*Year :* 2017

# INFRA-SLOW OSCILLATIONS IN THE BRAIN BALANCE SLEEP CONTINUITY AND FRAGILITY

Lecci Sandro

Lecci Sandro, 2017, INFRA-SLOW OSCILLATIONS IN THE BRAIN BALANCE SLEEP CONTINUITY AND FRAGILITY

Originally published at : Thesis, University of Lausanne

Posted at the University of Lausanne Open Archive http://serval.unil.ch
Document URN : urn:nbn:ch:serval-BIB_CEB4A6BAF63B7

UNIL | Université de Lausanne
Faculté de biologie et de médecine

**Département des Neurosciences Fondamentales**

# INFRA-SLOW OSCILLATIONS IN THE BRAIN BALANCE SLEEP CONTINUITY AND FRAGILITY

**Thèse de doctorat en Neurosciences**

présentée à la

Faculté de Biologie et de Médecine
de l'Université de Lausanne

par

**Sandro Lecci**

Biologiste diplômé de l'Université de Lausanne, Suisse

**Jury**

Prof. Micah Murray, Président
Prof. Anita Lüthi, Directeur
Prof. Paul Franken, Expert
Dr. Karim Benchenane, Expert

Thèse n° 204

**Lausanne 2017**

***Programme doctoral interuniversitaire en Neurosciences des Universités de Lausanne et Genève***

LEMANIC NEURO SCIENCE DOCTORAL SCHOOL

UNIL | Université de Lausanne

UNIVERSITÉ DE GENÈVE

UNIL | Université de Lausanne

UNIVERSITÉ DE GENÈVE

*Programme doctoral interuniversitaire en Neurosciences des Universités de Lausanne et Genève*

# Imprimatur

Vu le rapport présenté par le jury d'examen, composé de

| | |
|---|---|
| ***Président·e*** | Monsieur Prof. Micah **Murray** |
| ***Directeur·trice de thèse*** | Madame Prof. Anita **Lüthi** |
| ***Expert·e·s*** | Monsieur Prof. Paul **Franken** |
| | Monsieur Dr. Karim **Benchenane** |

le Conseil de Faculté autorise l'impression de la thèse de

**Monsieur Sandro Lecci**

Master en Biologie Médicale Université de Lausanne

intitulée

**INFRA-SLOW OSCILLATIONS IN THE BRAIN BALANCE SLEEP CONTINUITY AND FRAGILITY**

Lausanne, le 31 mars 2017

pour Le Doyen
de la Faculté de Biologie et de Médecine

Prof. Micah Murray

# TABLE OF CONTENT

# A. ACKNOWLEDGEMENTS

I am immensely thankful to my thesis director, Prof. Anita Lüthi.

Since I joined the Lab as a master student she took care of my needs and worries, always fully investing herself in finding a solution to have things working out in the best way, not just in the good way. Her innate leading attitude made me, and still makes me, always feel comfortable in every situation, and this, in my humble opinion, is what makes such a stressful, challenging, '*pàthos*'-genic, but still one of the nicest, periods of life easier to face. There is nothing I wish it would have gone differently in these last years.

I sincerely thank Dr. Laura Fernandez, my direct supervisor, for all the time she invested in guiding me throughout this journey. I consider myself lucky to have had a wonderful person like her as a point of reference in my daily work. She stopped whatever she was doing to help me or answer to my questions, without letting me go away having any single doubt. I am also grateful to Ralf Wimmer, my supervisor for the first months when I started. He managed to cultivate in me the interest in methodological approaches.

I owe to Chiara Pellegrini the endless scientific, moral and personal support she gave me at any time. Chiara is the kind of friend and colleague everybody should have on his/her side, I will never be able to give her back as much as she did for me.

I am extremely thankful to the rest of the Lüthi group for creating a fantastic working environment, I will never forget all the laughs we had together. In particular, Gil for his spontaneity, Romain for his efficiency in replicating what took me years to achieve (it is fulfilling!) and Elidie for her simplicity. In parallel, I am also thankful to the former lab members who already left the research group: Dr. Martina Perin, Dr. Zita Rovó and Dr. Simone Astori. They played a crucial role in shaping my scientific career.

I wish to express my gratitude to the collaborators in Germany: Freddy and Prof. Born. They contributed substantially to create a piece of artwork that I personally consider a gold standard, also concerning how collaborations should be established.

I am truly thankful to all the people I interacted with and that helped me in some way at the department to obtain my daily results. In particular Prof. Chatton, for all the technical support he provided and for the time spent chatting about electronics and informatics, Ing. Nicolas Liaudet for his precious help in programming, and Prof. Welker, for being extremely honest and straightforward in correcting my first draft of the article. I truly appreciated it.

I am also grateful for the support of funding agencies without which my thesis would not have been possible. These include the Swiss National Science Foundation and Etat de Vaud. Moreover, I could profit from travel grants from the Lemanic Neuroscience Doctoral School and from the Swiss Physiological Society that made me participate in international neuroscience meetings. I also had the chance to spend two weeks in the laboratory of Prof. Massimo Scanziani at UCSD thanks to travel support from the Swiss Physiological Society and from Prof. Lüthi's funding. This proved to be an invaluable experience for me in terms of seeing forefront experimental and analytical setting in neuroscience. Many thanks in particular to Dr. Riccardo Beltramo who spent a lot of time showing me his research activity and for his patience and willingness in guiding me into the analytical and technical aspects, which I will treasure for my future research activity.

Furthermore, I am extremely grateful to my friends in Lausanne and in Ticino, who always had a good word to say to make me smile again after a bad day and who were always there for a relaxing beer.

Finally, I wish to express my sincerest gratitude to my parents, who gave up many things to pay for my education, and to my brother Daniele, who helped me in many organizational aspects. They all believed in me, sometimes much more than me. I truly appreciate their efforts.

Lastly, I am infinitely thankful to Elena, the most important person in my life and mother of my son Simone, for everything she did, is doing and will do for me.

# B1. ABSTRACT

Sleep serves two opposing needs. It must provide continuity, for the restorative functions to take place, such as memory consolidation or metabolite clearance, and it must be fragile enough for sensing potential threats in the close environment. During sleep, a balance between these two fundamental aspects is to be kept as any imbalance may entrain potential pathological consequences. To date, how these two needs are kept in balance remains to be described.

Sleep spindles originate from the thalamo-cortical network, are abundant during non-rapid eye movement (non-REM) sleep in mammals and have been shown to play a crucial role in gating sensory information, potentially contributing to the partial sensory disconnection of this behavioral state. Sleep spindles are tightly coupled to slow oscillations (< 1 Hz) that, together with the delta frequency band (1 – 4 Hz), constitute another distinctive marker of non-REM sleep. Moreover, the depolarizing slow oscillation phase, when boosted, has been shown to promote memory consolidation, providing sleep continuity within defined temporal windows.

Through polysomnography recordings, we investigated the temporal dynamics of characteristic non-REM sleep frequency bands: the sigma power (that contains sleep spindles, 10 – 15 Hz) and the slow wave activity (SWA, slow oscillations + delta frequency band, 0.75 – 4 Hz) throughout consolidated non-REM sleep epochs in both mice and humans. We identify an infra-slow oscillatory component that dominates sigma power (0.02 Hz-oscillation) and is significantly less present in SWA and adjacent frequency bands. The 0.02 Hz-oscillation in sigma power was present in local cortical circuits in both species with a parietofrontal gradient.

We played noises to sleeping mice to study the relationship between the 0.02 Hz-oscillation in sigma power and the balance between sleep fragility and continuity. Mice woke up when noises were presented during the descending phase (fragility periods) and slept through it when presented in the ascending phase (continuity periods). Fragility periods also showed increased heart rate and low hippocampal ripple activity, a marker of offline memory processing. Conversely, continuity periods correlated with low heart rate and increased hippocampal ripple activity. Moreover, in humans, a stronger 0.02 Hz-oscillation correlated with better declarative memory performance

Therefore, the 0.02 Hz-oscillation in sigma power times the alternation between periods of continuity and fragility in both species, suggesting an evolutionary conserved mechanism modulating sensory perception during sleep.

# B2. RÉSUMÉ

Le sommeil combine deux besoins fondamentaux. Il doit être continu pour que ces fonctions restauratrices, comme la consolidation de la mémoire et l'élimination cellulaire des métabolites, puissent avoir lieu, mais en même temps aussi suffisamment fragile, pour détecter les dangers potentiels à proximité. Ces deux besoins sont gardés en équilibre pendant le sommeil. De nos jours, aucune description du mécanisme qui contrôle cet équilibre n'existe.

Les fuseaux du sommeil sont générés dans le réseau thalamo-cortical, ils sont prédominants pendant le sommeil de type non-rapid eye movement (non-REM), et ils jouent un rôle crucial dans le contrôle du flux sensoriel. Ils peuvent donc potentiellement contribuer à la déconnexion sensorielle typique du sommeil non-REM. Les fuseaux du sommeil sont aussi couplés avec les oscillations lentes, un autre marqueur caractéristique du sommeil non-REM et qui, ensemble avec la bande de fréquence delta (1 – 4 Hz), identifient la pression homéostatique du sommeil. De plus, la phase dépolarisante de l'oscillation lente, une fois entrainée, a été montrée comme étant bénéfique pour la consolidation de la mémoire, en fournissant une fenêtre temporelle qui peut promouvoir la continuité de sommeil.

Nous avons investigué, au moyen d'enregistrements polysomnographiques chez la souris et chez l'homme, les dynamiques temporelles des bandes de fréquences caractéristiques du sommeil non-REM, qui sont la puissance des fréquences sigma (qui intègrent les fuseaux du sommeil, 10 – 15 Hz) et l'activité des ondes lentes (SWA, composée des oscillations lentes et de la puissance des fréquences delta, 0.75 – 4 Hz), tout au long des périodes de sommeil consolidé. Nous avons identifié une composante oscillatoire infra-lente (à partir de maintenant appelée oscillation à 0.02 Hz), qui est prédominante pour la puissance sigma par rapport à SWA et à des bandes de fréquence contiguës. L'oscillation à 0.02 Hz dans la puissance sigma était présente dans des circuits corticaux locaux chez les deux espèces et présentait un gradient pariéto-frontal.

Pour investiguer la relation entre l'oscillation à 0.02 Hz de la puissance sigma et l'équilibre entre fragilité et continuité de sommeil, nous avons joué des sons à des souris qui étaient en train de dormir. Les souris se réveillaient seulement quand le son était joué dans la phase descendante (période de fragilité) et continuaient à dormir si le son était présenté dans la phase montante (période de continuité). Pendant les périodes de fragilité nous avons aussi mesuré une augmentation de la fréquence cardiaque et une baisse de l'activité des ondulations de l'hippocampe (Ripple activity), qui identifie le processus de mémorisation hors ligne. Les

périodes de continuité corrèlent avec une activité cardiaque basse et une haute présence de l'activité des ondulations de l'hippocampe. De plus, chez l'homme, l'oscillation à 0.02 Hz de la puissance sigma corrèle avec une meilleure performance dans une tâche qui teste la mémoire déclarative.

En conclusion, l'oscillation à 0.02 Hz de la puissance sigma définit l'alternation entre périodes de continuité et de fragilité chez les deux espèces, ce qui suggère la présence d'un mécanisme évolutionnaire conservé qui règle la perception sensorielle pendant le sommeil.

# C. INTRODUCTION

One of the most intriguing open question about sleep is, paradoxically, also one of the simplest: why do we sleep, what function does it serve? Understanding sleep as global phenomenon is a hobbyhorse of human being, most of it has been discovered and explained but we are far from having a complete knowledge of all its facets. In the last century, thanks to the technological advances, the scientific research has had an exponential boost in terms of quality and precision, therefore increasing the number of engaged people, invested money and, importantly, acquired knowledge. In 1989, J. Hobson wrote that "[…]*more has been learned about sleep in the past 60 years than in the preceding 6,000*" (cited by Madhu Kalia in (Kalia, 2006)), indicating how we, as scientists, seek for knowledge no matter what we already know, ergo "loving wisdom".

The interest in sleep dates since ancient civilizations. Unfortunately, our knowledge about science and sleep in the past is limited to the minority of writings remaining available today and to our ability to decipher them. Some rare Egyptian hieroglyphs report how fascinating was this behavioral state for the Egyptians, giving rise to personal interpretation. The importance of sleep and, consequently, of dreaming in the Egyptian culture is exposed in the Chester Beatty Papyrus (Kirsch, 2011 and references therein). It was believed that, during sleep, the eyes were truly open and the Gods were revealed; sleep was a journey to the star Sirius, where the source of higher consciousness resided. Many writings of Greek philosophers survived until today, they report the common interest in clarifying the role of sleep with respect to the body and the nature (Beare, 2009; Adam, 2009; Kirsch, 2011). Questioning the role of sleep is, of course, not restricted to past populations but still occurs nowadays. Another example comes from the Buddhism religion, where the sleep is seen as a period during which the person is not accountable of his/her actions and sleep itself reflects the consequences of his waking behavior: insomnia, for example, is caused by immorality. Some other populations, like the Aborigines, follow tribal rules and perform rituals to be assured of a good sleep (Scher, 2017).

Far from being an exhaustive listing of how perception and reflection on sleep evolved in different civilizations, these examples show how people care and wonder about having a good restful night, independently of their faith, education and knowledge. It is therefore a common belief to think that sleep plays a key role in our life, considering that we spend almost one third of our life in the bed and that the detrimental consequences of chronic sleep loss span

in multiple directions (Tobaldini et al., 2014; Tobaldini et al., 2016; Banks and Dinges, 2007; Jackson et al., 2013; Kreutzmann et al., 2015 and references therein).

Sleep is a universal behavioral state observed in all animals and insects studied so far; while all species profit from its function, its duration and intensity are highly variable. As reviewed by J. Siegel, there is no clear consensus on the relationship between sleep duration and physiological aspects such as body mass, brain size or alimentation habits (Siegel, 2005, 2009). However, it seems that it has been evolutionarily optimized with respect to the predator-prey relationship, not only concerning the duration and intensity but also its occurrence during the day-night cycle, even though this hypothesis has been questioned (discussed in Siegel, 2009). Irrespective of the hypothesis, it is curious to see how sleep behavior changes among different animals. For example, the big brown bat sleeps for almost 20 hours a day and is active at dusk when it can predate mosquitos and other flying insects. Its sleep-wake cycle has been optimized to a restricted period of time for several reasons: echolocation is energy demanding and a longer activity period would be unsustainable, and flying insects are mostly active at dusk when the sight of predatory birds gets worse (Siegel, 2009).

As the question of "*what really sleep is*" remains unanswered, or contains a considerably high subjective part, scientists focused more on "*what sleep is good for*". To answer this question, however, one has to shrink the field of interest as sleep does not serve a simple and unique function. In fact, apart from being trivially considered as "recharging", sleep has been shown to promote a series of disparate biological functions, such as immunity protection (Irwin, 2015; Marshall and Born, 2002), metabolic function and energy balance (Xie et al., 2013; Benington and Heller, 1995; Maquet, 1995), memory consolidation (Vorster and Born, 2015;Born, 2010; Marshall and Born, 2002), macromolecule biosynthesis (Mackiewicz et al., 2007) and emotional regulation (Baran et al., 2012; Perogamvros et al., 2013). During sleep, many different processes are simultaneously regulated and yet seemingly unrelated to each other. Therefore, the qualification of sleep based on its role in specific aspects helps us to contextualize and expand further its function but fails to characterize its absolute identity.

The ability to keep sensory disconnection (**sleep continuity**) and integration (**sleep fragility**) in balance is a requisite for sleep. Continuity and fragility are used here to describe sleep stability face to presentation to external stimuli, sleep is said to be continuous when a stimulus does not induce a state transition, whereas it is said to be fragile when the stimulus induces a behavioral state transition, thus fragmenting sleep. Most of the restorative functions, if not all of them, depend on its intact structure and maintaining sleep continuity is crucial for their functionality. However, how this relates to the other need of sleep, the fragility, has so far

been completely neglected. Keeping sensory disconnection and integration in balance allows the sleeper to profit from the restorative and beneficial aspects of sleep but, at the same time, helps him to maintain the integration of stimuli from the close environment (Hennevin et al., 2007). The concept of arousability during sleep reflects the strength of this balance and the easiness to wake up at a specific moment. A typical example comes from our daily experience: we might sleep over the noise made by the dump truck early in the morning but we wake up quickly as soon as our telephone rings, or, for example, we react differently when our name is presented together with other names and sounds during sleep (Oswald et al., 1960; McDonald et al., 1975). It is important to specify that the connotation and the intensity of the sensory stimulus play a critical role. Unpleasant stimuli are more likely to induce awakenings, but will barely be recognized if played at low intensity level (Portas et al., 2000). Sleep continuity is therefore an important feature of sleep as it allows for all the regenerative and protective aspects of sleep to work undisturbedly. It is germane to emphasize here the importance of this feature as any imbalance between sleep continuity and fragility may entrain pathological and detrimental consequences, as such imbalance could be linked to excessive daytime sleepiness (El-Ad and Korczyn, 1998; Zeman, 1998) or insomnia (Shekleton et al., 2014), which is increasingly linked to markers of hyperarousal in the central and autonomic nervous systems (Feige et al., 2013).

Importantly, sleep disturbances (or disorders related to sleep) are not only linked to internal factors, such as gene alteration, but may arise from the environment and an inappropriate lifestyle. In fact, since the introduction of artificial light, our lifestyle has changed dramatically by reducing sleeping time in advance of more entertainments and/or working hours (Cho et al., 2015), even though this theory has been recently challenged (Borniger et al., 2013). This, together with the increased consumption of caffeinated drinks, leads to an increased occurrence of sleep-related disturbances (Clark and Landolt, 2017). Recently, many efforts have been taken to improve either sleep quality or sleep environments (i.e. the sleep school established by Prof. Zulley (www.zulley.de)) as consequences of bad sleep have also implications on people close to us besides directly affecting our body and mental health. Therefore, despite being widely studied by scientists and non-scientific people, what makes our sleep good and restorative has not yet been discovered and will continue to be a key question at the center of the sleep research for the next years.

Investigating the mechanism that keeps sleep continuity and fragility in balance might certainly enlighten and clarify one, if not many, roles of sleep. Therefore, it might provide with useful indications on how sensory perception is attenuated, yet still kept, during sleep. In this

line, it will help us understand the neural basis of the cortical state during sleep. Furthermore, identifying the key player of that mechanism might provide with interesting targets for pharmacological intervention on sleep disturbances related to sleep continuity and/or fragility aiming to potentially ameliorate sleep quality.

In this report, I will introduce the methodological aspects of sleep research, and I will provide a general description of the mechanisms that regulate the sleep-wake cycle. Finally, I will summarize the current knowledge about specific fluctuations in brain activity, with a frequency of tens of seconds. Importantly, besides introducing the basic mechanisms that induce and maintain sleep, I will focalize my attention on the bidirectional switch between sleep continuity and fragility by reporting different *phaenomena* during sleep that occur with a time range of close to one minute (in the infra-slow range) and on the possible regulation of arousal threshold by these mechanisms. To present, there is no indication that such association might occur during sleep and that arousability varies on such a slow time scale.

# 1. Methodology of sleep research

## i. Techniques used in sleep research

Analyzing sleep as a behavioral state usually requires a multidimensional approach. Self-assessment of sleep through questionnaires reports personal experience, but there is a need in quantifying sleep quality based on measurable and objective parameters.

In the last centuries the widely accepted hypothesis was that sleep originated from the brain. The first findings of electrically driven information in the body arose in 1791 when Galvani demonstrated, on isolated frog legs, that a small current injection was capable of inducing muscle contractions (Piccolino, 1997). Thanks to the technological and electro-technical advances in the 19$^{th}$ and 20$^{th}$ century, it became possible to measure and record biological data using instruments that detect and amplify small electric currents generated by the body, first with galvanometers, and then with electroencephalograms (EEG). The galvanometer, a device that converts electrical activity into a magnetic moment, was one of the first instruments used for showing the presence of electrical activity in the intact brain and its extensive use laid the foundation for the development of more sophisticated and precise devices. Hans Berger is considered the father of the modern electrophysiology thanks to his tenacity and his perseverance in developing and using the EEG recording technique in the early ‘20s. The principle of EEG recording is based on the detection of small voltage variations between two metal electrodes, where high recorded value correlates with high difference of brain activity between the two electrodes. The EEG recording device allowed Berger to detect and record electrical activity from the human scalp, first in patients with skull defects and then in healthy subjects. His findings were first published in 1929 after many years spent improving the technique with different electrodes and using more sensitive galvanometers. This discovery is considered a milestone of medical investigation and research on the human brain as Berger made possible to see a reliable tracing of brain’s activity for the first time. Apart from its extensive use in epilepsy research, the EEG recordings setup was quickly adapted for sleep research and scientists took advantage of specific algorithms, such as the Fast Fourier Transform (FFT), to analyze its traces.

Although almost 100 years old, the EEG technique remains widely used nowadays and serves as standard technique to investigate brain activity. In parallel, other interesting techniques, such as functional Magnetic Resonance Imaging (fMRI) or magnetoencephalography (MEG), have been set up to study brain activity. fMRI combines the detection of hemoglobin saturation level together with the MRI scanning imaging. It predicts

that zones in the brain that are more active (i.e. during a specific visual or auditory task) will use much more oxygen than during a resting period, resulting therefore in a greater blood flow and differences in oxygenation in that brain area (reviewed in Buxton, 2013). fMRI temporal resolution is, however, lower compared to EEG recordings and is therefore not recommended for high resolution analysis, but recent reports propose mathematical approaches that overcome this problem (Mitra et al., 2015). The principle of the MEG technique is similar to the EEG technique and aims to detect small changes in the magnetic field caused by active neurons, it provides a better source localization but it is not favorable for sleep research because of the dimensions and postural restrictions (discussed in Barkley and Baumgartner, 2003). All these different techniques highlight in turn specific characteristics of brain activity, such as electric discharge, oxygen/glucose consumption but also water movement, as it is the case for the diffusion tensor imaging (reviewed in Assaf and Pasternak, 2008). Interestingly they can be combined for a more complete study but not all of them are suitable for sleep research for several reasons, such as space restraints or sounds produced by the machines running. Thanks to its non-invasiveness, temporal resolution, world-wide distribution and noiseless feature, the EEG technique is amongst the most suited for studying sleep and, in particular, the brain dynamics that control for arousability.

ii. Identification of vigilance states in the sleep-wake cycle

The identification of oscillatory components in the EEG traces allowed for the classification of two major sleeping states: the rapid-eye-movement (REM) sleep and the non-REM sleep. Rules for standardized scoring in humans have been proposed already in 1968 by Rechtschaffen and Kales (Rechtschaffen and Kales, 1968) and in 2007 the American Academy of Sleep Medicine provided a *Manual for the scoring of sleep and associated events* (Iber, 2007). These rules were proposed as reference method to standardize the scoring technique and have become the gold standard in sleep research (Himanen and Hasan, 2000). Hereafter I will summarize the hallmarks identifying the different vigilance states. It is important to mention here that other vigilance states are identified, such as the differentiation between active and quiet wakefulness, drowsiness, or the transitory intermediate state between non-REM sleep and REM sleep. The vigilance states with their spectral characteristics are summarized and exposed in Table 1 at page 12 and graphically shown in Figure 1 at page 13. Unless specified, the frequency bands and spectral characteristics are reported as for humans.

| Vigilance state | Oscillatory hallmark | Complementary information |
|---|---|---|
| **Wakefulness** | Alpha (α: 8 – 12 Hz)<br>Beta (β: 12 – 30 Hz)<br>Gamma (γ: 30 – 80 Hz) | Prominent muscular activity |
| **Non-REM sleep** | Delta (δ: 1.5 – 4 Hz)<br>Sigma (σ: 8 – 15 Hz)<br>Slow-Oscillations (< 1 Hz)<br>Sleep spindles<br>K-complexes | Disappearance of alpha rhythm<br>Increase of low frequencies<br>Decrease of muscular tone |
| **REM sleep** | Theta (θ: 4 – 10 Hz) | Decrease of amplitude<br>Mixed frequencies<br>Peripheral muscular atonia<br>Eye movements |

*Table 1: Frequency Hallmarks of Behavioral States*

Each behavioral state is composed of a mixture of oscillations detected through EEG recordings, subdivided into relative presence of frequency bands identified by Greek letters. The presence or not of these oscillations together defines the parameters used for sleep scoring.

Wakefulness is identified based on the presence of low-amplitude high-frequency oscillations (mainly α, β and γ) together with the detection of muscular activity. REM sleep is named after its peculiar rapid movement of the eyes and is characterized by peripheral muscular atonia together with the presence of frequencies in the theta frequency band. The EEG traces resemble wakefulness, hence its other name "sommeil paradoxal" (paradoxical sleep), as named by Michel Jouvet after describing it in cats (reviewed in Jouvet, 1967b). Non-REM sleep is characterized by prominent oscillations < 1 Hz, identified as slow oscillations (Steriade et al., 1993), and by rhythms in the δ range, which are typically referred to jointly as Slow Wave Activity (SWA) ranging from 0.75 – 4 Hz (Achermann and Borbely, 2003; Brown et al., 2012; Rasch and Born, 2013 and Weber and Dan, 2016). Other events characteristic of non-REM sleep are sleep spindles, waxing and waning oscillatory events of 8 – 15 Hz and lasting 0.5 – 3 s arising from the thalamo-cortical network (Steriade, 2006; Timofeev et al., 2012), and K-complexes, identified by the brief and large deflection in the EEG trace, are mostly described in human sleep and are often associated with sleep spindles (Halasz, 2005).

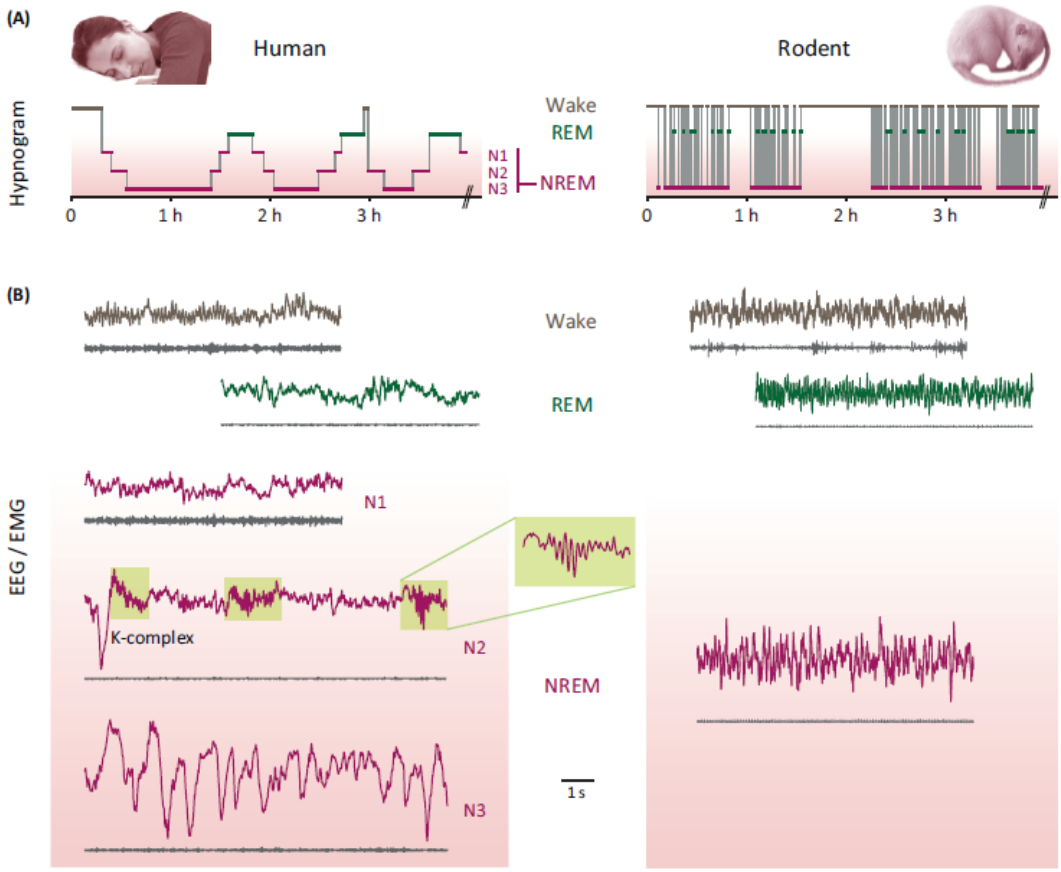


*Figure 1: Comparison between human and rodent hypnogram and behavioral states*

Humans and rodents share basic architectural and spectral characteristics of sleep. (A) Hypnogram of a sleeping human (left) and rodent (right) showing the cyclic behavioral state change between wakefulness, non-REM sleep states and REM sleep. (B) The behavioral states are identified based on peculiar spectral characteristics (exposed in Table 1 at page 12) that result from EEG recordings. Note the subdivision of human non-REM sleep into three stages corresponding to different sleep depth (N1-N3). Sleep spindles (yellow boxes) are predominantly present in non-REM sleep stage N2. Modified from Astori et al., 2013.

Non-REM sleep is accompanied with reduced muscular activity compared to wakefulness and, in humans, is differentiated into 3 different stages (N1 – N3 or stage1 – stage3, also reported as S1 – S3) that define sleep depth. The combination of EEG and electromyogram (EMG), together with optional recordings, such as oxygen saturation level, electrooculogram and respiratory monitoring is called polysomnography and allows for a more precise profiling of sleep stages.

Figure 1A provides an example of a typical hypnogram obtained from human and rodent polysomnography recordings (Astori et al., 2013). In humans, a sleep cycle is identified when the subject goes from light non-REM sleep state (N1) to deep non-REM sleep (N3), with the EEG trace displaying gradual changes towards low frequencies and high amplitudes, and back, together with a transition to REM sleep. The cyclic transitions between non-REM and REM

sleep lasts approximately 90 minutes. The EEG traces show gradual changes from high frequency and low amplitude to low frequency and high amplitude and indicates the transition between drowsiness (N1) and deep sleep (N3) (Figure 1B at page 13). Except for rapid awakenings, transitions between and within behavioral states are gradual and, sometimes, difficult to identify. The classification of sleep in behavioral states, as described above, reports the characteristic elements needed to perform an adequate scoring of the sleep-wake cycle.

Sleep in rodents shares common features to human sleep, such as the frequency bands and the cyclic alternation of behavioral states. However, when comparing these two species, particular care has to be taken. Critical differences are found, for example, related to the length of each bout of either non-REM or REM sleep is shorter (100 – 120 s) and there is so far no clear indication for light and deep non-REM sleep stages.

## 2. The timing of sleep

The regulation of sleep occurs at different levels, ranging from gene expression to the environment, with the modern 24/7 lifestyle being a critical factor, together with the waking history before bedtime. These levels at which sleep is regulated conjointly modulate and maintain transitions between behavioral states. The combined action of two processes, circadian and homeostatic, regulates the timing and structure of sleep. It summarizes the regulation of sleep as a function of all vigilance states and of their relative distribution, providing an indication of how sleep is timed with respect to the 24h day. As an example, sustained wakefulness results in a compensatory increase in sleep duration, indicating that its timing and duration strongly depend on the preceding waking experience. However, this relationship holds only until a saturating point is reached. In fact, as reported by Gulevich and colleagues (Gulevich et al., 1966), only 14.4 h of recovery sleep were observed after 264 h of continuous waking. Therefore, understanding how sleep is regulated requires the investigation of mechanisms that mediate sleep drive during wakefulness, as well as mechanisms that stabilize and maintain sleep once it has started.

In this chapter I will first summarize the regulation of sleep based on interaction between circadian and homeostatic processes, then I will focus on how sleep is regulated internally, by emphasizing the role of nuclei in the brainstem that control for the switch between wakefulness and non-REM sleep. Finally, I will briefly introduce the awakenings induced by external triggers, such as auditory stimulations. As these mechanisms have been extensively reviewed in literature, the following sections are based on key articles and reviews, with the goal of highlighting the aspects linked to the timing of sleep (Borbely, 1982; Mistlberger, 2005; Moore, 2007; Saper et al., 2001; Franken and Dijk, 2009; Brown et al., 2012).

### i. The two-process model of sleep regulation

To work during the day and sleep during the night seems trivial, but this precise timing is the result of hundreds of thousands of years of evolution. As mentioned in the preface, sleep periods were adapted to every species' environment and lifestyle (Siegel, 2009). In general, our everyday life is timed by the alternation of light and darkness and we evolved adapting our working habits to match the natural illumination period. The daily alternation between wakefulness and sleep follows a "*circadian*" rhythm (from the combination of two Latin words: *circa diēm*, meaning "approximately/around the day"). In parallel, a substantial fraction of our bodily functions has evolved to be homeostatically

regulated, that is, any excess is compensated by a counterbalancing drive in the opposite direction. In sleep, this is translated into compensatory mechanisms that occur at different levels.

Together, the circadian (sleep-wake independent) and the homeostatic (sleep-wake dependent) processes have been proposed to conjointly regulate sleep propensity throughout the day. Hereafter I will report the mechanisms of action of these two processes, first independently, then in mutual combination.

ii. The circadian process

Evidence for a circadian regulation of sleep was shown in 1964, with an experiment that aimed at studying the presence of fixed rhythms in a person not exposed to the natural illumination during three months. More specifically, the subject was left in a cave without any indication of the external time and could speak with the medical doctor only once a day. As soon as the subject changed his habits and went to sleep only when tired, his circadian period slightly augmented and his sleep onset time was delayed every day. After a couple of weeks he had lost almost 3 days (Mills, 1964). Further experiments identified the human circadian period to range between 23.8 and 24.5 h (Czeisler et al., 1999). This means that, even without an external biological clock, such as the sun, we can stick to a *circadian* rhythm based on our internal clock. Another evidence for a circadian regulation of sleep drive is ascertained through the forced desynchrony protocol (pioneered by Nathaniel Kleitman in 1939), which separates the circadian from the homeostatic process of sleep regulation (Dijk and Czeisler, 1994, 1995). More specifically, forcing subjects to adapt to a sleep-wake cycle shorter or longer than 24h results in sleep-onset times at different moments across several days, some of which are unfavorable according to the internal circadian cycle, such as in the afternoon hours, resulting in shorter sleep.

The experiment performed by Mills, together with similar evidence found in plants almost 200 years before by the work of the French astronomer Jean-Jacques de Mairan (cited in Volkov et al., 2012), suggested the presence of an internal clock that maintains the circadian period at about 24-25 hours without regular sunlight exposure and even in total darkness. The hypothalamus has been proposed as the center regulating the sleep/wake cycle (Richter, 1965; Richter, 1967; reviewed in Moore, 2007), as rats with lesions in this area showed a loss in the activity – rest cycle, among other impairments. Further studies identified the SupraChiasmatic Nucleus (SCN) as the nucleus responsible

for timing the internal circadian clock and the Retinohypothalamic tract as the critical pathway relaying light information from retina to the SCN (reviewed by Moore, 2007) that uses melanopsin, a light-sensitive protein located in retinal ganglion cells, as mediator (Gooley et al., 2001). Importantly, transplanting the SCN to a host with a lesioned SCN recovers the circadian function with the periodicity of the donor species (Ralph et al., 1990), and recordings of action potentials of cells from mice SCN explants in culture show a clear circadian rhythm with a period of ~24.1 h (Herzog et al., 1997).

Lesion experiments are extremely helpful in understanding how the circadian rhythm entrains the sleep-wake cycle. Lesions to SCN in rats result in a disrupted temporal occurrence of sleep and wakefulness but no major consequences in total sleep and wake time were found (Baker et al., 2005; Ibuka and Kawamura, 1975), even though SCN ablation in squirrel monkey (Edgar et al., 1993), and in some strains of mice (Easton et al., 2004) reported increased sleep time. The general consensus is that SCN lesions and ablations disrupt the circadian rhythm without affecting sleep homeostasis (Mistlberger et al., 1983; Tobler et al., 1983; Trachsel et al., 1992). SCN ablation affects the circadian alternation between wakefulness and sleep because of its extensive efferent connections to hypothalamus and brainstem nuclei that control for the sleep – wake cycle, which are briefly reported hereafter (for review see Mistlberger, 2005; Saper et al., 2001; Moore, 2007; Brown et al., 2012; and references therein).

The sleep promoting targets of SCN are the VentroLateralPreOptic area (VLPO) and the Median Preoptic Area (MnPO). Connections to the VLPO are assured through both direct and indirect wirings that include the DorsoMedial Hypothalamus (DMH), the subParaVentricularZone (sPVZ) and the Lateral Hypothalamus (LH) (more about these nuclei in chapter 3 at page 25). sPVZ is the major efferent of SCN cells and is connected to brainstem and hypothalamic nuclei controlling the sleep/wake cycle. Lesions to sPVZ disrupt the sleep/wake temporal organization, but have less effect on the circadian regulation of other parameters, such as body temperature. The VLPO is responsible for starting and maintaining non-REM sleep, therefore lesions to VLPO induce insomnia and reduce daily NREM sleep, but have only modest effects on the sleep-wake cycle. Similarly, lesions to MnPO induce insomnia without major consequences on the sleep/wake cycle. These results indicate that SCN is primarily connected to sleep-promoting nuclei, and that SCN lesions disrupt the temporal organization of sleep and wakefulness without impairing sleep homeostasis. In parallel, lesions to sleep promoting

targets of SCN, such as VLPO, induce insomnia without affecting the inner circadian clock.

SCN also projects to the wake-promoting posterior hypothalamus and to nuclei that are also involved in regulating sleep, such as DMH or LH, albeit to a lesser extent compared to the sPVZ innervations described above. Lesions to DMH impair the circadian sleep-wake cycle, feeding and locomotor activity but preserves daily fluctuations of body temperature and plasma melatonin, indicating the crucial role of DMH in regulating the sleep-wake cycle. Therefore, SCN itself controls the circadian regulation of biological functions acting as a relay nucleus between the SCN and specific area mediating active and wakefulness behaviors.

Together, these results indicate that SCN is the primary entrainment target of a pathway relying retinal light information to the inner brain, and the lesion of which causes a loss in the structure of the activity – rest cycle. Moreover, cellular activity of isolated SCN maintains the pacemaking circadian rhythm and grafting the SCN to another species causes adaptation of circadian rhythm to match the host cycle (Ralph et al., 1990).

Finally, SCN activity is regulated through a feedback mechanism that involves the brain according to the vigilance state and homeostatic sleep pressure through as yet unknown mechanisms (Buijs et al., 2003; Deboer et al., 2003). Additionally, SCN activity is also regulated through the feed-back action of melatonin secretion from the pineal gland (reviewed in Moore, 2007). In the evening SCN firing activity decreases because of the weaker illumination, resulting in increased melatonin synthesis and secretion, which further decreases SCN activity through activation of MT-1 G-protein coupled receptors (reviewed in Moore, 2007; Dubocovich, 2007). During the day, SCN activity inhibits melatonin synthesis. Melatonin administration in humans and non-human primates promotes sleep (Zhdanova et al., 2002; Zhdanova, 2005; Arendt, 2005) and is currently being used for preventing and/or treating the jet-lag effect (Herxheimer and Petrie, 2002).

SCN is considered as the major inner clock regulator that closely coordinates autonomic rhythms such as body temperature and sleep-wake cycle. Circadian fluctuations are, however, not restricted to brain tissues, nearly all cells and tissues present either molecular or cellular rhythmicity (Buijs et al., 2006; Kalsbeek et al., 2006; Stratmann and Schibler, 2006), and these oscillators in the entire body need to be continuously synchronized by the SCN through both endocrine and neural control (Schibler et al., 2015).

Therefore, besides directly modulating the neuronal activity of nuclei involved in the sleep/wake cycle, SCN also modulates the circadian secretion of hormones within the brain and the entire body.

It is interesting to mention that a possible presence of a circadian component in the human brain was reported long before the discovery of SCN activity as inner clock pacemaker. In fact, the vigilance of a sleep deprived person over many days has been shown to fluctuate with a circadian rhythm, having a peak in the afternoon at 4 PM and a nadir at 4 AM (Borbely, 1982). This means that, even though we are sleep-deprived during one night, our vigilance in the next morning is higher compared to our level in the night, indicating that a circadian process drives our need to be awake during the day. Similarly, sleep propensity also shows a circadian rhythmicity (Akerstedt, 1977) with nadir and peak coinciding with maximal and minimal body temperature, respectively (discussed in Borbely, 1982). Therefore, the peak of body temperature is reached at ~4 PM and is aligned to the nadir of sleep propensity distribution.

iii. Genes regulating the Circadian process and their mechanism of action

The mechanism regulating the circadian cycle involves a feedback loop controlled through transcription and translation of genes, which are highly conserved among animals (reviewed in Franken and Dijk, 2009). During the day, the transcription factors CLOCK and BMAL1, encoded by the genes *Clock* and *Bmal1,* are translated and make up the machinery controlling the circadian rhythm. Once heterodimerized, they drive the expression of two period genes (*Per1* and *Per2*) and two cryptochromes (*Cry1* and *Cry2*). The translated proteins PER and CRY form complexes that inhibit the CLOCK:BMAL1 complex, therefore inhibiting their own transcription once a certain level is reached (Mistlberger, 2005; Schibler et al., 2015). During the night, the PER-CRY complex is degraded and, consequently, the CLOCK:BMAL1 complex can drive again the transcription of the *Per* and *Cry* genes. Importantly, other clock genes have been shown to play key roles in the circadian machinery, such as the core gene *Rev-erbα,* which translated for a nuclear receptor that inhibits *Bmal1* expression (for extensive reviews see Lowrey and Takahashi, 2004; Brown et al., 2012 and references therein). Finally, tissues outside the SCN, and outside the brain, also express circadian clock genes (Hastings, 2003; Hastings et al., 2003), as it was shown by the circadian bioluminescence pattern emitted by transgenic rat cells lines of liver, lung and skeletal muscle kept *in vitro* expressing

luciferase in combination with the *Per1* gene (Yamazaki et al., 2000). The phase of peripheral oscillators is aligned to the SCN oscillation through signaling cascades that include glucocorticoid receptors and the serum response factor (Schibler et al., 2015).

iv. The homeostatic process

In parallel to the circadian regulation of sleep, it is well established that sleep also follows a homeostatic regulatory process, where sleep propensity is regulated at different levels with respect to the preceding sleep-wake history. First, a shortening of sleep onset time together with an increased time spent in deeper sleeping stage are observed. Then, changes in the spectral distribution of frequency bands during sleep also identify homeostatic regulations of sleep. The power levels of SWA in the EEG have been shown to reflect the prior sleep-wake history, with elevated values at sleep onset, which exponentially decrease as sleep progresses (Process S curve Figure 2 at page 21; Borbely, 1982; Tobler and Borbely, 1986; Franken et al., 1991b), yet it is now known that, at least in humans, the delta but not the slow wave component are homeostatically regulated (Achermann and Borbely, 1997; Rasch and Born, 2013; Vyazovskiy et al., 2011). Prolonged wake periods, usually achieved through sleep deprivation, result in a proportional increase in SWA level during recovery sleep (Franken et al., 1991b), whereas episodes of excessive diurnal sleep or napping before bedtime consistently reduce SWA level at night (Werth et al., 1996). This further establishes its role as a marker for homeostatic sleep pressure. Additionally, the homeostatic increase in SWA positively correlates with sleep depth (see Figure 2 at page 21 for more details). This positive association has been already described in 1937 by Loomis and colleagues (Loomis et al., 1937), who noted increased arousal threshold during periods with high SWA (also called slow wave sleep, SWS). This has been confirmed almost 30 years later with the experiments of Williams (Williams et al., 1964) and Goodenough (Goodenough et al., 1965) who report an increased arousal threshold to pain or acoustic stimuli during SWS compared to N2 sleep, a lighter stage where SWA is less present compared to SWS. Therefore, SWA is identified as a marker of sleep depth (Borbely et al., 1981; Dijk and Beersma, 1989).

Importantly, the dynamics of SWA as indicator of homeostatic regulation of sleep has been extensively studied during undisturbed sleep as well as in relation to sleep deprivation experiments or to changes in the light-dark cycle in rodents (Tobler et al.,

1990; Franken et al., 1991b; Franken et al., 1991a; Tobler et al., 1992), and all evidence indicates that it is a general property of mammalian sleep. Current ideas interpret changes in SWA in relation to alterations in synaptic strength. The theory behind the synaptic homeostasis hypothesis (also referred to as SHY) is based on neuronal synaptic refining occurring during sleep after accumulation of neuronal "fatigue" due to sustained firing during wakefulness. This results in a compensatory homeostatic recovery characterized by longer and more frequent silence periods, thus increasing the SWA level during sleep (Tononi and Cirelli, 2003; Rodriguez et al., 2016). However, the SHY hypothesis still awaits a firm mechanistic assessment in terms of how it can be based on neuronal discharge characteristics and modifications of synaptic transmission in both excitatory and inhibitory neurons.

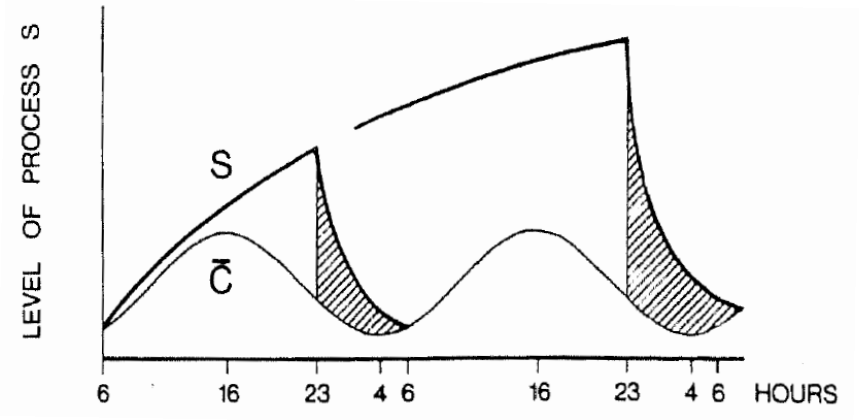


*Figure 2: Temporal dynamics of Homeostatic and Circadian processes of sleep regulation (modified from Borbely, 1982).*

The homeostatic process of sleep regulation (process S) is identified through measurement of SWA from the EEG recordings. Process S increases non-linearly across the day and decreases exponentially once sleep occurs. Increased sleep drive after sleep deprivation is reflected by the augmented level of SWA. Process $\bar{C}$ reflects the inverse function of the circadian fluctuation of fatigue perceived during sleep deprivation. The difference between the two curves indicates the sleep need (modified from Borbely1982).

During sleep, SWA has been shown to be temporally linked with activity of faster rhythms, such as sigma power (Uchida et al., 1991; Vyazovskiy et al., 2004), although their simultaneous presence is incompatible at the single neuronal level (Nunez et al., 1992; Steriade, 2003). While SWA decreases during sleep epochs, as well as during the resting phase, the activity within the spindle frequency band shows a complete opposite trend with a tendency to increase during sleep (Trachsel et al., 1988; Uchida et al., 1991), Additionally, SWA and sigma frequency band populate different vigilance states in humans, with the first being predominant in deeper non-REM sleep stages and the latter in lighter non-REM sleep stages (Uchida et al., 1991). Within non-REM sleep episodes

the power of the sigma frequency band has been shown to follow a U-shaped distribution, with high values at the beginning and at the end. This temporal correlation is evident during successful transitions between non-REM sleep and REM sleep (Wimmer et al., 2012) as well as during REM sleep attempts (Franken, 2002), where the characteristic increase in sigma power is coupled with a decrease in delta power shortly before the transition to REM sleep. These findings suggest that sigma power might cooperate with SWA into complex regulatory mechanisms occurring during sleep, at least in mammals. In fact, several reptiles lack the neural circuitry necessary to generate SWA suggesting that it might not be necessary to sleep homeostasis (reviewed in Greene and Frank, 2010).

Regulation of sleep homeostasis has been proposed to be mediated through different cellular and molecular mechanisms, several of which are induced by substances accumulating as a result of metabolic or synaptic activity during waking. The best characterized somnogen is adenosine, which accumulates throughout the day and with prolonged wakefulness as a product of ATP hydrolysis, whereas its level decreases during sleep (Porkka-Heiskanen et al., 1997). The extracellular accumulation of adenosine activates neurons in the VLPO, which could favor inhibition of wake-promoting nuclei (Gallopin et al., 2005), yet this has not yet been demonstrated. Alternative mechanisms of action for adenosine involve glial-mediated adenosine release that acts on basal forebrain (Halassa et al., 2009). Interfering with the sleep-promoting action of adenosine, through assumption of caffeine, confirms the role of adenosine in mediating sleep homeostasis (Landolt, 2008). Other somnogenic compounds related to sleep homeostasis include: uridine, oxidized glutathione, muramyl dipeptide and prostaglandin $D_2$, as well as sleep-inducing peptides, growth factors, cytokines, and neuromodulators, such as nitric oxide (reviewed in Brown et al., 2012).

The temporal dynamics and the intensity of SWA is thus a firmly established marker of the homeostatic regulation of sleep and these influence several measurable parameters of sleep depth related to its architecture, transition probabilities to other vigilance states, spectral composition and behavior, such as arousal threshold. In spite of the clarity of this measure, still little is known about the function of SWA, both for sleep function but also how exactly it affects the cortical state and its capability of sensory processing. On-going researches are currently being performed in multiple directions, aiming at, for example, investigating the contribution of SWA and reactive delta waves to sleep protection (Halasz

et al., 2014), identify their laminar profiles (Fiath et al., 2016), or, studying their role in memory consolidation through trans-cranial magnetic stimulations (Bellesi et al., 2014).

v. Sleep regulation through interaction between Circadian and Homeostatic processes

Borbely proposed in 1982 a sleep regulation model that combines the circadian and the homeostatic processes (Borbely, 1982) and that has been the leading model of sleep regulation ever since. The circadian process, reported as the mirror image of the fatigue curve during sleep deprivation (Process $\bar{C}$ in Figure 2 at page 21), indicates the sleep drive, whereas the homeostatic process (process S) corresponds to the SWA level. The difference between the two processes corresponds to the sleep propensity, which increases in the late afternoon reaching a peak value at the time of sleep onset (generally 11 PM). The validity of this model has been confirmed comparing simulated data with experimental data (discussed in Borbely, 1982; Kronauer et al., 1982; Akerstedt and Gillberg, 1981). The estimated sleep duration depending on sleep onset time closely matches the experimental data with a tendency to underestimate sleep duration when sleep onset time occurs around noon. A phase adjustment of the circadian component results in a close matching between simulated and experimentally obtained data (discussed in Borbely, 1982).

Although apparently segregated, the genes building the circadian clock machinery have been shown to have an effect in the homeostatic regulation of sleep, and, conversely, sleep homeostasis has an impact on expression of circadian gene (for review see Franken and Dijk, 2009 and Franken, 2013). As an example, mice having deficiencies in both core genes of the circadian machinery *Cry1* and *Cry2*, besides being arrhythmic when kept in constant conditions, report alteration in homeostatic markers, such as SWA and non-REM sleep bout consolidation (Wisor et al., 2008). This is explained by the increase in sleep need caused by the lack of CRY proteins. These animals live, therefore, under constant sleep pressure condition. Single knock-out animals for either gene do not report the same phenotype (Wisor et al., 2008). Furthermore, redox potential resulting from cell metabolism has a direct effect onto complexes regulating transcription of clock genes, such as CLOCK:BMAL1. *In vitro* experiments showed that an increased cellular metabolism induced increases in the amount of oxidized co-factors ($NAD^+$ and $NADP^+$), thus increasing the redox potential, which directly affects the transcription of clock genes. Energy metabolism, therefore, plays a role in modulating the circadian transcription of genes (discussed in Franken and Dijk, 2009).

Therefore, the two processes, initially described as independent, are tightly coupled to conjointly regulate the sleep need based on both internal and external factors, such as gene expression or light illumination and potential sleep restrictors, respectively. Additional experiments in mice having different genetic background report different homeostatic responses to sleep restriction (Franken et al., 2001) and seem to confirm the close relationship between genes and environment.

# 3. Neural control of sleep and wake states

In the previous section I reported the main findings and the implication of the two-process model of sleep regulation. This model describes and predicts the relationship between the circadian and homeostatic processes of sleep regulation, whose combination reports the sleep drive across the 24 h, as well as during sleep restriction. The hypnogram of mammalian sleep, as shown in Figure 1 at page 13, reports variations within sleep itself that indicate a complex internal regulation of the sleep-wake cycle. In this chapter, I will briefly expose the nuclei responsible for inducing and controlling non-REM sleep state in rodents. The mechanism that controls for the switch between behavioral states, as well as for their maintenance has been extensively reviewed (Saper et al., 2001; Saper et al., 2010; Brown et al., 2012; Schwartz and Kilduff, 2015; Jones, 2005), it is therefore not in the purpose of this thesis to list all the actors. I will rather emphasize the role of nuclei involved in the bidirectional switch between Non-REM and Wakefulness and describe briefly their mechanism of action. Unless elsewhere specified, the following sections are based on the aforementioned reviews.

## i. Historical crucial findings

The mechanism that regulates the switch between different stages has been hypothesized after the findings of different groups in France and the U.S. (Jouvet in Lyon, France, and Moruzzi&Magoun at the Northwestern University, USA) obtained in the middle of last century. The experiments performed by these groups aimed at identifying the region in the brain that controls sleep. Crucial for their research were findings of the Austrian Psychiatrist and Neurologist Constantin Von Economo, who studied the causes of the *encephalitis lethargica* plague that spread in Europe during and after the First World War (reviewed in Triarhou, 2006). He reported that people who had lesions in the posterior hypothalamus presented excessive sleepiness, whereas people with injuries in the preoptic area were insomniac. Therefore, he predicted that the preoptic area was responsible for inducing sleep and that the posterior hypothalamus was important for wakefulness. These results were confirmed by studies in monkey, rats, and cats (Triarhou, 2006; Saper et al., 2001 and references therein).

As reported by M. Jouvet in his scientific autobiography (Jouvet, 2004), as well as in his dedicated section on the website of the University of Lyon (Jouvet, 1967a), Moruzzi and Magoun identified a region in the midbrain that, when stimulated, arouses a slumbering animal and, when destructed, lead to permanent coma. This region was therefore named Reticular

Activating System (RAS) and was identified as responsible for the characteristic waking EEG pattern because of its widespread innervations to the neocortex. A few years later, Jouvet in France and Moruzzi himself in Italy reported that a brain cut between the pons and the midbrain in cats induce insomnia, indicating that sleep was generated in a lower brain area (reviewed in Gottesmann, 1988). In conclusion, these experiments revealed that the RAS in the brainstem was responsible for inducing and maintaining the wake state and that downstream nuclei control for the Non-REM and REM occurrence by modulating the RAS activity. The results of these experiments in cats are probably the first evidence for the complexity of how behavioral states are maintained and how transitions occur. During these last 60 years, many aspects have been further explored and clarified, but, at this moment, we are far from having completely understood the sleep-wake cycle.

ii. Maintaining wakefulness

As reported by Moruzzi and Magoun, the stimulation of the RAS in the midbrain induced awakenings, whereas its destruction leads to coma. More detailed experiments with use of fluorescent indicators (reviewed in Fuxe et al., 2010) revealed the presence of several nuclei in the RAS that expressed Noradrenalin, Serotonin and Acetylcholine: the Locus Coeruleus (LC), the dorsal Raphé (DR) and the Laterodorsal Tegmental – Pedunculo Pontine Nucleus (LDT/PPT), respectively (Figure 3A, page 30). Individual stimulation of each single neurotransmitter had similar consequences in inducing awakenings, causing the stereotypical EEG dynamics recorded form the scalp (reported in Jouvet, 1967b). Other nuclei have been found to contribute to the awakening process, e.g. the Tuberomamillary Nucleus (TMN, histamine), the Parabrachialis nucleus (PB, glutamate), the ventral Periaqueductal gray (vPAG, dopamine) and the Precoeruleus area (PC, glutamate). Cellular unit recordings, as well as immunocytochemistry approaches (such as c-FOS staining for identify active cells), are the basic tools used to identify the increased activity in wake-promoting nuclei in the brainstem. The RAS ascending projection, divided into two branches, innervates the thalamus, the hypothalamus and basal forebrain, contributing to spread the awakening drive throughout the cortex (Figure 3A, page 30). Projections to the thalamus stem from the cholinergic pedunculopontine (PPT) and Laterodorsal Tegmental nuclei (LDT). They innervate the intralaminar Thalamic nuclei and the thalamic reticular nucleus, which play a key role in regulating thalamic activity (Steriade et al., 1993). To confirm its wake-promoting role, stimulation of the PPT nucleus induces cortical EEG activation together with increased activity

in the γ frequency band (20 – 80 Hz) (Steriade et al., 1991), whereas muscimol injection, a GABA receptor agonist, inhibits the PPT-LDT nuclei and causes sleepiness (Lin et al., 1989). The second branch stems from LC and DR and projects to the hypothalamus and basal forebrain, where it joins the histaminergic fibers coming from the TMN as well as cholinergic afferents to the thalamus and cortex. The anatomical basis of the marked effects of the ARAS on the thalamocortical system is found in the wide divergence of axonal arborizations throughout all brain areas, as exemplified e.g. by the LC (reviewed by Benarroch, 2009; Schwarz and Luo, 2015).

Wakefulness is maintained through an excitatory drive carried out to the components of the ascending arousal system from a specific neuronal population of the LH, identified in 1998 by two research groups as Orexin-A and B, because of their food intake-promoting action (Sakurai et al., 1998), or Hypocretin positive neurons, because of their mRNA sequence close to secretin (de Lecea et al., 1998) (Figure 3, page 30). Shortly after, Lin and colleagues reported the direct link between the sleep disorder canine narcolepsy and a mutation in the hypocretin/orexin receptor 2 gene (Lin et al., 1999) Orexins receptors were found in the LC, TMN, in the midbrain Raphé and in the mesopontine reticular formation (Marcus et al., 2001; Trivedi et al., 1998). Orexin injection in the preoptic area near the VLPO promotes wakefulness and decreases non-REM and REM sleep time. As VLPO neurons do not express orexin receptors (Methippara et al., 2000), this mechanism could be due to presynaptic action onto monoaminergic axon terminals. Orexin therefore helps maintaining wakefulness by sending excitatory inputs to the ascending arousal system and by inhibiting the nuclei in the preoptic area responsible for inducing sleep. Orexin plays therefore an important role in maintaining wakefulness, in fact orexin-deficient mice show symptoms close to human Narcolepsy, with sudden transitions to REM sleep-like state together with total loss of muscle tone (Chemelli et al., 1999). Human Narcolepsy has been shown be associated with the absence of orexin in the hypothalamus and spinal fluid (Nishino et al., 2000; Peyron et al., 2000; Thannickal et al., 2000). The principal cause of orexin deficiency seems to be related to autoimmune attacks in genetically predisposed individuals (reviewed and discussed in Liblau et al., 2015).

Additionally, the postural muscular tone during wakefulness is maintained through descending projections from caudal pontine and medullary reticular formation nuclei onto motor neuron in the spinal cord. Together, the low voltage fast frequency of waking EEG is mediated through the increased activity of monoaminergic and cholinergic wake promoting brainstem nuclei.

iii. Falling asleep

The firing activity of PPT-LDT, LC, dorsal and medial Raphé, as well as TMN neurons has been shown to change depending on different behavioral states. As previously mentioned, it is elevated during wakefulness, decreased during non-REM sleep and almost abolished during REM sleep, except for PPT-LDT that increases its firing rate in this latter state (Steriade et al., 1990). Anterograde and retrograde tracing experiments reported the direct connection between the VLPO and components of the ascending arousal system, such as TMN (Sherin et al., 1996; Sherin et al., 1998), dorsal-medial Raphé and LC, even though with less innervation (Sherin et al., 1998; Steininger et al., 2001), and lateral hypothalamic area (Sherin et al., 1998) (Figure 3B, page 30). The majority of labelled cells in the VLPO are inhibitory expressing GABA and/or Galanine (Sherin et al., 1998). VLPO-preferred activity during sleep has been confirmed through c-FOS staining (Sherin et al., 1996) and through electrophysiological recording (Szymusiak and McGinty, 1989; Szymusiak et al., 1998), which reported a 2-fold increase in firing rate during sleep compared to wakefulness and a preference for increased firing rate during deep sleep after sleep deprivation. It is therefore likely that VLPO inhibitory activity on monoaminergic nuclei in the brainstem identifies the transition to non-REM sleep. In fact, a reduction of non-REM and REM sleep is observed after excitotoxic lesion of VLPO (Lu et al., 2000). Recent findings, however, indicate the presence of inhibitory GABAergic neurons in the LH that modulate the VLPO activity, as well as other wake-promoting nuclei. Chemogenetic activation of these cells promotes wakefulness by reducing VLPO inhibitory drive onto wake promoting nuclei. Conversely, their inhibition will no longer reduce VLPO activity and result in an increase in sleep (Venner et al., 2016). VLPO activity, together with nuclei in the LH, plays a crucial role in inducing and maintaining sleep. Since excitotoxic lesions of VLPO do not abolish sleep, other regions in the brain might be sleep promoting and, therefore, inhibit the arousal system similarly as the VLPO. Candidates are found in the Median Pre Optic area (mPOA) and basal forebrain (Modirrousta et al., 2004; Takahashi et al., 2009), whose cells have been shown to fire faster during sleep and to contain GABA as well (Suntsova et al., 2002; Gong et al., 2004). Moreover, the recently described GABAergic neurons in the LH seem to be directly linked to arousal-promoting structures as well (Venner et al., 2016). MnPO cells in the mPOA, in contrast, seem to positively reflect sleep homeostatic pressure as they also express c-fos during sleep deprivation and start to fire in advance of sleep (Gvilia et al., 2006). Finally, MnPO targets the VLPO (Chou et al., 2002; Uschakov et al., 2007) probably acting as a trigger, the lateral hypothalamic area, LC, dorsal Raphé but not the PPT-LDT nucleus (Suntsova et al., 2007; Uschakov et al., 2007). Muscimol infusion in the MnPO causes

prolonged wakefulness, whereas electrical stimulation or bicucculine (GABA-A receptor antagonist) enhances non-REM sleep (Suntsova et al., 2007).

Together, the activity of VLPO and of its upstream GABAergic inhibitory group of cells in the LH, as well as of other pre-Optic area, is crucial in controlling transitions to sleep by modulating the activity of wake-promoting brainstem nuclei.

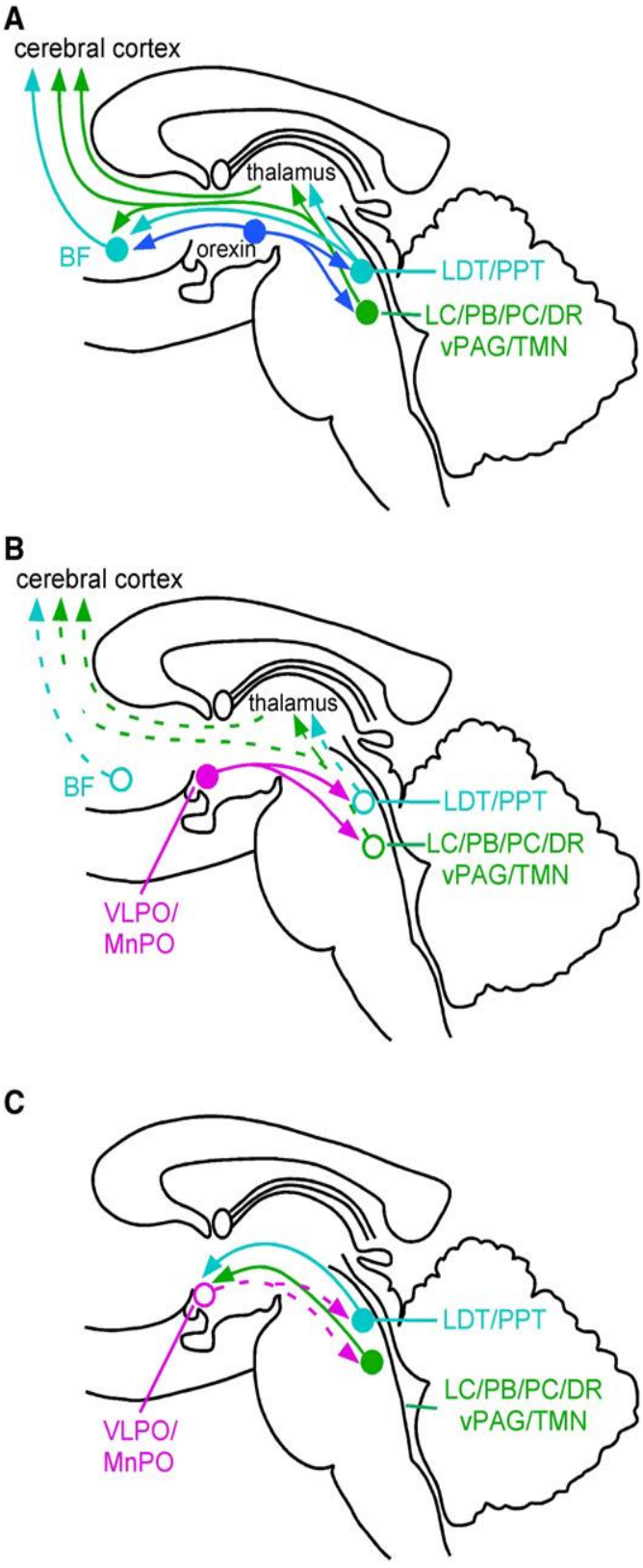


*Figure 3: Nuclei involved in the Sleep-Wake switch Adapted from Saper et al., 2010*

(A) Brainstem nuclei constitute the RAS and, together with hypothalamic nuclei and basal forebrain, control wakefulness. Cholinergic (Laterodorsal Tegmental and Pedunculo Pontine nuclei, light blue) and monoaminergic (Locus Coeruleus, Dorsal Raphe, ventral PeriAqueductalGray and tegmental nucleus) and glutamatergic (nucleus Parabrachialis, nucleus Precoeruleus fibers (green) innervate the thalamus, the basal forebrain and the cerebral cortex through two mayor pathways. Orexinergic fibers (dark blue) modulate the activity of wake promoting nuclei.
(B) Anterior hypothalamic nuclei (VentroLateral PreOptic area and Median PreOptic area, magenta) mediate sleep through inhibition onto the RAS nuclei. Reduced wake promoting action is shown with open circles and dotted arrows.
(C) The mutual inhibition between sleep promoting and wake promoting nuclei constitute the “Flip-Flop” model.

iv. The "Flip-Flop" model

Sleep and wakefulness are tightly intermingled during the subjective night of both mice and humans. During predomination of one state, for example wakefulness, the nuclei in the brainstem fire more rapidly, whereas the nuclei in the anterior hypothalamic area have a decreased firing rate. Conversely, during non-REM sleep the activity of anterior hypothalamic area is increased at the expense of a decreased activity in the wake-promoting brainstem. What is the mechanism that controls this bidirectional switch? The decreased firing rate in the VLPO during wakefulness is caused by inhibitory inputs from noradrenergic LC terminals, serotoninergic fibers belonging to median and dorsal Raphé as well as histaminergic afferences from the TMN (Chou et al., 2002). A newly discovered inhibitory connection between GABAergic LH cells and VLPO further contributes to modulate the VLPO activity (Venner et al., 2016). Noradrenaline and serotonin inhibit directly VLPO neurons, whereas histaminergic inhibition from the TMN is mediated through GABA and Galanin co-expression (Airaksinen et al., 1992; Kukko-Lukjanov and Panula, 2003) (Figure 3C, page 30). Nuclei in the PreOptic area (VLPO/MnPO) and nuclei in the RAS are therefore mutually inhibited, such that during wakefulness monoaminergic neurons in the brainstem inhibit VLPO/MnPO neurons and decrease their firing rate, whereas during non-REM sleep VLPO/MnPO neurons fire more rapidly and inhibit wake promoting nuclei in the arousal system. These, in turn, decrease their inhibitory drive onto VLPO neuron resulting in disinhibition and reinforcement. This mutual inhibition constitutes the "flip-flop" model, where the balance between monoaminergic excitatory activity and GABAergic inhibition is flipped generating the state transition. This mechanism works in both ways and stabilizes each behavioral state preventing the intrusion of intermediate stages that are potentially dangerous. In fact, a sufficient amount of either excitatory or inhibitory drive is needed to flip the balance, meaning that small physiological fluctuations in firing rate do not result in state change and behavioral state fragmentation. Without a proper flop-flop mechanism, non-REM sleep can intrude wakefulness and vice versa, resulting into quick and frequent appearances of drowsiness periods, which are biologically not suitable. Excluding any pathological condition, the gradual and slow modulation of homeostatic and circadian mechanism affects this balance and is translated into fast transitions between behavioral states. As soon as one actor is partially lost, the balance is shifted towards one or the other end and a homeostatic overcompensation occurs. For example, a lesion in the VLPO has been shown to reduce sleep time, causing an increase in sleep drive. The balance point is consequently shifted such that less "force" is needed to switch the firing

pattern and transitions towards sleep are more frequent, resulting in a higher sleep fragmentation (discussed in Saper et al., 2001).

The "flip-flop" mechanism, however, is not restricted to this mutual inhibition between wake-promoting brainstem nuclei and sleep promoting anterior hypothalamic nuclei. Both actors are modulated by cells in the hypothalamus, orexinergic neurons maintain wakefulness by simultaneously activating wake promoting nuclei and inhibiting sleep promoting nuclei, whereas GABAergic cells reduce VLPO activity to promote wakefulness.

Another evidence that support the flip-flop mechanism is the modulation in firing activity starting before the actual transition. This indicates that the balance is stressed until a critical point, which results in a state transition, is reached. As shown in Figure 4, which summarizes the results of many landmark studies, in a transition from non-REM sleep to wakefulness, the activity in the preoptic area starts decreasing some hundreds of millisecond before the actual transition, and the firing activity in the basal forebrain increased in the same time scales. Interestingly, activity in the LC starts to increase 2 seconds before and reaches a stable value one second before the transition.

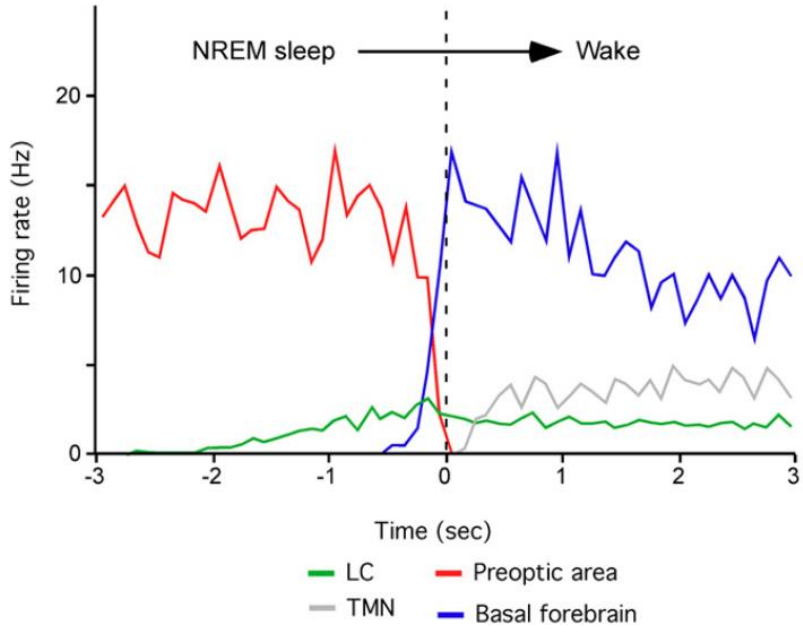


*Figure 4: Firing activity of nuclei involved in the sleep/wake cycle during a transition between non-REM sleep and Wakefulness. Adapted from Saper et al., 2010.*

During a representative switch between non-REM sleep and wake, the firing activity of the main actors that control the behavioral state change anticipate the actual transition as detected through visual scoring. LC starts to increase its firing rate seconds before whereas the basal forebrain a few hundreds of milliseconds before the transition. The inhibitory drive provided by the preoptic area, necessary to maintain non-REM sleep, decreases before the transition as well.

v. Sensory gating and wake up by external stimuli

Sensory gating during sleep is crucial to provide and maintain the right balance between sensory disconnection and integration. Out of the large body of work indicating that sleep is accompanied by reduced sensory perception, I summarize hereafter a selection of publications that report how sensory inputs are gated during sleep and which factor might influence the arousability. As hypothesized by Francis Crick in 1984 saying that "*If the thalamus is the gateway to the cortex, the reticular complex might be described as the guardian of the gateway.*" (Crick, 1984), the nucleus Reticularis Thalami might modulate the sensory flow from the thalamus to the cortex through its inhibitory drive onto thalamic nuclei. Supporting this idea, sleep spindles, oscillatory events arising from the thalamo-cortical network, have been shown to be involved in sensory gating, as, for example, the human cortical response to tones presented during a sleep spindle event suggests the recruitment of inhibitory components (Schabus et al., 2012) that might promote the sensory disconnection. In fact, spindle-rich nights, as well as an increased presence of oscillations close to the sigma frequency band, correlates with an increased arousal threshold (Dang-Vu et al., 2010, McKinney et al., 2011). Additionally, sustaining sleep spindles through genetic approaches results in an increased arousal threshold (Wimmer et al., 2012). Another evidence for decreased sensory perception during sleep has been attributed to the phase of cortical slow oscillations (<1Hz, as reported by Steriade et al., 1993). Cortico-thalamic cells show a decreased firing rate in response to stimuli presented during the silent state of slow oscillations compared to active states, thus supporting the idea that sensory gating is modulated instantaneously and strongly depends on the momentary oscillatory components detected through the EEG (Massimini et al., 2003, Rosanova and Timofeev, 2005).

All transitions presented in the previous chapter are considered spontaneous, that is, without any external trigger. Induced transitions, however, are more likely to present differences in firing activity dynamics as the system is immediately perturbed from the outside. Awakenings can be induced by almost every sensory modality, using sound, touch (Vibrotactile (Kato et al., 2004), nociceptive (Drewes et al., 1997) and thermal (Lavigne et al., 2000)), vision (Shang et al., 2008) and taste stimuli (Stuck et al., 2016). Smell, however, does not increase the arousal frequency during non-REM sleep (Stuck et al., 2007; Stuck, 2010). Hereafter I will focalize on the acoustic stimulation as a tool to drive induced awakenings as it is most frequently used and offers the least invasive approach to study stimulus-related awakenings. Whatever sound, before reaching the auditory cortex, travels through numerous synapses in the brainstem and thalamus. The Inferior Colliculus (IC), located in the midbrain,

belongs to the auditory pathway that relies the tympanum to the auditory cortex. It is thought to play a key role in frequency, duration and intensity discrimination of sounds (Caird et al., 1991; Yan et al., 2005; Malmierca et al., 2003; Malmierca et al., 2005; Shackleton et al., 2005). Moreover, it has been shown to be involved in defensive responses, such as fear and freezing, with increased arousal (Macedo et al., 2005). IC spontaneous activity during SWS is largely comparable to wakefulness, whereas it is increased during REM sleep and noise-elicited spikes do not differ between wakefulness and SWS (Torterolo et al., 2002). IC activity seems therefore not to be modulated by transitions between wakefulness and non-REM sleep. Interestingly, electrical stimulation of the IC in urethane anesthetized guinea pigs elicits comparable cortical responses similar to the ones induced by noise during wakefulness (Cabrera et al., 2013). Biological and non-biological relevant stimuli seem to follow different paths. It has been recently proposed that biologically significant auditory stimuli travel from the cochlear nucleus to the IC and from here they might induce cortical EEG activation through the basal forebrain, whereas non-biological relevant stimuli travel directly from the cochlear nuclei to the reticular formation (Cabrera et al., 2013), hence the awakening induced by non-familiar sounds. Electrical stimulation of an upstream nucleus of the IC, the medial geniculate body, induces cortical EEG activation in the auditory cortex only (Starzl and Magoun, 1951). The DR appear to be involved in the auditory induced awakenings, due to its strategic position between the IC and the basal forebrain (Dringenberg et al., 2006), emphasizing the critical role of the IC in relying information from the auditory pathway to the behavioral state control nuclei. In fact, the IC receives robust serotoninergic innervations (Klepper and Herbert, 1991; Hurley et al., 2002; Hurley and Pollak, 2001; Hurley and Pollak, 2005, for more information see Hall et al., 2010). Besides serotoninergic inputs, it has been shown through retrograde tracing that IC cells receive also cholinergic inputs from both ipsi- and contralateral PPT-LDT nuclei (Motts and Schofield, 2009), confirming the observations that Acetylcholine levels affect IC cell activity during noise exposure (Watanabe and Simada, 1973; Farley et al., 1983; Habbicht and Vater, 1996). Importantly, other mechanisms have been recently proposed to mediate behavioral responses, such as the multisensory neurons in the nucleus gigantocellularis that bidirectionally project to spinal cord neurons and to the brainstem-thalamic nuclei that mediate arousal (Pfaff et al., 2012).

This high intrinsic connectivity between nuclei of the auditory pathway and the nuclei involved in the sleep-wake cycle indicate a possible and plausible pathway originating in the brainstem and midbrain that could control the behavioral response to noise exposure (i.e. awakenings) without the cortical integration.

# 4. Infra-slow oscillations in the brain

The criteria used for scoring sleep in vigilance states take into account, in the case of polysomnography, oscillatory behaviors that occur from less than one event to hundreds of events per second. These oscillations are often grouped into frequency bands with relatively defined borders and are also associated with specific characteristics of the vigilance state. For example, as a big picture, α activity (8 – 12 Hz) in humans is predominant during the closed-eye quiet wakefulness state, during mental calculation or meditation, the faster γ activity dominates active wakefulness, and sleep spindles mostly populate stage 2 non-REM sleep. For a long time neglected, frequencies below the established frequency bands are gaining again interest in the last years. Evidence for very slow oscillations (also called infra-slow oscillations, < 0.1 Hz) in the brain was generated and described already in 1957 (Aladjalova, 1957). Importantly, it is germane to specify here that infra-slow is a general term identifying the temporal occurrence of phenomena, independently of their nature. Therefore, it is used to describe a variety of biological phenomena occurring at different levels, such as periodic variation in membrane potential, firing rate, field potentials, or even in neurovascular coupling.

This chapter reports the major descriptions of infra-slow oscillations in brain activity, with a particular interest in their potential behavioral correlate as indicators of periods of sleep continuity and fragility.

## i. The challenge of measuring infra-slow oscillations in the brain

Infra-slow oscillations recorded through conventional AC-based devices were often neglected because easily mistaken for recording artifacts. In fact, the saturation of the amplifier dynamic range at low frequencies (usually < 0.5 Hz) or slow voltage drifts due to changes in skin conductance or sweating (S. Fulda, personal communication) is the reason why conventional EEG recordings are equipped with a low cut filter (high-pass) that provides a stable recording (Vanhatalo et al., 2005). Therefore, as previously said, all brain activities occurring at frequencies lower than the built-in filter were overlooked, neglected, and sometimes misinterpreted, for a long period of time. This problem is solved with the use of Direct Current EEG/LFP recordings (DC-EEG/LFP), that allows for a reliable detection of infra-slow oscillations and which is now proposed as the standard technique in clinical research. DC-EEG recording devices make use of non-polarizable metal electrodes, such as gold or steel, because they avoid the capacitive coupling to the

external environment and, therefore, accumulation of charge that slowly drifts the signal (for review see Vanhatalo et al., 2005). For the sake of clarity, I will use the term Full-Band (fb, e.g. fbEEG) for referring to recordings where no low/high pass filters were applied.

ii. Infra-slow oscillations: from cellular activity to network synchronizations

Slow drifts in membrane potential were described in thalamocortical cells of cat and rat brain slices (Leresche et al., 1991). In a steady condition, these cells alternate between depolarization and subsequent hyperpolarization periods with a frequency of ~1 Hz. Additionally, a subset of neurons in the cat dorsal Lateral Geniculate Nucleus (dLGN) reported spindle-like depolarizations, intermingled with variant hyperpolarizing periods of 5 – 25 s, resulting in an infra-slow oscillation of ~0.1 Hz (Leresche et al., 1991). Intracellular recording of corticothalamic cells in anesthetized cats (Steriade et al., 1993) confirmed the presence of a slow oscillatory component *in vivo* (0.3 – 0.4 Hz). Bursts of action potentials are generated during the transient depolarization periods, which are sequentially alternated with silent hyperpolarization time-windows. Simultaneous recordings with cortical EEG electrodes identified the close relationship between cellular slow rhythmicity and slow oscillatory components of the EEG trace, opening the doors to the investigation of the coalescence between slow oscillations and faster rhythms. Studies in the ferret brain slices, oriented such that the connection between dLGN, reticular thalamic nucleus and visual cortical areas is maintained, further investigated the spindle-generating mechanism, which initiate through inhibitory potentials and spontaneously terminate in association with a transient depolarization that marks the refractory period (Bal and McCormick, 1996). During the refractory period, the threshold needed to generate an additional spindle wave is considerably higher (Kim et al., 1995) and it was not until this depolarization decayed over tens of seconds that the next spontaneous spindle wave was generated (Bal and McCormick, 1996). Lüthi and McCormick later showed that this depolarization was due to a persistent enhancement of a cationic hyperpolarization-activated cation current (Ih) through activation of a calcium-sensitive adenylyl cyclase (Lüthi and McCormick, 1998, 1999). Thalamocortical neurons possess thus intrinsic mechanisms of refractoriness that fall within the infra-slow range.

Sleep spindles arise from the thalamo-cortical network and play a crucial role in gating sensory information during sleep (reviewed in Lüthi, 2014), for example a high spindle rate during sleep corresponds to a higher probability of sleep stability in the face

of noises compared to low spindle rate during sleep (Dang-Vu et al., 2010), cortical activation is reduced when auditory stimuli are presented during a sleep spindle compared to a spindle free moment (Dang-Vu et al., 2011; Schabus et al., 2012), or the acoustic arousal threshold is increased in genetically modified mice, in which the sigma power is increased in non-REM sleep prior to transitions (Wimmer et al., 2012). Given this important feature, the temporal organization of sleep spindles is of crucial interest to investigate the balance between sleep fragility and continuity.

Infra-slow patterns have been found not only in LGN neurons *in vivo* and *in vitro* in anesthetized cat, but also during wakefulness in freely moving awake and anesthetized rats (Albrecht et al., 1998). Also, infra-slow firing activities have been found in other brain nuclei than the LGN and under different recording conditions, for example in basal ganglia (SubThalamic Nuclei and Globus Pallidus) of anesthetized rats (Allers et al., 2002), in LC and DR in freely-moving rats (Filippov et al., 2004), and also in a subset of neurons in primary visual cortex of freely-moving rats (Hengen et al., 2016).

Furthermore, there is evidence for physiopathological events, such as interictal epileptiform events or cyclic paroxysm generation, to occur at low periodicity and in phase with infra-slow oscillations (Vanhatalo et al., 2004) or to be coupled with infra-slow thalamic firing (Steriade and Contreras, 1995). Similar findings have been also shown in humans where subcortical nuclei are recorded from Parkinson and epilepsy patients during sleep, drowsiness and awakenings (Moiseeva and Aleksanian, 1986).

Infra-slow oscillations in cellular activity are, therefore, present in physiological and pathological conditions, in different species and in both cortical area and subcortical nuclei.

Infra-slow changes in steady membrane potential have direct measurable correlates in the EEG trace. Achermann and Bórbely analyzed the temporal power dynamics of frequency bands, such as the SWA and the Spindle Frequency Activity (SFA), in sleeping humans (Achermann and Borbely, 1997) seeking for indication of infra-slow periodicities as was previously reported (Leresche et al., 1991; Steriade et al., 1993). Achermann and Borbely obtained comparable results to the observations made by Leresche, and then by Steriade, using a completely different approach, thus providing with useful insights on the ongoing infra-slow activity without the use of intracellular, juxtacellular or fbEEG recordings (Achermann and Borbely, 1997).

fbEEG/LFP recordings report the presence of infra-slow oscillations in different brain regions in humans (Vanhatalo et al., 2004; Picchioni et al., 2011; Nir et al., 2008) and in rats (Filippov et al., 2004), during both wakefulness and sleep. Changes in infra-slow brain potential are found in human parietal and sensorimotor cortices (Linkenkaer-Hansen et al., 2001; Nikouline et al., 2001) and during acoustic or motor tasks (Leistner et al., 2010) using MEG recordings. Infra-slow oscillations, as well as slow oscillations (reviewed in Steriade, 2006), coalesce with faster EEG activities (> 1 Hz) (Vanhatalo et al., 2004), probing the tight cellular coupling in their generating mechanism. Together, direct sampling of network electrical and magnetic activity in the brain reveals the presence of a ubiquitous infra-slow component that orchestrates faster oscillations.

iii. Infra-slow activity in the neurovascular coupling

Biswal and colleagues in 1995 reported for the first time infra-slow oscillations in the blood oxygenation level dependent (BOLD) contrast imaging. More specifically they show that, in the resting human brain, the time course of low frequencies in regions activated by hand movement are temporally correlated and represent functional connectivity (Biswal et al., 1995). Further analysis on BOLD signals in human patients revealed the presence of resting state networks (RSNs, representing functionally interconnected areas in the brain that are simultaneously active) following an infra-slow activation pattern (Greicius et al., 2003; Raichle et al., 2001; Shulman et al., 1997; see Lee et al., 2013 for more details). Importantly, RSNs are conserved across subjects (Damoiseaux et al., 2006; De Luca et al., 2006 and Mantini et al., 2007). The Default Mode Network (DMN) is a particular RSN, identified through a set of interacting brain regions shown to be active when the subject is at wakeful rest and is not performing any task, but also during sleep (Raichle et al., 2001; Horovitz et al., 2008; Horovitz et al., 2009; Larson-Prior et al., 2009). Importantly, the DMN has been shown to oscillate at an infra-slow timescale in both healthy and schizophrenia subjects (Mingoia et al., 2012). Therefore, areas in the brain that belong to the same network, typical of wakeful rest and sleep, report an infra-slow oscillation in their neurovascular coupling. RNSs have been also found through analysis of fbEEG (Hiltunen et al., 2014 and references therein), therefore BOLD signals that identify RSNs are likely to arise from neuronal activation, rather than pure changes in blood flow. This suggests that the intrinsic brain connectivity remains unaltered during sleep compared to wakefulness, even though the EEG traces displays considerable differences. Furthermore, delimited independent regions in the brain have also been shown to be active

following an infra-slow time (for review see Palva and Palva, 2012 and references therein). Importantly, infra-slow fluctuations in hemodynamic sources are not limited to humans but are found also in Monkeys (Vincent et al., 2007; Logothetis et al., 2001), rats (Lu et al., 2012) and mice (Mechling et al., 2014), with equivalent properties.

Similar to infra-slow frequency components in fbEEG, BOLD infra-slow fluctuations have also been shown to be coupled to faster cortical activity in anesthetized rats (Pan et al., 2010, 2011; Pan et al., 2013) and monkeys (Magri et al., 2012) during spontaneous activity. These results have been achieved through parallel recording of scalp EEG and fMRI BOLD signals. Moreover, BOLD infra-slow fluctuations are also shown to be entrained by evoked responses (Goense and Logothetis, 2008; Logothetis et al., 2001; Huttunen et al., 2008).

Even though BOLD signals indirectly sample neuronal activations, evidence for neuronal-induced infra-slow brain potentials has been confirmed through voltage sensitive dye recording in awake and anesthetized mice (Chan et al., 2015). Moreover, increased BOLD fluctuations also positively correlate with neuronal plasticity (Canals et al., 2008), further corroborating its link to neuronal activity.

Together, the presence of infra-slow rhythmicity in single cell, nuclei or isolated networks, suggests that behavioral state control and maintenance during wakefulness and sleep not only occurs at momentary levels but might also depend on the phase of the ongoing infra-slow oscillations in the brain.

### iv. Potential roles of the infra-slow oscillation

Although being extensively studied in the last years, the roles of infra-slow oscillations in the brain remain unclear. It has been proposed to coordinate and organize the long-range cortico-cortical network (Buzsáki, 2006) organizing therefore the processes beyond consolidation of episodic memory (Picchioni et al., 2011). Moreover, it has been shown that sensory perception *per se* fluctuates in an infra-slow range, the successful detection of a threshold tactile stimulus in humans occurs in patches, where their macroscopic temporal distribution reveals an infra-slow oscillation in sensory perception (Monto et al., 2008).

Interestingly, astrocytic calcium dynamics has also been found to oscillate at infra-slow frequencies in cortex of anesthetized rats (Kuga et al., 2011) and in thalamic astrocytes of rat brain slices (Hughes et al., 2011). The potential role of astrocyte in memory formation and consolidation is gaining interest (De Pitta et al., 2016) This further

expand the pivotal importance of infra-slow oscillations in mechanisms controlling switches between behavioral states.

The slow oscillation itself has been proposed to organize the alternation of periods promoting memory consolidation with more fragile temporal windows. Faster rhythms, such as sleep spindles and hippocampal ripples, are nested within the depolarizing phase of the slow oscillation (reviewed in Rasch and Born, 2013). Entrainment of slow oscillations by auditory stimuli phase-locked to the depolarizing phase enhances the consolidation of declarative memory in humans, whereas out of phase stimuli remained ineffective (Ngo et al., 2013).

Infra-slow oscillations have been found in the cortex and in subcortical nuclei in several species during different behavioral states. They are correlated with attention, perception and memory consolidation suggesting for a primordial basal feature of the brain. This prompts to an evolutionary conserved phenomenon common to mammals and reptiles (Shein-Idelson et al., 2016) and that might be represent a basic time scale over which levels of arousals fluctuate on top of the major vigilance states.

## 5. Aim of the thesis

As for many diseases in our body, in order to re-establish the correct functionality of sleep in people suffering from sleep disorders we need to find the cause of its malfunction rather than aiming at reducing their symptoms. Disturbances in the mechanisms that regulate the daily timing of sleep, as well as the transitions between the vigilance states, have direct consequences on the general sleep health. Episodic disruptions of sleep homeostasis have mild effects, which we surely already experienced once in our life. However, when sleep disruption becomes chronic, it entrains a series of knock-on effects that have to be taken seriously because potentially threatening for our health. Most of the actors implied in transitions between behavioral states have been identified and we start to have a complete picture of their function. Important advances have been made with the introduction of techniques, such as optogenetics and chemogenetics, which allow precise stimulation or inhibition of these nuclei involved in the sleep-wake cycle, in terms of time latency and area of interest. State transitions can be therefore externally triggered, depicting the crucial role of these nuclei. However, a much finer regulatory process is thought to be implicated throughout the sleep, as it is evident from the presence of infra-slow oscillations identified in both neuronal and neurovascular networks. This is likely to represent the balance between two fundamental needs of sleep: its ability to be restorative, promoting continuity and memory consolidation, as well as to be sufficiently fragile, to identify potential threats in the close environment.

The aim of this thesis is to identify correlates of the balance between sleep continuity and fragility. We first established a valid measure that consistently reported the presence of this intrinsic variability. If this marker identifies periods of continuity and fragility, it should be differentially present in each of these two periods. Therefore, we investigated whether this marker successfully reports on differences in the sensory perception during sleep in mice. More specifically we exposed sleeping mice to a threshold level auditory stimulus that induce an equal amount of successful and unsuccessful arousals, termed sleeps-through. Finally, we aimed at identifying parallel measures that conjointly classify a sleep period as protective or fragile, these are the hippocampal ripple power, marker of offline memory processing, and heart rate, whose variability indicates variations in the sympathetic/parasympathetic balance.

In study II and III we genetically manipulated the nRT and the sensory thalamus, two nuclei implicated in the thalamo-cortical network that generates sleep spindles. The

nRT, in particular, plays an important role in gating sensory information during sleep. We aimed at further investigate their role in the sleep spindle generation by selectively delete genes that code for membrane channels and receptor, validating the effects in behavioral models.

In summary, this thesis provides with an identification of a marker that reports the balance between sleep fragility and continuity in both humans and mice. Since these two species share common features of sleep, such as the spectral components of vigilance states, but at the same time show striking differences in its timing and duration, we hypothesize the presence of a common evolutionary aspect that mediates a fundamental need of sleep. Furthermore, the identification of this actor opens the door to potential clinical intervention aiming at re-establishing the correct balance between sleep fragility and continuity.

# D. RESULTS

Study I:

**Coordinated infra-slow neural and cardiac oscillations mark fragility and offline periods in mammalian sleep**

Sandro Lecci, Laura M. J. Fernandez,* Frederik D. Weber,* Romain Cardis, Jean-Yves Chatton, Jan Born, Anita Lüthi

Sci Adv. 2017 Feb 8;3(2):e1602026.

During sleep we fall into a state of relative disconnection from the outside world, where we take advantage of the reduced sensory stimulations to rest, so that important beneficial functions, such as memory consolidation and metabolite clearance, can take over. At the same time, we need to keep a certain level of "background" attention, required to sample and scan the close environment seeking for salient stimuli. Keeping these two fundamental aspects in balance is essential to maintain our sleep health, any imbalance between them has detrimental effects. Despite its apparent uniformity, sleep is a highly heterogeneous state, whose complexity can be ascertained by its polysomnographic analysis in both rodents and humans. The aim of this study was to identify potential neuronal markers of non-REM sleep in the two species, which might rely, through their intrinsic variability, on the variant arousability level.

We investigated the temporal dynamics of the power level of frequency bands characteristic of non-REM sleep, SWA and sigma power, in both mice and humans. Sigma power shows the presence of an infra-slow oscillatory component, which is substantially reduced in adjacent frequency bands, in mice non-REM sleep and in human stage 2 non-REM sleep. Restricting the analysis to the individual fast spindle peak in humans also revealed the presence of the infra-slow oscillation, suggesting for a fundamental role of sleep spindles in its generating mechanism. To test whether the identified oscillation in sigma power mediates the alternation between periods of sleep continuity and fragility, we exposed mice sleeping in freely-moving conditions to threshold-level non-biologically relevant stimuli (white noise, 20 s long, 90 dB SPL). Mice woke up when the noise was played in the descending phase of sigma power, whereas they slept through it when played in the rising phase, thus subdividing sleep into 2 alternating periods of 20 – 25 s. We further show that sleep continuity periods are also marked by an increased presence of hippocampal ripple activity, indicating offline memory processing, and reduced sympathetic drive, as detected through heart rate monitoring.

Conversely, sleep fragility periods coincide with reduced hippocampal ripple activity and correlates with signs of increased sympathetic drive. Furthermore, in humans, subjects displaying a stronger infra-slow oscillation peak in the fast spindle frequency temporal dynamics, also performed better in a declarative memory task.

Together, we identify a previously undescribed oscillation, the 0.02 Hz oscillation in sigma power, that, together with markers of sympatovagal activity and memory processing, divides mice and humans non-REM sleep into periods of sleep continuity and fragility.

This publication represents the body of work of my doctoral thesis, I conceived most of the experimental approaches, developed and analyzed the majority of data, as well as substantially contributed in the coordination between the collaborators in different universities. I performed most of the EEG surgeries in mice, or trained a collaborator to do them, as well as performing the entire noise exposure experiment. I developed most of the analysis scripts needed to quantify and further analyze the infra-slow oscillation in mice.

Study II:

**Suppression of Sleep Spindle Rhythmogenesis in Mice with Deletion of $Ca_V3.2$ and $Ca_V3.3$ T-type $Ca^{(2+)}$ Channels**

Pellegrini Chiara, Lecci Sandro, Lüthi Anita, Astori Simone.
SLEEP 2016;39(4):875–885

Low-threshold discharges, essential for generating sleep rhythms, are enabled by low voltage-gated T-type $Ca^{2+}$ channels (T-Channels). Two isoforms, $Ca_V3.2$ and $Ca_V3.3$ (encoded by the genes *CACNA1h* and *CACNA1i*, respectively), are present in neurons of the *nucleus Reticularis thalami* (nRT), a shell of GABAergic interneurons that modulate the information flow in the thalamocortical system and plays a key role in the generation of sleep spindles. The contribution of T-channels to single cell burst discharge has been extensively studied. However, their coordinated role in network rhythmic activity requires elucidations.

We took advantage of the availability of genetically modified animals, lacking both genes *CACNA1h* and *CACNA1i* (hereafter identified as $Ca_V3$.DKO), to study their individual and conjoint role in nRt rhythmogenesis and the consequences to sleep behavior. The cellular, network and behavioral consequences of genetic deletion of $Ca_V3.3$ were previously described. Here, we report that nRt cells of mice lacking the $Ca_V3.2$ ($Ca_V3.2$KO) channel only maintain their cellular properties, whereas the double deletion fully abolished the nRt low-threshold spiking. Consequently, the EEG power spectrum of non-REM sleep in freely-behaving $Ca_V3.2$KO animals was undistinguishable from wild-type mice, whereas $Ca_V3$.DKO animals show a suppressed sigma power in advance of an increased delta frequency range. Moreover, although sleeping more time, the average non-REM bout duration in $Ca_V3$.DKO animals was substantially shorter. Therefore, the genetic-induced silencing in nRt busting activity affects *in primis* the sleep spindle generation, which has then consequences in sleep architecture, as well as in the slow waves rhythmogenesis.

The results of this study lay the foundations to further investigations about the critical role of an intact thalamocortical oscillatory network in the generation of infra-slow oscillations in sigma power.

My interest in computer science pushed me to develop my own standalone software, based on the Matlab engine, to perform standardized sleep analysis. Therefore, I coded a user-friendly program for whoever acquires data using our specific recording system, provided the recordings are of 12 h. The big amount of data to be analyzed indeed required a bioinformatic support, which is how I contributed to this article. The use of this software considerably

reduced the time needed to analyze the data, both by the user, who can easily group the all animals and perform the analysis of interest, and by the machine, exploiting the multi-core architecture of the processor. The output log file contains, as far as possible, all analysis and referenced values relative to standardized statistical tests.

Far from being fully optimized for a (non-)commercial distribution, this software is currently undergoing serious renovations to match the newly adopted recording techniques in the research group.

Study III:

**Phasic, nonsynaptic GABA-A receptor-mediated inhibition entrains thalamocortical oscillations**

Zita Rovó,* Ferenc Mátyás,* Péter Barthó, Andrea Slézia, Sandro Lecci, Chiara Pellegrini, Simone Astori, Csaba Dávid, Balázs Hangya, Anita Lüthi, and László Acsády.

J Neurosci. 2014 May 21; 34(21): 7137–7147.

GABAergic cells play a fundamental role in pacing rhythmic activity in different brain structures through their action on post-synaptic GABA-A receptors. These are located synaptically or extrasynaptically depending on their pentameric subunit assembly. Synaptic GABA-A receptors express the γ subunit, which is replaced by the δ subunit in its extrasynaptic isoform. Synaptic GABA-A receptors mediate phasic and fast inhibition, whereas extrasynaptic receptor mediate tonic and slow inhibition. This study aims at validating previous findings performed *in vitro* reporting the potential role of extrasynaptic GABA-A receptor recruited during nRt-mediated phasic inhibitory post synaptic currents. More specifically, through focal viral injections, synaptic GABA-A receptors were made unfunctional in restricted somatosensory thalamus, leaving the inhibitory drive from nRt cells to be excerted merely by extrasynaptic GABA-A receptors.

We report successful deletion of γ2 subunit in synaptic GABA-A receptor within the injection site, through both anatomical and electrophysiological investigations. Virally-infected TC cells do not show evoked inhibitory post-synaptic currents (eIPSCs) upon single or 10 Hz stimulation, indicating the unique recruitment of non-functional synaptic GABA-A receptors. Surprisingly, nRt stimulations evoked burst IPSCs in virally infected TC cells. This has been attributed to recruitment of extrasynaptic GABA-A in a phasic instead of a tonic manner. The phasic, extrasynaptic inhibition only was sufficient to promote rebound bursting in thalamocortical, as showed by juxtacellular recording in in two somatosensory nuclei in anesthetized mice. Despite the removal of phasic synaptic inhibition, the bursting mechanism of sleep spindles generation was preserved and most of the spindle oscillatory characteristics were maintained, with the exception of the decrease in intra-spindle frequency. Further analysis in freely moving animals, supported these results showing no difference in the sigma power (7-15 Hz) during periods of exits from non-REM sleep.

Here, I performed EEG surgeries, recordings and analysis in mice who were previously injected with either the virus expressing the Cre enzyme, to focally remove the subunit γ2 of

synaptic GABA-A receptors, or with a virus expressing the Green Fluorescent Protein. This experiment was crucial because it allowed to confirm in naturally sleeping freely-moving mice what has been found *in vitro* and in mice under anesthesia. Importantly, it brought onto the behavioral level the genetic manipulations made in a restricted brain region.

This high-resolution manipulation provides with useful application in the sleep pharmacology. In fact, synaptic GABA-A receptors are the target of many sedative-/hypnotic drugs, such as Zolpidem, who binds to the benziodiazepine binding site located between the γ and the α subunits. Focal removal of synaptic GABA-A receptor modifies the injection zone into a zolpidem-insensitive region. This allows to i) Study the role of extrasynaptic GABA-A receptor in generating sleep oscillations and, therefore, provides with potential target for future treatments of sleep desorders, and to ii) Study the effects of Zolpidem administration in the generation of infra-slow rhythmicities by sequentially targeting different brain regions. Zolpidem administration in mice transiently reduce the measured power in fast frequencies, that is, also sigma power. It is therefore likely that the hypnotic effect of Zolpidem is mediated through modulation of GABA-A receptors within the spindle generating network.

# E. DISCUSSION

Sleep serves opposing needs. It has to provide continuity for the restorative aspects to occur, such as memory consolidation, fatigue extinction or metabolite clearance, as well as to provide a certain degree of fragility to escape from potential threats. A good balance between these two aspects is generally unperceived but, as soon as our sleep tends towards one of the two ends, our general well-being is affected. To date, how these two needs are kept in balance remains unknown.

Sleep problems affect a large population and to simply sleep better is a common shared request. Insomnia is among the most frequent sleep disorders affecting approximately 30% in its episodic and 10% in its chronic form (Morin et al., 2006), but other sleep disorders, such as excessive daytime sleepiness, have a non-negligible occurrence as well (Lindberg et al., 1997). In general, the population is well aware of the consequences of these problems and over-the-counter drugs are available to provide with a first help (Culpepper and Wingertzahn, 2015). Sleep restriction to single nights has moderate consequences, such as the increased chance to catch a cold (Cohen et al., 2009), to get emotional (Yoo et al., 2007) or to be less focused and commit errors (Kaplan et al., 2017). However, when becomes chronic, it causes detrimental effects on the body and on mental health, for example the risks of cardiovascular accidents (Covassin and Singh, 2016), some cancer (Thompson et al., 2011; Thompson and Li, 2012) and obesity jumps (Liu et al., 2013). Besides affecting our health, chronic sleep restriction is potentially dangerous for people around us, the decreased level of attention can easily result in catastrophic accidents on working places and on the street. Investigating therefore the mechanism that keeps in balance the continuity and fragility aspects of sleep might indicate possible cause of, and therefore targets for, sleep related disturbances.

Beside the co-autorship publications, I invested the majority of my time in the project that aimed at investigating the mechanism behind the balance between sleep fragility and continuity, on which I focus the majority of this discussion. More specifically I focused my interest on identifying spectral markers that could indicate a modulation in the arousability state during non-REM sleep in rodent and the same analysis was extended to human recordings after a collaboration. Their causal relationship was tested using perturbing, non-emotional stimuli presented at the threshold level and the data were analyzed based on the different behavioral outcome, i.e. “Wake-up” and “Sleep-through”. I will cite hereafter references,

which I find most pertinent in the contextualization of my results and, wherever possible, I cite reviews that summarize and provide a complete description of the corresponding content.

## 1. Infra-slow oscillations are present in specific EEG power dynamics

To identify any indication of the balance between sleep fragility and continuity, we focused our interest on the temporal dynamics of the frequency bands that characterize non-REM sleep in mice and humans: SWA and sigma power. Therefore, long bouts of non-REM sleep were inspected in both human and mouse recordings. We report a previously undescribed oscillations of power dynamics conserved between both species. More specifically, the power value in the sigma frequency band, compared to SWA, oscillates with a period of 50 – 60 s, indicating that windows of high and low power are intermingled every 25 – 30 s. Adjacent frequency bands, such as theta and beta, show a decreased presence of the infra-slow component creating a distribution curve, in which sigma frequency band contains the highest level of an infra-slow oscillatory component.

The sigma frequency band contains sleep spindles, defined events of specific frequency and duration occurring during non-REM sleep, identified in humans and carnivores as oscillations in the ~8 – 16 Hz range (Aeschbach and Borbely, 1993; Contreras et al., 1997). In mice a more graded activity is found in the range 9 – 18 Hz (Wimmer et al., 2012). In order to compare the two species, we focused on the power value in the 10 – 15 Hz range, which contains sleep spindle events in humans and takes into account the continuous activity in this frequency band in mice. In humans, the individualized fast spindle peak correlates with sleep spindle density, therefore the fast spindle peak power dynamics were analyzed in parallel and is shown to oscillate at the similar frequency, corroborating the hypothesis that the modulation of sigma power over time may be due to different sleep spindle organization.

Infra-slow oscillations in brain activity, when reported through fbEEG recordings, refer to the low end scale of the spectrum of oscillations and have been described with a range having at least one order of magnitude (0.01 – 0.1 Hz). Because of the low-cut filtering, our recording setup was unable to detect them. However, the 0.02 Hz-oscillation that we identified results from the temporal dynamics of a specific frequency band and, as previously mentioned, does not directly depend on the use of direct-current EEG recordings. Moreover, distribution of infra-slow frequencies around the identified 0.02 Hz-peak is narrow and cannot be by a “scale-free” distribution of frequencies (He, 2014), as I also showed. Infra-slow oscillations in brain activity are coupled with faster rhythms (Vanhatalo et al., 2004), however, we report a

decreased, yet still present, infra-slow component for faster frequencies (beta and beta2 in humans). Nevertheless, evidence for the coupling between the 0.02 Hz-oscillation in different frequency bands and the infra-slow oscillation measured through fbEEG is not currently available. Simultaneous recording with fbEEG setups are needed to confirm this statement. It is important to emphasize here that infra-slow oscillations in power dynamics are not restricted to the sigma frequency band but are present in all analyzed frequency bands, even though to a weaker extent, indicating that mechanisms other than the thalamo-cortical network might be implicated in the generation of infra-slow oscillations.

When using fronto-parietal recordings, oscillatory components might result from focal activity detected by one of the two electrodes and not from a ubiquitous presence. Referential recordings in both rodents and humans show that individual cortical areas located along the fronto-parietal axis report the same infra-slow oscillation of power dynamics with parietal regions having an increased oscillatory component compared to frontal regions. The spatio-temporal spreading of infra-slow oscillations of power dynamics in the cerebral cortex has not yet been studied but will undoubtedly provide with useful indications about the origin and, possibly, their propagation direction.

Since such temporal dynamics are conserved across the analyzed species, it is likely that this phenomenon is shared by the same ancestral origin and, importantly, has to be considered in its absolute timing. We report an oscillation that is present with similar, if not equal, characteristics in species whose sleep architecture is extremely different (see Figure 1 at page 13).

Finally, our results are in contrast with recent findings concerning the temporal evolution of activity in specific frequency bands during epochs of non-REM sleep. More specifically, Watson and colleagues report a gradual increase in sigma power along the non-REM sleep episodes (Watson et al., 2016). However, their analysis is based on the average of non-REM sleep episodes having different durations and, to overcome this problem, they normalize in time bouts having different length. This results in the gradual cancellation of all dynamics present along the non-REM sleep episode with the exception of the last one, which has been shown to precede transitions to other behavioral states, such as REM sleep (Astori et al., 2011 and Rovo et al., 2014). Therefore, it is crucial to consider the intact temporal dynamics in single non-REM sleep epochs. We concluded therefore that the most suited approach for studying the infra-slow oscillations was to consider them as unitary elements whose identifying mark is their oscillatory frequency.

Together, the analysis of undisturbed sleep in both species reveal the presence of an oscillation with a supra-second periodicity (~50-60 s/cycle), where the sigma frequency band has the highest oscillatory component compared to adjacent frequency bands.

## 2. Infra-slow fluctuations in sigma power divide non-REM sleep into 2 phases

Scoring sleep *a posteriori* based on defined events, such as noise exposures in our case, allows for the identification of patterns that are directly involved in the analysis of interest. Through this approach in naturally sleeping mice, we have found a correlation between the phase of sigma power infra-slow oscillation and the behavioral outcome, suggesting its use as predictive agent. More specifically, when noise was presented during the ascending phase of sigma power infra-slow oscillation, the animals slept through it, whereas when it was presented during the descending phase, the animals woke up. The noise was chosen such that it caused an equal amount of wake-up and sleep-through, indicating that some existing parameter during sleep might flag the balance between sleep continuity and fragility. The duration and type of the noise likely play an important role, we chose a non-biologically relevant stimulus, i.e. the white noise, which persisted for 20 s, corresponding to approximately half of the infra-slow oscillation period. These characteristics are fundamental to avoid the emotional response given by the nature of the sound (Tacikowski et al., 2014; Shi, 2016), and to successfully stimulate the system during the infra-slow oscillation. It is noteworthy to remind here that all noises were presented without knowledge of the ongoing spectral components and that animals are habituated to noise exposure to remove the novelty effect of an unknown sound.

Existing knowledge in the field reports that a minimal sleep bout duration of 60 s is necessary to prevent cognitive impairment in mice performing a novel object recognition task (Rolls et al., 2011), supporting our findings of an existing alternation between sleep fragility and continuity that occurs every ~50 s that, when extensively disrupted, can lead to cognitive impairment. Moreover, associations between sleep stability and specific spectral components, in particular with the density of sleep spindles in humans, has already been proposed (Dang-Vu et al., 2010), yet without a clear temporal distribution of these protective periods.

## 3. Arguments corroborating sleep continuity

We have found a subdivision of non-REM sleep into two alternating periods of sleep continuity and fragility. Sleep continuity periods are identified by the ascending phase of sigma power infra-slow fluctuations, as noises fail to induce awakenings when presented in this period. Hypothesizing that a specific sleep segment promotes continuity, it should indicate ongoing processes in support of it. Memory consolidation has been correlated with good healthy sleep (Rasch and Born, 2013; Cellini, 2016) and can therefore be used as marker for sleep continuity. We measured hippocampal ripple activity in mice (150 – 250 Hz), which has been shown to positively correlate with learning and indicates offline memory processing (Buzsáki, 2015). Simultaneous analysis of hippocampal ripple power and sigma power reveals a positive correlation with a constant time lag, indicating specifically that an increase in ripple power precedes sigma power rises. This suggests that memory consolidation preferentially occurs when sigma power indicates a sleep continuity period. Conversely, hippocampal ripple power is low during sleep fragility periods. A potential importance for the 0.02 Hz-oscillation in memory consolidation was probed in humans by investigating the correlation between the 0.02 Hz-peak of sigma power infra-slow oscillation and the cognitive performance assessed through declarative memory tests. We report a positive correlation between the 0.02 Hz-peak and the score of memory performance, suggesting that a higher occurrence and/or strength of infra-slow oscillations in sigma power, which would be equivalent to more frequent or stronger continuity periods, positively supports memory consolidation. Together, albeit based on very different approaches, experiments in both species report a positive correlation between infra-slow oscillations in sigma power and memory consolidation or hippocampal ripple activity.

Changes in sympathovagal balance, as detected through heart rate measurements (quantified as the RR interval) have been shown to anticipate awakenings from non-REM sleep (Sforza et al., 2000; Kuo et al., 2008, see Silvani and Dampney, 2013 for an extensive review). Moreover, the analysis of RR intervals reveals the presence of slow and infra-slow oscillatory components that are differently modulated during sleep through differences in sympathetic/parasympathetic system activity as compared to wakefulness (Somers et al., 1993; Billman, 2011). Therefore, increases or decreases in instantaneous heart rate might mirror periods of fragility or continuity. We monitored autonomic activity through measurement of heart rate during sleep in both mice and humans. Increase in heart rate, which typically reflects a shift of the sympathetic/parasympathetic balance towards a greater sympathetic influence, might indicate preparation for awakening, crucial for qualifying as a fragility period. Conversely, low and stable heart rate activity might indicate continuity periods. In mice we report an anticorrelation between heart rate activity and sigma power infra-slow oscillation.

During periods of continuity, heart rate was stable and low, possibly helping in stabilizing the sleep period. Importantly, in humans the correlation between heart rate and 0.02 Hz-oscillation in sigma power is time shifted compared to mice, suggesting a different organization of cardiac coordination to brain rhythms, a subject that is discussed in the next chapter.

Together, the coincidence of factors, such as memory consolidation, hippocampal ripple power and autonomic drive seem to confirm the presence of continuity periods timed by the infra-slow oscillations in sigma power.

Importantly, besides sharing similar and comparable spectral characteristics, sleep in the two species is essentially different. While humans show more consolidated states with less transitions across behavioral states, mice have a highly fragmented sleep, resulting therefore in shorter sleeping bouts. When comparing the infra-slow oscillations in sigma power, mouse non-REM sleep is comparable to N2 stage in humans, where fast sleep spindles are more prevalent (Mölle et al., 2011). Restricting our analysis to stage N2 also reveals a higher correlation between fast spindle infra-slow peak and declarative memory. Along these lines, one might be tempted to speculate that the evolution of SWS, during which sensory disconnection is more pronounced, might be the consequence of evolution in sessile/sedentary species, in which the presence of a deeper sleeping state might not be an endangerment.

## 4. Arguments corroborating sleep fragility

Succeeding to a sleep continuity period, sleep fragility completes one infra-slow oscillation, Periods of sleep fragility are identified by the decreasing phase of the 0.02 Hz-oscillation of sigma power, as noises presented there induced awakenings in mice. As it is the case for sleep continuity periods, other parameters are also supporting the evidence of sleep fragility periods. Similarly to what described for sleep continuity periods, we show a decreased hippocampal ripple power in mice during the descending phase of sigma power. This suggests a decreased level of memory consolidation when the animal is in a state where a mild threshold stimulus is sufficient to induce an awakening. Consolidate memory during this periods would therefore not be sustainable as subjected to potential excessive sleep disruptions. This has indeed confirmed with an experiment, where cognitive performance was tested in mice, whose sleep was interrupted such that single sleep bouts were not exceeding a desired length (Rolls et al., 2011). When individual sleep bout length was reduced below 60 seconds, the animal showed an impaired cognitive performance on the next day. Therefore, it seems that sleep needs at least 60 s to assure memory consolidation. This observation supports our finding that

memory consolidation is restricted to periods of sleep continuity, as sleep bouts of less than 60 s are too short to provide with at least one continuity and one fragility period.

Sleep fragility periods are also associated with increased instantaneous heart rate, suggesting a preparatory period awakening. Heart rate has been shown to change seconds before spontaneous transitions (Silvani and Dampney, 2013). This seems to be a requirement to face the abrupt increases associated with an awakening. We show in mice that heart rate increases during periods of sleep fragility, that is, when the animal is more susceptible to external sensory stimuli. This supports the idea that, during this period, the mouse has to be potentially ready to wake up as soon as a threatening stimulus is perceived. The conjoint presence of these factors supports our finding of sleep fragility periods intermingled with sleep continuity periods in an infra-slow time scale.

In humans, however, this association is time-shifted and cannot be confirmed for several reasons: 1) We need to first establish the correlation between sleep spindles, heart rate and periods of fragility and continuity with a similar experimental approach as in mice and 2) we need to consider that cardiac control in mice occurs within different time frames as in mice, as it can be inferred by the faster heart rate.

## 5. Potential cellular mechanisms involved

In my thesis, I provided a first description of the basis aspects concerning the infra-slow oscillations in sigma power and its behavioral correlate. However, a full description of the mechanism behind this phenomenon is required as the reported results prompt for important implications in sleep medicine. Identifying the molecular actors responsible for the generation of these oscillations is crucial to propose potential pharmacological targets.

As sleep spindles contribute to the sigma frequency band (Aeschbach and Borbely, 1993; Contreras et al., 1997) and the fast spindle peak in humans presents a high infra-slow oscillatory component, they might be the primary actors involved in the generation and modulation of the 0.02 Hz-oscillation. The mechanisms of sleep spindle generation have been extensively studied and reviewed (Astori et al., 2013; Lüthi, 2014), I will provide here a short description of their cellular and molecular characteristics, necessary to contextualize the results obtained in study II and III and to relate them to the infra-slow oscillations in sigma power.

Sleep spindles are generated within the thalamo-cortical (TC) network, a loop involving the cerebral cortex, the thalamic nuclei and the nucleus Reticularis Thalami (nRT). The burst firing of TC cells, essential for the generation of sleep spindles, is entrained by the rhythmic

inhibition from the nRT cells. This results in a resonating oscillation generated within the TC and nRT cells, which is synchronized within thalamic regions by the cortical afferents. To sustain the burst discharge, a specialized group of ion channels, receptors and intra-cellular mechanism is present in nRT neurons. A group of calcium channels, belonging to the low-voltage gated T-type family, is among the main actors behind the burst discharge generation. During non-REM sleep, nRT cells are gradually hyperpolarized, this facilitates the opening of the T-type calcium channels that cause the bursting firing through rapid and transient membrane depolarization. Cells in the nRT express two different T-type calcium channels, encoded by the genes *$Ca_V3.2$* (*CACNA1h*) and *$Ca_V3.3$* (*CACNA1i*). Genetic deletion of the gene *$Ca_V3.3$* cause a reduction in cellular T-current, thus affecting the burst generation. Mice lacking this gene show therefore an impaired bursting in nRT cells *in vitro*. However, the contribution of the channel encoded by the gene *$Ca_V3.2$* to the bursting activity has not yet been defined.

In the study II, Pellegrini and colleagues, including myself, studied the nRT cellular properties after a single or double deletion of both calcium channels and aimed at clarifying their role in the sleep spindle rhythmogenesis using both *in vitro* and *in vivo* approaches (Pellegrini et al., 2016). Deficiency in $Ca_V3.2$ gene did not alter nRT cellular properties, whereas deletion of the gene $Ca_V3.3$ reduced, but not abolished, the low-threshold $Ca^{2+}$ current. Combined deletion of both channels fully abolished the T-current and, consequently, the rebound oscillatory bursts were absent. This was reflected in a general decrease in sigma power detected through EEG recording in mice sleeping undisturbedly in freely-moving conditions. However, whether these animals also show infra-slow oscillations in the sigma power remains to be determined. These animals could provide with a direct demonstration, whether an intact thalamo-cortical network is necessary and indispensable for generating and maintaining infra-slow oscillations in sigma power.

In study III, Rovo and colleagues, including myself, investigated the role of GABAergic synaptic inhibition within the thalamo-cortical loop by performing focal removal of the γ2 subunit in GABA-A receptor in the somatosensory thalamus (Rovo et al., 2014). GABA-A receptors, classified in synaptic and extrasynaptic based on their subunit composition and position in the synaptic cleft, have also different inhibitory firing patterns: phasic and tonic, respectively. Their pentameric assembly is theoretically limitless (Farrant and Nusser, 2005), but specific subunits (Essrich et al., 1998) take distinct roles in receptor trafficking. Here, the goal was to remove only synaptic GABA-A receptors to test their role in thalamocortical rhythm generation. For this purpose, we virally deleted the γ2 subunit that is responsible for synaptic localization of GABA-A receptors. As a result, only extrasynaptic GABA-A

receptors, which do not require the γ subunit (Nusser et al., 1998), remain functional. Importantly, the expression pattern of other synaptic GABA-A receptor subunits was also decreased, while the expression of a4, a thalamically expressed extrasynaptic subunit, remained unaltered. We obtained a completely unexpected result: during bursting activity, these remaining extra-synaptic receptor switch from tonic to phasic inhibition and the oscillatory inhibition in the TC network is maintained. Field potential recordings, as well as polysomnography recordings, report no relevant modification in sigma power and sleep spindle generation after the focal loss of function of synaptic GABA-A receptors. Therefore, the phasic inhibition controlling the sleep spindle generation is independent of the γ2 subunit and therefore of synaptic GABA-A receptors.

Interestingly, Zolpidem's hypnotic action is also mediated through binding to GABA-A receptor benzodiazepine binding site, located between the α and the γ subunits. Zolpidem is a widely used hypnotic drug prescribed for humans and also used in animals. It induces sleep and, in mice, it has been shown to depress faster oscillations, including the sigma frequency band (Kopp et al., 2004). Since the γ subunit is crucial for Zolpidem's pharmacodynamics, its deletion in mice makes them zolpidem-insensitive, as it is the case for the knock-in F77I mutation (Uygun et al., 2016). Preliminary results in control mice indicate that sigma power infra-slow oscillations were reduced approximately by half after zolpidem injection, therefore its hypnotic action could be mediated through acting on GABA-A receptors.

To conclude, virally mediated focal deletion of GABA-A receptor γ subunit offers a unique model to study Zolpidem's effect on the generation and control of sigma power infra-slow oscillations. Sequential targeting of different brain area might help disentangling the mechanism behind their generation.

## 6. Use of terminology and limitations

Some words and terms used to describe the findings were borrowed from specific fields. It is worth to mention here the intentions by which these words were used and the potential misinterpretation that they might cause. More specifically, the term "fragility" has been used here to describe a specific period of non-REM sleep where the presence of a stimulus can potentially induce an awakening, hence fragmenting sleep. This is conceptually different from the meaning itself of the word that alludes at sleep being essentially more fragile. Without external stimulations, sleep will not be interrupted. Similarly, with the term "continuity" we indicate the subsequent period where, again, the presence of a noise does not induce an

awakening. Sleep is said therefore to promote continuity, which has the same significance as saying that sleep is less fragile when exposed to the same stimulus. Additionally, the continuity promoted during the specific phase of the infra-slow oscillation is different than a state of temporarily-increased sleep depth, as markers of sleep depth, such as SWA, do not clearly go along with it. In spite of what the word "continuity" might suggest, sleep is definitely not more continuous during this time window, it will promote continuity only once a stimulus is presented there. Finally, the predominance of infra-slow oscillations in sigma power during S2 in humans might wrongly indicate that stage S2 is similar to mice non-REM sleep. As mentioned in the introduction, non-REM sleep in rodents is not differentiated into stages as it is the case in humans, even though some attempts have been proposed (J.-C. Compte, personal communication/unpublished data).

We present here results obtained from experiments performed in mice and humans. Although these two species share common feature of sleep, such as transitions between behavioral stated and their spectral hallmarks, from a macroscopic point of view their sleep is strikingly different. Sleep cycles in humans last for more than one hour whereas in mice a new cycle starts after a couple of minutes, resulting therefore in an extremely fragmented architecture of sleep. Despite this, however, the spectral temporal dynamics during sleep remain similar and comparable (Astori et al., 2013).

Performing experiments in different species requires an adaptation of the protocols. We tried to provide with parallel intervention as much as possible, considering that the experiments in the two species were performed in different universities and constant coordination was required to proof check the validity of the experiments.

Scoring of sleep in humans is performed with a temporal resolution of 30 s, whereas in mice it is generally done using 4 s-time windows. Therefore, the analysis protocols have been modified to extract information with the same time resolution using different approaches. Adaptation of analytical approaches were applied to offline analysis, this allowed us to calmly modify the protocols to compare the results between the two species. However, for what concerns online analysis and experiments, such as noise exposures and memory performance tests, we extracted as much information as possible from existing datasets. We have not yet started additional sets of experiments in mice, for testing memory performance correlation with sigma power infra-slow oscillation peak, and in humans, for testing the continuity and fragility periods using noise exposures. The identification of a similar correlative memory test and protocol for mice would have taken too much time, but is under consideration as future experiment. Similarly, the 20 s white noise at 90 dB used in mice might not have the good

intensity to test the threshold level of the balance between sleep fragility and continuity in humans. Therefore, apart for the noise exposures, which indeed require the acquisition of new datasets, we investigated the presence of hippocampal ripple power, which has been shown to report on offline memory processing (Buzsáki, 2015).

We identify the periods of continuity and fragility using sounds that cover approximately half of the 0.02 Hz-oscillation period. Noises were presented without knowledge of the existing oscillation, therefore we sampled conditions where it started over all phases. Using shorter sounds will definitely be helpful to better identify the moment of switch between the two periods. For this purpose, increasing the sampling frequency of our dataset will be of precious help. In fact, we are currently using consecutive windows of 4 s each to calculate the spectral power of the EEG trace, resulting in a representation of the 0.02 Hz-oscillation with 10-15 points.

The correlation between sigma power infra-slow oscillation and the behavioral outcome in mice is obtained through offline analysis. Although this approach reveals a clear subdivision of sleep into fragility and continuity periods based on the existing oscillation, an effective causality relationship between the two has to be identified and confirmed. Inferring causal relationship between co-occurring phenomena, such as the infra-slow oscillation in sigma power and the behavioral outcome, from *a posteriori* analysis requires direct confirmations through positive and negative controls. This point will be further discussed in section 7. *Ongoing experiments and future directions*.

The presence of the 0.02 Hz-oscillation in different frequency bands might be the reflection of other processes, cortical or subcortical, or might orchestrate other networks responsible for the balance between sleep fragility and continuity. As long as the mechanism behind the generation of these oscillations is not fully described, the cause-effect relationship cannot be confirmed.

Finally, we used genetically modified animals, such as the $Ca_V3.2$ and 3.3 knock-out mice, where the gene of interest is deleted constitutively in every tissue. Although not lethal in our case, results obtained through this approach have to be contextualized with respect of potential homeostatic and compensatory mechanisms that could overcome that specific genetic loss. More direct approaches, such as focal deletion (or gene insertion gain of function mutation) or even reversible alterations through optogenetic or chemogenetic approaches, are preferred.

# 7. Ongoing experiments and future directions

Additional experiments aiming at identifying the mechanisms generating the infra-slow oscillations, as well as their implication in sensory perception, are currently being performed but are in a preliminary state, thus they are not presented here as results. Therefore, I will discuss hereafter all the current ideas, hypothesis and methodological approaches we are performing and considering to perform in order to disentangle the mechanisms and role of infra-slow oscillations in sigma power. More specifically, thanks to a thorough collaboration with the lab members, our interests are spanning in multiple directions trying to cover different aspects of this newly described phenomenon.

1) **Can we confirm the results in both species with parallel interventions?** Provide with parallel intervention in both species is crucial to identify potential ancestral origins behind the process of generation and regulation of infra-slow oscillations. Identifying the correct threshold stimulus that reports the same, or similar, subdivision of non-REM sleep into fragility and continuity period in humans will undoubtedly open new doors to behavioral experimentation for testing sleep stability under the effect of different hypnotics.

2) **Can we confirm the causal link between the phase of infra-slow oscillation and the fragility or continuity period of sleep?** Online detection of the infra-slow oscillation in sigma power, and application of specific algorithms that identify the ideal moment to play the noise to induce an awakening, are currently being developed. In our specific case, closed-loop stimulation protocols provide crucial approaches to study the causal link between two observed phenomena. Therefore, the noise will be played based on the sigma power infra-slow oscillation phase as a positive control, and randomly as negative control.

Closed-loop stimulations are widely used in fundamental research, for example to create explicit memory (de Lavilleon et al., 2015) or to enhance (Ngo et al., 2013), and has a potential role in clinical medicine, for example to attenuate the symptoms of Parkinson's disease (Kern et al., 2016) or to automatically maintain blood glucose level within the ranges in Diabetes's patients (Thabit et al., 2016).

3) **How are sleep spindles contributing to the 0.02 Hz-oscillation in sigma power?** To confirm that infra-slow oscillations in sigma power are related to thalamo-cortical sleep spindle generation, we are setting up an analysis protocol that extracts sleep spindles from LFP recordings in head-restrained sleeping mice (Fernandez et al., 2016) and correlates their position and characteristics, such as cycle number and frequency, with the phase of the 0.02 Hz-oscillation. LFP recordings in different brain areas, as reported in study I, will indicate any

spatio-temporal organization between sleep spindles and sigma power infra-slow oscillation. Moreover, the application of this approach to genetically modified animals, such as $Ca_V3.3$ and DKO (double knock-out for 3.2 and 3.3 genes), will help characterizing the role of sleep spindles.

4) **Are brainstem nuclei, such as the LC, involved in generating the 0.02 Hz-oscillation?**

Its close interplay between cortical activity and autonomic function control, where the baroreflex arc represents an indicator, prompts to a brainstem-located generation and control of infra-slow oscillations. The high connectivity between sleep/wake controlling nuclei and nuclei controlling for the sympathetic/parasympathetic balance, such as the nucleus tractor solitary (Silvani et al., 2015), identifies the noradrenergic Locus Coeruleus as one possible orchestrating actor. Noradrenergic innervations stemming from the LC are present throughout the entire brain cortex (reviewed in Saper et al., 2010) and might coordinate the cortico-thalamic synchronization of sleep spindles, hence potentially modulating the infra-slow oscillations in sigma power. We performed a preliminary experiment where we intraperitoneally injected DSP-4, a neurotoxic agent that selectively disrupts the noradrenergic fibers of the LC (Fritschy and Grzanna, 1989; reviewed in Ross and Stenfors, 2015). As the cortical remaining noradrenergic innervations after the injection were heterogeneous and not constant across animals, we concluded that a different approach could provide with more reliable results. Therefore, we are considering to record LC firing activity, together with cortical EEG recordings, in animals expressing light-sensitive receptors in LC (ChannelRhodopsin (ChR2) and Halorhodopsin (NpHR)). This approach allows us to investigate, in animals sleeping in freely-moving condition, whether i) LC reduced activity during non-REM sleep (Aston-Jones and Bloom, 1981; Eschenko et al., 2012) correlates with infra-slow oscillations in sigma power and heart rate and ii) whether direct optogenetic modulation of LC activity has consequences to the 0.02 Hz-oscillation in sigma power and/or heart rate.

5) **Do peripheral modulations of heart rate affect the 0.02 Hz-oscillation?**

To clarify the interaction between autonomic control and sigma power infra-slow oscillations, we are currently performing experiments, in which we modulate the cardiac activity using either sympathetic or vagal blockers (Atenolol or Methylatropine, respectively) (Pham et al., 2009). The results will indicate, whether external modulation of cardiac control by increasing, decreasing and stabilize the heart rate has direct consequences on sigma power infra-slow oscillations. Consequently, this might indicate, whether a plausible feedback control between

the two phenomena exists, thus proposing that cardiac activity reflects fragility and continuity periods and its monitoring might help identifying them.

6) **Does memory consolidation in mice depend on intact 0.02 Hz-oscillations?** Since the 0.02 Hz-oscillation positively correlates with declarative memory consolidation in humans, and with hippocampal ripple power in mice, an index for offline memory processing, perturbation of sleep aiming at disrupting the infra-slow oscillation might provide with useful indications on the mechanism of memory consolidation. In fact, excessive sleep fragmentation in mice has been shown to reduce the performance in memory related tasks (Rolls et al., 2011). We are thus considering an experiment in mice that combines learning, sleep monitoring with LFP electrodes and memory recall.

7) **Is the cortical processing affected by the infra-slow oscillation phase**? The auditory cortical evoked potential provides with useful information and indications about the cortical processing of an auditory stimulus. We are currently recording cortical evoked potential in primary auditory cortex, as well as primary somatosensory cortex, during natural sleep in head-restrained mice. Importantly, we use 10 ms-long clicks instead of the 20 s white noise to avoid constant processing that might affect the shape of the evoked potential. We hypothesize that the cortical integration of sounds presented at different phases of the sigma power infra-slow oscillation reflects the subdivision of sleep into periods of fragility and continuity, thus identifying potential cellular networks implied in this balance. We address this question through two different approaches. First, we present clicks with a pseudo-random interval to sleeping mice while recording their cortical activity. This will result in the coverage of all phases of the infra-slow oscillation and will therefore provide with important indications on the temporal fluctuation of sensory integration. Second, through the help of a customized feed-back control (see point 6 above), the LFP signals will be analyzed online and clicks will be presented at specific phases (i.e. during the descending or ascending phase). The results will eventually confirm the paradigm that periods of continuity and fragility are timed by the infra-slow oscillation in sigma power.

8) **Can we enhance or reduce the cortical integration during specific phases of the infra-slow oscillation?** As a parallel experiment of point 7) we are setting up a similar protocol that includes the modulation of cortical activity during non-REM sleep through optogenetic approaches. We aim to enhance or reduce the inhibitory drive, for example acting on the somatostatin expressing interneurons. Somatostatin interneurons have been shown to target the apical dendrites of layer 5 pyramidal neurons and to down-regulate their activity (Silberberg and Markram, 2007; Murayama et al., 2009). In a similar experimental approach, Takahashi

and colleagues (Takahashi et al., 2016) report an increase in the whisker detection threshold in rats when somatostatin interneurons in the barrel cortex are optogenetically activated during stimulus presentation. Therefore, increasing the inhibitory drive of somatostatin interneurons in the auditory cortex during sleep might help investigating the cortical integration depending on the infra-slow oscillation phase.

9) **Is the infra-slow oscillation homeostatically regulated?**
A series of analysis is required to further investigate this phenomenon. More specifically it is important to show whether the infra-slow oscillation in sigma power is most prominent during specific moments of sleep and, as it provides an indication of sleep quality, whether it is also homeostatically regulated. We restricted our analysis to the first 100 min of the resting phase; that is, when the subjects sleep the most. It will be therefore very important to provide the profile of infra-slow oscillations throughout the entire resting phase and to also assess it in terms of sleep architecture and after increased sleep drive (sleep deprivation). Different dynamics of how the infra-slow oscillation evolves along a non-REM sleep bout might precede transitions to different behavioral states.

# 8. Conclusion

To conclude, in this thesis I report the description of a novel oscillatory component, the infra-slow oscillation in sigma power, which times the alternation between sleep fragility and continuity. The brain keeps windows of 25-30 s open to sample the close environment during the fragility periods, where the presence of a threshold stimulus can potentially induce a preventive awakening. The same stimulus presented during the opposing temporal window, termed continuity period, impacts on a system that is currently promoting continuity and, therefore, does not induce an awakening. Fragility and continuity periods additionally correlate with cardiac activity and marker of memory consolidation, which further support the subdivision of sleep into these two stages. The infra-slow fluctuation in sigma power is thus a good candidate to report the ongoing balance between sleep fragility and continuity.

This newly described oscillation, which we show to be correlated with memory consolidation and the temporal organization of sleeping periods with high or low susceptibility to external noises, might have a potential role in sampling sleep quality. The presence of this oscillation in subjects suffering from sleep disorder has not yet been tested but we estimate it could report on the imbalance between sleep fragility and continuity. If added to the palette of parameters used for sleep investigation in hospitals it could potentially give more indications about the extent of the existing sleep disturbances.

Hypnotic drugs, such as zolpidem, are widely used among people suffering from insomnia because of its rapid sleep-inducing action. By binding to the benzodiazepine site on GABA-A receptor, it potentiates its inhibitory action throughout the entire brain. Recently, genetic modification approaches aimed at developing mice, which were zolpidem insensitive in specific areas or nuclei. Moreover, sigma power has been shown to be largely reduced after zolpidem administration. Zolpidem hypnotic action might be mediated through modulation of the sigma power infra-slow oscillation. Therefore, localizing the target area of zolpidem, which controls for the generation of infra-slow oscillations in sigma power might provide with more precise pharmacological target to treat sleep disturbances.

Together, these results indicate the presence of a continuous mechanisms during non-REM sleep in both mice and humans that coordinate in time the alternation of periods promoting wither sleep continuity or fragility, thus reporting their balance.

# F. REFERENCES

Achermann P, Borbely AA (1997) Low-frequency (< 1 Hz) oscillations in the human sleep electroencephalogram. Neuroscience 81:213-222.

Achermann P, Borbely AA (2003) Mathematical models of sleep regulation. Front Biosci 8:s683-693.

Adam F (2009) The Book of Prognostics - Hippocrates. In. http://classics.mit.edu/Hippocrates/prognost.10.10.html.

Aeschbach D, Borbely AA (1993) All-night dynamics of the human sleep EEG. J Sleep Res 2:70-81.

Airaksinen MS, Alanen S, Szabat E, Visser TJ, Panula P (1992) Multiple neurotransmitters in the tuberomammillary nucleus: comparison of rat, mouse, and guinea pig. J Comp Neurol 323:103-116.

Akerstedt T (1977) Inversion of the sleep wakefulness pattern: effects on circadian variations in psychophysiological activation. Ergonomics 20:459-474.

Akerstedt T, Gillberg M (1981) The circadian variation of experimentally displaced sleep. Sleep 4:159-169.

Aladjalova NA (1957) Infra-slow rhythmic oscillations of the steady potential of the cerebral cortex. Nature 179:957-959.

Albrecht D, Royl G, Kaneoke Y (1998) Very slow oscillatory activities in lateral geniculate neurons of freely moving and anesthetized rats. Neurosci Res 32:209-220.

Allers KA, Ruskin DN, Bergstrom DA, Freeman LE, Ghazi LJ, Tierney PL, Walters JR (2002) Multisecond periodicities in basal ganglia firing rates correlate with theta bursts in transcortical and hippocampal EEG. J Neurophysiol 87:1118-1122.

Arendt J (2005) Melatonin in humans: it's about time. J Neuroendocrinol 17:537-538.

Assaf Y, Pasternak O (2008) Diffusion tensor imaging (DTI)-based white matter mapping in brain research: a review. J Mol Neurosci 34:51-61.

Aston-Jones G, Bloom FE (1981) Activity of norepinephrine-containing locus coeruleus neurons in behaving rats anticipates fluctuations in the sleep-waking cycle. J Neurosci 1:876-886.

Astori S, Wimmer RD, Luthi A (2013) Manipulating sleep spindles--expanding views on sleep, memory, and disease. Trends Neurosci 36:738-748.

Astori S, Wimmer RD, Prosser HM, Corti C, Corsi M, Liaudet N, Volterra A, Franken P, Adelman JP, Luthi A (2011) The Ca(V)3.3 calcium channel is the major sleep spindle pacemaker in thalamus. Proc Natl Acad Sci U S A 108:13823-13828.

Baker FC, Angara C, Szymusiak R, McGinty D (2005) Persistence of sleep-temperature coupling after suprachiasmatic nuclei lesions in rats. Am J Physiol Regul Integr Comp Physiol 289:R827-838.

Bal T, McCormick DA (1996) What stops synchronized thalamocortical oscillations? Neuron 17:297-308.

Banks S, Dinges DF (2007) Behavioral and physiological consequences of sleep restriction. J Clin Sleep Med 3:519-528.

Baran B, Pace-Schott EF, Ericson C, Spencer RM (2012) Processing of emotional reactivity and emotional memory over sleep. J Neurosci 32:1035-1042.

Barkley GL, Baumgartner C (2003) MEG and EEG in epilepsy. J Clin Neurophysiol 20:163-178.

Beare JI (2009) On Sleep and Sleeplessness - Aristotle. In. http://classics.mit.edu/Aristotle/sleep.html.

Bellesi M, Riedner BA, Garcia-Molina GN, Cirelli C, Tononi G (2014) Enhancement of sleep slow waves: underlying mechanisms and practical consequences. Front Syst Neurosci 8:208.

Benarroch EE (2009) The locus ceruleus norepinephrine system: functional organization and potential clinical significance. Neurology 73:1699-1704.

Benington JH, Heller HC (1995) Restoration of brain energy metabolism as the function of sleep. Prog Neurobiol 45:347-360.

Billman GE (2011) Heart rate variability - a historical perspective. Front Physiol 2:86.

Biswal B, Yetkin FZ, Haughton VM, Hyde JS (1995) Functional connectivity in the motor cortex of resting human brain using echo-planar MRI. Magn Reson Med 34:537-541.

Borbely AA (1982) A two process model of sleep regulation. Hum Neurobiol 1:195-204.

Borbely AA, Baumann F, Brandeis D, Strauch I, Lehmann D (1981) Sleep deprivation: effect on sleep stages and EEG power density in man. Electroencephalogr Clin Neurophysiol 51:483-495.

Born J (2010) Slow-wave sleep and the consolidation of long-term memory. World J Biol Psychiatry 11 Suppl 1:16-21.

Borniger JC, Weil ZM, Zhang N, Nelson RJ (2013) Dim light at night does not disrupt timing or quality of sleep in mice. Chronobiol Int 30:1016-1023.

Brown RE, Basheer R, McKenna JT, Strecker RE, McCarley RW (2012) Control of sleep and wakefulness. Physiol Rev 92:1087-1187.

Buijs RM, van Eden CG, Goncharuk VD, Kalsbeek A (2003) The biological clock tunes the organs of the body: timing by hormones and the autonomic nervous system. J Endocrinol 177:17-26.

Buijs RM, Scheer FA, Kreier F, Yi C, Bos N, Goncharuk VD, Kalsbeek A (2006) Organization of circadian functions: interaction with the body. Prog Brain Res 153:341-360.

Buxton RB (2013) The physics of functional magnetic resonance imaging (fMRI). Rep Prog Phys 76:096601.

Buzsáki G (2006) Rhythms of the brain. Oxford ; New York: Oxford University Press.

Buzsáki G (2015) Hippocampal sharp wave-ripple: A cognitive biomarker for episodic memory and planning. Hippocampus 25:1073-1188.

Cabrera G, Cavelli M, Lopez C, Rodriguez-Servetti Z, Vanini G, Chase MH, Falconi A, Torterolo P (2013) Wakefulness-promoting role of the inferior colliculus. Behav Brain Res 256:82-94.

Caird DM, Palmer AR, Rees A (1991) Binaural masking level difference effects in single units of the guinea pig inferior colliculus. Hear Res 57:91-106.

Canals S, Beyerlein M, Keller AL, Murayama Y, Logothetis NK (2008) Magnetic resonance imaging of cortical connectivity in vivo. Neuroimage 40:458-472.

Cellini N (2016) Memory consolidation in sleep disorders. Sleep Med Rev.

Chan AW, Mohajerani MH, LeDue JM, Wang YT, Murphy TH (2015) Mesoscale infraslow spontaneous membrane potential fluctuations recapitulate high-frequency activity cortical motifs. Nat Commun 6:7738.

Chemelli RM, Willie JT, Sinton CM, Elmquist JK, Scammell T, Lee C, Richardson JA, Williams SC, Xiong Y, Kisanuki Y, Fitch TE, Nakazato M, Hammer RE, Saper CB, Yanagisawa M (1999) Narcolepsy in orexin knockout mice: molecular genetics of sleep regulation. Cell 98:437-451.

Cho Y, Ryu SH, Lee BR, Kim KH, Lee E, Choi J (2015) Effects of artificial light at night on human health: A literature review of observational and experimental studies applied to exposure assessment. Chronobiol Int 32:1294-1310.

Chou TC, Bjorkum AA, Gaus SE, Lu J, Scammell TE, Saper CB (2002) Afferents to the ventrolateral preoptic nucleus. J Neurosci 22:977-990.

Clark I, Landolt HP (2017) Coffee, caffeine, and sleep: A systematic review of epidemiological studies and randomized controlled trials. Sleep Med Rev 31:70-78.

Cohen S, Doyle WJ, Alper CM, Janicki-Deverts D, Turner RB (2009) Sleep habits and susceptibility to the common cold. Arch Intern Med 169:62-67.

Contreras D, Destexhe A, Sejnowski TJ, Steriade M (1997) Spatiotemporal patterns of spindle oscillations in cortex and thalamus. J Neurosci 17:1179-1196.

Covassin N, Singh P (2016) Sleep Duration and Cardiovascular Disease Risk: Epidemiologic and Experimental Evidence. Sleep Med Clin 11:81-89.

Crick F (1984) Function of the thalamic reticular complex: the searchlight hypothesis. Proc Natl Acad Sci U S A 81:4586-4590.

Culpepper L, Wingertzahn MA (2015) Over-the-Counter Agents for the Treatment of Occasional Disturbed Sleep or Transient Insomnia: A Systematic Review of Efficacy and Safety. Prim Care Companion CNS Disord 17.

Czeisler CA, Duffy JF, Shanahan TL, Brown EN, Mitchell JF, Rimmer DW, Ronda JM, Silva EJ, Allan JS, Emens JS, Dijk DJ, Kronauer RE (1999) Stability, precision, and near-24-hour period of the human circadian pacemaker. Science 284:2177-2181.

Damoiseaux JS, Rombouts SA, Barkhof F, Scheltens P, Stam CJ, Smith SM, Beckmann CF (2006) Consistent resting-state networks across healthy subjects. Proc Natl Acad Sci U S A 103:13848-13853.

Dang-Vu TT, McKinney SM, Buxton OM, Solet JM, Ellenbogen JM (2010) Spontaneous brain rhythms predict sleep stability in the face of noise. Curr Biol 20:R626-627.

Dang-Vu TT, Bonjean M, Schabus M, Boly M, Darsaud A, Desseilles M, Degueldre C, Balteau E, Phillips C, Luxen A, Sejnowski TJ, Maquet P (2011) Interplay between spontaneous and induced brain activity during human non-rapid eye movement sleep. Proc Natl Acad Sci U S A 108:15438-15443.

de Lavilleon G, Lacroix MM, Rondi-Reig L, Benchenane K (2015) Explicit memory creation during sleep demonstrates a causal role of place cells in navigation. Nat Neurosci 18:493-495.

de Lecea L, Kilduff TS, Peyron C, Gao X, Foye PE, Danielson PE, Fukuhara C, Battenberg EL, Gautvik VT, Bartlett FS, 2nd, Frankel WN, van den Pol AN, Bloom FE, Gautvik KM, Sutcliffe JG (1998) The hypocretins: hypothalamus-specific peptides with neuroexcitatory activity. Proc Natl Acad Sci U S A 95:322-327.

De Luca M, Beckmann CF, De Stefano N, Matthews PM, Smith SM (2006) fMRI resting state networks define distinct modes of long-distance interactions in the human brain. Neuroimage 29:1359-1367.

De Pitta M, Brunel N, Volterra A (2016) Astrocytes: Orchestrating synaptic plasticity? Neuroscience 323:43-61.

Deboer T, Vansteensel MJ, Detari L, Meijer JH (2003) Sleep states alter activity of suprachiasmatic nucleus neurons. Nat Neurosci 6:1086-1090.

Dijk DJ, Beersma DG (1989) Effects of SWS deprivation on subsequent EEG power density and spontaneous sleep duration. Electroencephalogr Clin Neurophysiol 72:312-320.

Dijk DJ, Czeisler CA (1994) Paradoxical timing of the circadian rhythm of sleep propensity serves to consolidate sleep and wakefulness in humans. Neurosci Lett 166:63-68.

Dijk DJ, Czeisler CA (1995) Contribution of the circadian pacemaker and the sleep homeostat to sleep propensity, sleep structure, electroencephalographic slow waves, and sleep spindle activity in humans. J Neurosci 15:3526-3538.

Drewes AM, Nielsen KD, Arendt-Nielsen L, Birket-Smith L, Hansen LM (1997) The effect of cutaneous and deep pain on the electroencephalogram during sleep--an experimental study. Sleep 20:632-640.

Dringenberg HC, Sparling JS, Frazer J, Murdoch J (2006) Generalized cortex activation by the auditory midbrain: Mediation by acetylcholine and subcortical relays. Exp Brain Res 174:114-123.

Dubocovich ML (2007) Melatonin receptors: role on sleep and circadian rhythm regulation. Sleep Med 8 Suppl 3:34-42.

Easton A, Meerlo P, Bergmann B, Turek FW (2004) The suprachiasmatic nucleus regulates sleep timing and amount in mice. Sleep 27:1307-1318.

Edgar DM, Dement WC, Fuller CA (1993) Effect of SCN lesions on sleep in squirrel monkeys: evidence for opponent processes in sleep-wake regulation. J Neurosci 13:1065-1079.

El-Ad B, Korczyn AD (1998) Disorders of excessive daytime sleepiness--an update. J Neurol Sci 153:192-202.

Eschenko O, Magri C, Panzeri S, Sara SJ (2012) Noradrenergic neurons of the locus coeruleus are phase locked to cortical up-down states during sleep. Cereb Cortex 22:426-435.

Essrich C, Lorez M, Benson JA, Fritschy JM, Luscher B (1998) Postsynaptic clustering of major GABAA receptor subtypes requires the gamma 2 subunit and gephyrin. Nat Neurosci 1:563-571.

Farley GR, Morley BJ, Javel E, Gorga MP (1983) Single-unit responses to cholinergic agents in the rat inferior colliculus. Hear Res 11:73-91.

Farrant M, Nusser Z (2005) Variations on an inhibitory theme: phasic and tonic activation of GABA(A) receptors. Nat Rev Neurosci 6:215-229.

Feige B, Baglioni C, Spiegelhalder K, Hirscher V, Nissen C, Riemann D (2013) The microstructure of sleep in primary insomnia: an overview and extension. Int J Psychophysiol 89:171-180.

Fernandez LM, Comte JC, Le Merre P, Lin JS, Salin PA, Crochet S (2016) Highly Dynamic Spatiotemporal Organization of Low-Frequency Activities During Behavioral States in the Mouse Cerebral Cortex. Cereb Cortex.

Fiath R, Kerekes BP, Wittner L, Toth K, Beregszaszi P, Horvath D, Ulbert I (2016) Laminar analysis of the slow wave activity in the somatosensory cortex of anesthetized rats. Eur J Neurosci 44:1935-1951.

Filippov IV, Williams WC, Frolov VA (2004) Very slow potential oscillations in locus coeruleus and dorsal raphe nucleus under different illumination in freely moving rats. Neurosci Lett 363:89-93.

Franken P (2002) Long-term vs. short-term processes regulating REM sleep. J Sleep Res 11:17-28.

Franken P (2013) A role for clock genes in sleep homeostasis. Curr Opin Neurobiol 23:864-872.

Franken P, Dijk DJ (2009) Circadian clock genes and sleep homeostasis. Eur J Neurosci 29:1820-1829.

Franken P, Tobler I, Borbely AA (1991a) Sleep homeostasis in the rat: simulation of the time course of EEG slow-wave activity. Neurosci Lett 130:141-144.

Franken P, Chollet D, Tafti M (2001) The homeostatic regulation of sleep need is under genetic control. J Neurosci 21:2610-2621.

Franken P, Dijk DJ, Tobler I, Borbely AA (1991b) Sleep deprivation in rats: effects on EEG power spectra, vigilance states, and cortical temperature. Am J Physiol 261:R198-208.

Fritschy JM, Grzanna R (1989) Immunohistochemical analysis of the neurotoxic effects of DSP-4 identifies two populations of noradrenergic axon terminals. Neuroscience 30:181-197.

Fuxe K, Dahlstrom AB, Jonsson G, Marcellino D, Guescini M, Dam M, Manger P, Agnati L (2010) The discovery of central monoamine neurons gave volume transmission to the wired brain. Prog Neurobiol 90:82-100.

Gallopin T, Luppi PH, Cauli B, Urade Y, Rossier J, Hayaishi O, Lambolez B, Fort P (2005) The endogenous somnogen adenosine excites a subset of sleep-promoting neurons via A2A receptors in the ventrolateral preoptic nucleus. Neuroscience 134:1377-1390.

Goense JB, Logothetis NK (2008) Neurophysiology of the BOLD fMRI signal in awake monkeys. Curr Biol 18:631-640.

Gong H, McGinty D, Guzman-Marin R, Chew KT, Stewart D, Szymusiak R (2004) Activation of c-fos in GABAergic neurones in the preoptic area during sleep and in response to sleep deprivation. J Physiol 556:935-946.

Goodenough DR, Lewis HB, Shapiro A, Jaret L, Sleser I (1965) Dream Reporting Following Abrupt and Gradual Awakenings from Different Types of Sleep. J Pers Soc Psychol 2:170-179.

Gooley JJ, Lu J, Chou TC, Scammell TE, Saper CB (2001) Melanopsin in cells of origin of the retinohypothalamic tract. Nat Neurosci 4:1165.

Gottesmann C (1988) What the cerveau isole preparation tells us nowadays about sleep-wake mechanisms? Neurosci Biobehav Rev 12:39-48.

Greene RW, Frank MG (2010) Slow wave activity during sleep: functional and therapeutic implications. Neuroscientist 16:618-633.

Greicius MD, Krasnow B, Reiss AL, Menon V (2003) Functional connectivity in the resting brain: a network analysis of the default mode hypothesis. Proc Natl Acad Sci U S A 100:253-258.

Gulevich G, Dement W, Johnson L (1966) Psychiatric and EEG observations on a case of prolonged (264 hours) wakefulness. Arch Gen Psychiatry 15:29-35.

Gvilia I, Xu F, McGinty D, Szymusiak R (2006) Homeostatic regulation of sleep: a role for preoptic area neurons. J Neurosci 26:9426-9433.

Habbicht H, Vater M (1996) A microiontophoretic study of acetylcholine effects in the inferior colliculus of horseshoe bats: implications for a modulatory role. Brain Res 724:169-179.

Halassa MM, Florian C, Fellin T, Munoz JR, Lee SY, Abel T, Haydon PG, Frank MG (2009) Astrocytic modulation of sleep homeostasis and cognitive consequences of sleep loss. Neuron 61:213-219.

Halasz P (2005) K-complex, a reactive EEG graphoelement of NREM sleep: an old chap in a new garment. Sleep Med Rev 9:391-412.

Halasz P, Bodizs R, Parrino L, Terzano M (2014) Two features of sleep slow waves: homeostatic and reactive aspects--from long term to instant sleep homeostasis. Sleep Med 15:1184-1195.

Hall IC, Rebec GV, Hurley LM (2010) Serotonin in the inferior colliculus fluctuates with behavioral state and environmental stimuli. J Exp Biol 213:1009-1017.

Hastings MH (2003) Circadian clocks: self-assembling oscillators? Curr Biol 13:R681-682.

Hastings MH, Reddy AB, Maywood ES (2003) A clockwork web: circadian timing in brain and periphery, in health and disease. Nat Rev Neurosci 4:649-661.

He BJ (2014) Scale-free brain activity: past, present, and future. Trends Cogn Sci 18:480-487.

Hengen KB, Torrado Pacheco A, McGregor JN, Van Hooser SD, Turrigiano GG (2016) Neuronal Firing Rate Homeostasis Is Inhibited by Sleep and Promoted by Wake. Cell 165:180-191.

Hennevin E, Huetz C, Edeline JM (2007) Neural representations during sleep: from sensory processing to memory traces. Neurobiol Learn Mem 87:416-440.

Herxheimer A, Petrie KJ (2002) Melatonin for the prevention and treatment of jet lag. Cochrane Database Syst Rev:CD001520.

Herzog ED, Geusz ME, Khalsa SB, Straume M, Block GD (1997) Circadian rhythms in mouse suprachiasmatic nucleus explants on multimicroelectrode plates. Brain Res 757:285-290.

Hiltunen T, Kantola J, Abou Elseoud A, Lepola P, Suominen K, Starck T, Nikkinen J, Remes J, Tervonen O, Palva S, Kiviniemi V, Palva JM (2014) Infra-slow EEG fluctuations are correlated with resting-state network dynamics in fMRI. J Neurosci 34:356-362.

Himanen SL, Hasan J (2000) Limitations of Rechtschaffen and Kales. Sleep Med Rev 4:149-167.

Horovitz SG, Fukunaga M, de Zwart JA, van Gelderen P, Fulton SC, Balkin TJ, Duyn JH (2008) Low frequency BOLD fluctuations during resting wakefulness and light sleep: a simultaneous EEG-fMRI study. Hum Brain Mapp 29:671-682.

Horovitz SG, Braun AR, Carr WS, Picchioni D, Balkin TJ, Fukunaga M, Duyn JH (2009) Decoupling of the brain's default mode network during deep sleep. Proc Natl Acad Sci U S A 106:11376-11381.

Hughes SW, Lorincz ML, Parri HR, Crunelli V (2011) Infraslow (<0.1 Hz) oscillations in thalamic relay nuclei basic mechanisms and significance to health and disease states. Prog Brain Res 193:145-162.

Hurley LM, Pollak GD (2001) Serotonin effects on frequency tuning of inferior colliculus neurons. J Neurophysiol 85:828-842.

Hurley LM, Pollak GD (2005) Serotonin modulates responses to species-specific vocalizations in the inferior colliculus. J Comp Physiol A Neuroethol Sens Neural Behav Physiol 191:535-546.

Hurley LM, Thompson AM, Pollak GD (2002) Serotonin in the inferior colliculus. Hear Res 168:1-11.

Huttunen JK, Grohn O, Penttonen M (2008) Coupling between simultaneously recorded BOLD response and neuronal activity in the rat somatosensory cortex. Neuroimage 39:775-785.

Iber C, Ancoli-Israel, S., Chesson, A. and Quan, S.F. (2007) The AASM Manual for the Scoring of Sleep and Associated Events: Rules, Terminology and Technical Specification: American Academy of Sleep Medicine.

Ibuka N, Kawamura H (1975) Loss of circadian rhythm in sleep-wakefulness cycle in the rat by suprachiasmatic nucleus lesions. Brain Res 96:76-81.

Irwin MR (2015) Why sleep is important for health: a psychoneuroimmunology perspective. Annu Rev Psychol 66:143-172.

Jackson ML, Croft RJ, Kennedy GA, Owens K, Howard ME (2013) Cognitive components of simulated driving performance: Sleep loss effects and predictors. Accid Anal Prev 50:438-444.

Jones BE (2005) From waking to sleeping: neuronal and chemical substrates. Trends Pharmacol Sci 26:578-586.

Jouvet M (1967a) The states of sleep. In. https://sommeil.univ-lyon1.fr/articles/jouvet/scientific_american/print.php: Scientific American.

Jouvet M (1967b) Neurophysiology of the states of sleep. Physiol Rev 47:117-177.

Jouvet M (2004) How sleep was dissociated into two states: telencephalic and rhombencephalic sleep? Arch Ital Biol 142:317-326.

Kalia M (2006) Neurobiology of sleep. Metabolism 55:S2-6.

Kalsbeek A, Palm IF, La Fleur SE, Scheer FA, Perreau-Lenz S, Ruiter M, Kreier F, Cailotto C, Buijs RM (2006) SCN outputs and the hypothalamic balance of life. J Biol Rhythms 21:458-469.

Kaplan J, Ventura J, Bakshi A, Pierobon A, Lackner JR, DiZio P (2017) The influence of sleep deprivation and oscillating motion on sleepiness, motion sickness, and cognitive and motor performance. Auton Neurosci 202:86-96.

Kato T, Montplaisir JY, Lavigne GJ (2004) Experimentally induced arousals during sleep: a cross-modality matching paradigm. J Sleep Res 13:229-238.

Kern K, Naros G, Braun C, Weiss D, Gharabaghi A (2016) Detecting a Cortical Fingerprint of Parkinson's Disease for Closed-Loop Neuromodulation. Front Neurosci 10:110.

Kim U, Bal T, McCormick DA (1995) Spindle waves are propagating synchronized oscillations in the ferret LGNd in vitro. J Neurophysiol 74:1301-1323.

Kirsch DB (2011) There and back again: a current history of sleep medicine. Chest 139:939-946.

Klepper A, Herbert H (1991) Distribution and origin of noradrenergic and serotonergic fibers in the cochlear nucleus and inferior colliculus of the rat. Brain Res 557:190-201.

Kopp C, Rudolph U, Tobler I (2004) Sleep EEG changes after zolpidem in mice. Neuroreport 15:2299-2302.

Kreutzmann JC, Havekes R, Abel T, Meerlo P (2015) Sleep deprivation and hippocampal vulnerability: changes in neuronal plasticity, neurogenesis and cognitive function. Neuroscience 309:173-190.

Kronauer RE, Czeisler CA, Pilato SF, Moore-Ede MC, Weitzman ED (1982) Mathematical model of the human circadian system with two interacting oscillators. Am J Physiol 242:R3-17.

Kuga N, Sasaki T, Takahara Y, Matsuki N, Ikegaya Y (2011) Large-scale calcium waves traveling through astrocytic networks in vivo. J Neurosci 31:2607-2614.

Kukko-Lukjanov TK, Panula P (2003) Subcellular distribution of histamine, GABA and galanin in tuberomamillary neurons in vitro. J Chem Neuroanat 25:279-292.

Kuo TB, Shaw FZ, Lai CJ, Yang CC (2008) Asymmetry in sympathetic and vagal activities during sleep-wake transitions. Sleep 31:311-320.

Landolt HP (2008) Sleep homeostasis: a role for adenosine in humans? Biochem Pharmacol 75:2070-2079.

Larson-Prior LJ, Zempel JM, Nolan TS, Prior FW, Snyder AZ, Raichle ME (2009) Cortical network functional connectivity in the descent to sleep. Proc Natl Acad Sci U S A 106:4489-4494.

Lavigne G, Zucconi M, Castronovo C, Manzini C, Marchettini P, Smirne S (2000) Sleep arousal response to experimental thermal stimulation during sleep in human subjects free of pain and sleep problems. Pain 84:283-290.

Lee MH, Smyser CD, Shimony JS (2013) Resting-state fMRI: a review of methods and clinical applications. AJNR Am J Neuroradiol 34:1866-1872.

Leistner S, Sander TH, Wuebbeler G, Link A, Elster C, Curio G, Trahms L, Mackert BM (2010) Magnetoencephalography discriminates modality-specific infraslow signals less than 0.1 Hz. Neuroreport 21:196-200.

Leresche N, Lightowler S, Soltesz I, Jassik-Gerschenfeld D, Crunelli V (1991) Low-frequency oscillatory activities intrinsic to rat and cat thalamocortical cells. J Physiol 441:155-174.

Liblau RS, Vassalli A, Seifinejad A, Tafti M (2015) Hypocretin (orexin) biology and the pathophysiology of narcolepsy with cataplexy. Lancet Neurol 14:318-328.

Lin JS, Sakai K, Vanni-Mercier G, Jouvet M (1989) A critical role of the posterior hypothalamus in the mechanisms of wakefulness determined by microinjection of muscimol in freely moving cats. Brain Res 479:225-240.

Lin L, Faraco J, Li R, Kadotani H, Rogers W, Lin X, Qiu X, de Jong PJ, Nishino S, Mignot E (1999) The sleep disorder canine narcolepsy is caused by a mutation in the hypocretin (orexin) receptor 2 gene. Cell 98:365-376.

Lindberg E, Janson C, Gislason T, Bjornsson E, Hetta J, Boman G (1997) Sleep disturbances in a young adult population: can gender differences be explained by differences in psychological status? Sleep 20:381-387.

Linkenkaer-Hansen K, Nikouline VV, Palva JM, Ilmoniemi RJ (2001) Long-range temporal correlations and scaling behavior in human brain oscillations. J Neurosci 21:1370-1377.

Liu Y, Wheaton AG, Chapman DP, Croft JB (2013) Sleep duration and chronic diseases among U.S. adults age 45 years and older: evidence from the 2010 Behavioral Risk Factor Surveillance System. Sleep 36:1421-1427.

Logothetis NK, Pauls J, Augath M, Trinath T, Oeltermann A (2001) Neurophysiological investigation of the basis of the fMRI signal. Nature 412:150-157.

Loomis AL, Harvey EN, Hobart GA (1937) Cerebral states during sleep, as studied by human brain potentials. J Exp Psychol:127-144.

Lowrey PL, Takahashi JS (2004) Mammalian circadian biology: elucidating genome-wide levels of temporal organization. Annu Rev Genomics Hum Genet 5:407-441.

Lu H, Zou Q, Gu H, Raichle ME, Stein EA, Yang Y (2012) Rat brains also have a default mode network. Proc Natl Acad Sci U S A 109:3979-3984.

Lu J, Greco MA, Shiromani P, Saper CB (2000) Effect of lesions of the ventrolateral preoptic nucleus on NREM and REM sleep. J Neurosci 20:3830-3842.

Lüthi A (2014) Sleep Spindles: Where They Come From, What They Do. Neuroscientist 20:243-256.

Lüthi A, McCormick DA (1998) Periodicity of thalamic synchronized oscillations: the role of Ca2+-mediated upregulation of Ih. Neuron 20:553-563.

Lüthi A, McCormick DA (1999) Modulation of a pacemaker current through Ca(2+)-induced stimulation of cAMP production. Nat Neurosci 2:634-641.

Macedo CE, Martinez RC, de Souza Silva MA, Brandao ML (2005) Increases in extracellular levels of 5-HT and dopamine in the basolateral, but not in the central, nucleus of amygdala induced by aversive stimulation of the inferior colliculus. Eur J Neurosci 21:1131-1138.

Mackiewicz M, Shockley KR, Romer MA, Galante RJ, Zimmerman JE, Naidoo N, Baldwin DA, Jensen ST, Churchill GA, Pack AI (2007) Macromolecule biosynthesis: a key function of sleep. Physiol Genomics 31:441-457.

Magri C, Schridde U, Murayama Y, Panzeri S, Logothetis NK (2012) The amplitude and timing of the BOLD signal reflects the relationship between local field potential power at different frequencies. J Neurosci 32:1395-1407.

Malmierca MS, Hernandez O, Rees A (2005) Intercollicular commissural projections modulate neuronal responses in the inferior colliculus. Eur J Neurosci 21:2701-2710.

Malmierca MS, Hernandez O, Falconi A, Lopez-Poveda EA, Merchan M, Rees A (2003) The commissure of the inferior colliculus shapes frequency response areas in rat: an in vivo study using reversible blockade with microinjection of kynurenic acid. Exp Brain Res 153:522-529.

Mantini D, Perrucci MG, Del Gratta C, Romani GL, Corbetta M (2007) Electrophysiological signatures of resting state networks in the human brain. Proc Natl Acad Sci U S A 104:13170-13175.

Maquet P (1995) Sleep function(s) and cerebral metabolism. Behav Brain Res 69:75-83.

Marcus JN, Aschkenasi CJ, Lee CE, Chemelli RM, Saper CB, Yanagisawa M, Elmquist JK (2001) Differential expression of orexin receptors 1 and 2 in the rat brain. J Comp Neurol 435:6-25.

Marshall L, Born J (2002) Brain-immune interactions in sleep. Int Rev Neurobiol 52:93-131.
Massimini M, Rosanova M, Mariotti M (2003) EEG slow (approximately 1 Hz) waves are associated with nonstationarity of thalamo-cortical sensory processing in the sleeping human. J Neurophysiol 89:1205-1213.
McDonald DG, Schicht WW, Frazier RE, Shallenberger HD, Edwards DJ (1975) Studies of information processing in sleep. Psychophysiology 12:624-629.
McKinney SM, Dang-Vu TT, Buxton OM, Solet JM, Ellenbogen JM (2011) Covert waking brain activity reveals instantaneous sleep depth. PLoS One 6:e17351.
Mechling AE, Hubner NS, Lee HL, Hennig J, von Elverfeldt D, Harsan LA (2014) Fine-grained mapping of mouse brain functional connectivity with resting-state fMRI. Neuroimage 96:203-215.
Methippara MM, Alam MN, Szymusiak R, McGinty D (2000) Effects of lateral preoptic area application of orexin-A on sleep-wakefulness. Neuroreport 11:3423-3426.
Mills JN (1964) Circadian Rhythms during and after Three Months in Solitude Underground. J Physiol 174:217-231.
Mingoia G, Wagner G, Langbein K, Maitra R, Smesny S, Dietzek M, Burmeister HP, Reichenbach JR, Schlosser RG, Gaser C, Sauer H, Nenadic I (2012) Default mode network activity in schizophrenia studied at resting state using probabilistic ICA. Schizophr Res 138:143-149.
Mistlberger RE (2005) Circadian regulation of sleep in mammals: role of the suprachiasmatic nucleus. Brain Res Brain Res Rev 49:429-454.
Mistlberger RE, Bergmann BM, Waldenar W, Rechtschaffen A (1983) Recovery sleep following sleep deprivation in intact and suprachiasmatic nuclei-lesioned rats. Sleep 6:217-233.
Mitra A, Snyder AZ, Tagliazucchi E, Laufs H, Raichle ME (2015) Propagated infra-slow intrinsic brain activity reorganizes across wake and slow wave sleep. Elife 4.
Modirrousta M, Mainville L, Jones BE (2004) Gabaergic neurons with alpha2-adrenergic receptors in basal forebrain and preoptic area express c-Fos during sleep. Neuroscience 129:803-810.
Moiseeva NI, Aleksanian ZA (1986) Slow-wave oscillations of the multi-unit activity average frequency in the human brain during drowsiness and sleep. Electroencephalogr Clin Neurophysiol 63:431-437.
Mölle M, Bergmann TO, Marshall L, Born J (2011) Fast and slow spindles during the sleep slow oscillation: disparate coalescence and engagement in memory processing. Sleep 34:1411-1421.
Monto S, Palva S, Voipio J, Palva JM (2008) Very slow EEG fluctuations predict the dynamics of stimulus detection and oscillation amplitudes in humans. J Neurosci 28:8268-8272.
Moore RY (2007) Suprachiasmatic nucleus in sleep-wake regulation. Sleep Med 8 Suppl 3:27-33.
Morin CM, LeBlanc M, Daley M, Gregoire JP, Merette C (2006) Epidemiology of insomnia: prevalence, self-help treatments, consultations, and determinants of help-seeking behaviors. Sleep Med 7:123-130.
Motts SD, Schofield BR (2009) Sources of cholinergic input to the inferior colliculus. Neuroscience 160:103-114.
Murayama M, Perez-Garci E, Nevian T, Bock T, Senn W, Larkum ME (2009) Dendritic encoding of sensory stimuli controlled by deep cortical interneurons. Nature 457:1137-1141.
Ngo HV, Martinetz T, Born J, Molle M (2013) Auditory closed-loop stimulation of the sleep slow oscillation enhances memory. Neuron 78:545-553.

Nikouline VV, Linkenkaer-Hansen K, Huttunen J, Ilmoniemi RJ (2001) Interhemispheric phase synchrony and amplitude correlation of spontaneous beta oscillations in human subjects: a magnetoencephalographic study. Neuroreport 12:2487-2491.

Nir Y, Mukamel R, Dinstein I, Privman E, Harel M, Fisch L, Gelbard-Sagiv H, Kipervasser S, Andelman F, Neufeld MY, Kramer U, Arieli A, Fried I, Malach R (2008) Interhemispheric correlations of slow spontaneous neuronal fluctuations revealed in human sensory cortex. Nat Neurosci 11:1100-1108.

Nishino S, Ripley B, Overeem S, Lammers GJ, Mignot E (2000) Hypocretin (orexin) deficiency in human narcolepsy. Lancet 355:39-40.

Nunez A, Curro Dossi R, Contreras D, Steriade M (1992) Intracellular evidence for incompatibility between spindle and delta oscillations in thalamocortical neurons of cat. Neuroscience 48:75-85.

Nusser Z, Sieghart W, Somogyi P (1998) Segregation of different GABAA receptors to synaptic and extrasynaptic membranes of cerebellar granule cells. J Neurosci 18:1693-1703.

Oswald I, Taylor AM, Treisman M (1960) Discriminative responses to stimulation during human sleep. Brain 83:440-453.

Palva JM, Palva S (2012) Infra-slow fluctuations in electrophysiological recordings, blood-oxygenation-level-dependent signals, and psychophysical time series. Neuroimage 62:2201-2211.

Pan WJ, Thompson GJ, Magnuson ME, Jaeger D, Keilholz S (2013) Infraslow LFP correlates to resting-state fMRI BOLD signals. Neuroimage 74:288-297.

Pan WJ, Thompson G, Magnuson M, Majeed W, Jaeger D, Keilholz S (2010) Simultaneous FMRI and electrophysiology in the rodent brain. J Vis Exp.

Pan WJ, Thompson G, Magnuson M, Majeed W, Jaeger D, Keilholz S (2011) Broadband local field potentials correlate with spontaneous fluctuations in functional magnetic resonance imaging signals in the rat somatosensory cortex under isoflurane anesthesia. Brain Connect 1:119-131.

Pellegrini C, Lecci S, Luthi A, Astori S (2016) Suppression of Sleep Spindle Rhythmogenesis in Mice with Deletion of CaV3.2 and CaV3.3 T-type Ca(2+) Channels. Sleep 39:875-885.

Perogamvros L, Dang-Vu TT, Desseilles M, Schwartz S (2013) Sleep and dreaming are for important matters. Front Psychol 4:474.

Peyron C et al. (2000) A mutation in a case of early onset narcolepsy and a generalized absence of hypocretin peptides in human narcoleptic brains. Nat Med 6:991-997.

Pfaff DW, Martin EM, Faber D (2012) Origins of arousal: roles for medullary reticular neurons. Trends Neurosci 35:468-476.

Pham H, Bonham AC, Pinkerton KE, Chen CY (2009) Central neuroplasticity and decreased heart rate variability after particulate matter exposure in mice. Environ Health Perspect 117:1448-1453.

Picchioni D, Horovitz SG, Fukunaga M, Carr WS, Meltzer JA, Balkin TJ, Duyn JH, Braun AR (2011) Infraslow EEG oscillations organize large-scale cortical-subcortical interactions during sleep: a combined EEG/fMRI study. Brain Res 1374:63-72.

Piccolino M (1997) Luigi Galvani and animal electricity: two centuries after the foundation of electrophysiology. Trends Neurosci 20:443-448.

Porkka-Heiskanen T, Strecker RE, Thakkar M, Bjorkum AA, Greene RW, McCarley RW (1997) Adenosine: a mediator of the sleep-inducing effects of prolonged wakefulness. Science 276:1265-1268.

Portas CM, Krakow K, Allen P, Josephs O, Armony JL, Frith CD (2000) Auditory processing across the sleep-wake cycle: simultaneous EEG and fMRI monitoring in humans. Neuron 28:991-999.

Raichle ME, MacLeod AM, Snyder AZ, Powers WJ, Gusnard DA, Shulman GL (2001) A default mode of brain function. Proc Natl Acad Sci U S A 98:676-682.

Ralph MR, Foster RG, Davis FC, Menaker M (1990) Transplanted suprachiasmatic nucleus determines circadian period. Science 247:975-978.

Rasch B, Born J (2013) About sleep's role in memory. Physiol Rev 93:681-766.

Rechtschaffen A, Kales A (1968) A Manual for Standardised Terminology, Techniques and Scoring System for Sleep Stages in Normal Subjects: United States Department of Healts and Welfare.

Richter CP (1967) Sleep and activity: their relation to the 24-hour clock. Res Publ Assoc Res Nerv Ment Dis 45:8-29.

Richter D (1965) Biochemical changes during sleep. Verh Dtsch Ges Inn Med 71:819-826.

Rodriguez AV, Funk CM, Vyazovskiy VV, Nir Y, Tononi G, Cirelli C (2016) Why Does Sleep Slow-Wave Activity Increase After Extended Wake? Assessing the Effects of Increased Cortical Firing During Wake and Sleep. J Neurosci 36:12436-12447.

Rolls A, Colas D, Adamantidis A, Carter M, Lanre-Amos T, Heller HC, de Lecea L (2011) Optogenetic disruption of sleep continuity impairs memory consolidation. Proc Natl Acad Sci U S A 108:13305-13310.

Rosanova M, Timofeev I (2005) Neuronal mechanisms mediating the variability of somatosensory evoked potentials during sleep oscillations in cats. J Physiol 562:569-582.

Ross SB, Stenfors C (2015) DSP4, a selective neurotoxin for the locus coeruleus noradrenergic system. A review of its mode of action. Neurotox Res 27:15-30.

Rovo Z, Matyas F, Bartho P, Slezia A, Lecci S, Pellegrini C, Astori S, David C, Hangya B, Luthi A, Acsady L (2014) Phasic, nonsynaptic GABA-A receptor-mediated inhibition entrains thalamocortical oscillations. J Neurosci 34:7137-7147.

Sakurai T et al. (1998) Orexins and orexin receptors: a family of hypothalamic neuropeptides and G protein-coupled receptors that regulate feeding behavior. Cell 92:1 page following 696.

Saper CB, Chou TC, Scammell TE (2001) The sleep switch: hypothalamic control of sleep and wakefulness. Trends Neurosci 24:726-731.

Saper CB, Fuller PM, Pedersen NP, Lu J, Scammell TE (2010) Sleep state switching. Neuron 68:1023-1042.

Schabus M, Dang-Vu TT, Heib DP, Boly M, Desseilles M, Vandewalle G, Schmidt C, Albouy G, Darsaud A, Gais S, Degueldre C, Balteau E, Phillips C, Luxen A, Maquet P (2012) The Fate of Incoming Stimuli during NREM Sleep is Determined by Spindles and the Phase of the Slow Oscillation. Front Neurol 3:40.

Scher R (2017) How Ancient Cultures Made Sense of Sleep. In. https://vanwinkles.com/ancient-interpretations-about-sleep.

Schibler U, Gotic I, Saini C, Gos P, Curie T, Emmenegger Y, Sinturel F, Gosselin P, Gerber A, Fleury-Olela F, Rando G, Demarque M, Franken P (2015) Clock-Talk: Interactions between Central and Peripheral Circadian Oscillators in Mammals. Cold Spring Harb Symp Quant Biol 80:223-232.

Schwartz MD, Kilduff TS (2015) The Neurobiology of Sleep and Wakefulness. Psychiatr Clin North Am 38:615-644.

Schwarz LA, Luo L (2015) Organization of the locus coeruleus-norepinephrine system. Curr Biol 25:R1051-1056.

Sforza E, Jouny C, Ibanez V (2000) Cardiac activation during arousal in humans: further evidence for hierarchy in the arousal response. Clin Neurophysiol 111:1611-1619.

Shackleton TM, Arnott RH, Palmer AR (2005) Sensitivity to interaural correlation of single neurons in the inferior colliculus of guinea pigs. J Assoc Res Otolaryngol 6:244-259.

Shang Y, Griffith LC, Rosbash M (2008) Light-arousal and circadian photoreception circuits intersect at the large PDF cells of the Drosophila brain. Proc Natl Acad Sci U S A 105:19587-19594.

Shein-Idelson M, Ondracek JM, Liaw HP, Reiter S, Laurent G (2016) Slow waves, sharp waves, ripples, and REM in sleeping dragons. Science 352:590-595.

Shekleton JA, Flynn-Evans EE, Miller B, Epstein LJ, Kirsch D, Brogna LA, Burke LM, Bremer E, Murray JM, Gehrman P, Lockley SW, Rajaratnam SM (2014) Neurobehavioral performance impairment in insomnia: relationships with self-reported sleep and daytime functioning. Sleep 37:107-116.

Sherin JE, Shiromani PJ, McCarley RW, Saper CB (1996) Activation of ventrolateral preoptic neurons during sleep. Science 271:216-219.

Sherin JE, Elmquist JK, Torrealba F, Saper CB (1998) Innervation of histaminergic tuberomammillary neurons by GABAergic and galaninergic neurons in the ventrolateral preoptic nucleus of the rat. J Neurosci 18:4705-4721.

Shi Z (2016) My name or yours? Event-related potential correlates of self-name processing. Neuroreport 27:542-547.

Shulman GL, Fiez JA, Corbetta M, Buckner RL, Miezin FM, Raichle ME, Petersen SE (1997) Common Blood Flow Changes across Visual Tasks: II. Decreases in Cerebral Cortex. J Cogn Neurosci 9:648-663.

Siegel JM (2005) Clues to the functions of mammalian sleep. Nature 437:1264-1271.

Siegel JM (2009) Sleep viewed as a state of adaptive inactivity. Nat Rev Neurosci 10:747-753.

Silberberg G, Markram H (2007) Disynaptic inhibition between neocortical pyramidal cells mediated by Martinotti cells. Neuron 53:735-746.

Silvani A, Dampney RA (2013) Central control of cardiovascular function during sleep. Am J Physiol Heart Circ Physiol 305:H1683-1692.

Silvani A, Calandra-Buonaura G, Benarroch EE, Dampney RA, Cortelli P (2015) Bidirectional interactions between the baroreceptor reflex and arousal: an update. Sleep Med 16:210-216.

Somers VK, Dyken ME, Mark AL, Abboud FM (1993) Sympathetic-nerve activity during sleep in normal subjects. N Engl J Med 328:303-307.

Starzl TE, Magoun HW (1951) Organization of the diffuse thalamic projection system. J Neurophysiol 14:133-146.

Steininger TL, Gong H, McGinty D, Szymusiak R (2001) Subregional organization of preoptic area/anterior hypothalamic projections to arousal-related monoaminergic cell groups. J Comp Neurol 429:638-653.

Steriade M (2003) The corticothalamic system in sleep. Front Biosci 8:d878-899.

Steriade M (2006) Grouping of brain rhythms in corticothalamic systems. Neuroscience 137:1087-1106.

Steriade M, Contreras D (1995) Relations between cortical and thalamic cellular events during transition from sleep patterns to paroxysmal activity. J Neurosci 15:623-642.

Steriade M, Nunez A, Amzica F (1993) A novel slow (< 1 Hz) oscillation of neocortical neurons in vivo: depolarizing and hyperpolarizing components. J Neurosci 13:3252-3265.

Steriade M, Dossi RC, Pare D, Oakson G (1991) Fast oscillations (20-40 Hz) in thalamocortical systems and their potentiation by mesopontine cholinergic nuclei in the cat. Proc Natl Acad Sci U S A 88:4396-4400.

Steriade M, Datta S, Pare D, Oakson G, Curro Dossi RC (1990) Neuronal activities in brain-stem cholinergic nuclei related to tonic activation processes in thalamocortical systems. J Neurosci 10:2541-2559.

Stratmann M, Schibler U (2006) Properties, entrainment, and physiological functions of mammalian peripheral oscillators. J Biol Rhythms 21:494-506.

Stuck BA (2010) Chemosensory processing during sleep. HNO 58:564-568.

Stuck BA, Moutsis TT, Bingel U, Sommer JU (2016) Chemosensory stimulation during sleep - Arousal responses to gustatory stimulation. Neuroscience 322:326-332.

Stuck BA, Stieber K, Frey S, Freiburg C, Hormann K, Maurer JT, Hummel T (2007) Arousal responses to olfactory or trigeminal stimulation during sleep. Sleep 30:506-510.

Suntsova N, Szymusiak R, Alam MN, Guzman-Marin R, McGinty D (2002) Sleep-waking discharge patterns of median preoptic nucleus neurons in rats. J Physiol 543:665-677.

Suntsova N, Guzman-Marin R, Kumar S, Alam MN, Szymusiak R, McGinty D (2007) The median preoptic nucleus reciprocally modulates activity of arousal-related and sleep-related neurons in the perifornical lateral hypothalamus. J Neurosci 27:1616-1630.

Szymusiak R, McGinty D (1989) Sleep-waking discharge of basal forebrain projection neurons in cats. Brain Res Bull 22:423-430.

Szymusiak R, Alam N, Steininger TL, McGinty D (1998) Sleep-waking discharge patterns of ventrolateral preoptic/anterior hypothalamic neurons in rats. Brain Res 803:178-188.

Tacikowski P, Cygan HB, Nowicka A (2014) Neural correlates of own and close-other's name recognition: ERP evidence. Front Hum Neurosci 8:194.

Takahashi K, Lin JS, Sakai K (2009) Characterization and mapping of sleep-waking specific neurons in the basal forebrain and preoptic hypothalamus in mice. Neuroscience 161:269-292.

Takahashi N, Oertner TG, Hegemann P, Larkum ME (2016) Active cortical dendrites modulate perception. Science 354:1587-1590.

Thabit H, Hartnell S, Allen JM, Lake A, Wilinska ME, Ruan Y, Evans ML, Coll AP, Hovorka R (2016) Closed-loop insulin delivery in inpatients with type 2 diabetes: a randomised, parallel-group trial. Lancet Diabetes Endocrinol.

Thannickal TC, Moore RY, Nienhuis R, Ramanathan L, Gulyani S, Aldrich M, Cornford M, Siegel JM (2000) Reduced number of hypocretin neurons in human narcolepsy. Neuron 27:469-474.

Thompson CL, Li L (2012) Association of sleep duration and breast cancer OncotypeDX recurrence score. Breast Cancer Res Treat 134:1291-1295.

Thompson CL, Larkin EK, Patel S, Berger NA, Redline S, Li L (2011) Short duration of sleep increases risk of colorectal adenoma. Cancer 117:841-847.

Timofeev I, Bazhenov M, Seigneur J, Sejnowski T (2012) Neuronal Synchronization and Thalamocortical Rhythms in Sleep, Wake and Epilepsy. In: Jasper's Basic Mechanisms of the Epilepsies, 4th Edition (Noebels JL, Avoli M, Rogawski MA, Olsen RW, Delgado-Escueta AV, eds). Bethesda (MD).

Tobaldini E, Pecis M, Montano N (2014) Effects of acute and chronic sleep deprivation on cardiovascular regulation. Arch Ital Biol 152:103-110.

Tobaldini E, Costantino G, Solbiati M, Cogliati C, Kara T, Nobili L, Montano N (2016) Sleep, sleep deprivation, autonomic nervous system and cardiovascular diseases. Neurosci Biobehav Rev.

Tobler I, Borbely AA (1986) Sleep EEG in the rat as a function of prior waking. Electroencephalogr Clin Neurophysiol 64:74-76.

Tobler I, Borbely AA, Groos G (1983) The effect of sleep deprivation on sleep in rats with suprachiasmatic lesions. Neurosci Lett 42:49-54.

Tobler I, Franken P, Scherschlicht R (1990) Sleep and EEG spectra in the rabbit under baseline conditions and following sleep deprivation. Physiol Behav 48:121-129.

Tobler II, Franken P, Trachsel L, Borbely AA (1992) Models of sleep regulation in mammals. J Sleep Res 1:125-127.

Tononi G, Cirelli C (2003) Sleep and synaptic homeostasis: a hypothesis. Brain Res Bull 62:143-150.

Torterolo P, Falconi A, Morales-Cobas G, Velluti RA (2002) Inferior colliculus unitary activity in wakefulness, sleep and under barbiturates. Brain Res 935:9-15.

Trachsel L, Tobler I, Borbely AA (1988) Electroencephalogram analysis of non-rapid eye movement sleep in rats. Am J Physiol 255:R27-37.

Trachsel L, Edgar DM, Seidel WF, Heller HC, Dement WC (1992) Sleep homeostasis in suprachiasmatic nuclei-lesioned rats: effects of sleep deprivation and triazolam administration. Brain Res 589:253-261.

Triarhou LC (2006) The percipient observations of Constantin von Economo on encephalitis lethargica and sleep disruption and their lasting impact on contemporary sleep research. Brain Res Bull 69:244-258.

Trivedi P, Yu H, MacNeil DJ, Van der Ploeg LH, Guan XM (1998) Distribution of orexin receptor mRNA in the rat brain. FEBS Lett 438:71-75.

Uchida S, Maloney T, March JD, Azari R, Feinberg I (1991) Sigma (12-15 Hz) and delta (0.3-3 Hz) EEG oscillate reciprocally within NREM sleep. Brain Res Bull 27:93-96.

Uschakov A, Gong H, McGinty D, Szymusiak R (2007) Efferent projections from the median preoptic nucleus to sleep- and arousal-regulatory nuclei in the rat brain. Neuroscience 150:104-120.

Uygun DS, Ye Z, Zecharia AY, Harding EC, Yu X, Yustos R, Vyssotski AL, Brickley SG, Franks NP, Wisden W (2016) Bottom-Up versus Top-Down Induction of Sleep by Zolpidem Acting on Histaminergic and Neocortex Neurons. J Neurosci 36:11171-11184.

Vanhatalo S, Voipio J, Kaila K (2005) Full-band EEG (FbEEG): an emerging standard in electroencephalography. Clin Neurophysiol 116:1-8.

Vanhatalo S, Palva JM, Holmes MD, Miller JW, Voipio J, Kaila K (2004) Infraslow oscillations modulate excitability and interictal epileptic activity in the human cortex during sleep. Proc Natl Acad Sci U S A 101:5053-5057.

Venner A, Anaclet C, Broadhurst RY, Saper CB, Fuller PM (2016) A Novel Population of Wake-Promoting GABAergic Neurons in the Ventral Lateral Hypothalamus. Curr Biol 26:2137-2143.

Vincent JL, Patel GH, Fox MD, Snyder AZ, Baker JT, Van Essen DC, Zempel JM, Snyder LH, Corbetta M, Raichle ME (2007) Intrinsic functional architecture in the anaesthetized monkey brain. Nature 447:83-86.

Volkov A, Waite AJ, Wooten JD, Markin VS (2012) Circadian rhythms in biologically closed electrical circuits of plants. Plant Signal Behav 7:282-284.

Vorster AP, Born J (2015) Sleep and memory in mammals, birds and invertebrates. Neurosci Biobehav Rev 50:103-119.

Vyazovskiy VV, Achermann P, Borbely AA, Tobler I (2004) The dynamics of spindles and EEG slow-wave activity in NREM sleep in mice. Arch Ital Biol 142:511-523.

Vyazovskiy VV, Olcese U, Hanlon EC, Nir Y, Cirelli C, Tononi G (2011) Local sleep in awake rats. Nature 472:443-447.

Watanabe T, Simada Z (1973) Pharmacological properties of cat's collicular auditory neurons. Jpn J Physiol 23:291-308.

Watson BO, Levenstein D, Greene JP, Gelinas JN, Buzsaki G (2016) Network Homeostasis and State Dynamics of Neocortical Sleep. Neuron 90:839-852.

Weber F, Dan Y (2016) Circuit-based interrogation of sleep control. Nature 538:51-59.
Werth E, Dijk DJ, Achermann P, Borbely AA (1996) Dynamics of the sleep EEG after an early evening nap: experimental data and simulations. Am J Physiol 271:R501-510.
Williams HL, Hammack JT, Daly RL, Dement WC, Lubin A (1964) Responses to Auditory Stimulation, Sleep Loss and the Eeg Stages of Sleep. Electroencephalogr Clin Neurophysiol 16:269-279.
Wimmer RD, Astori S, Bond CT, Rovo Z, Chatton JY, Adelman JP, Franken P, Luthi A (2012) Sustaining sleep spindles through enhanced SK2-channel activity consolidates sleep and elevates arousal threshold. J Neurosci 32:13917-13928.
Wisor JP, Pasumarthi RK, Gerashchenko D, Thompson CL, Pathak S, Sancar A, Franken P, Lein ES, Kilduff TS (2008) Sleep deprivation effects on circadian clock gene expression in the cerebral cortex parallel electroencephalographic differences among mouse strains. J Neurosci 28:7193-7201.
Xie L, Kang H, Xu Q, Chen MJ, Liao Y, Thiyagarajan M, O'Donnell J, Christensen DJ, Nicholson C, Iliff JJ, Takano T, Deane R, Nedergaard M (2013) Sleep drives metabolite clearance from the adult brain. Science 342:373-377.
Yamazaki S, Numano R, Abe M, Hida A, Takahashi R, Ueda M, Block GD, Sakaki Y, Menaker M, Tei H (2000) Resetting central and peripheral circadian oscillators in transgenic rats. Science 288:682-685.
Yan J, Zhang Y, Ehret G (2005) Corticofugal shaping of frequency tuning curves in the central nucleus of the inferior colliculus of mice. J Neurophysiol 93:71-83.
Yoo SS, Gujar N, Hu P, Jolesz FA, Walker MP (2007) The human emotional brain without sleep--a prefrontal amygdala disconnect. Curr Biol 17:R877-878.
Zeman A (1998) Persistent vegetative state. Lancet 351:144.
Zhdanova IV (2005) Melatonin as a hypnotic: pro. Sleep Med Rev 9:51-65.
Zhdanova IV, Geiger DA, Schwagerl AL, Leclair OU, Killiany R, Taylor JA, Rosene DL, Moss MB, Madras BK (2002) Melatonin promotes sleep in three species of diurnal nonhuman primates. Physiol Behav 75:523-529.

# G. ARTICLES

NEUROSCIENCE



# Coordinated infraslow neural and cardiac oscillations mark fragility and offline periods in mammalian sleep

Sandro Lecci,[1] Laura M. J. Fernandez,[1]* Frederik D. Weber,[2]* Romain Cardis,[1] Jean-Yves Chatton,[1] Jan Born,[2] Anita Lüthi[1]†

**Rodents sleep in bouts lasting minutes; humans sleep for hours. What are the universal needs served by sleep given such variability? In sleeping mice and humans, through monitoring neural and cardiac activity (combined with assessment of arousability and overnight memory consolidation, respectively), we find a previously unrecognized hallmark of sleep that balances two fundamental yet opposing needs: to maintain sensory reactivity to the environment while promoting recovery and memory consolidation. Coordinated 0.02-Hz oscillations of the sleep spindle band, hippocampal ripple activity, and heart rate sequentially divide non–rapid eye movement (non-REM) sleep into offline phases and phases of high susceptibility to external stimulation. A noise stimulus chosen such that sleeping mice woke up or slept through at comparable rates revealed that offline periods correspond to raising, whereas fragility periods correspond to declining portions of the 0.02-Hz oscillation in spindle activity. Oscillations were present throughout non-REM sleep in mice, yet confined to light non-REM sleep (stage 2) in humans. In both species, the 0.02-Hz oscillation predominated over posterior cortex. The strength of the 0.02-Hz oscillation predicted superior memory recall after sleep in a declarative memory task in humans. These oscillations point to a conserved function of mammalian non-REM sleep that cycles between environmental alertness and internal memory processing in 20- to 25-s intervals. Perturbed 0.02-Hz oscillations may cause memory impairment and ill-timed arousals in sleep disorders.**

## INTRODUCTION

All mammals benefit from sleep in fundamental aspects for brain and body (*1*, *2*). For sleep to be beneficial, it must be of sufficient duration and physiological continuity. Conversely, sleep needs to retain a certain degree of fragility, because all sleeping organisms remain capable of a behavioral arousal response to salient stimuli and potential threats. To date, it is unclear how sleep generates advantageous effects while maintaining sensory responsiveness and how the two opposite needs for continuity and fragility are balanced. Recently, given the enormous differences in sleep fragmentation between mammalian species (*3*), the idea of universal beneficial functions of sleep for all mammals has even been challenged (*4*).

Ongoing electrical rhythms in the thalamocortical loops of the sleeping brain are central to disrupt sensory information processing. Among these, sleep spindles are particularly efficient in attenuating the likelihood that sensory stimuli arrive in cortex (*5*, *6*). Spindles are electroencephalographic hallmarks of non–rapid eye movement (non-REM) sleep in the sigma (10 to 15 Hz) power range that occur preferentially during human "light" sleep (*7*) and that last for ~0.5 to 3 s throughout mammals (*8*). Sensory processing thus varies momentarily along with the spectral dynamics of thalamocortical rhythms and contributes to sleep fragility (*9*). Non-REM sleep is also accompanied by marked changes in the autonomic system, notably including decreases in heart rate that recover before transitions to REM sleep or awakening (*10*). Therefore, periods of sleep fragility, during which awakenings are more likely to occur, should involve the autonomic system. To date, however, an analysis of sleep fragility periods based on a combined assessment of sensory processing, spectral dynamics, and autonomic parameters has not been carried out. Moreover, how fragility phases interchange with phases of continuity and how these concur with hallmarks of memory processing during sleep remain open questions.

[1]Department of Fundamental Neurosciences, University of Lausanne, 1005 Lausanne, Switzerland. [2]Institute of Medical Psychology and Behavioral Neurobiology, University of Tübingen, 72076 Tübingen, Germany.
*These authors contributed equally to this work.
†Corresponding author. Email: anita.luthi@unil.ch

## RESULTS

### Undisturbed non-REM sleep in mice shows a 0.02-Hz oscillation in sigma power

To examine whether mouse non-REM sleep shows microarchitectural dynamics indicative of variable fragility, we used polysomnography [electroencephalography (EEG)/electrocorticography (ECoG) and electromyography (EMG)] in freely moving mice (*11*) and inspected the temporal evolution of two major spectral bands characteristic for non-REM sleep: the slow-wave activity (SWA; 0.75 to 4 Hz) and the sigma (10 to 15 Hz) power band (*8*). Epochs of non-REM sleep were selected during the first 100 min after onset of the light phase [zeitgeber time 0 (ZT0)], during which mice slept ~63% of their time ($n$ = 18 mice). During this period, non-REM sleep occurred in bouts ranging from 8 to >512 s in duration, with a mean length of 108.6 ± 8.1 s. Both sigma power and SWA were elevated during non-REM sleep and decreased during waking or REM sleep (Fig. 1A and fig. S1). Unexpectedly, we noticed that sigma power, but not SWA, displayed marked variations that recurred periodically in both short and long non-REM sleep bouts (Fig. 1B and fig. S1). We assessed the dynamics of sigma power across time for consolidated non-REM sleep periods ≥96 s (mean duration, 180.4 ± 8.8 s) (fig. S2). This revealed a predominant frequency of 0.021 ± 0.001 Hz (Fig. 1C) in a fast Fourier transform (FFT), corresponding to a cycle length of 47.6 ± 2.1 s. In contrast, such a prominent peak was not present for the SWA time course (Fig. 1C), and it was markedly weaker in frequency bands adjacent to the sigma band ($n$ = 18; Friedman's test, $P = 7.9 \times 10^{-5}$; Fig. 1D). Further analyses and computational simulations confirmed that sigma power oscillated robustly in the 0.02-Hz frequency range (fig. S3). First, a 0.02-Hz oscillation emerged when the analysis was restricted to long non-REM sleep bouts (≥192 s, corresponding to 32.08% of all the

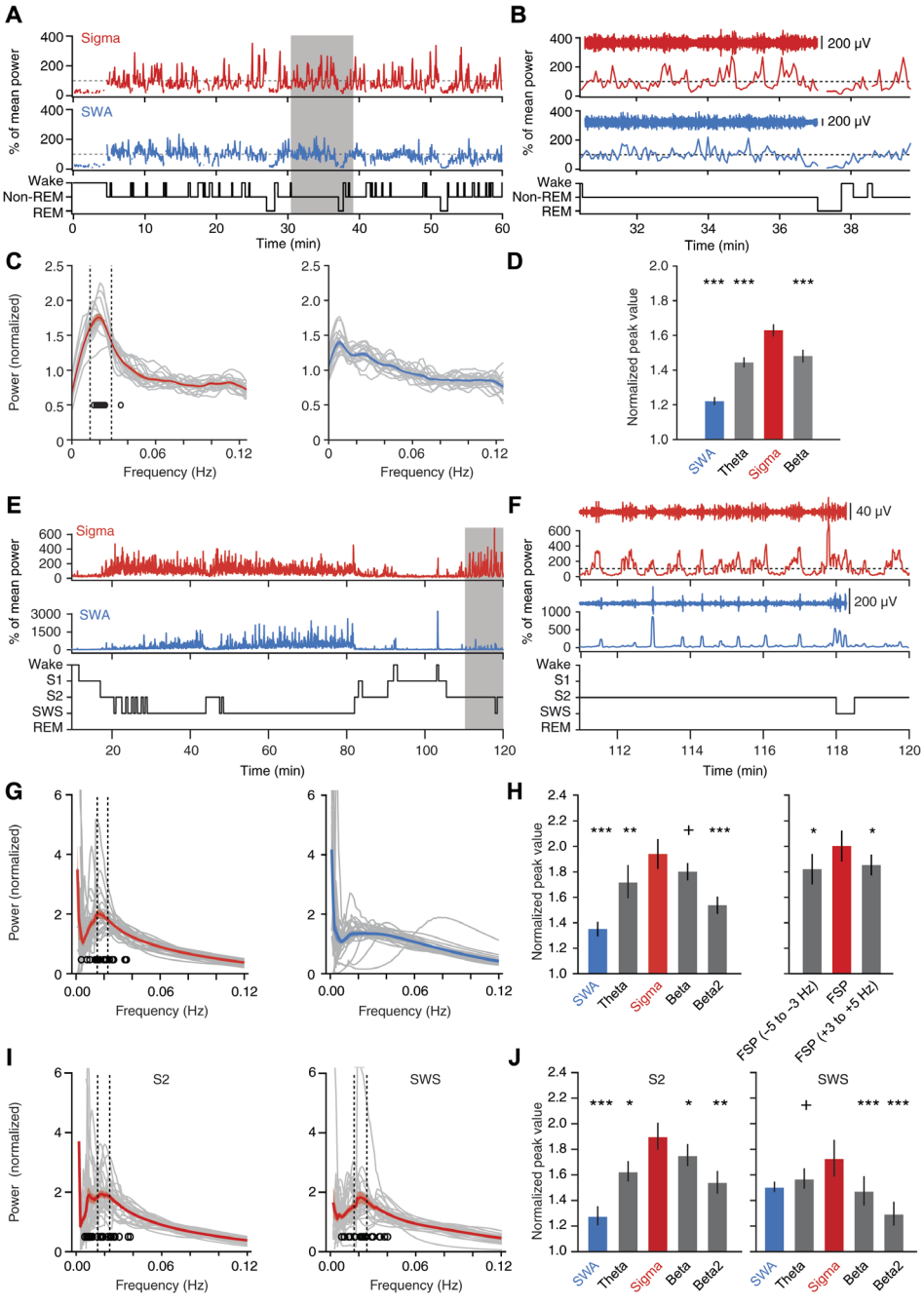


**Fig. 1. The 0.02-Hz oscillation in sigma power in undisturbed non-REM sleep of mice and humans.** (**A** to **D**) Sleep analysis in freely moving mice ($n$ = 18). (A and B) Sigma (red; 10 to 15 Hz) and SWA (blue; 0.75 to 4 Hz) power time course for a single mouse, with hypnograms shown below. Gray-shaded area in (A) is expanded in (B), with aligned band-pass–filtered ECoG traces. (C) FFT of power time course for sigma (left) and SWA (right) for individual mice (gray traces, $n$ = 18) and for the average across mice (color + shading, means ± SEM). Open circles denote FFT peaks obtained from Gaussian fits (their SD was 0.015 Hz). Vertical dotted lines indicate mean peak frequency ± 0.5 SD. Minor ticks are added to indicate the 0.02-Hz value on the frequency axis. (D) Mean peak values from (C) for sigma power, SWA, theta (6 to 10 Hz), and beta (16 to 20 Hz) bands (Friedman rank sum test; $P = 4.9 \times 10^{-8}$, post hoc Wilcoxon signed-rank tests relative to sigma power, $P = 7.63 \times 10^{-6}$ for SWA; $P = 3.81 \times 10^{-5}$ for theta; $P = 1.53 \times 10^{-5}$). (**E** to **J**) Sleep analysis in humans ($n$ = 27). (E and F) Same as (A) and (B) for a single human subject (sigma, 10 to 15 Hz; SWA, 0.5 to 4 Hz). (G) Power spectral profiles for sigma power and SWA time course during non-REM sleep (S2 + SWS) graphed as in (C). The open circles indicate the peak of Gaussian fits, which show an SD of 0.008 Hz. (H) Left: Same as (D), calculated over all non-REM sleep (theta, 4 to 8 Hz; beta, 16 to 20 Hz; beta2, 20 to 24 Hz). Same statistics as (D): $P = 3.5 \times 10^{-4}$; post hoc Wilcoxon signed-rank tests with $P = 9.5 \times 10^{-6}$ for SWA; $P = 0.009$ for theta; $P = 0.095$ for beta; $P = 4.3 \times 10^{-4}$ for beta2. Right: Individual fast spindle power peaks (FSP ± 1 Hz) and adjacent frequency bands. Same statistics as in (C): $P = 0.034$ for Friedman rank sum test; $P = 0.015$ for −5 to −3 Hz; $P = 0.032$ for +3 to +5 Hz. (I) Same analysis as (G), restricted to S2 or to SWS and sigma power. (J) Left: Power analysis as in (H) restricted to S2 sleep revealed a prominent peak for sigma power over other frequency bands ($n$ = 27; Friedman rank sum test, $P = 8.5 \times 10^{-6}$, followed by Wilcoxon signed-rank tests with respect to sigma power; $P = 2.5 \times 10^{-6}$ for SWA; $P = 0.023$ for theta; $P = 0.011$ for beta; $P = 0.002$ for beta2). Right: As left for SWS only (same statistics as the left panel: $P = 1.8 \times 10^{-4}$; $P = 0.11$ for SWA; $P = 0.052$ for theta; $P = 6 \times 10^{-4}$ for beta; $P = 1.6 \times 10^{-4}$ for beta2). $^{+}P < 0.1$, $^{*}P < 0.05$, $^{**}P < 0.01$, $^{***}P < 0.001$.

bouts ≥96 s) (fig. S3, A to F), demonstrating that sigma power cycles on a 50-s time scale during consolidated non-REM sleep. Second, computational simulations indicated that a true sinusoidal component at ~0.02 Hz rather than scale-free power dynamics underlay the peak in the FFT (fig. S3, G to J). Third, autocorrelations displayed side peaks with a periodicity of 52.6 ± 0.83 s (paired *t* test compared to shuffled data, $t = 3.82$, $P = 0.0015$; fig. S4, A and B). These combined results demonstrate that mouse non-REM sleep contains a 0.02-Hz oscillation of sigma power dynamics, corresponding to a periodicity of ~50 s.

### Undisturbed non-REM sleep in humans shows a 0.02-Hz oscillation in sigma power

To explore whether this infraslow 0.02-Hz oscillation exists in higher mammals, we carried out a comparable power analysis for human sleep (fig. S5). As expected, sigma power was high during stage 2 (S2) sleep (light sleep) and declined during slow-wave sleep (SWS; "deep" sleep) (*7*) when SWA emerged (Fig. 1E and fig. S6). The 0.02-Hz oscillation was present in the sigma power band (10 to 15 Hz) with maximal amplitudes comparable to those in mice (Fig. 1F and fig. S7) but was attenuated in the SWA band (Fig. 1, G and H). When analyzed across all non-REM sleep (S2 + SWS), human sigma power oscillations had a periodicity of 0.019 ± 0.001 Hz ($n = 27$), corresponding to a cycle length of 52.6 ± 2.6 s, comparable to mice. The sigma power band showed the most pronounced dynamics of around 0.02 Hz, while adjacent frequency bands displayed distinctly weaker periodicity ($n = 27$; Friedman's test, $P < 3.5 \times 10^{-4}$; Fig. 1H). Furthermore, SWA lacked prominent infraslow dynamics and showed a minor spectral peak (Fig. 1H). In humans, there are fast (12 to 15 Hz) and slow spindles (9 to 12 Hz), with the former being prevalent during S2 and providing a distinct peak in individual power spectra (*12*). When focusing our analysis on the fast spindles, we found that 0.02-Hz oscillations emerged strongest in a 2-Hz band around the fast spindle peak (FSP; 13.16 ± 0.12 Hz) and fell off in adjacent bands (Fig. 1H). The 0.02-Hz oscillation of sigma power appeared to be more prominent in S2 than in SWS (Fig. 1, I and J). Autocorrelations confirmed the oscillatory nature of sigma power dynamics, displaying side peaks with a periodicity of 53.0 ± 2.73 s (Wilcoxon signed-rank test for periodicity, $P = 0.026$; fig. S4, C and D). Together, these data unravel a 0.02-Hz oscillation common to both human and mouse non-REM sleep that is prevalent for sigma power and most prominent for fast spindles in human non-REM sleep.

### The 0.02-Hz oscillation shows regional specificity in both mice and humans

To assess whether 0.02-Hz oscillations were present in local cortical circuits, we performed multisite referential local field potential (LFP) recordings across four cortical areas in combination with polysomnography in sleeping head-fixed mice ($n = 6$). Under these recordings conditions, the three major vigilance states wake, non-REM, and REM sleep showed spectral profiles comparable to those of freely moving animals (fig. S8). The 0.02-Hz oscillation in sigma power of non-REM sleep was present in the simultaneously recorded EEG and LFP signals (Fig. 2, A and B), yet the latter showed that the amplitude of the oscillation depended on cortical area [$n = 6$ mice; repeated-measures (RM) analysis of variance (ANOVA) for factors "frequency" and "area"; $F_{1,5} = 145.8$, $P = 6.88 \times 10^{-5}$; $F_{4,20} = 19.23$, $P = 1.25 \times 10^{-6}$; Fig. 2C]. Primary (SI) and secondary (SII) somatosensory cortices showed a major 0.02-Hz peak in the sigma compared to the SWA power time course ($n = 6$; paired *t* test, $t = 17.88$, $P = 1.01 \times 10^{-5}$ for SI; $t = 5.72$, $P = 0.0023$ for SII; Fig. 2D), yet this peak was minor in auditory cortex (AC) and medial prefrontal cortex (mPFC) ($n = 6$; paired *t* test, $t = 2.83$, $P = 0.037$ for AC; $t = 2.02$, $P = 0.1$ for mPFC).

The topography of 0.02-Hz oscillations in humans was assessed in an additional group of $n = 24$ subjects with full-night polysomnographic recordings (Fig. 3A and fig. S6). These data confirmed that the 0.02-Hz oscillation in sigma power was more pronounced during S2 than SWS. Furthermore, the 2-Hz band around the FSP was the strongest oscillatory component in these comparisons (fig. S6C). The 0.02-Hz oscillations showed a maximum over parietal derivations for power in both the sigma and the FSP band and declined toward anterior central and frontal areas. However, the relative dominance of the 0.02-Hz oscillation in the sigma and FSP bands over adjacent frequency bands and SWA persisted along the parietofrontal axis (Fig. 3B).

### The 0.02-Hz oscillation divides non-REM sleep into periods of high and low fragility to acoustic noise

If 0.02-Hz oscillations are relevant for sleep fragility and continuity, then they should be accompanied by a varying arousability of mice in response to external stimuli. We chose acoustic stimuli such that they lasted half a cycle of the 0.02-Hz oscillation (20 s). This long-duration noise would probe the propensity to arouse over the sustained periods of low and high sigma power and hence reveal whether these corresponded to states of distinct fragility. A white noise stimulus of 90-dB sound pressure level (SPL) yielded an arousal success rate of 38.7 ± 8.6% ($n = 10$), as assessed by polysomnography (Fig. 4A), and trials were post hoc–classified on the basis of ECoG (EEG)/EMG data in "wake-up" or "sleep-through" trials (Fig. 4B). Noise was played as soon as the mouse was in consolidated non-REM sleep (for ≥40 s) and at most once every 4 min, without knowledge of the oscillation phase. In a wake-up trial from a single mouse, sigma power was at its maximum before noise onset, such that noise exposure fell within a phase of declining power. In contrast, for a sleep-through trial of the same mouse, sigma power had just exited the trough, and noise was played within the phase of incrementing power (Fig. 4C). This phase difference between wake-up and sleep-through trials was robust when calculated across trials and mice (wake-up, $n = 9$ mice; sleep-through, $n = 10$ mice; RM ANOVA for factors "time" and "behavioral outcome"; $F_{4.78,81.27} = 3.81$, $P < 0.0042$, after Greenhouse-Geisser correction; Fig. 4D, left). Moreover, the time course corresponded to the 0.02-Hz oscillations during undisturbed sleep (Fig. 4D, right; see also Fig. 1), whereas SWA time course was indistinguishable between the wake-up and sleep-through trials (wake-up, $n = 9$ mice; sleep-through, $n = 10$ mice; RM ANOVA for factors "time" and "behavioral outcome"; $F_{4.84,82.20} = 1.86$, $P = 0.11$, after Greenhouse-Geisser correction; Fig. 4E). Therefore, as shown schematically in Fig. 4F, the 0.02-Hz sigma power oscillations seem to divide mouse non-REM sleep into alternating periods of successive high and low responsiveness to external stimuli. To test this hypothesis, we analyzed the phases of the 0.02-Hz oscillation before noise onset and found that values for the wake-up and sleep-through trials fell onto opposite halves in a polar plot of oscillation phases (Fig. 4, G and H). Therefore, wake-ups and sleep-throughs occur during declining and rising sigma power levels, respectively. As wake-ups took place either early or late during the 20-s noise exposure, we asked whether the declining sigma power phase could be further subdivided according to the occurrence of wake-ups. Sigma power was significantly lower for early (taking place within <8 s after noise onset) than for late (12 to 16 s after noise onset) wake-ups (early arousals, $n = 6$; late arousals, $n = 9$; RM ANOVA for factors "time" and "behavioral

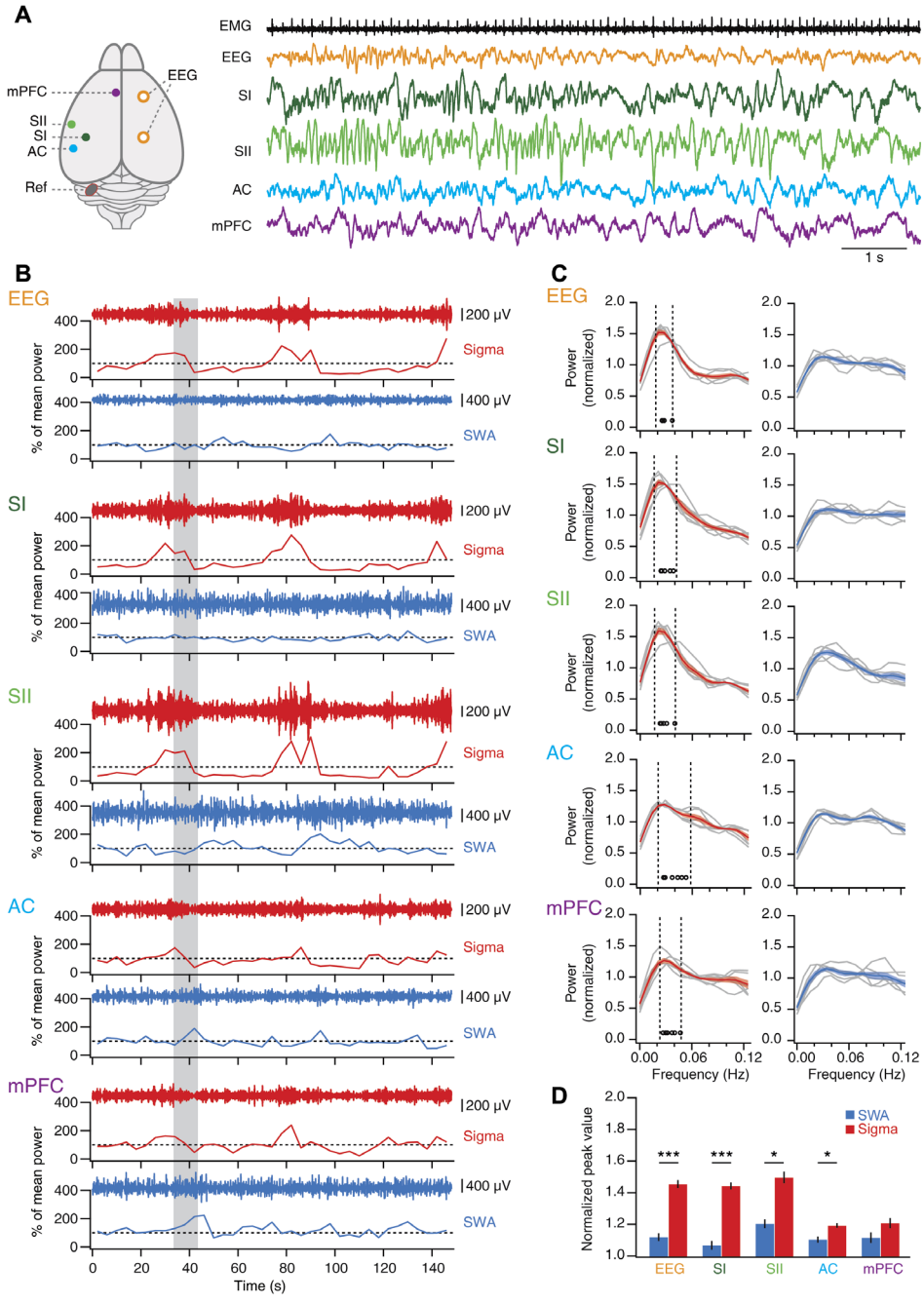


**Fig. 2. The 0.02-Hz oscillation is present in local cortical areas and predominates in somatosensory cortex.** (**A**) Top view of mouse brain with indication of recording sites and with corresponding representative traces obtained during non-REM sleep scored on the basis of EEG/EMG recordings. (**B**) Sigma (red) and SWA (blue) power time course for a single non-REM sleep bout recorded simultaneously from all areas. The gray-shaded area indicates the time corresponding to the traces in (A). Dotted lines indicate 100%. (**C**) FFT of power time course for sigma (left) and SWA (right) for individual mice (gray traces, $n = 6$) and for the average across mice (color + shading, means ± SEM). Open circles denote FFT peaks obtained from Gaussian fits. Vertical dotted lines indicate mean peak frequency ± 0.5 SD. (**D**) Mean peak values from (C) for sigma power and SWA for all brain areas and EEG recordings, analyzed as in Fig. 1D. RM ANOVA with factors "area" and "frequency"; area, $P = 1.25 \times 10^{-6}$; frequency, $P = 6.88 \times 10^{-5}$; post hoc paired $t$ tests; EEG, $t = 11.19$, $P = 9.93 \times 10^{-5}$; SI, $t = 17.88$, $P = 1.01 \times 10^{-5}$; SII, $t = 5.72$, $P = 0.0023$; AC, $t = 2.83$, $P = 0.037$; mPFC, $t = 2.02$, $P = 0.1$; $^{*}P < 0.01$, $^{***}P < 0.001$. SI and SII, primary and secondary somatosensory cortex; AC, auditory cortex; mPFC, medial prefrontal cortex; Ref, reference.

outcome"; $F_{4,52} = 2.72$, $P = 0.04$; fig. S9), suggesting a phase advancement for early over late arousals. The progression into the declining sigma power period thus reflects the entry into a period of sleep fragility. Last, we asked whether the total duration of the non-REM sleep before noise exposure affected responsiveness. Both wake-up and sleep-through trials were broadly distributed across the range of non-REM sleep bout durations in mice (fig. S10), ruling out bout duration as a determinant of behavioral outcome to noise exposure.

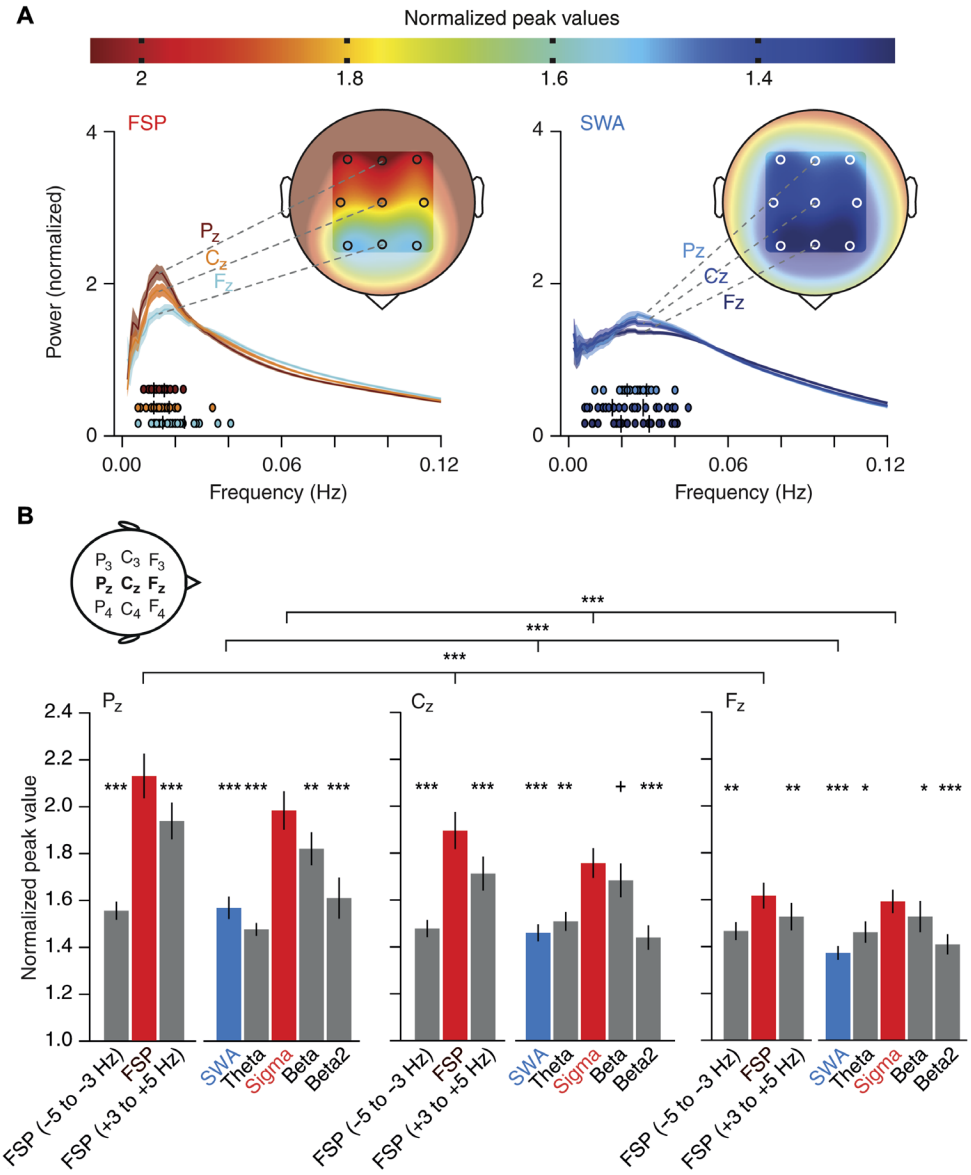


**Fig. 3. Regional cortical topology of the 0.02-Hz oscillation in humans.** (**A**) Top: Color scale that indicates the mean normalized power values calculated from the average 0.02-Hz oscillation band (±0.5 SD around average peak values) during non-REM sleep. Bottom: The power spectral profiles for the FSP band (FSP ± 1 Hz, ~13 Hz, left) and the SWA band (right) averaged across subjects (color + shading, means ± SEM) displayed for representative midline electrodes ($F_Z$, $C_Z$, and $P_Z$); analysis as in Fig. 1G. Coloring for power spectral profiles and each subject's 0.02-Hz oscillation peak (filled circles underneath the power spectral profiles) corresponds to normalized peak values in the color scale. Insets show human head with an approximate topography of the mean normalized peak power values for all nine EEG electrodes ($F_3$, $F_Z$, $F_4$, $C_3$, $C_Z$, $C_4$, $P_3$, $P_Z$, and $P_4$). (**B**) Mean (±SEM) normalized peak values for FSP band and adjacent frequency bands (FSP −5 to −3 Hz and FSP +3 to +5 Hz), as well as sigma power (10 to 15 Hz), SWA (0.5 to 4 Hz), theta (4 to 8 Hz), beta (16 to 20 Hz), and beta2 (20 to 24 Hz) bands separate for the three midline electrodes ($F_Z$, $C_Z$, and $P_Z$); analysis as in Fig. 1H with data from the participants of the memory study ($n = 24$). Additional Friedman rank sum test between three midline electrodes for FSP band ($P = 3.5 \times 10^{-8}$), sigma ($P = 6.35 \times 10^{-9}$), and SWA ($P = 2.8 \times 10^{-6}$) (top three horizontal lines), with post hoc–paired comparisons along decreases from $P_z$ to $C_z$ as well as $C_z$ to $F_z$ separate for those three frequency bands (Wilcoxon signed-rank test, all $P_s < 0.0036$). For consistency with the core study analyses, which relied on nonparametric statistics, the same statistical tests were performed here. $^{+}P < 0.1$, $^{*}P < 0.05$, $^{**}P < 0.01$, $^{***}P < 0.001$ for Wilcoxon signed-rank test relative to FSP band (left bar groups) and relative to the sigma band (right bar groups).

## The offline periods are coordinated with hippocampal ripples

We further characterized the 0.02-Hz oscillation by examining the timing of ripples (150 to 250 Hz) in the CA1 area of the hippocampus, which represent an established index for offline memory processing (*13*). Sigma power and ripple power were correlated such that ripple activity augmentations preceded sigma power rises by ~4 s ($n = 6$; fig. S11). Thus, hippocampal ripple activity was high during periods of increasing sigma power, during which mice maintained sleep while being exposed to noise. This suggests that more pronounced 0.02-Hz oscillations strengthen offline consolidation of hippocampus-dependent memory.

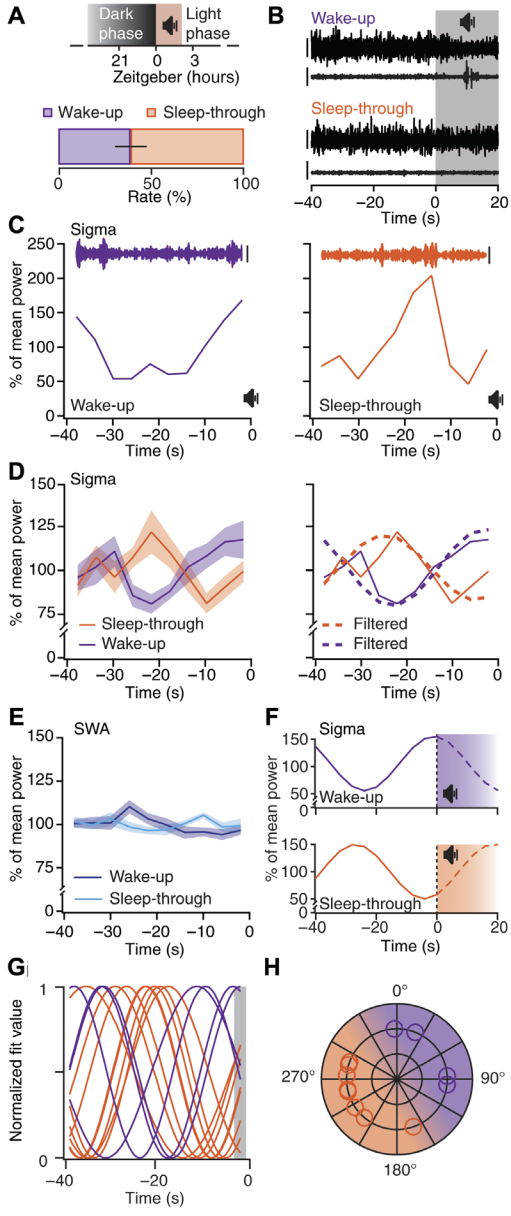


**Fig. 4. The 0.02-Hz oscillation imposes periods of high and low fragility to acoustic noise.** (**A**) Top: Acoustic stimulation protocol. Bottom: Percentage (means ± SEM) of wake-up and sleep-through trials ($n$ = 10 mice). (**B**) Representative EEG (ECoG) (upper trace)/EMG (lower trace) traces from wake-up and sleep-through trials. Gray-shaded area indicates period of noise exposure. Scale bars, 400 and 80 μV for EEG(ECoG)/EMG. (**C**) Time course of sigma power for the 40 s of non-REM sleep before noise onset for a wake-up (violet) and a sleep-through (orange) trial [same data as (B)]. Insets show corresponding band-pass–filtered (10 to 15 Hz) EEG (ECoG) traces. Scale bars, 200 μV. (**D**) Left: Means ± SEM sigma power time course for wake-up and sleep-through trials ($n$ = 9 and 10, respectively; RM ANOVA for factors "time" and "behavioral outcome", Greenhouse-Geisser–corrected, $P < 0.0042$). Right: Overlay of the traces from the left, once unfiltered (continuous line) and once band-pass–filtered (dotted lines) for the frequencies corresponding to 0.02-Hz oscillation peak ± 1 width (see Fig. 1C). (**E**) Means ± SEM SWA time course as in (D) [same statistics as in (D), $P$ = 0.11]. (**F**) Projected time course of sigma power during noise exposure for wake-up and sleep-through trials. (**G**) Waveforms for average wake-up ($n$ = 4) and sleep-through ($n$ = 8) trials obtained through sinusoidal fits. (**H**) Polar representation of sigma power phases decoded from (G) (shaded area; 0°, peak), with shading of corresponding intervals for high (purple) and low (orange) responsiveness to stimulation.

### The strength of the 0.02-Hz oscillation correlates with overnight consolidation of declarative memory in humans

To explore the role of 0.02-Hz oscillations in memory consolidation, we correlated the explicit postsleep recall on an episodic memory task (presented before sleep) in humans with oscillation peaks and conventional measures of spindle density (*14*). Recall correlated with the individual peak of 0.02-Hz oscillations in the fast spindle band during all-night non-REM sleep ($r$ = 0.45, $P$ = 0.027; $n$ = 24; Fig. 5A), while correlation was absent for SWA ($r$ = −0.24; Fig. 5B). The correlation episodic memory recall appeared to be most robust for the 0.02-Hz oscillation over centroparietal sites ($C_4$, $C_Z$, $P_4$, and $P_Z$; $P_s < 0.043$). The 0.02-Hz oscillation peak also correlated with the mean fast spindle density ($r$ = 0.51, $P$ = 0.011; Fig. 5C), but not with overall spindle count ($P > 0.38$). Spindle measures per se (such as spindle density and spindle count) in this analysis were not significantly correlated with episodic memory recall (all $P_s > 0.15$). These data are the first indications that the periodic clustering of spindle activity on a 50-s time scale is a critical determinant for offline memory consolidation.

### The online periods are coordinated with heart rate changes

To test our hypothesis that changes in heart rate accompany the period of fragility to external stimuli, we monitored heart rate along with non-REM sleep in both mice and humans. In mice, through measuring interbeat intervals from the nuchal EMG (fig. S12), we found that heart rate increased and fluctuated around elevated values when sigma power oscillations were declining (Fig. 6, A and B), yielding a cross-correlation function with a prominent negative peak at ~0 s (Fig. 6, B and E). In humans, heart rate alterations also correlated with sigma power, but with a clear time lag. Here, heart rate declined rapidly once sigma power had reached a peak and increased gradually during sigma power minima (Fig. 6, C and D), before subsequent sigma peaks by ~5 s (Fig. 6F). Thus, although with different phase relations that could be related to differences in the kinetics and mechanisms of neural coupling to the heart in both species, cardiovascular activity is coordinated with brain oscillations that mark arousability.

## DISCUSSION

Sleep has to reconcile the needs for continuity and fragility. Here, we uncovered a 0.02-Hz oscillation in mouse and human non-REM sleep with characteristics that qualify it as a hallmark for how sleep balances these conflicting needs. First, the 0.02-Hz oscillation is most prominent in a frequency band that contains neural rhythms associated with the gating of sensory information during sleep. Second, it is coordinated with an established physiological correlate of offline memory processing and with modulation of autonomic status. Third, the 0.02-Hz oscillation phase is linked to wake-up from sleep in mice and to the extent of overnight memory consolidation in humans. This dual behavioral relevance in two different species suggests that the 0.02-Hz oscillation provides a unitary temporal scale of mammalian non-REM sleep over which both beneficial effects and maintained reactivity to the environment are balanced.

### The 0.02-Hz oscillation in sigma power results from a periodic recurrence of sleep spindles

The 10- to 15-Hz frequency band analyzed here contains sleep spindles, a well-described sleep rhythm that is a thalamocortically generated and visually obvious hallmark of the non-REM sleep EEG in

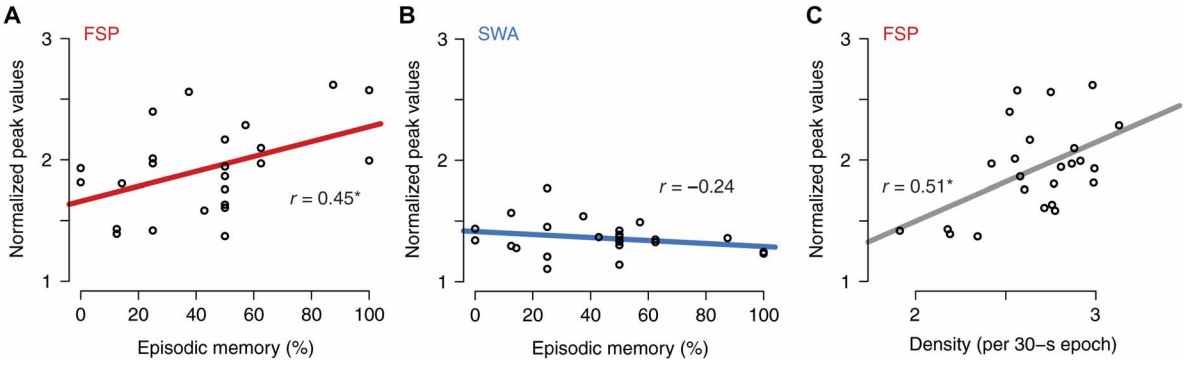


**Fig. 5. Sleep benefit in episodic memory correlates with the strength of the 0.02-Hz oscillation in the FSP band (FSP ± 1 Hz).** (**A**) Correlation of episodic memory recall (that is, recall of objects in their spatiotemporal context) with normalized peak values of FSP band. Pearson's *r* values are given in all panels (*$P$ = 0.027). (**B**) Same for SWA band ($P$ = 0.26). (**C**) Normalized power in FSP band was positively associated with the density of fast spindles (*$P$ = 0.011). Analyses were performed on the average of all parietocentral EEG electrodes ($C_3$, $C_Z$, $C_4$, $P_3$, $P_Z$, and $P_4$) for the FSP band, and across frontal electrodes ($F_3$, $F_Z$, and $F_4$) for the SWA band, as these sites correspond to the locations with the highest overall power in the respective bands.

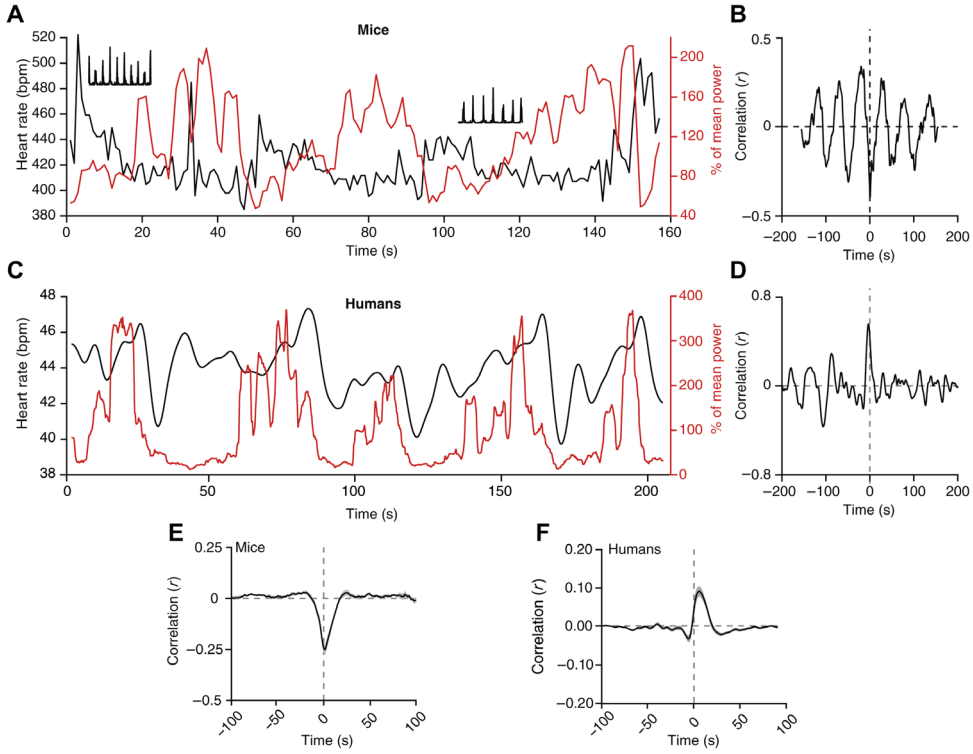


**Fig. 6. The 0.02-Hz oscillation aligns with heart rate changes in both mice and humans.** (**A**) Representative non-REM sleep bout with simultaneous recording of sigma power (red trace) and heart rate [black trace; in beats per minute (bpm)]. Insets show 1-s period of corresponding raw data (squared) to illustrate R-wave detection in EMG traces. (**B**) Cross-correlogram between sigma power and heart rate for traces in (A). (**C**) Same as (A) for a single human subject. (**D**) Corresponding cross-correlogram as (B). (**E** to **F**) Mean cross-correlogram for mice ($n$ = 12) (E) and humans ($n$ = 27) (F). Shadowing represents means ± SEM.

humans and carnivores between ~8 and 16 Hz (*7*, *15*). Mouse EEG traces show a more continuous and graded activity in the 9- to 18-Hz band that is best quantified through mean power levels (*11*). For species comparisons, we focused here on power dynamics in the 10- to 15-Hz band. The oscillatory pattern we found accords with the slow recurrence of discrete spindles over intervals of tens of seconds in humans and carnivores (*16*, *17*). Moreover, the much narrower individualized fast spindle band (around 13 Hz) oscillated most vigorously on a 0.02-Hz scale and correlated with the density of discrete spindles. Therefore, sleep spindles and fast spindles in particular are primary constituents of the 0.02-Hz oscillation. As adjacent frequency bands also show clear yet weaker 0.02-Hz oscillations, neural rhythm generators other than the thalamocortical spindle-generating circuits could contribute. In this context, it is noteworthy that the 8- to 13-Hz alpha band was recently associated with enhanced fragility of non-REM sleep in humans (*9*).

## The 0.02-Hz time scale is a fundamental property of mammalian non-REM sleep

Aside from shared spectral hallmarks and regulatory mechanisms, mouse and human non-REM sleep are strikingly different, in particular with

respect to their architecture. In this study, we have now identified a temporal scale that is relevant for both S2 in humans and non-REM sleep in mice. We also have shown that mouse non-REM sleep shares several of the basic neural and autonomic characteristics of S2. These similarities will undoubtedly contribute to emerging questions on the specific benefits provided by S2 to sleep and in particular to sleep-dependent memory consolidation. We exemplify this here through demonstrating that the 0.02-Hz amplitude of fast spindles is a predictor of overnight declarative memory consolidation. Recent human research specifically linking S2 to strengthened hippocampal-cortical connectivity (*18*) and to procedural memory (*19*) is now open for reassessment in rodents in terms of novel temporal and spatial aspects of spindle organization.

The 0.02-Hz oscillation likely acts to provide an organizational time scale for non-REM sleep in other mammalian species. Carnivores, such as cats and ferrets, show periodically recurring spindle events at intervals of 10 to 40 s (*16*). Slow periodicities occur in brainstem arousal systems in sleeping rats (*20*). Beyond mammals, the Australian reptile *Pogona vitticeps* sleeps in alternating low (<4 Hz)– and high-frequency (10 to 30 Hz)–dominated states in cycles of 60 to 80 s (*21*).

The infraslow frequency of 0.02 Hz is strikingly similar to the periodicity found for cycling blood oxygen level–dependent imaging signals observed in brain subnetworks during rest (*22*) and non-REM sleep (*23*) that are conserved across rodents, monkeys, and humans (*24*) and that result from varying brain integration during sleep (*25*). Although the link between infraslow periodicities in electrophysiological and functional magnetic resonance imaging signals remains to be established, the shared oscillation frequency suggests that it represents an evolutionarily conserved time frame over which neural and hemodynamic sleep rhythms are coordinated.

### The 0.02-Hz oscillation renders human sleep S2 a functionally unique sleep stage

The predominance of 0.02-Hz oscillations for fast spindles in S2 of human non-REM sleep functionally sets S2 apart from SWS. Over a 50-s time scale, an S2-specific spindle amassment in parietal areas yields a qualitatively different spatiotemporal spindle pattern than in SWS, where cortically driven spindle grouping predominates (*8*). It remains to be determined how these diverse organizational hierarchies contribute to the differential alignment of fast and slow spindles with slow waves (*12*). To what extent the 0.02-Hz oscillation will be important for observed differences in local versus global recurrence of spindles during S2 and SWS (*26*), as well as for proposed frameworks on active systems consolidation (*27*), remains an additional area of future investigation.

### The online period of the 0.02-Hz oscillation facilitates wake-up in response to acoustic stimuli

Cortical responses to acoustic stimuli show an enhanced late inhibitory component of the evoked sensory responses during spindles (*6*, *28*), which is a neural correlate for disrupted cortical processing. The fragility period of the 0.02-Hz oscillation, corresponding to low spindle occurrence, could thus be accompanied by a suppression of these inhibitory components. However, the transition to full-blown awakening additionally requires an activation of brainstem arousal systems, such as the noradrenergic locus coeruleus that effectively arouses the thalamocortical system (*29*) and discharges phasically during alerting stimuli (*30*). Periodicities in sleep's fragility to acoustic stimuli could be modulated through periodic patterns in excitability of this and/or additional subcortical arousal-promoting systems, which so far have not been investigated with respect to infraslow rhythms in activity during non-REM sleep (*20*).

Although a protective function of sleep spindles for arousals is well established, the role of the 0.02-Hz oscillation for arousability in humans will need to be ascertained to more comprehensively address the parallels between human sleep S2 and mouse non-REM sleep reported here. However, we caution here against a simple transfer of approaches between species. Not only do mice and humans differ in terms of subcortical and cortical mechanisms of sensory processing; stimulus attributes such as frequency composition also have different ecological valence (*31*). In humans, exposure to sounds mimicking those found in everyday life was previously used to assess resilience to sleep disruption and therefore seems suitable to address the role of the 0.02-Hz oscillation for sleep fragility in humans (*9*, *32*).

### The offline period of the 0.02-Hz oscillation promotes memory consolidation

The observed offline periods with reduced responsiveness to external noise might favor internal memory processing, as they coincide with enhanced ripple power, a sign for memory replay of recently experienced episodes (*13*). Human fast spindles predominate in sensorimotor areas and augment following learning (*33*) together with hippocampal ripples (*34*–*36*), a phenomenon that is crucial for memory consolidation (*1*, *37*). Our findings reveal the alignment of ripples and spindles within 25-s intervals that concur during periods of low fragility to noise. These data support the idea of a minimally required unit of uninterrupted sleep and provides a compelling explanation why optogenetically fragmenting non-REM sleep to periods shorter than 30 to 60 s disrupts memory consolidation (*38*). Corroborating the link to memory consolidation, we present the first evidence in humans that more pronounced 0.02-Hz oscillations in the spindle band correlated with enhanced hippocampus-dependent episodic memory after sleep. This further substantiates the idea that the temporal grouping of spindles, rather than their overall occurrence, is central to sleep-dependent memory consolidation.

### Alternative roles of the 0.02-Hz oscillation in non-REM sleep

Several facets of the 0.02-Hz oscillation support a role in subdividing sleep into fragility and offline periods, yet it undoubtedly serves roles that could complement or add to the ones presented here. These additional roles could include promotion of oscillatory signaling in signaling pathways in neurons and astrocytes, with implications for sleep-dependent gene transcription and synapse function. More generally, slow metabolic or energetic processes that result from, or contribute to, modified neuronal excitability during sleep (*39*) could evolve over infraslow time scales. Notably, oscillations in the 0.02-Hz range have also been reported in the EEG alpha and theta band activity during waking rest periods in humans (*40*). Furthermore, infraslow oscillations were observed in a broader frequency range (0.01 to 0.1 Hz) during a somatosensory detection task carried out in fully awake subjects (*41*), raising the possibility that neural variations on a 50-s time scale may be common to several vigilance states.

### Infraslow periodicities observed in clinical settings

Important clinical clues to infraslow periodicities in sleep fragility come from the "cyclic alternating pattern" (CAP) that is prominent in sleep disorder patients, consisting of visually identifiable alternations in EEG synchrony over periods of 10 to 60 s (*42*). Similar to

the 0.02-Hz oscillation, these are coordinated with autonomic parameters and signs of elevated arousability, such as body movements. However, unlike the 0.02-Hz oscillation, the CAP occurs throughout all sleep stages with wide variations in its spectral composition, occurrence of epileptic seizures in humans (*43*), and hippocampal interneuron discharges in sleeping rats (*44*).

## CONCLUSIONS

In conclusion, the 0.02-Hz infraslow oscillation reflects sleep's arbitration between maintaining readiness for arousal and continuity for offline processing. The oscillation provides a supraordinate temporal framework that, as we show here, controls sleep's alternation between fragility and continuity, and which might likewise explain previously established links between sleep EEG rhythms, cardiac activity, hemodynamic fluctuations, and offline memory consolidation mechanisms (*22*, *23*, *45*) that occur on a 50-s time scale during sleep. Hypothalamic and brainstem circuits coordinating autonomic output with cortical state, possibly through diencephalic relays, are likely generators of the infraslow rhythm, which could affect cortical excitability (*46*, *47*). Therefore, we speculate that the 0.02-Hz infraslow oscillation reflects an inverse bottom-up oscillatory control between online and offline states, counterbalancing cortically driven faster sleep rhythms that organize brain activity in a top-down manner.

## MATERIALS AND METHODS

### Animal husbandry and experimental groups

Mice were housed in a temperature- and humidity-controlled environment with a 12-hour light/dark cycle (lights on from 9:00 a.m. to 9:00 p.m.). Food and water were administered ad libitum. Surgery for combined EEG (ECoG)/EMG electrode implantation was performed on a total of 26 5- to 7-week-old male C57BL/6J mice, bred in our colonies, as previously described by Wimmer *et al.* (*11*). For head-fixed conditions, eight C57BL/6J male mice of the same age were implanted for the EEG/EMG/LFP recordings. All experimental procedures complied with the Swiss National Institutional Guidelines on Animal Experimentation and were approved by the Swiss Cantonal Veterinary Office Committee for Animal Experimentation.

### Surgeries for polysomnography and LFP recordings in mice

For EEG (ECoG)/EMG surgeries, mice were anesthetized with isoflurane (1 to 2%, $O_2$ and $N_2O$ mixture), and two gold-plated screws (1.1-mm diameter) (*48*) were gently inserted into the skull over the right hemisphere to obtain a frontoparietal derivation; four additional screws were inserted for implant stabilization. Two gold wires were inserted into the neck muscle for EMG recordings. A male-to-female connector was soldered to EEG (ECoG) and EMG electrodes, and the implant was covered with two-component epoxy glue (RelyX, 3M ESPE Dental Products; or G-CEM, GC Corporation) and dental cement (Paladur, Heraeus Kulzer GmbH). Paracetamol (2 mg/ml) was diluted into the drinking water for at least 10 days of recovery after the surgery, and an additional week of adaptation was given after the animals were tethered to a commutator (Dragonfly Inc.) via custom-made counterbalanced cables. Surgery for head-fixed LFP electrode implantation was performed under isoflurane anesthesia (1 to 2%, $O_2$ and $N_2O$ mixture) on eight mice (*49*). Above the left hemisphere, small craniotomies were drilled (<0.5-mm diameter) to chronically implant LFP tungsten microelectrodes (FHC; 10 to 12 megohms) in the following areas of interest: AC (bregma posterior, −2.5 mm; lateral, 3.9 mm; surface depth, 1.0 mm), SI (bregma posterior, −1.7 mm; lateral, 3.0 mm; surface depth, 0.9 mm), SII (bregma posterior, −0.7 mm; lateral, 4.2 mm; surface depth, 1.0 mm), mPFC (prelimbic and infralimbic area: bregma anterior, +1.8 mm; lateral, 0.3 mm; surface depth, 1.85 mm), and CA1 (bregma posterior, −2.5 mm; lateral, 2 mm; surface depth, 1.3 mm). A silver wire (Harvard Apparatus) was positioned in contact with the bone above the cerebellum and used as a neutral reference to record referential LFP signals. Over the right hemisphere, a light metal implant was glued to the bone, and two EEG gold-plated wires were chronically implanted to record differential frontoparietal EEG signals similar to those of the freely moving animals. For EMG electrodes, two gold pellets were inserted into the neck. Carprofen (5 mg/kg subcutaneously) and paracetamol were provided during recovery from surgery. Mice were daily habituated by gradually increasing the amount of time in the head-fixed condition and by rewarding with sweet water after each session.

### Mouse polysomnographic and LFP recordings

EEG (ECoG)/EMG signals were recorded in freely moving mice, acquired and amplified using an Embla amplifier (gain 2000×), digitized at 2 kHz, and down-sampled to 200 Hz using Somnologica version 3.3.1 software (Embla System). The EEG (ECoG) and EMG traces were high-pass–filtered at 0.7 and 10 Hz, respectively. A 48-hour baseline sleep-wake recording under undisturbed conditions was obtained for every animal, and only the 100 min after light onset for the two consecutive days was used for further analysis to assess a data set homogeneous with respect to time of day. Recordings of LFPs were obtained from head-fixed mice habituated to sleep (fig. S8). The EEG (ECoG)/EMG signals allowed to assess the behavioral state during the sleep-wake cycle recordings and, together with LFP signals, were amplified (1000×) and acquired through Plexon Systems (16-channel Multiple Acquisition Processor system). More specifically, the signals were sampled at 1 kHz, high-pass–filtered at 0.8 Hz, and low-pass–filtered at 300 Hz. LFP electrode positions were labeled at the end of all recordings through electrocoagulation before transcardiac perfusion with 4% paraformaldehyde in 0.1 M phosphate buffer (under pentobarbital anesthesia, 60 mg/kg), through current injections (50 μA, 8 s), and post hoc compared to the stereotactic atlas after coronal slicing (100-μm sections) (fig. S8). Mice with an unprecise electrode localization were excluded from specific analyses. Head-fixed mice were not exposed to noise stimuli.

### Scoring of rodent polysomnographic and LFP data

All sessions involving freely moving animals were visually scored using a 4-s epoch resolution, and power spectra were determined as previously described by Wimmer *et al.* (*11*). Whenever an abnormal discharge was present or the behavioral state was unclear, the epoch was scored as an artifact corresponding to the closest behavioral state and was omitted for any spectral analysis. For any 4-s epoch to be included in the spectral time course, it had to be preceded and followed by another epoch belonging to the same behavioral state excluding artifacts. A vigilance state file and a spectral file (FFT, 0.75 to 90 Hz with 0.25-Hz steps) were exported from Somnologica for every 4-s epoch and for every recording session. Under the head-fixed condition, scoring was based on combined EEG/EMG/LFP data and involved the selection of consolidated non-REM sleep bouts ≥45 s, excluding transitional periods to REM sleep or waking. Power spectra were calculated with a 4-s window resolution. Scoring of

EEG/LFP/EMG signals was performed using Igor Pro version 6.3 (WaveMetrics Inc.) customized semiautomated routines.

### Human subjects and sleep recordings

Human data obtained from 27 healthy men (22.5 ± 0.49 years of age; range, 18 to 28 years of age) who participated in a previous pharmacological study included overnight polysomnographic and electrocardiographic (ECG) recordings (*50*) (further referred to as "core study") (the core analyses are presented in Figs. 1 and 6, and figs. S3, S4, S6A, and S7). Data for Figs. 3 and 5, and fig. S6 (B and C) were obtained from a sample that included 14 subjects taking part in a memory study (*14*) that was extended by 10 more subjects ($n$ = 24, further referred to as "memory study"). The memory study also included standard polysomnographic full-night EEG recordings with a higher density of electrode sites.

All subjects had a regular sleep-wake pattern, did not take any medications at the time of the experiments, and were nonsmokers. Acute and chronic illness was excluded by medical history, routine laboratory investigation, and additional physical examination in the core study. The subjects of the core study were synchronized by daily activities and nocturnal rest with a more fixed sleep schedule, whereas the subjects of the memory study were instructed to keep their regular sleep schedule. Memory tasks were timed according to their regular sleeping time. All subjects spent one adaptation night in the laboratory to habituate to the experimental setting. For the core study, only data from placebo nights were included in the analysis. For the memory study, only the sleep group subjects were included. All participants gave written informed consent before participating, and both studies were approved by the local ethics committee.

Polysomnographic recordings included EEG from $C_3$ and $C_4$ electrode sites (International 10–20 system; reference: linked electrodes at the mastoids, ground at $F_{pz}$), EMG (*musculus mentalis*), and electrooculography (around the eyes), with the memory study data set using additional EEG sites ($F_3$, $F_Z$, $F_4$, $C_3$, $C_Z$, $C_4$, $P_3$, $P_Z$, and $P_4$). Electrode impedances were kept below 5 kilohms. Signals were amplified (BrainAmp, Brain Products), digitized (sampling rate >200 Hz), and filtered (EEG and electrooculogram between 0.3 and 35 Hz and EMG between 10 and 100 Hz).

### Scoring of human EEG data and sleep EEG parameter analyses

Sleep stages were scored offline in 30-s epochs by an experienced scorer according to standard criteria (*51*). Further analysis of the core study was focused on the first 210 min starting with sleep onset of undisturbed sleep that was expected to contain long uninterrupted epochs rich in S2 as well as SWS and good cardiac recording quality. The analysis of the memory study used the entire sleep period. The proportion of stage 1, S2, SWS (the sum of stage 3 and stage 4), non-REM sleep (sum of S2 and SWS), REM sleep, wakefulness after sleep onset, movement time, and sleep latencies was determined. Sleep onset was defined with reference to lights off by the first occurrence of an S1 sleep epoch followed by S2 sleep. For simplicity, EEG analysis focused on $C_3$ channel mainly used for sleep scoring in the core study, whereas analyses in the memory group used all nine recording sites. Data of subsequent analyses were down-sampled to 100 Hz to facilitate computation. Analysis was performed in MATLAB 2013b (MathWorks) using custom-made scripts, FieldTrip (www.ru.nl/neuroimaging/fieldtrip) (*52*), and for analysis of standard sleep parameters including spindle and SWA analysis using the SpiSOP tool (www.spisop.org). For the correlation of the standard sleep parameters with memory and with the strength of the 0.02-Hz oscillation, the average of all parietocentral EEG electrodes ($C_3$, $C_Z$, $C_4$, $P_3$, $P_Z$, and $P_4$) was taken for the spindle band analyses, and the average of the frontal electrodes ($F_3$, $F_Z$, and $F_4$) was taken for the SWA band analysis, because these locations correspond to the sites with the highest overall power in the respective bands.

Briefly, power spectral analyses of non-REM sleep were calculated on consecutive artifact-free 5-s segments of non-REM sleep, which overlapped in time by 4 s along the entire recording period. Each segment was tapered by a single Hanning window before applying an FFT that resulted in interval power spectra with a frequency bin resolution of 0.2 Hz. Power spectra were then averaged across all segments (Welch's method). Mean power density from the spectra was calculated in the frequency band for slow waves (0.5 to 4 Hz) and in the sigma band (10 to 15 Hz). Concrete fast spindles and slow waves during non-REM sleep were analyzed according to previously published algorithms (*12*, *54*). For each individual and channel, their densities (per 30-s epoch of non-REM sleep), counts, mean amplitudes, and lengths were calculated.

For the identification of slow waves, the signal in each channel during non-REM sleep epochs was filtered between 0.5 and 3.5 Hz (−3 dB roll-off) using a digital finite impulse response (FIR) filter (Butterworth, order of 4). Next, all intervals of time with consecutive positive-to-negative zero crossings were marked as putative slow waves if their durations corresponded to a frequency between 0.5 and 1.11 Hz (*53*), yet these were excluded in case their amplitude was >1000 μV (as these were considered artifacts) or when both negative and positive half-wave amplitudes lay between −15 and +10 μV. A slow wave was identified if its negative half-wave peak potential was lower than the mean negative half-wave peak of all putatively detected slow oscillations in the respective EEG channel, and also only if the amplitude of the positive half-wave peak was larger than the mean positive half-wave amplitude of all other putatively detected slow waves within this channel.

For the detection of fast spindles, the EEG signal was filtered with a band-pass around the individual FSP (see "Analysis of 0.02-Hz oscillations in humans") with a ±1-Hz range (−3 dB cutoff). Then, using a sliding window with a size of 0.2 s, the root mean square (RMS) was computed, and the resulting signal was smoothed in the same window with a moving average. A spindle was detected when the smoothed RMS signal exceeded an individual amplitude threshold by 1.75 × SD of the filtered signal in this channel at least once and additionally exceeded a lower threshold of 1.5 × SD for 0.5 to 3 s. The crossings of the lower threshold marked the beginning and end of each spindle and quantified their length. Spindle amplitude was defined by the voltage difference between the largest trough and the largest peak. Spindles were excluded for amplitudes >200 μV.

### Analysis of 0.02-Hz oscillations in mice

The scheme in fig. S2 summarizes the analysis steps for undisturbed non-REM sleep in mice. From the scored data, all non-REM sleep bouts ≥24 epochs (each epoch corresponding to 4 s, thus ≥96 s of uninterrupted non-REM sleep) were selected in the first 100 min at ZT0 for two consecutive light phases, regardless of the amount of non-REM sleep (fig. S2A). The spectral files of all 4-s epoch across all non-REM sleep (red lines in hypnogram in fig. S2A) were then used to calculate an arithmetic mean FFT per mouse. In recordings from head-fixed sleeping mice, an average non-REM sleep spectral

profile was calculated across the entire recording for each mouse (810 to 3210 s).

Figure S2B shows how the time course of spectral power was analyzed in 4-s bins for the following frequency bands: SWA (0.75 to 4 Hz), theta (6 to 10 Hz), sigma (10 to 15 Hz), and beta (16 to 20 Hz). To do this, the power values from the 4-s FFTs for each frequency band were normalized to the average non-REM sleep FFT calculated across all non-REM sleep (fig. S2A) and plotted against time, yielding the line graphs in Figs. 1 (A and B) and 6A, and figs. S1, S2B, and S12.

The spectral profiles of these power time courses of each non-REM sleep bout were obtained through calculating an FFT (fig. S2C) with Hamming window method, which revealed all power values in the infraslow frequency range (<0.125 Hz). The choice of a minimal bout length of 24 epochs, corresponding to ≥96 s, preserved at least two cycles of the 0.02-Hz oscillation detected here. A mean spectral profile was calculated for every mouse through averaging across the interpolated absolute FFTs obtained from each power profile of each non-REM sleep bout (fig. S2C, right).

Control analyses were carried out to ensure the robustness of peak detection (as shown in fig. S3). For the analysis of scale-free behavior, similar FFT calculations for a simulated scale-free power profile ($1/f$) with equal bout length distribution did not yield a peak unless a 0.02-Hz sine wave was added (fig. S3, G to J). Before FFT calculation, the average power value for each frequency band was subtracted from each non-REM sleep bout to prevent large power increases at extremely small frequencies; however, the 0.02-Hz peaks were also present without this offset. Autocorrelations were calculated for original and shuffled sigma power data of these long non-REM bouts for each mouse (fig. S4, A and B).

The mean FFT obtained per mouse was normalized to its own mean. Similarly, in EEG (ECoG)/LFP recordings, the FFTs over the power data mentioned above were obtained for each non-REM sleep bout using a Hamming window and means calculated as before (Fig. 2). Leaving out the Hamming window did not affect the result.

Last, to determine peak and SDs of the FFTs, we performed a Gaussian fit (one term). Peak location and SD values were obtained from the fitted curve and used to calculate the average peak value in the range (peak ± 0.5 × SD). These values were used to calculate average peak values in all other frequency bands (Fig. 1D). By choosing a mean that is determined not only by the single data point of the peak but also by the spread of values around 1 full SD, we take into account that the exact peaks might not be identical for all frequency bands.

The peak ± SD frequencies of the FFT for sigma power were also used to calculate a band-pass (FIR)–filtered trace of sigma power time course before noise onset (Fig. 4D) and to reconstruct the oscillations in Fig. 4F. The peak ± SD frequencies of the FFT for sigma power were also used for the phase analysis in Fig. 4 (G and H). Here, the sigma power time courses in the prestimulus period were fit to a sinus function with a frequency constrained by these limits. The phase of these sinusoids was read for the wake-up and sleep-through trials in which both a peak and a trough lay within the fitted period. This was the case for 4 of 9 wake-up and 8 of 10 sleep-through sigma power time courses.

In noise exposure experiments, the time courses of sigma power and SWA in the 40-s prestimulus period were averaged across animals after sorting the trials on the basis of their outcome (wake-up or sleep-through trials). For any successful trial, the values in both sigma and SWA frequency bands were expressed in percentage with respect to the average non-REM sleep power spectrum in the 40-s prestimulus period (Fig. 4, C and E). Because of this normalization, 0.02-Hz oscillations had smaller amplitudes than those in Fig. 1. A total of $n = 1$ of 10 animals did not wake up in any of the noise exposures and did not contribute to the power calculations (Fig. 4, D and E). Later analysis showed that, in this mouse, only two noise exposures were successful, and both of these fell onto the rising phase of the sigma power oscillation. Analysis of phase was carried out with phase convention peak of 0° and trough of 180°, as described above.

Ripple activity time course was quantified from the LFP recording in the CA1 area. The signal was first filtered between 150 and 250 Hz and then squared. The values were averaged in a 4-s bin, and a cross-correlation was performed against the corresponding sigma power from channel SI (resampled at 1 Hz) using the ripple activity trace as "source wave."

### Analysis of 0.02-Hz oscillations in humans

The scheme in fig. S5 summarizes the analysis steps for human non-REM sleep. An analysis similar to that in mice was performed on consecutive 30-s intervals of non-REM sleep EEG (further referred to as bouts) of the first 210 min of sleep and free of artifacts or movement arousals for the core study data set (fig. S5A) and was extended to the full-night sleep in the memory group data set (Figs. 3 and 5). The analysis differed from that in mice to account for dissimilarities in sleep patterns of humans (for example, longer bouts). For each EEG signal of a bout, the power spectra were calculated every 0.1 s in the 0.5- to 24-Hz range in steps of 0.2 Hz with a continuous wavelet transform using Morlet wavelets with length of four cycles. At every time point, the average power in the bands was calculated in frequency bands equivalent to mice: SWA (0.5 to 4 Hz), theta (4 to 8 Hz), sigma (10 to 15 Hz), individual beta (16 to 20 Hz), and beta2 (20 to 24 Hz). This resulted in a detailed power time course for each respective frequency band (fig. S5B).

After visual confirmation that the power time course in the sigma and SWA bands corresponded to real spindle and SWA activity, the temporal resolution was reduced to highlight activity changes in the infraslow periodicity. Therefore, a symmetric moving average was applied in a 4-s time window to match the resolution of the mouse data. As in mice, the average absolute values of the non-REM sleep spectral composition were used for normalization by setting them to 100% (Fig. 1, E and F). The first 100 min of concatenated non-REM sleep was used for this normalization to account for interindividual differences in the amount of non-REM sleep and to match the time interval used for the analysis in mice [fig. S5, A (bottom) and C].

To establish the spectral profile of these power time courses, the spectra of the power time courses for each frequency band were obtained for all non-REM sleep bouts lasting ≥120 s (≥4 epochs) (fig. S5A, bottom). For this, a Morlet wavelet analysis was performed in each interval on the previously calculated power time courses for respective frequency bands that aimed for a frequency resolution of 0.001 Hz in the range 0.001 to 0.12 Hz with time steps of 0.5 s. To obtain one power spectrum for each bout, we then averaged the resulting signal across time steps along the duration of the bout (fig. S5D).

Last, the spectral profile of the 0.02-Hz oscillation of all frequency bands for all non-REM sleep was calculated by averaging the spectral values across all the non-REM sleep bouts of the subject, weighted by their duration. As in mice, the spectral profile obtained per subject was normalized to its own mean. To determine peak and

SDs of each power spectrum, a Gaussian fit (three terms) was performed on the normalized power from single subjects. The peak location and SD values were obtained from the fitted curve and used to calculate the average peak value in the range (peak ± 0.5 × SD) (Fig. 1, G and H). Accounting for the larger variability in individual peak values between human subjects and frequency bands as compared to mice, the respective range of each frequency band was used to approximate the highest possible average peak values. Using the range from the sigma band for averaging of peak values in all frequency bands essentially yielded the same results reported here.

To address specificity of the 0.02-Hz oscillation to spindles, we repeated the analysis for a frequency band tailored to the individual spindle band of each subject. Thus, for each subject, the frequency band was centered to its FSP that was determined according to previously described standard methods (*12*, *54*), and that is specified here briefly. Power spectra containing the sigma band (8 to 18 Hz) were calculated in the same way as reported above but using consecutive artifact-free 10-s intervals of non-REM sleep, which overlapped in time by 5 s with a frequency resolution of 0.1 Hz. The FSP was visually identified for each subject from the individual power spectra of non-REM sleep epochs as power maxima within the sigma band (*12*). Although slow spindles contribute to the sigma band, they were not considered because of their prevalence mainly during SWS and tight temporal association with fast spindles (*12*).

Control analyses for humans in figs. S3 and S4 including using minimal bout lengths of double (≥240 s; fig. S3, D to F) or triple the length (≥360 s), changing Morlet wavelet cycle length to seven cycles for better frequency resolution, skipping the normalization steps, or comparing the power fluctuations in the full spectrum (in smaller bands of 1 Hz from 1 to 24 Hz, instead of broader specific bands) essentially yielded the same results reported here. Autocorrelations were calculated as in mice for original and shuffled sigma power profile data of non-REM sleep. To more closely match the respective analyses in mice, the data were split in all possible continuous 240-s segments and down-sampled to 1 Hz (this analysis is referred to as 240-s bouts; see fig. S4, C and D).

### White noise exposure during polysomnographic recordings in sleeping mice

A subset of 10 mice implanted for polysomnography was habituated to the experimental noise stimulus during the period of tethering after surgery through playing noises six to eight times per light phase. During the experimental trials, animals were exposed, four at a time, to white noise pulses of 90-dB SPL lasting 20 s, generated through custom-written LabVIEW procedure (National Instruments Corporation). The duration of the noise was chosen such that it covered half a cycle of the 0.02-Hz oscillation and because mice woke up or slept through it at comparable rates. The arousal success rate was defined as the fraction of wake-up trials within all accepted trials. In a preliminary experimental series, a 20-s pulse at 80 dB was found to lead to an insufficient number of wake-up trials, with the arousal success rate <30%, whereas a 4-s pulse at 100 dB led to arousals in more than 90% of the cases. Noise was played randomly in the first 100 min at ZT0, but the following conditions had to be fulfilled: At least one of the four mice was in non-REM sleep for ≥40 s, as assessed through online monitoring of EEG (ECoG)/EMG traces, and the previous noise had been played ≥4 min before. The experimenter was blind to the spectral composition of non-REM sleep during the noise exposure experiment, such that noises were played without knowledge of the sigma power phase. Wake-ups were identified on the basis of characteristic alterations of EEG/EMG signals, namely, the decrease in amplitude and increase in frequency for the EEG trace, combined with the detection of muscular activity from the EMG electrodes (Fig. 4B). The animals were exposed several times to the noise in each recording session. The 20-s pulse was played 14.0 ± 0.3 (minimally 9) times per mouse, of which 8.6 ± 0.4 (minimally two per mouse) trials were successful, meaning that the mouse did not wake up in the prestimulus period or in the first 4 s of noise exposure. EEG (ECoG)/EMG traces were scored blind with respect to noise exposure times.

### Study procedures and memory assessment in humans

In the core study, subjects arrived at the laboratory at 9:00 p.m. for experimental preparation, and sleep was allowed between 11:00 p.m. (lights off) and 7:00 a.m. Subjects underwent blood sampling via an intravenous forearm catheter, which was connected to a long thin tube and enabled blood collection from an adjacent room without disturbing the subject's sleep and unnoticed by all subjects (*14*).

The memory study demonstrated a twofold better recall of episodic memory when task performance was followed by nocturnal sleep compared to postlearning daytime wakefulness (*14*). Here, we only used the subjects of the sleep group, for which the procedures were as follows: Encoding of the memory task took place in the evening (between ~8:00 p.m. and 11:00 p.m.). One hour after encoding, and in accordance with their usual sleep habits, participants went to bed (lights off) for an 8-hour sleep period in the laboratory with polysomnographic recordings. The retrieval phase started 1 hour after awakening. The episodic memory task described in detail by Weber *et al.* (*14*) required the encoding of faces (events) embedded in a spatial context (that is, different locations on a screen) and a temporal context (that is, different faces at the different locations were presented in two experimental episodes separated by a 1-hour interval). During encoding, participants remained unaware that the task was aimed at memory testing but were instructed to keep focused on the experimental episodes presented on the screen.

For recall testing during the retrieval phase after sleep, old and novel faces were presented, and the subjects had to indicate (by mouse clicks) whether a face was new or presented during one of the task episodes, and for the latter, whether it occurred in the first or second episode and at which location it occurred. Episodic memory, that is, "what-where-when" memory, was determined by the percentage of the faces that were correctly identified as occurring in one of the episodes (that is, "what"), and for which the participant also correctly indicated the episode (that is, "what-when") and the location (that is, "what-where") it occurred, minus the locations for which the participant had forgotten that they were occupied with any face in a final separate recall test (false "where-when" memory).

### Analysis of heart rate in mice and humans

The instantaneous heart rate was extracted from the nuchal EMG recording in freely moving or head-fixed mice and calculated from the ECG recordings in humans. In $n = 12$ mice (eight freely moving and four head-fixed), the heart rate was quantified through detection of R waves in the EMG trace filtered between 20 and 300 Hz. Reliability of this signal was confirmed through standard ECG recording in one mouse (fig. S12) (*55*). Peak or threshold detections were used, with equal results. In the latter case, threshold was set as

the mean + 3.5 × SD of the EMG signal. We then calculated the interval between two successive peaks (R-R interval) for all consolidated non-REM sleep bouts ≥45 s. Occasionally, R waves were classified as aberrant because they were either below threshold or artifactual because of muscle twitches, which corresponded to 1.41% of all intervals. In freely moving animals, all non-REM sleep bouts ≥96 s were used. The number of non-REM sleep bouts per head-fixed animal included in the analysis ranged from 10 to 42 bouts (mean number of bouts, 22.3 ± 7.2). The R-R intervals were then binned (1 s) and converted into beats per minute. In humans, the heart rate was determined across artifact-free consecutive non-REM sleep intervals on the basis of R-R intervals. R waves were detected by first filtering the ECG signal with a high-pass filter of 20 Hz [infinite impulse response (IIR); designed for a stopband of 15 Hz with −100-dB attenuation, with two filter passings and no time shift] and then applying a low-pass filter at 45 Hz (IIR; filter order of 4, with two filter passings and no time shift). To obtain a clear signal amplitude envelope describing the R wave, we calculated the absolute values of the Hilbert transform of the signal. Then, the signal was down-sampled to 100 Hz to facilitate computation. R-wave peaks were automatically identified as maxima in the envelope signal if they were at least 0.2 s apart (minimal heart refractory period) and reached above a threshold of 2 SDs from overall envelope signal values. This method was visually confirmed in each subject to validate correct R-wave peak detection in all epochs. Instantaneous heart rate at every R-wave peak was then determined by duration between consecutive R-R intervals.

For cross-correlating time courses of heart rate (in beats per minute) and sigma power in mice, the sigma power trace was interpolated to match the 1-Hz sampling rate of the heart rate trace. In humans, it was smoothed in a 4-s moving symmetric time window, and both sigma power and heart rate traces were resampled at 100 Hz by interpolation. The 120-s intervals were $z$-transformed (by subtracting the mean and dividing by the SD). In both mice and humans, the cross-correlation was performed using the heart rate signal as source wave. In both species, the cross-correlograms were first averaged within and then across subjects. In humans, all of the above procedures were repeated separately for S2 and SWS epochs instead of non-REM sleep epochs but reported solely for the oscillation peak analysis.

### Experimental design and statistics

Group size in mice matched the minimum required to obtain a statistical power of 0.8. Power analyses were carried out on the basis of effect sizes obtained from preliminary data sets. Group size in humans was chosen to obtain a statistical power of 0.95 for similar effect sizes, as observed in mice. Statistical power was calculated using G*Power version 3.1.9.2. Data normality was tested using the Shapiro-Wilk $W$ test, and parametric or nonparametric statistical tests were chosen accordingly. The Wilcoxon signed-rank test was used for nonparametric matched pair comparisons, whereas paired two-tailed Student's $t$ tests (referred to as $t$ test in text and legends) were used as parametric statistical tests. RM ANOVA was used as parametric statistical test to study the within-subjects effect of behavioral outcome and/or the between-subjects effect. To assess equality of variances for the RM ANOVA, we calculated the Mauchly's test of sphericity. Whenever equality of variances was rejected, the univariate adjusted Greenhouse-Geisser correction was applied. Friedman rank sum test was used as a nonparametric test to study within-subjects effect in case parametric model parameters of an ANOVA violated assumptions of normality. Statistical tests were calculated using JMP version 10.0.0 (SAS Institute Inc.), Igor Pro, and the R programming language (2.15.0, R Core Team) [The R Development Core Team, The R Foundation for Statistical Computing (www.r-project.org/foundation), 2007]. $P < 0.05$ was considered statistically significant. If not mentioned otherwise, $P$ values were reported uncorrected for multiple comparisons, as taking these into account did not alter the main results. For the purpose of comparison between mice and humans, all data in bar graphs are presented as means ± SEM, even if not normally distributed (Fig. 1, D, H, and J). All indications of $n$ refer to either mice or humans. Time course graphs, as well as data in the main text, are presented as means ± SEM.

## SUPPLEMENTARY MATERIALS

Supplementary material for this article is available at http://advances.sciencemag.org/cgi/content/full/3/2/e1602026/DC1

fig. S1. The 0.02-Hz oscillation is prominent for sigma power throughout both short and long non-REM sleep bouts in mice.
fig. S2. Scheme of analysis for 0.02-Hz oscillations in mice.
fig. S3. The 0.02-Hz oscillation is robust against the choice of non-REM sleep bout length for analysis and does not result from an 1/$f$ power dependence.
fig. S4. The sigma power dynamics in both mice and humans show a periodicity on a 0.02-Hz time scale, as assessed through autocorrelations.
fig. S5. Scheme of analysis for 0.02-Hz oscillations in humans.
fig. S6. Sleep parameters for the participants of the studies in humans and predominance of 0.02-Hz oscillations in S2 sleep.
fig. S7. The 0.02-Hz oscillation is prominent for sigma power throughout early non-REM sleep in humans.
fig. S8. Sleep in head-fixed animals reproduces the three major vigilance states and their spectral characteristics found in freely moving animals.
fig. S9. Acoustic stimuli causing early or late wake-ups fall onto late or early portions of the declining sigma power phase, respectively.
fig. S10. Wake-up and sleep-through trials do not depend on previous sleep duration.
fig. S11. Ripple power increases precede sigma power elevations.
fig. S12. Nuchal EMG recordings faithfully detect the R-waves of the heartbeat in mice.

## REFERENCES AND NOTES


1. B. Rasch, J. Born, About sleep's role in memory. *Physiol. Rev.* **93**, 681–766 (2013).
2. J. M. Krueger, M. G. Frank, J. P. Wisor, S. Roy, Sleep function: Toward elucidating an enigma. *Sleep Med. Rev.* **28**, 46–54 (2016).
3. S. S. Campbell, I. Tobler, Animal sleep: A review of sleep duration across phylogeny. *Neurosci. Biobehav. Rev.* **8**, 269–300 (1984).
4. J. M. Siegel, Sleep viewed as a state of adaptive inactivity. *Nat. Rev. Neurosci.* **10**, 747–753 (2009).
5. T. T. Dang-Vu, M. Bonjean, M. Schabus, M. Boly, A. Darsaud, M. Desseilles, C. Degueldre, E. Balteau, C. Phillips, A. Luxen, T. J. Sejnowski, P. Maquet, Interplay between spontaneous and induced brain activity during human non-rapid eye movement sleep. *Proc. Natl. Acad. Sci. U.S.A.* **108**, 15438–15443 (2011).
6. M. Elton, O. Winter, D. Heslenfeld, D. Loewy, K. Campbell, A. Kok, Event-related potentials to tones in the absence and presence of sleep spindles. *J. Sleep Res.* **6**, 78–83 (1997).
7. D. Aeschbach, A. A. Borbély, All-night dynamics of the human sleep EEG. *J. Sleep Res.* **2**, 70–81 (1993).
8. S. Astori, R. D. Wimmer, A. Lüthi, Manipulating sleep spindles—Expanding views on sleep, memory, and disease. *Trends Neurosci.* **36**, 738–748 (2013).
9. S. M. McKinney, T. T. Dang-Vu, O. M. Buxton, J. M. Solet, J. M. Ellenbogen, Covert waking brain activity reveals instantaneous sleep depth. *PLOS ONE* **6**, e17351 (2011).
10. E. Sforza, C. Jouny, V. Ibanez, Cardiac activation during arousal in humans: Further evidence for hierarchy in the arousal response. *Clin. Neurophysiol.* **111**, 1611–1619 (2000).
11. R. D. Wimmer, S. Astori, C. T. Bond, Z. Rovó, J.-Y. Chatton, J. P. Adelman, P. Franken, A. Lüthi, Sustaining sleep spindles through enhanced SK2-channel activity consolidates sleep and elevates arousal threshold. *J. Neurosci.* **32**, 13917–13928 (2012).
12. M. Mölle, T. O. Bergmann, L. Marshall, J. Born, Fast and slow spindles during the sleep slow oscillation: Disparate coalescence and engagement in memory processing. *Sleep* **34**, 1411–1421 (2011).
13. G. Buzsáki, Hippocampal sharp wave-ripple: A cognitive biomarker for episodic memory and planning. *Hippocampus* **25**, 1073–1188 (2015).
14. F. D. Weber, J. Wang, J. Born, M. Inostroza, Sleep benefits in parallel implicit and explicit measures of episodic memory. *Learn. Mem.* **21**, 190–198 (2014).

15. D. Contreras, A. Destexhe, T. J. Sejnowski, M. Steriade, Spatiotemporal patterns of spindle oscillations in cortex and thalamus. *J. Neurosci.* **17**, 1179–1196 (1997).
16. M. Steriade, D. A. McCormick, T. J. Sejnowski, Thalamocortical oscillations in the sleeping and aroused brain. *Science* **262**, 679–685 (1993).
17. E. Werth, P. Achermann, D.-J. Dijk, A. A. Borbély, Spindle frequency activity in the sleep EEG: Individual differences and topographical distribution. *Electroencephalogr. Clin. Neurophysiol.* **103**, 535–542 (1997).
18. K. C. Andrade, V. I. Spoormaker, M. Dresler, R. Wehrle, F. Holsboer, P. G. Sämann, M. Czisch, Sleep spindles and hippocampal functional connectivity in human NREM sleep. *J. Neurosci.* **31**, 10331–10339 (2011).
19. S. Laventure, S. Fogel, O. Lungu, G. Albouy, P. Sévigny-Dupont, C. Vien, C. Sayour, J. Carrier, H. Benali, J. Doyon, NREM2 and sleep spindles are instrumental to the consolidation of motor sequence memories. *PLOS Biol.* **14**, e1002429 (2016).
20. G. Aston-Jones, F. E. Bloom, Activity of norepinephrine-containing locus coeruleus neurons in behaving rats anticipates fluctuations in the sleep-waking cycle. *J. Neurosci.* **1**, 876–886 (1981).
21. M. Shein-Idelson, J. M. Ondracek, H.-P. Liaw, S. Reiter, G. Laurent, Slow waves, sharp waves, ripples, and REM in sleeping dragons. *Science* **352**, 590–595 (2016).
22. D. Mantini, M. G. Perrucci, C. Del Gratta, G. L. Romani, M. Corbetta, Electrophysiological signatures of resting state networks in the human brain. *Proc. Natl. Acad. Sci. U.S.A.* **104**, 13170–13175 (2007).
23. M. Fukunaga, S. G. Horovitz, P. van Gelderen, J. A. de Zwart, J. M. Jansma, V. N. Ikonomidou, R. Chu, R. H. R. Deckers, D. A. Leopold, J. H. Duyn, Large-amplitude, spatially correlated fluctuations in BOLD fMRI signals during extended rest and early sleep stages. *Magn. Reson. Imaging* **24**, 979–992 (2006).
24. H. Lu, Q. Zou, H. Gu, M. E. Raichle, E. A. Stein, Y. Yang, Rat brains also have a default mode network. *Proc. Natl. Acad. Sci. U.S.A.* **109**, 3979–3984 (2012).
25. M. Boly, V. Perlbarg, G. Marrelec, M. Schabus, S. Laureys, J. Doyon, M. Pélégrini-Issac, P. Maquet, H. Benali, Hierarchical clustering of brain activity during human nonrapid eye movement sleep. *Proc. Natl. Acad. Sci. U.S.A.* **109**, 5856–5861 (2012).
26. Y. Nir, R. J. Staba, T. Andrillon, V. V. Vyazovskiy, C. Cirelli, I. Fried, G. Tononi, Regional slow waves and spindles in human sleep. *Neuron* **70**, 153–169 (2011).
27. L. Genzel, M. C. W. Kroes, M. Dresler, F. P. Battaglia, Light sleep versus slow wave sleep in memory consolidation: A question of global versus local processes? *Trends Neurosci.* **37**, 10–19 (2014).
28. M. Schabus, T. T. Dang-Vu, D. P. J. Heib, M. Boly, M. Desseilles, G. Vandewalle, C. Schmidt, G. Albouy, A. Darsaud, S. Gais, C. Degueldre, E. Balteau, C. Phillips, A. Luxen, P. Maquet, The fate of incoming stimuli during NREM sleep is determined by spindles and the phase of the slow oscillation. *Front. Neurol.* **3**, 40 (2012).
29. M. E. Carter, O. Yizhar, S. Chikahisa, H. Nguyen, A. Adamantidis, S. Nishino, K. Deisseroth, L. De Lecea, Tuning arousal with optogenetic modulation of locus coeruleus neurons. *Nat. Neurosci.* **13**, 1526–1533 (2010).
30. K. Takahashi, Y. Kayama, J. S. Lin, K. Sakai, Locus coeruleus neuronal activity during the sleep-waking cycle in mice. *Neuroscience* **169**, 1115–1126 (2010).
31. K. K. Ohlemiller, S. M. Jones, K. R. Johnson, Application of mouse models to research in hearing and balance. *J. Assoc. Res. Otolaryngol.* **17**, 493–523 (2016).
32. T. T. Dang-Vu, S. M. McKinney, O. M. Buxton, J. M. Solet, J. M. Ellenbogen, Spontaneous brain rhythms predict sleep stability in the face of noise. *Curr. Biol.* **20**, R626–R627 (2010).
33. S. Gais, M. Mölle, K. Helms, J. Born, Learning-dependent increases in sleep spindle density. *J. Neurosci.* **22**, 6830–6834 (2002).
34. O. Eschenko, W. Ramadan, M. Mölle, J. Born, S. J. Sara, Sustained increase in hippocampal sharp-wave ripple activity during slow-wave sleep after learning. *Learn. Mem.* **15**, 222–228 (2008).
35. M. Mölle, O. Eschenko, S. Gais, S. J. Sara, J. Born, The influence of learning on sleep slow oscillations and associated spindles and ripples in humans and rats. *Eur. J. Neurosci.* **29**, 1071–1081 (2009).
36. Z. Clemens, M. Mölle, L. Erőss, R. Jakus, G. Rásonyi, P. Halász, J. Born, Fine-tuned coupling between human parahippocampal ripples and sleep spindles. *Eur. J. Neurosci.* **33**, 511–520 (2011).
37. N. Maingret, G. Girardeau, R. Todorova, M. Goutierre, M. Zugaro, Hippocampo-cortical coupling mediates memory consolidation during sleep. *Nat. Neurosci.* **19**, 959–964 (2016).
38. A. Rolls, D. Colas, A. Adamantidis, M. Carter, T. Lanre-Amos, H. C. Heller, L. de Lecea, Optogenetic disruption of sleep continuity impairs memory consolidation. *Proc. Natl. Acad. Sci. U.S.A.* **108**, 13305–13310 (2011).
39. F. Ding, J. O'Donnell, Q. Xu, N. Kang, N. Goldman, M. Nedergaard, Changes in the composition of brain interstitial ions control the sleep-wake cycle. *Science* **352**, 550–555 (2016).
40. P. Novak, V. Lepicovska, C. Dostalek, Periodic amplitude modulation of EEG. *Neurosci. Lett.* **136**, 213–215 (1992).
41. S. Monto, S. Palva, J. Voipio, J. M. Palva, Very slow EEG fluctuations predict the dynamics of stimulus detection and oscillation amplitudes in humans. *J. Neurosci.* **28**, 8268–8272 (2008).
42. L. Parrino, R. Ferri, O. Bruni, M. G. Terzano, Cyclic alternating pattern (CAP): The marker of sleep instability. *Sleep Med. Rev.* **16**, 27–45 (2012).
43. S. Vanhatalo, J. M. Palva, M. D. Holmes, J. W. Miller, J. Voipio, K. Kaila, Infraslow oscillations modulate excitability and interictal epileptic activity in the human cortex during sleep. *Proc. Natl. Acad. Sci. U.S.A.* **101**, 5053–5057 (2004).
44. M. Penttonen, N. Nurminen, R. Miettinen, J. Sirviö, D. A. Henze, J. Csicsvári, G. Buzsáki, Ultra-slow oscillation (0.025 Hz) triggers hippocampal afterdischarges in Wistar rats. *Neuroscience* **94**, 735–743 (1999).
45. R. Kaplan, M. H. Adhikari, R. Hindriks, D. Mantini, Y. Murayama, N. K. Logothetis, G. Deco, Hippocampal sharp-wave ripples influence selective activation of the default mode network. *Curr. Biol.* **26**, 686–691 (2016).
46. A. Silvani, R. A. L. Dampney, Central control of cardiovascular function during sleep. *Am. J. Physiol. Heart Circ. Physiol.* **305**, H1683–H1692 (2013).
47. E. V. Golanov, J. R. C. Christensen, D. J. Reis, Neurons of a limited subthalamic area mediate elevations in cortical cerebral blood flow evoked by hypoxia and excitation of neurons of the rostral ventrolateral medulla. *J. Neurosci.* **21**, 4032–4041 (2001).
48. G. M. Mang, P. Franken, Sleep and EEG phenotyping in mice. *Curr. Protoc. Mouse Biol.* **2**, 55–74 (2012).
49. L. M. Fernandez, J.-C. Comte, P. Le Merre, J.-S. Lin, P.-A. Salin, S. Crochet, Highly dynamic spatiotemporal organization of low-frequency activities during behavioral states in the mouse cerebral cortex. *Cereb. Cortex* 10.1093/cercor/bhw311 (2017).
50. L. Besedovsky, J. Born, T. Lange, Endogenous glucocorticoid receptor signaling drives rhythmic changes in human T-cell subset numbers and the expression of the chemokine receptor CXCR4. *FASEB J.* **28**, 67–75 (2014).
51. A. Rechtschaffen, A. Kales, *A Manual of Standardized Terminology, Techniques and Scoring System for Sleep of Human Subjects* (U.S. Department of Health, Education and Welfare, 1968).
52. R. Oostenveld, P. Fries, E. Maris, J.-M. Schoffelen, FieldTrip: Open source software for advanced analysis of MEG, EEG, and invasive electrophysiological data. *Comput. Intell. Neurosci.* **2011**, 156869 (2011).
53. H.-V. V. Ngo, T. Martinetz, J. Born, M. Mölle, Auditory closed-loop stimulation of the sleep slow oscillation enhances memory. *Neuron* **78**, 545–553 (2013).
54. M. Mölle, L. Marshall, S. Gais, J. Born, Grouping of spindle activity during slow oscillations in human non-rapid eye movement sleep. *J. Neurosci.* **22**, 10941–10947 (2002).
55. C. Jin, J. Zhang, X. Li, X. Yang, J. Li, J. Liu, Injectable 3-D fabrication of medical electronics at the target biological tissues. *Sci. Rep.* **3**, 3442 (2013).


**Acknowledgments:** We are grateful to all laboratory members for constructive discussions and detailed reading of the manuscript. We thank N. Liaudet for help with MATLAB, R. Kraftsik for help with statistical analysis, L. Besedovsky for providing the human sleep recordings, and J.-Y. Wang for providing sleep and memory data in humans. We are grateful to P. Franken, D. McCormick, and P. Salin for the critical input; M. Tafti and R. Gervais for the stimulating discussions; and J. Brumberg, M. Celio, P. Franken, S. Fulda, M. Tafti, and E. Welker for the careful reading of earlier versions of the manuscript. Basic Igor Pro routines were provided by S. Crochet. This work was possible thanks to the Physiology Department of the University of Lausanne, which provided the room for the mouse sleep experimentation, and the Werner Reichardt Centre for Integrative Neuroscience within the University of Tübingen, which provided computational infrastructure. **Funding:** Funding was provided by the Swiss National Science Foundation (grants 31003A_146244 and 31003A_166318) and the Etat de Vaud and the Deutsche Forschungsgemeinschaft (SFB 654 "Plasticity and Sleep"). **Author contributions:** S.L. and A.L. conceived the original study in mice, which was extended and rewritten in interaction with F.D.W. and J.B., who contributed the human findings. L.M.J.F. performed the LFP recordings and developed the analyses. S.L. performed all mouse experiments. R.C. contributed to the polysomnographic recordings in undisturbed mice. J.-Y.C. developed the noise generator in LabVIEW. S.L., L.M.J.F., F.D.W., R.C., and A.L. analyzed the data. S.L., L.M.J.F., F.D.W., and R.C. prepared the figures. A.L. wrote the manuscript together with S.L., F.D.W., L.M.J.F., and J.B. **Competing interests:** The authors declare that they have no competing interests. **Data and materials availability:** All data needed to evaluate the conclusions in the paper are present in the paper and/or the Supplementary Materials. Additional data related to this paper may be requested from the authors. Computer codes used to generate the results can be provided upon request. Code for spindle (peak) and slow wave detection as well as general power analysis of human data is publicly available at www.spisop.org.

Submitted 25 August 2016
Accepted 19 December 2016
Published 8 February 2017
10.1126/sciadv.1602026

**Citation:** S. Lecci, L. M. J. Fernandez, F. D. Weber, R. Cardis, J.-Y. Chatton, J. Born, A. Lüthi, Coordinated infraslow neural and cardiac oscillations mark fragility and offline periods in mammalian sleep. *Sci. Adv.* **3**, e1602026 (2017).

BASIC SCIENCE

# Suppression of Sleep Spindle Rhythmogenesis in Mice with Deletion of $Ca_V3.2$ and $Ca_V3.3$ T-type $Ca^{2+}$ Channels

Chiara Pellegrini, MSc; Sandro Lecci, MSc; Anita Lüthi, PhD; Simone Astori, PhD

*Department of Fundamental Neurosciences, University of Lausanne, Lausanne, Switzerland*

**Study Objectives:** Low-threshold voltage-gated T-type $Ca^{2+}$ channels (T-channels or $Ca_V3$ channels) sustain oscillatory discharges of thalamocortical (TC) and *nucleus Reticularis thalami* (nRt) cells. The $Ca_V3.3$ subtype dominates nRt rhythmic bursting and mediates a substantial fraction of spindle power in the NREM sleep EEG. $Ca_V3.2$ channels are also found in nRt, but whether these contribute to nRt-dependent spindle generation is unexplored. We investigated thalamic rhythmogenesis in mice lacking this subtype in isolation ($Ca_V3.2$KO mice) or in concomitance with $Ca_V3.3$ deletion ($Ca_V3$.double-knockout (DKO) mice).
**Methods:** We examined discharge characteristics of thalamic cells and intrathalamic evoked synaptic transmission in brain slices from wild-type, $Ca_V3.2$KO and $Ca_V3$.DKO mice through patch-clamp recordings. The sleep profile of freely behaving $Ca_V3.2$KO and $Ca_V3$.DKO mice was assessed by polysomnographic recordings.
**Results:** $Ca_V3.2$ channel deficiency left nRt discharge properties largely unaltered, but additional deletion of $Ca_V3.3$ channels fully abolished low-threshold whole-cell $Ca^{2+}$ currents and bursting, and suppressed burst-mediated inhibitory responses in TC cells. $Ca_V3$.DKO mice had more fragmented sleep, with shorter NREM sleep episodes and more frequent microarousals. The NREM sleep EEG power spectrum displayed a relative suppression of the σ frequency band (10–15 Hz), which was accompanied by an increase in the δ band (1–4 Hz).
**Conclusions:** Consistent with previous findings, $Ca_V3.3$ channels dominate nRt rhythmogenesis, but the lack of $Ca_V3.2$ channels further aggravates neuronal, synaptic, and EEG deficits. Therefore, $Ca_V3.2$ channels can boost intrathalamic synaptic transmission, and might play a modulatory role adjusting the relative presence of NREM sleep EEG rhythms.
**Keywords:** sleep spindles, sleep architecture, nucleus Reticularis thalami
**Citation:** Pellegrini C, Lecci S, Lüthi A, Astori S. Suppression of sleep spindle rhythmogenesis in mice with deletion of $Ca_V3.2$ and $Ca_V3.3$ T-type $Ca^{2+}$ channels. *SLEEP* 2016;39(4):875–885.

**Significance**
Sleep spindles are recurrent brain electrical oscillations typical for non-rapid-eye-movement sleep that protect the sleeping brain from external disturbance, sustain memory reinforcement in neuronal circuits and appear to be altered in several psychiatric disorders. We succeeded in suppressing sleep spindles in mice by genetically deleting the two low-voltage-gated $Ca^{2+}$ channels responsible for rhythmic electrical discharges of cells in the *nucleus Reticularis thalami*, also known as the thalamic spindle pacemaker. Our findings help dissecting the genetic make-up of sleep rhythmogenesis and offer a mouse model to examine the pathophysiological consequences of disrupting sleep spindles.

## INTRODUCTION

Low voltage-gated T-type $Ca^{2+}$ channels (T-channels) enable neurons to produce low-threshold discharges that are essential for the generation of sleep rhythms, but that occur also in motor control and olfaction.[1–6] Furthermore, T-channels may lead to aberrant bursting in neurons exposed to abnormal electrical activity.[1,7,8] T-channels are encoded by three genes, *CACNA1g*, *CACNA1h* and *CACNA1i* that give rise to the subtypes $Ca_V3.1$, $Ca_V3.2$, and $Ca_V3.3$, respectively, characterized by different biophysical properties and expression patterns.[9,10] T-channels are most abundant in thalamus, where they exhibit regional specificity: whereas $Ca_V3.1$ channel mRNA is restricted to excitatory thalamocortical (TC) cells, e.g., in the ventrobasal nucleus (VB), mRNA for both $Ca_V3.2$ and $Ca_V3.3$ channels is present in the *nucleus Reticularis thalami* (nRt),[10,11] a shell of GABAergic cells modulating the information flow in the thalamocortical system.[12]

Genetic manipulations of $Ca_V3$ channels have yielded substantial insight into the mechanisms of oscillatory activity of neuronal cells. However, in contrast to the well-established role of T-channels in single-cell burst discharge, how these channels contribute to network rhythmic activity has only partially progressed since the generation of knock-out (KO) animals. Furthermore, in at least some cases, the relation between the cellular effects of T-channel subtype deletion and the purported role of burst discharges in EEG rhythms remains obscure. For example, $Ca_V3.1$ channels are clearly responsible for low-threshold bursting in TC cells. However, both increases and decreases in the δ power (1–4 Hz) of the NREM sleep EEG were observed in animals lacking $Ca_V3.1$ channels.[13,14] Therefore, a long-standing tenet on the TC cell clock-like burst discharges as basis for the EEG δ rhythm[15,16] could not yet be confirmed based on $Ca_V3$ channel genetics.

We have previously shown that the $Ca_V3.3$ subtype is the major source of low-threshold $Ca^{2+}$ spikes in nRt cell dendrites.[17] In $Ca_V3.3$KO mice, nRt repetitive burst discharges were strongly reduced, leading to an impaired inhibitory drive onto TC cells. Furthermore, consistent with the previously recognized implication of the nRt in sleep spindle pacemaking, EEG power in the σ frequency range (10–15 Hz) was weakened at transitions between NREM and REM sleep in $Ca_V3.3$KO animals. There were no other major changes in EEG frequency bands, which indicated a $Ca_V3.3$-specific decrease in sleep spindle rhythmogenesis.[17]

Although $Ca_V3.3$-deficiency led to a reduction in sleep spindles, a substantial portion of power increase remained present in the σ frequency band at NREM sleep exit, suggesting that other cellular mechanisms contributing to these thalamocortical rhythms exist. A major candidate is the $Ca_V3.2$-current that has been identified in nRt cells,[18] and that appears to be the target of several modulatory extracellular and intracellular signaling molecules.[19] To date, $Ca_V3.2$ channels are implicated in peripheral nociception and neuropathic pain, and might be involved in

specific forms of thalamic processing, e.g., relay of nociceptive inputs.[20–22] In addition, the expression of $Ca_V3.2$ channels can be modified in pathological conditions, e.g., in animal models of epilepsy.[7] Whether and how $Ca_V3.2$ channels contribute to thalamic sleep rhythmogenesis has yet not been ascertained.

Here, we examined the consequences of silencing $Ca_V3$-mediated nRt rhythmogenesis on the EEG profile of mice harboring a deletion of *$Ca_V3.2$* and *$Ca_V3.3$* genes ($Ca_V3$.DKO). Whereas a lack of the $Ca_V3.2$ subtype alone in $Ca_V3.2$KO mice did not cause major alterations to nRt cellular properties, $Ca_V3$.DKO mice showed a fully abolished nRt low-threshold spiking and strongly impaired intrathalamic GABAergic transmission. In freely behaving $Ca_V3.2$KO mice, the EEG power spectrum during NREM sleep was indistinguishable from that of wild-type animals. By contrast, in $Ca_V3$.DKO mice, relative EEG power in the σ frequency range during NREM sleep was suppressed and accompanied by an increase in the δ frequency range. Although $Ca_V3$.DKO mice spent globally more time in NREM sleep during the light phase, NREM sleep episodes were of shorter duration compared to wild-type animals. Thus, silencing low-threshold bursts in nRt neurons not only affects spindle generation, but also alters slow wave rhythmogenesis, likely due to deficient inhibitory drive onto TC cells.

## METHODS

### Animal Handling and Genotyping

All procedures were approved by the Veterinary Office of the Canton de Vaud. C57Bl/6J (wild-type), homozygous $Ca_V3.2$KO and homozygous $Ca_V3$.DKO mice were maintained under a 12:12h light/dark schedule (Zeitgeber time ZT 0: 7AM for animals used for electrophysiological recordings; 9AM for polysomnographic recordings). Homozygous $Ca_V3.2$KO mice were obtained from heterozygous breeders ($Ca_V3.2$*het*) from the *Cacna1h*-KO mouse line,[23] originally generated on a mixed C57Bl/6J-129S3 background that was backcrossed into the C57Bl/6J background for 4 generations and has since been backcrossed into the C57Bl/6J background for over 10 years. Homozygous $Ca_V3$.DKO mice were obtained by crossing the $Ca_V3.2$KO and the C57Bl/6J-*Cacna1i*-KO ($Ca_V3.3$KO) mouse line.[17] First, $Ca_V3.2$*het*/$Ca_V3.3$*het* mice were generated from $Ca_V3.2$*het* and homozygous $Ca_V3.3$KO mice. Second, $Ca_V3.2$*het*/$Ca_V3.3$*het* were interbred, and the obtained $Ca_V3.2$*het*/$Ca_V3.3$KO mice were selected as final breeders for the generation of $Ca_V3$.DKO mice. The percentage of homozygous $Ca_V3$.DKO mice at the time of genotyping (P8-12) was below Mendelian expectation (< 10%), suggesting high perinatal mortality. The genotype was determined by PCR using the following primers (5'–3') for the *CACNA1h* gene, following a protocol provided by Heinz Beck's laboratory at the University of Bonn: CACNA1hF: ATTCAAGGGCTTCCACAGGGTA; CACNA1hR: CATCTCAGGGCCTCTGGACCAC; CACNA1hNeo: GCTAAAGCGCATGCTCCAGACTG, yielding products of 480 bp for wild-type and 330 bp for $Ca_V3.2$KO mice. For the *CACNA1i* gene, primers were: CACNA1iF: CTGCTGTGGTACCCTCCTGTC; CACNA1iR: GACAGGGTACCTGCTGCATG; EN-2SA-3R: GGGTTCGTGTCCTACAACAC, yielding products of 900 bp for wild-type and 545 bp for $Ca_V3.3$KO mice.[17]

### Electrophysiological Recordings and Analyses

Acute horizontal brain slices (300 µm-thick) were prepared at ZT 5–6 from 3–4 week-old animals of either sex, as previously described.[17,24] In the recording chamber, slices were constantly superfused with oxygenated artificial CSF (ACSF) at 30–32°C containing (in mM): 125 NaCl, 25 $NaHCO_3$, 2.5 KCl, 1.25 $NaH_2PO_4$, 1.2 $MgCl_2$, 2 $CaCl_2$, 25 glucose, 1.7 L(+)-ascorbic acid. Visually identified nRt and TC neurons were whole-cell patched with borosilicate glass pipettes (TW150F-4, WPI). For recordings of passive membrane properties and spike discharges, pipettes (3–5 MΩ) were filled with an intracellular solution containing (in mM): 140 $KMeSO_4$, 10 KCl, 10 HEPES, 0.1 EGTA, 4 Mg-ATP, 0.2 Na-GTP, 10 phosphocreatine (290–300 mOsm, pH 7.25). A liquid junction potential of −10 mV was taken into account. For T-current isolation, patch pipettes (2–3 MΩ) were filled with the following solution (in mM): 135 tetramethylammonium hydroxide (TMA-OH), 40 HEPES, 10 EGTA, 2 $MgCl_2$, 4 Mg-ATP, titrated to pH 7.2 with 100 mM hydrofluoric acid (HF). The extracellular solution was supplemented with 1 µM tetrodotoxin. A liquid junction potential of −2 mV was corrected for. T-current density and activation curve were estimated as previously described.[17] For IPSC recordings in TC cells, pipettes (3–4 MΩ) were filled with (in mM): 127 CsGluconate, 10 HEPES, 2 BAPTA, 6 $MgCl_2$, 2 Mg-ATP, 0.2 Na-GTP, 10 phosphocreatine, 2.5 QX-314 (290–300 mOsm, pH 7.25). In TC neurons voltage-clamped at −30 mV, postsynaptic responses were evoked by monopolar stimulation in the internal capsule with an ACSF-filled glass electrode, in the absence of glutamatergic blockers. IPSC charge transfer was calculated as the integral of the current trace during 1s from response onset. For EPSP recordings in nRt cells, pipettes were filled with the $KMeSO_4$-based solution described above, and ACSF was supplemented with 0.1 mM picrotoxin and 0.01 mM glycine. Current-clamp recordings were conducted with automatic bridge-balance of pipette resistance. Glutamatergic afferents were electrically stimulated in the internal capsule with a paired-pulse protocol (50 ms interval). Inputs of cortical origin were selected based on the short-term facilitation of the postsynaptic responses,[25] as assessed by the ratio of the initial slopes of voltage responses to 2$^{nd}$ and 1$^{st}$ stimuli. The probability of eliciting a low-threshold spike was estimated by the presence of a burst discharge in the 2$^{nd}$ response (as opposed to tonic firing or lack of discharge). At least 8 paired-pulse responses were evoked in nRt cells held at −80 mV by current injections.

Series resistance ($R_s$) was monitored throughout recordings by brief voltage pulses, and data were rejected for $R_s$ changes > 25%. Data were acquired through a Digidata1320 digitizer. Signals were amplified through a Multiclamp700B amplifier (Molecular Devices), sampled at 20 kHz and filtered at 10 kHz using Clampex10 (Molecular Devices). Clampfit10 (Molecular Devices) and Igor Pro 6 (WaveMetrics) were used for data analysis.

### Chemicals

All standard salts and chemicals were purchased from SigmaAldrich, except the following: $KMeSO_4$ (ICN Biomedicals); L(+)-ascorbic acid (VWR Prolabo); Tetrodotoxin, (Latoxan); QX-314-Cl (Alomone Labs), picrotoxin (Abcam).

### Polysomnographic Recordings and Analyses

Electroencephalographic (EEG/ECoG) and electromyographic (EMG) recordings were performed in male $Ca_V3.2$KO mice, $Ca_V3$.DKO mice and wild-type mice chronically implanted with electrodes for differential fronto-parietal EEG and nuchal muscle EMG, as previously described.[17,26] EEG electrodes were 2 gold-plated screws (1.1 mm diameter) implanted on the right hemisphere ~1.5 mm frontal to the bregma and ~1.5 mm frontal to the lambda, respectively, both at ~1.5 mm from the central fissure. Four further screws were inserted on the 2 hemispheres at symmetrical positions to stabilize the pin connector. EMG electrodes were gold wires with a diameter of 0.2 mm. The whole implant was fixed to the skull with a first layer of resin cement (RelyX, 3-M, or G-CEM, GC America Inc.) and then covered with Paladur (Heraeus Kulzer). At the time of surgery, animals were 6–9 weeks old. $Ca_V3$.DKO mice had slightly lower body weights (wild-type: 22.3 ± 0.9 g, n = 8 vs. $Ca_V3.2$KO: 21.8 ± 0.7 g, n = 8, and $Ca_V3$.DKO: 19.3 ± 0.9 g, n = 8; P = 0.058, one-way ANOVA). During one week of post-surgery recovery, mice received paracetamol (2 mg/mL) in drinking water. Animals were allowed one additional week to habituate once electrode implants were connected to the tethering cables. Polysomnographic acquisitions were performed in 48 h-long sessions with groups of 4 animals. The analog EEG and EMG signals were first amplified (gain 2000 x), and then high-pass filtered at 0.7 Hz and 10 Hz, respectively. Data were digitized at 2 kHz and down-sampled to 200 Hz through Somnologica 3.3.1 software (Embla System). Vigilance states were visually scored as wakefulness, NREM or REM sleep based on EEG/EMG signals according to well-established criteria.[26] Power spectra were determined from 48-h long recordings using discrete-Fourier transformation between 0.75 to 90 Hz (0.25 Hz bins) for consecutive 4-s epochs. For spectral analysis, a given epoch was rejected when an adjacent epoch was scored to a different vigilance state or contained movement artifacts. On average, 74% ± 5% of the total waking time, 93% ± 1% of the total NREM sleep time and 75% ± 2% of the total REM sleep time were included in the spectral analysis of wild-type animals. The corresponding values for $Ca_V3.2$KO mice are 82% ± 6%, 94% ± 1%, 84% ± 1%, and, for $Ca_V3$.DKO mice, 74% ± 7%, 91% ± 1% and 76% ± 4%. Mean power spectra were calculated as the average of all artifact-free 4-s epochs of the corresponding vigilance state during both light and dark phase. Sigma power at NREM-to-REM sleep transition was determined according to previously described procedures,[3,26] with % σ power expressed relative to the mean values at min 0.5–1.5 after the transition to REM sleep. Microarousals were defined as waking episodes of ≤ 16 s duration preceded and followed by at ≥ 5 and ≥ 4 NREM sleep episodes, respectively. EEG analyses were performed with customized semi-automated routines written in Matlab v8.5 R2015a (The Mathworks).

### Statistical Analyses

Data are presented as mean ± SEM, with "n" indicating the number of cells for *in vitro* recordings, and number of animals for EEG datasets. The use of parametric or nonparametric statistical tests was based on the normal distribution of the data. One-way ANOVA and repeated measures ANOVA were performed in JMP.10 (SAS Institute Inc.), followed by post hoc Student *t*-test, with significance accepted for $\alpha < 0.05$. Greenhouse-Geisser (G-G) correction was applied to account for violation of sphericity (Mauchly test), where necessary. Cumulative distributions of bouts of behavioral states were compared with the Kolmogorov-Smirnov test in Matlab, with a significance level of 0.01.

## RESULTS

### Abolishment of nRt Low-Threshold Burst Discharges in $Ca_V3$.DKO Mice

In acute brain slices from wild-type, $Ca_V3.2$KO and $Ca_V3$.DKO mice, we compared basic electrophysiological parameters of nRt neurons by means of whole-cell patch-clamp recordings (Figure 1). No overt difference between genotypes was present for values of resting membrane potential ($V_{rmp}$: wild-type, −64.6 ± 2.6 mV; $Ca_V3.2$KO, −67.9 ± 2.6 mV; $Ca_V3$.DKO, −70.9 ± 3.1 mV), cell capacitance ($C_m$: wild-type, 78.7 ± 7 pF; $Ca_V3.2$KO, 85.9 ± 10 pF; $Ca_V3$.DKO, 80.0 ± 5 pF), and input resistance ($R_i$: wild-type, 204.8 ± 31.4 MΩ; $Ca_V3.2$KO, 207.4 ± 34.2 MΩ; $Ca_V3$.DKO, 227.5 ± 24.9 MΩ) (wild-type, n = 11 cells; $Ca_V3.2$KO, n = 9; $Ca_V3$.DKO, n = 9; for all parameters P > 0.05, one-way ANOVA; Figure 1A). Current responses to hyperpolarizing voltage steps, which include activation of inwardly rectifying and HCN channels, were also comparable (Figure 1B). Moreover, tonic firing elicited by depolarizing current injections (400 ms) from a holding potential of −70 mV displayed similar input-output relationships (wild-type, n = 9; $Ca_V3.2$KO, n = 8; $Ca_V3$.DKO, n = 9; Figure 1C). We noticed a tendency of $Ca_V3$.DKO neurons to sustain prolonged tonic firing, whereas wild-type and $Ca_V3.2$KO often displayed strong accommodation after the first 200 ms of depolarization. We quantified spiking frequency during the second half of the 400 ms-long depolarization, and found a consistent tendency for an increase in $Ca_V3$.DKO neuron firing rate (e.g. 400 pA step: wild-type, 26.7 ± 17.8 Hz; $Ca_V3.2$KO, 26.8 ± 10.1 Hz; $Ca_V3$.DKO, 43.9 ± 11.7 Hz; P > 0.05). This is consistent with a previous study reporting on increased propensity of $Ca_V3$.DKO nRt cells to generate tonic firing during prolonged step depolarization (> 1 s).[27]

We next examined low-threshold spiking generated at the offset of brief hyperpolarizing current steps (Figure 2). Wild-type cells (n = 10) displayed rhythmic low-threshold $Ca^{2+}$ spikes accompanied by bursts of $Na^+$ action potentials, the number of which varied depending on the initial membrane potential. Typically, bursts discharges were best elicited at $V_m$ values in the range between −70 mV and −55 mV. Interestingly, in nRt cells from $Ca_V3.2$KO mice, no significant change in repetitive bursting was found (P > 0.05; n = 9; Figure 2C, 2D). Inter-burst intervals measured for discharges elicited from −70 mV also did not differ between genotypes (interval between initial APs of the first and second burst: wild-type, 168 ± 16 ms, n = 6; $Ca_V3.2$KO, 181 ± 14 ms, n = 8; P > 0.05, unpaired *t*-test). By contrast, $Ca_V3$.DKO mice displayed a complete lack of oscillatory low-threshold spiking, as previously reported.[27] Occasionally, a single action potential appeared in $Ca_V3$.DKO cells at

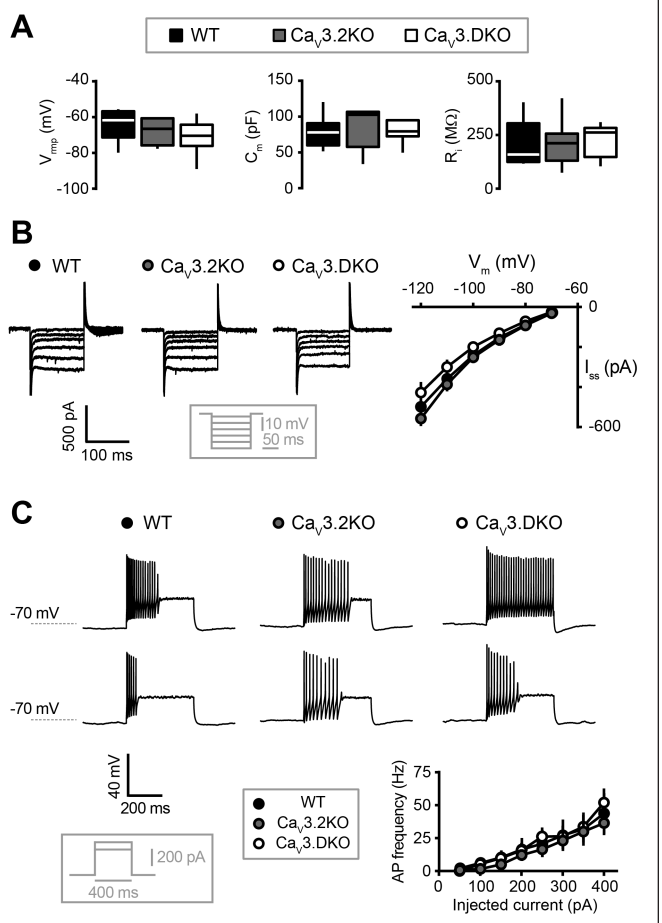


**Figure 1**—Lack of overt changes in passive properties and tonic discharge of nRt cells of $Ca_V3.2KO$ and $Ca_V3.DKO$ mice. **(A)** Box-and-whisker plots with values of resting membrane potential ($V_{rmp}$), membrane capacitance ($C_m$) and input resistance ($R_i$) of nRt cells from wild-type (WT, n = 11), $Ca_V3.2KO$ (n = 9) and $Ca_V3.DKO$ (n = 9) mice. The midline in each box represents the median, the whiskers are 10$^{th}$ and 90$^{th}$ percentiles. **(B)** Left, representative current responses to hyperpolarizing voltage steps from −60 mV for all genotypes. Inset: protocol. Right, steady-state current ($I_{ss}$) for WT (n = 10), $Ca_V3.2KO$ (n = 9) and $Ca_V3.DKO$ (n = 9) nRt cells over a range of voltages. **(C)** Top, representative tonic discharges in WT, $Ca_V3.2KO$ and $Ca_V3.DKO$ nRt cells elicited by positive current injections from −70 mV. Bottom, average discharge frequency of tonic action potentials (APs) during the 400 ms over a range of positive currents injected (WT, n = 9; $Ca_V3.2KO$, n = 8; $Ca_V3.DKO$, n = 9; P > 0.05). Inset: current-clamp protocol.

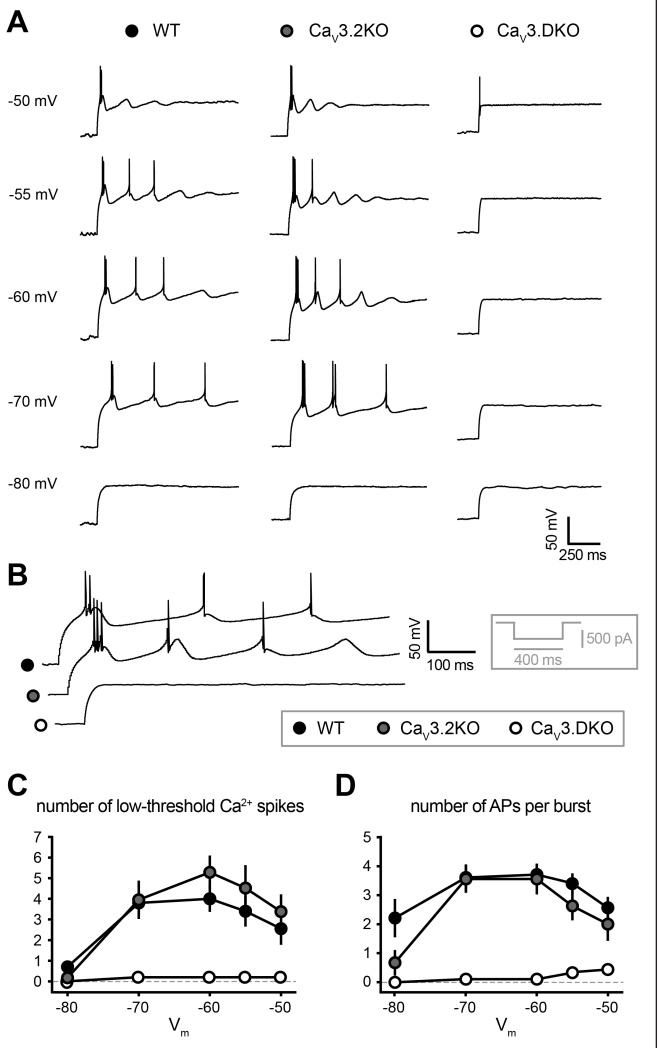


**Figure 2**—Suppression of oscillatory low-threshold bursting in nRt cells from $Ca_V3.DKO$ mice. **(A)** Representative traces of low-threshold bursting in WT, $Ca_V3.2KO$ and $Ca_V3.DKO$ nRt cells elicited at the offset of negative current injections from different membrane potentials, as indicated. **(B)** Expanded traces from **(A)** at −60 mV. Inset: current-clamp protocol. **(C)** Number of low-threshold $Ca^{2+}$ spikes and **(D)** number of action potentials (APs) during the first burst in WT (n = 10), $Ca_V3.2KO$ (n = 9), and $Ca_V3.DKO$ (n = 9) mice.

the offset of hyperpolarizing steps applied from more depolarized membrane potentials (−50 mV, observed in 4 of 9 cells).

Next, we quantified the contribution of $Ca_V3.2$ channels to isolated low-threshold $Ca^{2+}$ currents (T-currents) that were elicited by increasing depolarizing steps applied to nRt cells voltage-clamped at −100 mV (Figure 3). Compared to wild-type cells, currents from $Ca_V3.2KO$ cells displayed a slight prolongation of inactivation kinetics ($\tau_{w,\ decay}$ at −60 mV: wild-type, 58.9 ± 4.5 ms, n = 9; $Ca_V3.2KO$, 83.1 ± 10.9 ms, n = 8; P = 0.07, unpaired *t*-test; Figure 3A), consistent with previous data from younger (2 week-old) $Ca_V3.2KO$ mice.[18] Activation kinetics were equivalent (10% to 90% rise time at −60 mV: wild-type, 6.8 ± 0.6 ms, n = 9; $Ca_V3.2KO$, 6.1 ± 0.5 ms, n = 8; P > 0.05, unpaired *t*-test; Figure 3A). Current density and activation curve were comparable, with no significant modification in the estimated $V_{half}$ (wild-type, −71.1 ± 1.0 mV, n = 9; $Ca_V3.2KO$, −69.8 ± 1.7 mV, n = 8; P > 0.05, unpaired *t*-test; Figure 3B). In $Ca_V3.DKO$ mice, no detectable T-currents were generated across the entire range of voltage steps (n = 9).

Together, deletion of $Ca_V3.2$ and $Ca_V3.3$ channels completely abolished T-currents in nRt cells, with a consequent suppression of repetitive oscillatory low-threshold discharges. The absence of the $Ca_V3.2$ subtype did not induce overt changes in the single-cell electrophysiological profile, confirming the dominant role of $Ca_V3.3$ channels in setting nRt cells responsiveness to somatic voltage fluctuations.[17] However, it is also well known that the electrotonic properties of the thin nRt cell

dendrites hamper proper space-clamp, which prevents the controlled activation of voltage-dependent conductances in distal compartments.[28] This could be one reason for which a $Ca_V3.2$-current component went undetected in our somatic whole-cell recordings.

### Impaired Intrathalamic GABAergic Transmission in $Ca_V3$.DKO Mice

We next examined the impact of $Ca_V3.2$ and $Ca_V3.3$ channel deletion on synaptic transmission and excitability within intrathalamic networks, which are both relevant for sleep rhythm generation.[17,29] We first verified whether thalamocortical (TC) cells in the ventrobasal nucleus (VB) continue to generate low-threshold discharges via $Ca_V3.1$ channels[13,14] when their synaptic partners in the nRt are burst-deficient. TC cells from wild-type, $Ca_V3.2$KO and $Ca_V3$.DKO mice displayed comparable responses to hyperpolarizing current injections, which reliably elicited low-threshold spikes crowned by the same number of action potentials (number of APs in bursts generated by a current injection of −250 pA: wild-type, 2.8 ± 0.4, n = 9; $Ca_V3.2$KO, 2.5 ± 0.5, n = 6; $Ca_V3$.DKO, 2.2 ± 0.4, n = 6; $P > 0.05$, one-way ANOVA; Figure 4A).

Low-threshold bursting of nRt generates phasic inhibitory currents in TC cells comprising a fast and a slow component, mediated by synaptic and non-synaptic $GABA_A$ receptors, respectively.[29,30] In TC cells held at −30 mV using low $Cl^-$-based electrodes we evoked IPSCs by electrically stimulating the internal capsule, while leaving excitatory transmission intact, thus permitting the recruitment of nRt cell discharges by glutamatergic inputs. In wild-type mice, evoked responses in TC cells typically consisted of multiphasic "burst IPSCs" (bIPSCs) at stimulation intensities > 100 μA, with a sequence of fast events riding on a slower current envelope, previously reported to result from presynaptic burst discharge.[17,29,31] Deletion of $Ca_V3.2$ channels decreased the charge transfer of bIPSCs elicited at higher intensities (250–300 μA: wild-type, 91.0 ± 21.1 pC, n = 7; $Ca_V3.2$KO, 50.7 ± 10.7 pC, n = 8; $P < 0.05$ one-way ANOVA; Figure 4B). By contrast, in TC cells from $Ca_V3$.DKO, only small monophasic IPSCs lacking the waveform typical for bIPSCs could be evoked, and the charge transfer was strongly diminished (250–300 μA: $Ca_V3$.DKO, 13.5 ± 3.6 pC, n = 7; $P < 0.01$ compared to wild-type; Figure 4B). Finally, we examined the responsiveness of nRt cells to cortical glutamatergic inputs, which are thought to initiate spindle rhythmogenesis by activating low-threshold conductances in nRt dendrites.[32,33] In current-clamped nRt cells at −80 mV, we evoked EPSPs of cortical origin by selecting responses that exhibited short-term facilitation upon paired-pulse stimulation in the internal capsule.[25] Paired-pulse ratio of the initial slope of voltage responses was comparable between genotypes (wild-type, 2.2 ± 0.2, n = 8; $Ca_V3.2$KO, 2.4 ± 0.2, n = 7; $Ca_V3$.DKO, 2.7 ± 0.4, n = 6; $P > 0.05$ one-way ANOVA; Figure 4C). In wild-type and in $Ca_V3.2$KO mice, the second stimulus typically elicited a low-threshold burst, with an occurrence of 68% ± 8% and 52% ± 15%, respectively. In $Ca_V3$.DKO mice, no bursting was generated ($P < 0.01$ Wilcoxon test, compared to the other genotypes), despite the sufficient depolarization provided by the second stimulus (on average 12.5 ± 1.2 mV), which occasionally elicited a single suprathreshold action potential (in 2 of 6 cells).

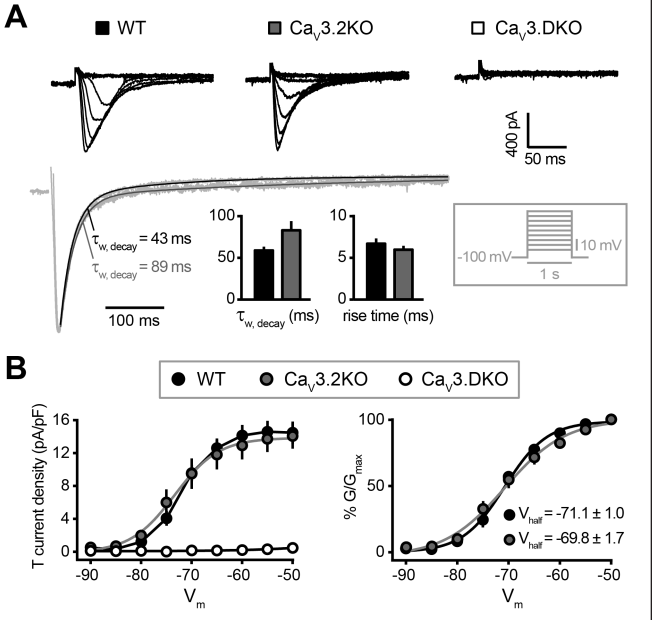


**Figure 3**—Elimination of low-threshold $Ca^{2+}$ currents in nRt cells from $Ca_V3$.DKO mice. **(A)** Top, isolated low-threshold $Ca^{2+}$ currents elicited by depolarizing steps from −100 mV in WT, $Ca_V3.2$KO and $Ca_V3$.DKO nRt cells. Bottom, representative traces scaled to peak and bar graphs showing mean values for decay time constant ($\tau_{w, decay}$) and rise time (10% to 90%) from WT and $Ca_V3.2$KO (WT, n = 9; $Ca_V3.2$KO, n = 8; $P > 0.05$). Inset: voltage-clamp protocol. **(B)** T-current density for all genotypes (left) and activation curve (right) of the T-currents for WT and $Ca_V3.2$KO with estimated $V_{half}$ (WT: −71.1 ± 1.0 mV, n = 9; $Ca_V3.2$KO: −69.8 ± 1.7 mV, n = 8; $P > 0.05$). In $Ca_V3$.DKO mice, no detectable T-currents were generated across the whole range of voltage steps (n = 9).

Together, these data reveal a pronounced deficit in the intrathalamic GABAergic transmission in $Ca_V3$.DKO mice, which is due to an impaired capability of nRt in generating low-threshold discharges. Although the deletion of $Ca_V3.2$ channels did not appear to affect nRt repetitive bursts in response to somatic current injections, $Ca_V3.2$KO mice displayed a reduction in the charge transfer of bIPSCs. This discrepancy between somatically and synaptically elicited bursting suggests that $Ca_V3.2$ deletion affects the efficacy of excitatory inputs in recruiting nRt dendritic $Ca^{2+}$ conductances.

### EEG Sleep Profile of $Ca_V3.2$KO and $Ca_V3$.DKO Mice

The lack of low-threshold bursting in nRt cells from $Ca_V3$.DKO mice predicted a marked deregulation of thalamic sleep rhythmogenesis. In particular, we expected $Ca_V3$.DKO mice to exhibit deficits in sleep spindle generation, which depends on nRt bursting and on reverberatory activity within the nRt-TC loop.[32,34,35] We performed polysomnographic recordings in freely behaving wild-type (n = 8), $Ca_V3.2$KO mice (n = 8), and $Ca_V3$.DKO mice (n = 8) chronically implanted with EEG/EMG electrodes and recorded under undisturbed conditions for 48 h. In the following, we describe sleep architecture and EEG power spectra during NREM sleep, REM sleep, and waking in the three genotypes.

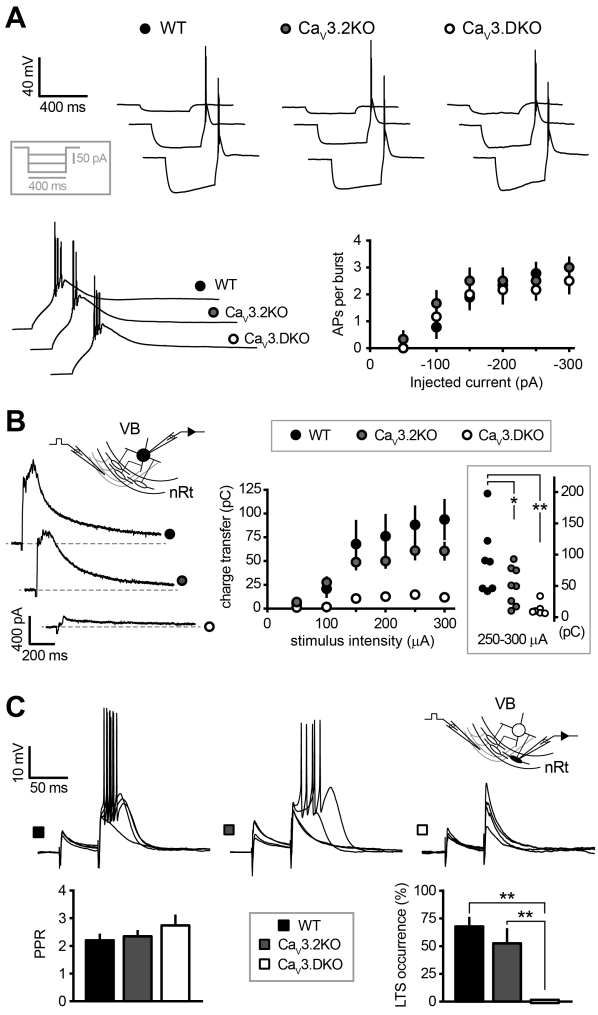


**Figure 4**—Consequences of $Ca_V3.2$ and $Ca_V3.3$ channel deletion for nRt-TC GABAergic transmission. **(A)** Top, representative traces of rebound bursting elicited by hyperpolarizing current injections discharges in TC neurons held at −70 mV. Inset: current-clamp protocol. Bottom left, expanded traces shown in **(A)** for a −150 pA step of current injection. Bottom right, the number of action potentials per burst across a range of injected current did not change between genotypes (WT, n = 9, $Ca_V3.2$KO, n = 6, $Ca_V3.3$DKO, n = 6; P > 0.05). **(B)** Left, example traces of evoked IPSCs recorded in TC cells at −30 mV upon electrical stimulation in the internal capsule. Inset, recording configuration showing site of stimulation in the internal capsule while recording from a TC cell in the ventrobasal nucleus (VB). Right, charge transfer across a range of stimulus intensities for all genotypes showing a minor and a strong decrease in the $Ca_V3.2$KO and $Ca_V3.3$DKO mice, respectively, compared to WT animals. Inset shows mean responses to higher stimulus intensities (250–300 μA) (WT, n = 7, $Ca_V3.2$KO, n = 8; $Ca_V3.3$DKO, n = 7; one-way ANOVA, P < 0.05; **P < 0.01, *P < 0.05, post hoc unpaired *t*-test). **(C)** Top, examples of postsynaptic responses evoked in nRt cells at −80 mV upon stimulation of cortical afferents. Inset, recording configuration showing stimulation site in the internal capsule. Paired-pulse stimuli (50 ms interval) were delivered to select for responses of cortical origin based on short-term facilitation. Bottom, bar graphs showing mean values of paired-pulse ratio (PPR), measured from the initial slope of voltage responses, and occurrence of low-threshold spiking (LTS) on the second stimulus (WT, n = 8, $Ca_V3.2$KO, n = 7; $Ca_V3.3$DKO, n = 6; one-way ANOVA, P > 0.05 for PPR and Wilcoxon test, P < 0.05 for LTS occurrence; **P < 0.01 nonparametric multiple comparison).

$Ca_V3.2$KO mice spent similar amounts of time in the different vigilance states as compared to wild-type animals, except for a slight reduction in NREM sleep during the dark phase ($F_{2.0,\ 21.3}$ = 2.8, P = 0.08; Figure 5A). During the light phase, $Ca_V3.3$DKO mice spent, on average, more time in NREM sleep and less time in waking, as compared to wild-type and $Ca_V3.2$KO mice ($F_{2.4,\ 25.3}$ = 6.6, P < 0.01). Inspection of sleep bout length revealed that NREM sleep episodes of long duration (> 252 s) occurred more frequently in $Ca_V3.2$KO mice, whereas bouts of intermediate duration (32–252 s) were predominant in $Ca_V3.3$DKO mice at the expense of long episodes ($F_{2.0,\ 21.3}$ = 12.3, P < 0.01; Figure 5B). By contrast, no alterations were found in episode length and global time spent in REM sleep ($F_{2.6,\ 27.2}$ = 2.3, P > 0.05; Figure 5A, 5B) or in the number of transitions from NREM to REM sleep (per hour of NREM sleep: 6.0 ± 0.5 in wild-type vs. 6.7 ± 0.4 in $Ca_V3.2$KO mice, and 5.8 ± 0.4 in $Ca_V3.3$DKO mice, P > 0.05). The changes in NREM sleep architecture appeared to be counterbalanced by alterations in waking episodes. Compared to wild-type and $Ca_V3.2$KO mice, $Ca_V3.3$DKO mice spent more time in brief and intermediate periods of wakefulness (< 32 s, 32–124 s, $F_{2.1,\ 22.5}$ = 11.6, P < 0.01; Figure 6A), and, interestingly, NREM sleep episodes were more frequently interrupted by microarousals (per hour of NREM sleep: 13.2 ± 1.1 microarousals in wild-type vs. 8.8 ± 0.9 in $Ca_V3.2$KO mice, and 17.6 ± 0.9 in $Ca_V3.3$DKO mice, P < 0.01 for both KO genotypes compared to wild-type). Thus, although $Ca_V3.3$DKO mice spent globally more time in NREM sleep episodes, these were of shorter duration, and sleep was generally more disrupted by short awakenings.

Next, we examined EEG power spectra of NREM and REM sleep. Absolute values of NREM sleep EEG power did not significantly differ between genotypes, although $Ca_V3.3$DKO mice appeared to show an increase in the low-frequency range (slow-wave activity, SWA, 0.75–4 Hz) during both light and dark phase (Figure 5C).

To examine the relative contribution of specific spectral frequencies to the global EEG profile, and to account for inter-individual variations in EEG signal amplitude, we compared percentage EEG power values obtained by normalizing each frequency bin to the total power for each behavioral state (Figure 5D). Whereas wild-type and $Ca_V3.2$KO mice had largely superimposable NREM sleep power spectra, significant differences were visible in $Ca_V3.3$DKO mice ($F_{2.7,\ 27.9}$ = 4.5, P < 0.05). In particular, a marked reduction occurred across the whole σ frequency range (10–15 Hz: 0.57% ± 0.03% in wild-type vs. 0.56% ± 0.03% in $Ca_V3.2$KO mice, and 0.41% ± 0.01% in $Ca_V3.3$DKO mice; P < 0.01, post hoc unpaired *t*-test). A compromised spindle rhythmogenesis in $Ca_V3.3$DKO mice was also found when EEG power dynamics were analyzed at transitions between NREM and REM sleep, which are spindle-rich periods.[17,26] In the NREM sleep epochs preceding REM sleep, σ power typically exhibits a surge, which is accompanied by a decrease in δ power, indicative of reduced sleep depth. $Ca_V3.2$KO mice displayed a partially reduced σ power surge, which, in $Ca_V3.3$DKO mice, was further diminished (570 ± 43% in wild-type vs. 438 ± 15% in $Ca_V3.3$DKO mice and 328 ± 15% in $Ca_V3.3$DKO mice; P < 0.01, Figure 5E) and also preceded by a lower level of basal σ power. In contrast to the changes

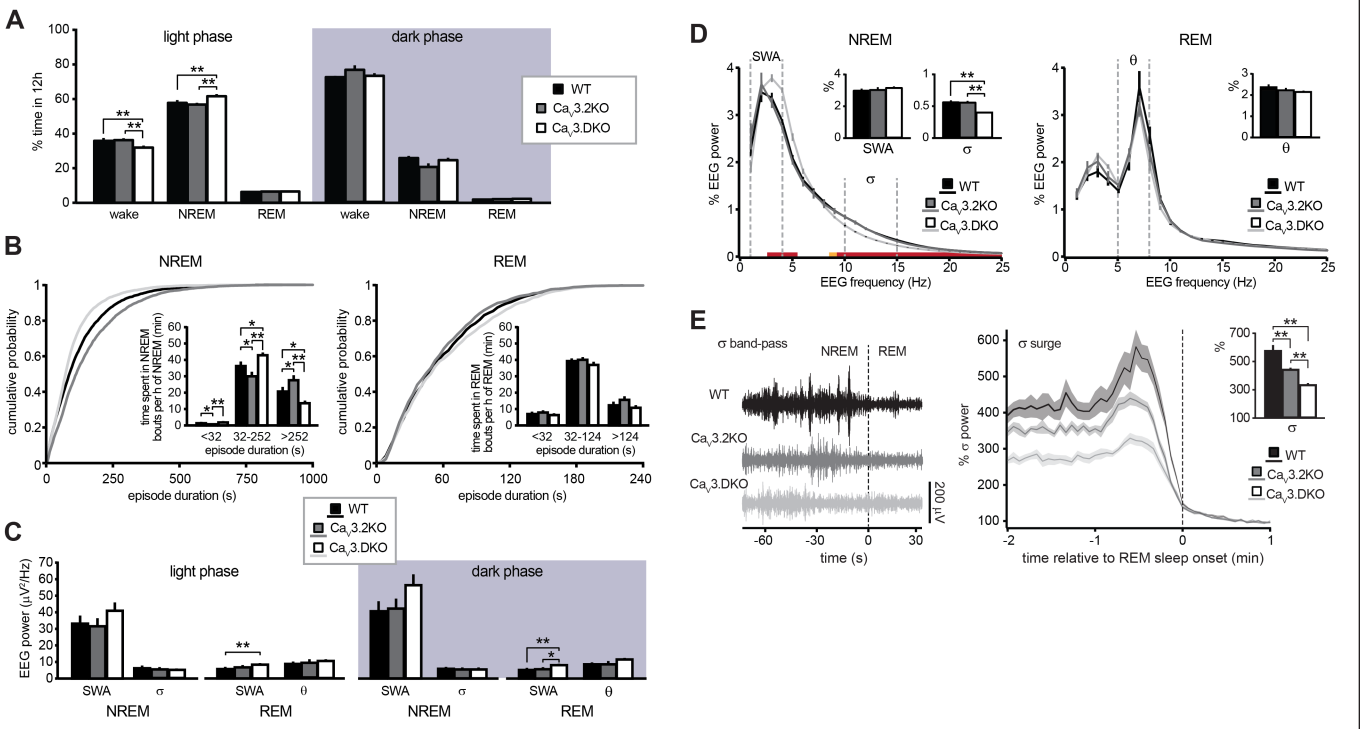


**Figure 5**—Comparison of the EEG sleep profile of WT, $Ca_V3.2$KO, and $Ca_V3$.DKO mice. **(A)** Time spent in wake, NREM and REM sleep, expressed in % of 12 h and separated for light and dark period, for WT (n = 8), $Ca_V3.2$KO (n = 8), and $Ca_V3$.DKO (n = 8) mice. During the light phase, $Ca_V3$.DKO showed an increased amount of NREM sleep, while waking was reduced (state × genotype interaction: $F_{2.4, 25.3} = 6.6$, $P < 0.05$; **$P < 0.01$, post hoc unpaired *t*-test). No change occurred during the dark phase ($F_{2.0, 21.3} = 2.8$, $P > 0.05$). **(B)** Cumulative distributions of NREM and REM sleep episode duration pooled for light and dark phase. Statistical significance was tested with K-S statistics ($P < 0.01$ between all genotypes for NREM sleep). Insets, histograms of time spent in short, intermediate and long episodes per hour of corresponding sleep (duration × genotype interaction: $F_{2.0, 21.3} = 12.3$, $P < 0.01$ for NREM sleep and $F_{2.6, 27.2} = 2.3$, $P > 0.05$ for REM sleep; *$P < 0.05$, **$P < 0.01$, post hoc unpaired *t*-test). **(C)** Mean absolute power of relevant frequency bands during NREM or REM sleep separated for light and dark phase (SWA (0.75–4 Hz), σ (10–15 Hz), and θ (5–8 Hz); one-way ANOVA, $P < 0.05$ and $P < 0.01$ for SWA of light and dark phase, respectively; *$P < 0.05$, **$P < 0.01$, post hoc unpaired *t*-test). **(D)** Normalized EEG power spectrum between 0.75 and 25 Hz for NREM (left) and REM (right) sleep. Red and orange lines on the x axes delineate intervals of frequency for $Ca_V3$.DKO mice with a significant difference compared to WT and $Ca_V3.2$KO mice, with $P < 0.01$ and $P < 0.05$, respectively, tested with post hoc unpaired *t*-test after repeated measures ANOVA (genotype × frequency interaction: $F_{2.7, 27.9} = 4.5$, $P < 0.05$ for NREM sleep and $F_{3.2, 33.4} = 1.8$, $P > 0.05$ for REM sleep). Dotted lines indicate frequency ranges for SWA (0.75–4 Hz), σ (10–15 Hz), and θ (5–8 Hz) bands used for the mean values presented in the bar graphs in the insets (one-way ANOVA, $P < 0.05$ for σ; **$P < 0.01$, post hoc unpaired *t*-test). **(E)** Left, examples of σ band-pass-filtered EEG recordings containing NREM-to-REM sleep transitions (occurring at time zero). Right, time course of mean EEG power in the σ band at NREM-to-REM sleep transitions in WT (n = 8), $Ca_V3.2$KO (n = 8), and $Ca_V3$.DKO (n = 8) mice during light and dark phase. Data were normalized to the mean power from 0.5 to 1.5 min after the transition to REM sleep. Shaded areas represent SEM. The dashed line at zero indicates REM sleep onset. Bar graph represents peak values of % σ power before REM sleep onset (one-way ANOVA, $P < 0.01$; **$P < 0.01$, post hoc unpaired *t*-test).

in σ power, relative EEG power in the low-frequency range was globally unaltered (0.75–4 Hz: 3.0% ± 0.1% in wild-type vs. 3.0% ± 0.2% in $Ca_V3$.DKO mice and 3.2% ± 0.1% in $Ca_V3$.DKO mice; $P > 0.05$, post hoc unpaired *t*-test). Interestingly, however, in $Ca_V3$.DKO mice a significant increase was obtained when the higher range of δ frequencies was considered (2–4 Hz: 3.2 ± 0.1% in wild-type vs. 3.2 ± 0.1% in $Ca_V3.2$KO mice and 3.6 ± 0.1% in $Ca_V3$.DKO mice, $P < 0.05$ for $Ca_V3$.DKO mice compared to wild-type and $Ca_V3.2$KO; post hoc unpaired *t*-test).

The normalized EEG power spectrum of REM sleep was not significantly altered in $Ca_V3.2$KO and $Ca_V3$.DKO mice ($F_{3.2, 33.4} = 1.8$, $P > 0.05$; Figure 5D). A slight increase in the higher range of δ frequencies during REM sleep seemed to gradually appear with *$Ca_V3$* single and double deletion (2–4 Hz: 1.70% ± 0.11% in wild-type vs. 1.86% ± 0.13% in $Ca_V3.2$KO mice and 1.93% ± 0.03% in $Ca_V3$.DKO mice; $P > 0.05$). A difference in SWA was visible for absolute values of REM sleep EEG power of $Ca_V3$.DKO mice ($P < 0.01$ compared to wild-type, for both phases; Figure 5C).

Absolute values of waking EEG power of $Ca_V3$.DKO mice exhibited a general increase across frequency bands during both light and dark phase compared to wild-type and $Ca_V3.2$KO mice ($P < 0.01$ for both phases; Figure 6B). The relative contribution of the distinct frequency bands to the normalized power spectra was different ($F_{5.6, 59.5} = 3.48$, $P < 0.01$), in particular at frequency ranges corresponding to the α (8–12 Hz) and the β (12–20 Hz) band that displayed, on average, a significant reduction (8–12 Hz and 12–20 Hz: 0.89% ± 0.05% and 0.29% ± 0.01% in wild-type vs. 0.94% ± 0.05% and 0.28% ± 0.01% in $Ca_V3.2$KO mice, and 0.70% ± 0.02% and 0.25% ± 0.01% in $Ca_V3$.DKO mice, $P < 0.01$ for $Ca_V3$.DKO

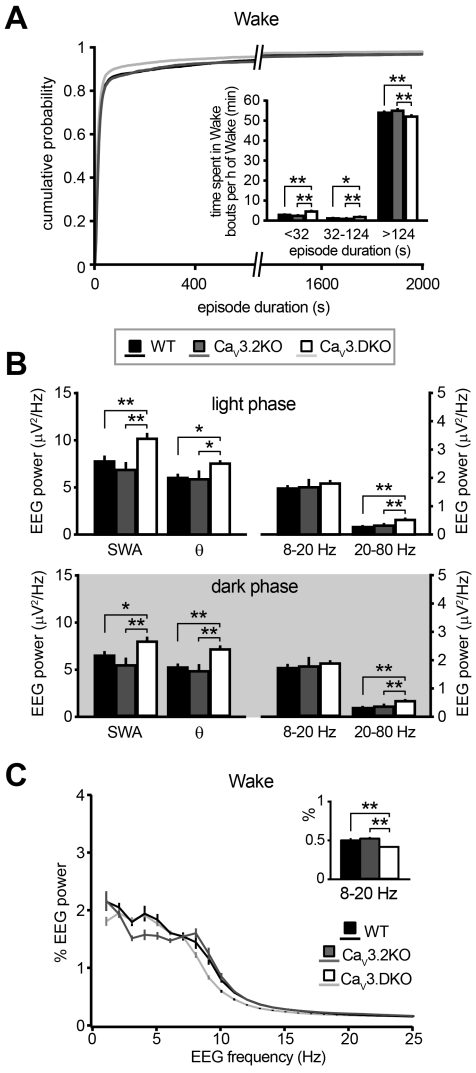


**Figure 6**—Comparison of wake EEG profile of wild-type, $Ca_V3.2$KO, and $Ca_V3$.DKO mice. **(A)** Cumulative distributions of wake episode durations during both light and dark phase. Statistical significance was tested with K-S statistics (P < 0.01 between all genotypes). Inset, histogram showing time spent in short, intermediate and long episodes per hour of wake (duration × genotype: $F_{2.1, 22.5} = 11.6$, P < 0.01; *P < 0.05, **P < 0.01, post hoc unpaired *t*-test). **(B)** Mean absolute power of relevant frequency bands separated for light and dark phase (SWA (0.75–4 Hz), θ (5–8 Hz); *P < 0.05, **P < 0.01, post hoc unpaired *t*-test after one-way ANOVA). **(C)** Normalized EEG spectral power between 0.75 and 25 Hz during waking (genotype × frequency interaction: $F_{5.6, 59.5} = 3.48$, P < 0.01). Inset, mean values of normalized EEG power in the frequency range 8–20 Hz for WT, $Ca_V3.2$KO, and $Ca_V3$.DKO (one-way ANOVA, P < 0.01; **P < 0.01, post hoc unpaired *t*-test).

mice compared to wild-type and $Ca_V3.2$KO, post hoc unpaired *t*-test; Figure 6C).

Altogether, analysis of sleep EEG power indicates distinct contributions of $Ca_V3.2$ and $Ca_V3.3$ channels to thalamocortical rhythmogenesis. *$Ca_V3.2$* single deletion did not cause major alterations to the spectral profile of NREM sleep. However, some differences in σ power dynamics were observed at transitions between NREM and REM sleep, i.e., at periods of enhanced sleep spindle rhythmogenesis. *$Ca_V3.2$* and *$Ca_V3.3$* double deletion induced a marked decrease in the relative contribution of the σ frequency range that was also evident in the average NREM sleep power spectrum, consistent with a constitutive impairment in sleep spindle rhythmogenesis. Additionally, the EEG power in the δ frequency range was augmented. $Ca_V3$.DKO mice spent more time in NREM sleep, but the predominance of short NREM sleep episodes together with the increase in microarousals indicates a more fragmented sleep architecture.

## DISCUSSION

This work contributes to clarify the roles of $Ca^{2+}$ channels for thalamic oscillations and sleep rhythms. In line with previous results, our data provide further evidence for a dominant role of $Ca_V3.3$ subtype in sustaining nRt low-threshold bursting and in activating the intrathalamic loop that underlies spindle pacemaking. In addition, our findings point at a modulatory function of the $Ca_V3.2$ subtype for nRt excitability, which might be involved in dynamically changing the strength of thalamic oscillations, e.g., by boosting sleep spindle rhythmogenesis at NREM to REM transitions. Based on these observations, we propose that the co-expression of $Ca_V3.2$ and $Ca_V3.3$ subtypes in nRt underlies distinct aspects of this pacemaker structure in rhythmogenesis. In addition, the lack of low-threshold $Ca^{2+}$ currents in $Ca_V3$.DKO mice excludes a functional contribution of the $Ca_V3.1$ subtype, although molecular analyses have also identified the presence of this isoform in nRt cells.[36]

Our study was largely based on a comparative analysis of single KOs for $Ca_V3.2$ channels and the DKO lacking both $Ca_V3.2$ and $Ca_V3.3$ channels (Figure 7). We found that removal of $Ca_V3.2$ channels alone did not cause major alterations to nRt discharge, consistent with previous reports indicating a major contribution of $Ca_V3.3$ channels.[17,18] In particular, low-threshold oscillatory bursting typical for NREM sleep rhythms, such as sleep spindles, was largely preserved in $Ca_V3.2$KO mice, and the underlying T-currents were comparable with wild-type levels.

We have analyzed cell excitability by applying somatic voltage steps, which might amplify the activation of proximal $Ca_V3$ channels and underestimate the contribution of distal compartments, especially in the case of the elongated dendrites of nRt neurons.[37] Are $Ca_V3.2$ channels preferentially located in distal dendritic branches? T-currents in nucleated patches from younger mice were shown to display higher $Ni^{2+}$ sensitivity and faster inactivation kinetics than whole-cell T-currents, indicating that, at least during development, $Ca_V3.2$ channels are mainly located at proximal sites.[28]

We have further characterized the capability of $Ca_V3$ channels to generate nRt discharge when synaptically recruited. Upon stimulation of glutamatergic inputs onto nRt, bIPSCs could still be evoked in TC cells of $Ca_V3.2$KO mice, although with a reduced charge transfer, whereas this form of GABAergic transmission was impaired by *$Ca_V3.3$* ablation.[17] Synaptic recruitment of $Ca_V3.3$ channels is hence obligatory for bIPSC generation, whereas $Ca_V3.2$ channels additionally appear to boost synaptic transmission mediated through burst discharge. A modulatory function for

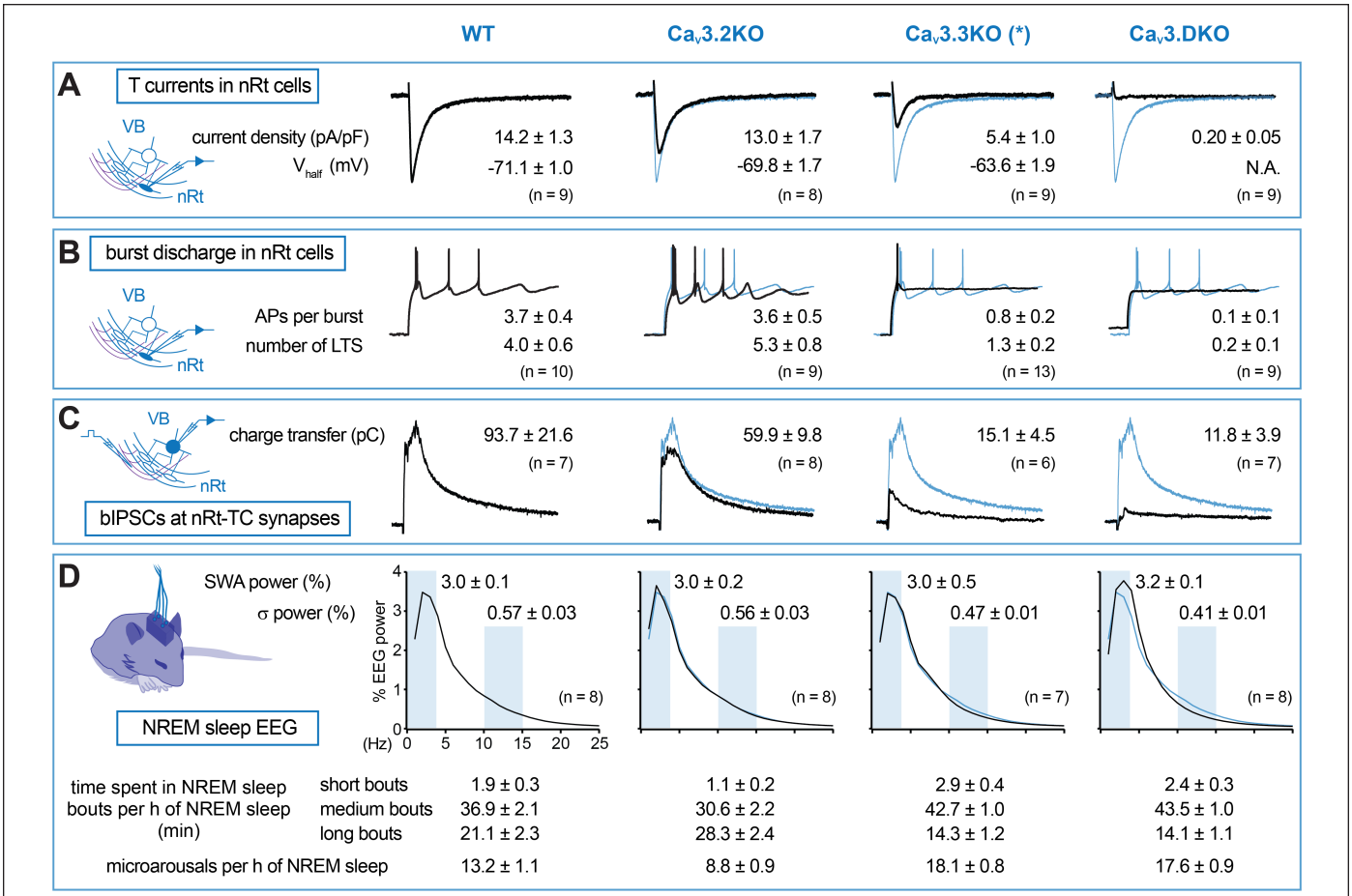


**Figure 7**—Summary of cellular and sleep data from mice with genetic deletions of $Ca_V3$ genes. **(A)** Low-threshold $Ca^{2+}$ currents (T-currents) elicited in nRt cells by somatic depolarization are strongly reduced by *$Ca_V3.3$* single and *$Ca_V3.2xCa_V3.3$* double ablation ($Ca_V3$.DKO). Traces show representative T-currents in all genotypes generated by a +40 mV depolarizing step from −100 mV holding potential. Mean values for T-current density (+40 mV depolarization) and for $V_{half}$ (estimated from the whole activation curve) are specified for each genotype. **(B)** The repetitive low-threshold bursting elicited in nRt cells at the offset of somatic current injections is preserved in $Ca_V3$.2KO mice, strongly impaired in $Ca_V3$.3KO mice, and completely abolished in $Ca_V3$.DKO mice. Traces are representative burst discharges in all genotypes, generated by a 400-ms-long hyperpolarization of −500 pA from −60 mV. Mean values for number of action potentials (APs) within the first burst and number of repetitive low-threshold $Ca^{2+}$ spikes (LTS) are reported. **(C)** $Ca_V3$ channels differentially contribute to the inhibitory postsynaptic currents elicited in TC cells by burst discharge (bIPSCs) of nRt cells, which is evoked by electric stimulation of glutamatergic afferents. *$Ca_V3.2$* deletion partially reduces multiphasic currents, which are abolished by additional *$Ca_V3.3$* ablation. Average values of inhibitory charge transfer (generated by stimuli of 250–300 μA) are reported on top of representative bIPSCs. **(D)** Power spectra of NREM sleep are not altered in $Ca_V3$.2KO mice. *$Ca_V3.3$* deletion causes a selective reduction in the σ frequency range (10–15 Hz), which becomes more pronounced in case of *$Ca_V3.2xCa_V3.3$* ablation. Additionally, $Ca_V3$.DKO mice exhibit a marked increase in EEG power in the δ frequency range (2–4 Hz). Normalized NREM sleep EEG power spectrum between 0.75 and 25 Hz are shown, with shaded boxes indicating relevant intervals of frequency: SWA (0.75–4 Hz) and σ (10–15 Hz) and average values on the top. Bottom, mean values of time spent in short (< 32 s), intermediate (32–252 s), and long ( > 252 s) episodes of NREM sleep and number of microarousals per hour of NREM sleep, indicating that *$Ca_V3.3$* deletion is sufficient to cause deficits in sleep consolidation. In each panel, the scheme on the left represents the recording configuration, and the blue traces on the right are wild-type data superimposed on the traces from the other genotypes for comparison. (*) $Ca_V3$.3KO data are reported from reference[17]. The NREM sleep power spectrum is presented here with normalized % values.

$Ca_V3.2$ channels, as opposed to a constitutive function of the dominating $Ca_V3.3$ channels, would be consistent with the well-documented sensitivity of the $Ca_V3.2$ channel to redox agents and to intracellular kinases[19] and might be important for use-dependent regulation of thalamocortical oscillations. An interesting open question is whether distinct $Ca_V3$ channel subunits are differentially recruited by cortical and thalamic glutamatergic inputs impinging onto nRt dendrites, thus modulating the feed-forward inhibition of TC cells in a subtype-specific manner.

Whereas $Ca_V3.3$-KO nRt cells showed a residual low-threshold $Ca^{2+}$ spike carried by $Ca_V3.2$ channels,[17] $Ca_V3$.DKO mice displayed a complete lack of dendritic T-currents and rebound oscillatory bursting. This resulted in the abolishment of bIPSCs in TC cells, predicting disturbances in thalamic rhythms.[29] The striking effects on nRt excitability and intrathalamic synaptic transmission were indeed reflected by changes in the EEG sleep profile of $Ca_V3$.DKO mice. Corroborating our previous studies on the role of $Ca_V3.3$ channels in σ power, we found again a marked decrease in the σ power

surge when both $Ca_V3$ channel subtypes are lacking. Additionally, $Ca_V3$.DKO mice also showed a reduced σ band in the normalized NREM sleep power spectrum. This suggests a more pronounced impairment in sleep spindle rhythmogenesis, as compared to $Ca_V3$.3KO mice, which is consistent with the full disappearance of bIPSCs in the DKOs. Comparison of cellular and sleep data from this study and from our previous report on $Ca_V3$.3KO mice[17] reveals how the progressive impairment in nRt and intrathalamic excitability caused by *$Ca_V3.2$* and *$Ca_V3.3$* single and double ablation is accompanied by increasing deficits in NREM sleep power characteristics (Figure 7). Notably, $Ca_V3$.3KO mice and $Ca_V3$.DKO mice present a similar rearrangement of NREM sleep bouts and a higher incidence of microarousals, as compared to wild-type and $Ca_V3$.2KO animals, indicating that $Ca_V3$.3 deletion is largely sufficient to deregulate sleep consolidation. Surprisingly, $Ca_V3$.2KO mice appear to have more consolidated NREM sleep, with bouts of longer duration less frequently interrupted by microarousals. Notably, $Ca_V3$.2KO mice spent less time in NREM sleep during the dark phase, suggesting a compensatory upregulation of NREM sleep duration during the light phase. The reason for this difference during the active phase is likely to be independent of thalamocortical rhythmogenesis. $Ca_V3$.2 channels are highly expressed in the basal ganglia circuit, in limbic and in cortical areas.[10] Constitutive deletion of this channel has been reported to generate phenotypes not directly related to thalamocortical rhythmogenesis, such as elevated anxiety and impaired memory.[38–40] Interestingly, concomitant deletion of $Ca_V3$.3 channels appears to override the effect of single $Ca_V3$.2 channel deletion on NREM sleep bout distribution. This indicates that the lack of the major T channel subtype for nRt rhythmogenesis imposes a dominant effect of impaired thalamocortical rhythmogenesis on sleep architecture.

In $Ca_V3$.DKO mice, the EEG-related phenotype was not specific to the σ range, but extended to EEG power between 2–4 Hz, belonging to the δ band, which was augmented. As a result, the balance between intrathalamic networks, providing the basis for sleep spindles, and thalamocortical circuitry, implicated in SWA, was affected more severely in the $Ca_V3$.DKO mice. Indeed, it has been previously shown that σ and δ power are negatively correlated during NREM sleep,[41–43] which was explained by a greater extent of membrane hyperpolarization of TC cells during δ rhythm generation in deep NREM sleep that precluded spindle rhythmicity. This current work now observes such a σ-δ power opposition through genetic means and suggests that the level of nRt excitability through $Ca_V3$ channels and the resulting bIPSC generation is a decisive factor for the σ/δ ratio apparent in the EEG.

Contrary to what would be expected from studies on pharmacological blockade of $GABA_A$R-mediated transmission in thalamic nuclei, $Ca_V3$.DKO mice did not display aberrant hypersynchronous rhythms, such as the 3 Hz spike-and-wave discharge.[29,44] The emergence of these pathological oscillations was explained by a disinhibition of thalamic nuclei.[44,45] Such hyperoscillations did not take place in the $Ca_V3$.DKO mice because GABAergic transmission in intrathalamic circuitry was not fully abolished, and some level of inhibition through tonic nRt discharge remained. Nevertheless, the imbalance between glutamatergic and GABAergic input onto TC cells in $Ca_V3$.DKO mice could favor intrinsic rhythmicity of TC neurons in the δ range at the expense of 10 Hz-nRt-TC reverberations.

Despite the augmented contribution of δ waves, sleep was more fragmented in $Ca_V3$.DKO mice. These mice spent globally more time in NREM sleep than wild-type animals, but in episodes of shorter duration. The concomitant increase in waking bouts of short duration and the higher occurrence of microarousals support the conclusion that $Ca_V3$.DKO mice experienced a more fragmented sleep, which is consistent with the well-established link between spindles and sleep consolidation.[32] These data also support the view that manipulation of spindles can alter sleep architecture independently of δ waves, as previously reported in mice with a genetic overexpression of small-conductance type 2 $K^+$ channels, which improved sleep quality without altering SWA.[46]

Altogether, deletion of the additional source of low-threshold $Ca^{2+}$ spike in nRt cells aggravated the sleep phenotype of $Ca_V3$.3KO mice, indicating a role of $Ca_V3$.2 channels in boosting nRt cell excitability and rhythmogenesis. Thus, the $Ca_V3$.DKO mice might represent a valuable model to study the involvement of nRt rhythmogenesis in pathophysiology, as already reported in the case of absence epilepsy.[27] The clinical relevance of $Ca_V3$.DKO mice remains a subject of further studies. Intriguingly, the deficits in sleep spindles strongly hint at the presence of a schizophrenic endophenotype.[47]

## REFERENCES


1. Beenhakker MP, Huguenard JR. Neurons that fire together also conspire together: is normal sleep circuitry hijacked to generate epilepsy? Neuron 2009;62:612–32.
2. Crunelli V, Cope DW, Hughes SW. Thalamic T-type $Ca^{2+}$ channels and NREM sleep. Cell Calcium 2006;40:175–90.
3. Cueni L, Canepari M, Adelman JP, Lüthi A. $Ca^{2+}$ signaling by T-type $Ca^{2+}$ channels in neurons. Pflügers Arch 2009;457:1161–72.
4. Ly R, Bouvier G, Schonewille M, et al. T-type channel blockade impairs long-term potentiation at the parallel fiber-Purkinje cell synapse and cerebellar learning. Proc Natl Acad Sci U S A 2013;110:20302–7.
5. Otsu Y, Marcaggi P, Feltz A, et al. Activity-dependent gating of calcium spikes by A-type $K^+$ channels controls climbing fiber signaling in Purkinje cell dendrites. Neuron 2014;84:137–51.
6. Egger V, Svoboda K, Mainen ZF. Dendrodendritic synaptic signals in olfactory bulb granule cells: local spine boost and global low-threshold spike. J Neurosci 2005;25:3521–30.
7. Becker AJ, Pitsch J, Sochivko D, et al. Transcriptional upregulation of $Ca_V3.2$ mediates epileptogenesis in the pilocarpine model of epilepsy. J Neurosci 2008;28:13341–53.
8. Shin HS, Cheong EJ, Choi S, Lee J, Na HS. T-type $Ca^{2+}$ channels as therapeutic targets in the nervous system. Curr Opin Pharmacol 2008;8:33–41.
9. Perez-Reyes E. Molecular physiology of low-voltage-activated T-type calcium channels. Physiol Rev 2003;83:117–61.
10. Talley EM, Cribbs LL, Lee JH, Daud A, Perez-Reyes E, Bayliss DA. Differential distribution of three members of a gene family encoding low voltage-activated (T-type) calcium channels. J Neurosci 1999;19:1895–911.
11. Liu XB, Murray KD, Jones EG. Low-threshold calcium channel subunit $Ca_V3.3$ is specifically localized in GABAergic neurons of rodent thalamus and cerebral cortex. J Comp Neurol 2011;519:1181–95.
12. Fuentealba P, Steriade M. The reticular nucleus revisited: intrinsic and network properties of a thalamic pacemaker. Prog Neurobiol 2005;75:125–41.

13. Anderson MP, Mochizuki T, Xie J, et al. Thalamic $Ca_V3.1$ T-type $Ca^{2+}$ channel plays a crucial role in stabilizing sleep. Proc Natl Acad Sci U S A 2005;102:1743–8.
14. Lee J, Kim D, Shin HS. Lack of delta waves and sleep disturbances during non-rapid eye movement sleep in mice lacking $\alpha 1_G$-subunit of T-type calcium channels. Proc Natl Acad Sci U S A 2004;101:18195–9.
15. Dossi RC, Nuñez A, Steriade M. Electrophysiology of a slow (0.5-4 Hz) intrinsic oscillation of cat thalamocortical neurones in vivo. J Physiol 1992;447:215–34.
16. Leresche N, Jassik-Gerschenfeld D, Haby M, Soltesz I, Crunelli V. Pacemaker-like and other types of spontaneous membrane potential oscillations of thalamocortical cells. Neurosci Lett 1990;113:72–7.
17. Astori S, Wimmer RD, Prosser HM, et al. The $Ca_V3.3$ calcium channel is the major sleep spindle pacemaker in thalamus. Proc Natl Acad Sci U S A 2011;108:13823–8.
18. Joksovic PM, Nelson MT, Jevtovic-Todorovic V, et al. $Ca_V3.2$ is the major molecular substrate for redox regulation of T-type $Ca^{2+}$ channels in the rat and mouse thalamus. J Physiol 2006;574:415–30.
19. Iftinca MC, Zamponi GW. Regulation of neuronal T-type calcium channels. Trends Pharmacol Sci 2009;30:32–40.
20. Bourinet E, Alloui A, Monteil A, et al. Silencing of the $Ca_V3.2$ T-type calcium channel gene in sensory neurons demonstrates its major role in nociception. EMBO J 2005;24:315–24.
21. Liao YF, Tsai ML, Chen CC, Yen CT. Involvement of the $Ca_V3.2$ T-type calcium channel in thalamic neuron discharge patterns. Mol Pain 2011;7:43.
22. Sekiguchi F, Kawabata A. T-type calcium channels: functional regulation and implication in pain signaling. J Pharmacol Sci 2013;122:244–50.
23. Chen CC, Lamping KG, Nuno DW, et al. Abnormal coronary function in mice deficient in $\alpha_{1H}$ T-type $Ca^{2+}$ channels. Science 2003;302:1416–8.
24. Cueni L, Canepari M, Luján R, et al. T-type $Ca^{2+}$ channels, SK2 channels and SERCAs gate sleep-related oscillations in thalamic dendrites. Nat Neurosci 2008;11:683–92.
25. Astori S, Lüthi A. Synaptic Plasticity at Intrathalamic Connections via $Ca_V3.3$ T-type $Ca^{2+}$ channels and GluN2B-containing NMDA receptors. J Neurosci 2013;33:430–4.
26. Franken P, Malafosse A, Tafti M. Genetic variation in EEG activity during sleep in inbred mice. Am J Physiol 1998;275:R1127–37.
27. Lee SE, Lee J, Latchoumane C, et al. Rebound burst firing in the reticular thalamus is not essential for pharmacological absence seizures in mice. Proc Natl Acad Sci U S A 2014;111:11828–33.
28. Joksovic PM, Bayliss DA, Todorovic SM. Different kinetic properties of two T-type $Ca^{2+}$ currents of rat reticular thalamic neurones and their modulation by enflurane. J Physiol 2005;566:125–42.
29. Rovó Z, Mátyás F, Barthó P, et al. Phasic, nonsynaptic GABA-A receptor-mediated inhibition entrains thalamocortical oscillations. J Neurosci 2014;34:7137–47.
30. Herd MB, Brown AR, Lambert JJ, Belelli D. Extrasynaptic $GABA_A$ receptors couple presynaptic activity to postsynaptic inhibition in the somatosensory thalamus. J Neurosci 2013;33:14850–68.
31. Sun YG, Wu CS, Renger JJ, Uebele VN, Lu HC, Beierlein M. GABAergic synaptic transmission triggers action potentials in thalamic reticular nucleus neurons. J Neurosci 2012;32:7782–90.
32. Astori S, Wimmer RD, Lüthi A. Manipulating sleep spindles - expanding views on sleep, memory, and disease. Trends Neurosci 2013;36:738–48.
33. Lüthi A. Sleep spindles: where they come from, what they do. Neuroscientist 2013;20:243–56.
34. McCormick DA, Bal T. Sleep and arousal: thalamocortical mechanisms. Annu Rev Neurosci 1997;20:185–215.
35. Steriade M. Grouping of brain rhythms in corticothalamic systems. Neuroscience 2006;137:1087–106.
36. McKay BE, McRory JE, Molineux ML, et al. $Ca_V3$ T-type calcium channel isoforms differentially distribute to somatic and dendritic compartments in rat central neurons. Eur J Neurosci 2006;24:2581–94.
37. Warren RA, Jones EG. Maturation of neuronal form and function in a mouse thalamo-cortical circuit. J Neurosci 1997;17:277–95.
38. Chen CC, Shen JW, Chung NC, Min MY, Cheng SJ, Liu IY. Retrieval of context-associated memory is dependent on the $Ca_V3.2$ T-type calcium channel. PLoS One 2012;7:e29384.
39. Chung NC, Huang YH, Chang CH, et al. Behavior training reverses asymmetry in hippocampal transcriptome of the $Ca_V3.2$ knockout mice. PLoS One 2015;10:e0118832.
40. Gangarossa G, Laffray S, Bourinet E, Valjent E. T-type calcium channel $Ca_V3.2$ deficient mice show elevated anxiety, impaired memory and reduced sensitivity to psychostimulants. Front Behav Neurosci 2014;8:92.
41. Nuñez A, Curro Dossi R, Contreras D, Steriade M. Intracellular evidence for incompatibility between spindle and delta oscillations in thalamocortical neurons of cat. Neuroscience 1992;48:75–85.
42. Uchida S, Maloney T, March JD, Azari R, Feinberg I. Sigma (12-15 Hz) and delta (0.3-3 Hz) EEG oscillate reciprocally within NREM sleep. Brain Res Bull 1991;27:93–6.
43. Vyazovskiy VV, Achermann P, Borbély AA, Tobler I. The dynamics of spindles and EEG slow-wave activity in NREM sleep in mice. Arch Ital Biol 2004;142:511–23.
44. Castro-Alamancos MA. Neocortical synchronized oscillations induced by thalamic disinhibition in vivo. J Neurosci 1999;19:RC27.
45. Paz JT, Bryant AS, Peng K, et al. A new mode of corticothalamic transmission revealed in the $Gria4^{-/-}$ model of absence epilepsy. Nat Neurosci 2011;14:1167–73.
46. Wimmer RD, Astori S, Bond CT, et al. Sustaining sleep spindles through enhanced SK2-channel activity consolidates sleep and elevates arousal threshold. J Neurosci 2012;32:13917–28.
47. Ferrarelli F, Tononi G. The thalamic reticular nucleus and schizophrenia. Schizophr Bull 2011;37:306–15.

## ACKNOWLEDGMENTS

The authors are grateful to Kevin P. Campbell for the permission of using the $Ca_V3.2$ knock-out mouse line, and to Heinz Beck for providing animal breeders. We thank Laura M.J. Fernandez for help with data analysis and Thi Dung Hau Iuliano-Dao for mouse genotyping.

## SUBMISSION & CORRESPONDENCE INFORMATION

Submitted for publication June, 2015
Submitted in final revised form October, 2015
Accepted for publication October, 2015
Address correspondence to: Simone Astori, PhD or Anita Lüthi, PhD, Department of Fundamental Neurosciences, University of Lausanne, Rue du Bugnon 9, CH-1005 Lausanne; Tel: +41 21 692 5294; Fax: +41 21 692 5105; Email: simone.astori@unil.ch or anita.luthi@unil.ch

## DISCLOSURE STATEMENT

This was not an industry supported study. This work was supported by the Swiss National Science Foundation (Ambizione grant PZ00P3_136761 to S.A. and grant 31003A-146244 to A.L.) and Etat de Vaud. The authors have indicated no financial conflicts of interest.

Systems/Circuits

# Phasic, Nonsynaptic GABA-A Receptor-Mediated Inhibition Entrains Thalamocortical Oscillations

**Zita Rovó,[1,2]* Ferenc Mátyás,[1]* Péter Barthó,[1] Andrea Slézia,[1] Sandro Lecci,[2] Chiara Pellegrini,[2] Simone Astori,[2] Csaba Dávid,[1] Balázs Hangya,[3,4] Anita Lüthi,[2] and László Acsády[1]**

[1]Laboratory of Thalamus Research, Institute of Experimental Medicine, Hungarian Academy of Sciences, Budapest H-1083, Hungary, [2]Department of Fundamental Neurosciences, University of Lausanne, Lausanne CH-1005, Switzerland, [3]Cold Spring Harbor Laboratory, Cold Spring Harbor, New York 11724, and [4]Laboratory of Cerebral Cortex Research, Institute of Experimental Medicine, Hungarian Academy of Sciences, Budapest H-1083, Hungary

**GABA-A receptors (GABA-ARs) are typically expressed at synaptic or nonsynaptic sites mediating phasic and tonic inhibition, respectively. These two forms of inhibition conjointly control various network oscillations. To disentangle their roles in thalamocortical rhythms, we focally deleted synaptic, γ2 subunit-containing GABA-ARs in the thalamus using viral intervention in mice. After successful removal of γ2 subunit clusters, spontaneous and evoked GABAergic synaptic currents disappeared in thalamocortical cells when the presynaptic, reticular thalamic (nRT) neurons fired in tonic mode. However, when nRT cells fired in burst mode, slow phasic GABA-AR-mediated events persisted, indicating a dynamic, burst-specific recruitment of nonsynaptic GABA-ARs. *In vivo*, removal of synaptic GABA-ARs reduced the firing of individual thalamocortical cells but did not abolish slow oscillations or sleep spindles. We conclude that nonsynaptic GABA-ARs are recruited in a phasic manner specifically during burst firing of nRT cells and provide sufficient GABA-AR activation to control major thalamocortical oscillations.**

## Introduction

A wealth of data indicate a major role of GABAergic cells in pacing various rhythms via GABA-A receptors (GABA-ARs) in the cortex (Sanchez-Vives and McCormick, 2000; Blatow et al., 2003), hippocampus (Cobb et al., 1995; Wulff et al., 2009), and thalamus (von Krosigk et al., 1993). GABA-ARs are classified into two fundamentally distinct types of receptors, synaptic and extrasynaptic receptors that mediate phasic and tonic inhibition, respectively. Exactly what type of inhibition governs oscillatory activity is presently unclear. The pentameric GABA-ARs can be assembled in theoretically limitless combinations with various types of subunits (Farrant and Nusser, 2005). For the synaptic clustering of GABA-ARs, the γ2 subunit is essential (Essrich et al., 1998). Receptors containing the γ2 subunit typically have rapid kinetics, low sensitivity to GABA, and prompt desensitization, enabling them to conduct fast inhibitory postsynaptic events, typical for phasic inhibition (Brickley et al., 1999). GABA-ARs containing δ instead of γ subunits are abundant in extrasynaptic membranes (Nusser et al., 1998; Wei et al., 2003; Farrant and Nusser, 2005; Belelli et al., 2009), have higher sensitivity to GABA, and are activated by ambient GABA. These extrasynaptic receptors are primarily responsible for a slow, persistent (i.e., tonic) chloride current (Hamann et al., 2002; Wei et al., 2003; Cope et al., 2005; Bright et al., 2007, 2011).

More recently, evidence is accumulating for a third type of GABA-AR-triggered inhibition. This spillover-mediated transmission is caused by diffusion of GABA from the synaptic cleft and allows activation of GABA-ARs in extrasynaptic locations (Capogna and Pearce, 2011), resulting in phasic inhibition with slowed-down kinetics. The time course and amplitude of synaptic inhibition are an important determinant of the oscillation frequency; therefore, it is critical to determine the contribution of these three types of GABA-AR-mediated inhibition to naturally occurring brain rhythms.

Thalamus is one of the brain regions abundantly expressing both synaptic and extrasynaptic receptors and it is known to be involved in large-scale brain oscillations important for states of vigilance, notably sleep. Thalamocortical (TC) cells express only a few of the potential combinations of GABA-AR subunits (Pirker et al., 2000). Synaptic receptors mainly incorporate α1,

Received Oct. 14, 2013; revised March 12, 2014; accepted April 13, 2014.

Author contributions: A.L. and L.A. designed research; Z.R., F.M., P.B., A.S., S.L., C.P., S.A., and C.D. performed research; Z.R., F.M., P.B., S.L., C.P., S.A., C.D., B.H., A.L., and L.A. analyzed data; Z.R., F.M., A.L., and L.A. wrote the paper.

This work was supported by SciEX-NMS, Swiss National Science Foundation, Foundation 450ème, Fonds Jean Falk-Variant, Hungarian Eötvös Scholarship, Hungarian Scientific Research Fund (NF101773, T109754), The Wellcome Trust, and the National Office for Research and Technology (Neurogen). F.M. and P.B. are János Bolyai Research fellows. S.A. is a Swiss National Science Foundation Ambizione Fellow. B.H. received support from the Swartz Foundation and Marie Curie International Outgoing Fellowship within the European Union Seventh Framework Programme for Research and Technological Development. We thank Werner Sieghart for providing primary antibodies; Barna Dudok for providing secondary antibodies; Krisztina Faddi for excellent technical help; and László Barna, the Nikon Microscopy Center at IEM, Nikon Austria GmbH, and Auro-Science Consulting Ltd for kindly providing microscopy support.

The authors declare no competing financial interests.

*Z.R. and F.M. contributed equally to this work.

This article is freely available online through the *J Neurosci* Author Open Choice option.

Correspondence should be addressed to either of the following: Dr. László Acsády, Laboratory of Thalamus Research, Institute of Experimental Medicine, Hungarian Academy of Sciences, PO Box 67, 1450 Budapest, Hungary, E-mail: acsady@koki.hu; or Dr. Anita Lüthi, Department of Fundamental Neurosciences, University of Lausanne, Bugnon 9, CH-1005, Lausanne, Switzerland, E-mail: anita.luthi@unil.ch.

DOI:10.1523/JNEUROSCI.4386-13.2014

$\beta$2/3, and $\gamma$2 subunits, whereas nonsynaptic receptors contain $\alpha$4, $\beta$2/3, and $\delta$ subunits. Major pacemakers for rhythms in thalamic circuits are the GABAergic cells of the nucleus reticularis thalami (nRT). Recent *in vitro* data indicate that extrasynaptic receptors can be recruited during nRT-mediated phasic IPSCs (Herd et al., 2013). This raises the possibility that sleep-related oscillations are partially driven by a population of molecularly distinct GABA-ARs located outside the synapse. However, whether and to what extent phasic activation of extrasynaptic GABA-ARs is capable of driving normal rhythms *in vivo* are not clear. As many sedative–hypnotic agents target synaptic GABA-ARs (Winsky-Sommerer, 2009), elucidating the contribution of nonsynaptic GABA-Rs to sleep oscillations is of great interest for further drug development. In this study, we unraveled a significant role for extrasynaptic receptors in sleep oscillations by using localized, virus-mediated gene-knock-out of synaptic $\gamma$2-GABA-ARs in the thalamus, leaving only extrasynaptic inhibition intact.

## Materials and Methods

*Mice and stereotactic surgery.* Adult *GABAAR*$\gamma 2^{771}$*lox* and C57BL/6J mice from both genders were used for the experiments. Mice were entrained to a 12 h light/dark cycle with food and water available *ad libitum*. All experimental procedures were performed according to the ethical guidelines of the Institute of Experimental Medicine of the Hungarian Academy of Sciences and the University of Lausanne and approved by the local Ethical Committees and Veterinary Offices of the Canton de Vaud. Surgeries and experiments were done under ketamine/xylazine anesthesia (ketamine, 83 mg/kg; xylazine, 3.3 mg/kg), except in animals where spindles were recorded. In the latter cases, urethane (0.012–0.015 g/100 g body weight) was used as anesthetic. AAV2/1-CMV-CRE (AAV-Cre) and/or AAV2/1-CMV-eGFP (AAV-GFP) viruses (100–300 nl; $10^{12}$ GC/ml; Vector Biolabs) were injected at a rate of 50–100 nl/min into the somatosensory thalamus (from bregma: anteroposterior −1.6 to 1.9 mm and mediolateral 1.4–1.8 mm; dorsoventral 2.8–3.2 from the surface).

*Histology and immunocytochemistry.* Animals were transcardially perfused first with saline, then with ~150 ml of fixative solution containing 2%–4% PFA in 0.1 M phosphate buffer (PB). Tissue blocks were cut on a Vibratome (Leica) into 50 $\mu$m coronal sections. After extensive washes and incubation in blocking solution containing 10% of normal goat serum or donkey serum and 0.5% Triton-X, recorded and labeled TC cells were visualized using streptavidin-conjugated fluorescent immunoglobulin tagged with a fluorescent protein (Cy3 or Alexa-488; in 1:2000 for 2 h at room temperature) or avidin-biotin complex (Vector Laboratories; 1:300, 2 h) developed by nickel-intensified diaminobenzidine, as a chromogen. Identifying the phenotype of the recorded cells, anti-Cre recombinase fluorescent staining was performed using monoclonal mouse anti-Cre antibody (Millipore; 1:3000, overnight at room temperature) and with Cy3-(Jackson ImmunoResearch Laboratories) or Alexa-488-conjugated anti-mouse secondary antibody (Invitrogen) (1:500; 2 h at room temperature). For precise localization of the recorded cells or the silicon probe tracks, vesicular glutamate transporter type 2 (vGluT2; guinea pig or mouse anti-vGluT2, 1:3000, Millipore) or parvalbumin (rabbit anti-PV; 1:3000, Baimbridge) counterstaining was used and labeled with Cy5or A647-conjugated secondary antibodies. In control animals, the counterstaining was performed using ImmPRESS anti-mouse or rabbit IG Polymer detection kit.

*In vitro* biocytin-labeled cells were visualized following one of the above-described protocols. The fixative solution contained 2% of PFA (~150 ml per animal); 50 $\mu$m coronal sections were cut, washed, cryoprotected in 30% sucrose in 0.1 M PB overnight, and freeze thawed over liquid nitrogen. For simple fluorescent double stainings, after incubating the sections in blocking solution (10% normal goat serum for 30 min), sections were treated with monoclonal anti-Cre antibody raised in mouse or rabbit (1:30,000 and 1:12,000; Millipore and Covance, respectively; overnight at room temperature) and one of the following antibodies: mouse anti-NeuN (1:3000, Millipore Bioscience Research Reagents), mouse anti-gephyrin (1:1000, Synaptic System), anti-GABA transporter type 1 (GAT1, Millipore) and type 3 (GAT3, Millipore) overnight at room temperature. The primer antibodies were visualized with corresponding fluorescent secondary antibodies (Alexa-488-, -Cy3-, or -Cy5-conjugated IGs). Finally, sections were mounted on slides and covered with Vectashield (Vector Laboratories).

For the visualization of GABA-AR subunits after the treatment with one of the anti-Cre antibodies, the sections were treated with biotinylated goat anti-mouse or -rabbit secondary antibody (1:300, at room temperature for 2 h) and amplified with Tyramide (Invitrogen, 1:50, 15 min). Next, the sections were digested in pepsin (0.2–0.3 mg/ml in 20% HCl solution made with 0.1 M PB; 7 min at 37°C), then incubated in rabbit anti-$\gamma$2 (1:4000, Synaptic System), rabbit anti-$\alpha$1 (1:500, W. Sieghart, Brain Research Institute, Vienna, Austria), or guinea-pig anti-$\alpha$1 (1:500, Frontier Institute) or rabbit anti-$\alpha$4 (1:500, W. Sieghart, Brain Research Institute, Vienna, Austria) overnight at room temperature. The Cre immunostaining was visualized with streptavidin-conjugated Alexa-488, while the other antibodies with corresponding Cy3 or Cy5-conjugated secondary IGs (at room temperature for 2 h). Finally, the sections were mounted.

Photographs were taken using either Zeiss Axioplan 2 equipped with DP70 digital camera (Olympus), Olympus FluoView FV1000 or Nikon ECLIPSE Ni-E confocal laser scanning systems. For the quantitative receptor localization, AAV-Cre ($n = 4$) and AAV-GFP ($n = 4$) injected animals were used. In each animal, 3–33 regions of interest (ROIs, area 23,000–30,0000 $\mu m^2$) were analyzed. To determine the abundance of GABA-AR subunits, the images were thresholded and gray values of pixels were registered in ROIs defined in appropriate optical sections of image stacks in FIJI (Schindelin et al., 2012); then the data were exported to a spreadsheet. For the preparation of figures, when necessary, brightness and contrast were adjusted using Adobe Photoshop CS4 (Adobe Systems) applied to whole images only.

For data acquisition of Stochastic Optical Reconstruction Microscopy (STORM) images, the method described by Dani et al., 2010 was used; 20 $\mu$m sections (without freeze thawing) were treated similarly as described above with the following exceptions. Normal horse serum (10%) was used for blocking, the pepsin-digestion step was shorter (3 min), and fluorescent secondary antibodies, specific for STORM, were used: horse anti-rabbit Alexa-405/Alexa-647 (1:50; generous gift from B. Dudok, Institute of Experimental Medicine, Budapest, Hungary) visualizing the GABAergic axonal varicosities labeled via guinea-pig antivesicular GABA transporter (vGAT, 1:6000, Synaptic System) and horse anti-guinea-pig-CY3/A647 (1:50; generous gift from B. Dudok) marking the $\gamma$2 content of the postsynaptic elements. Finally, the sections were placed on coverslips, uncovered, and stored at 4°C. Directly before image acquisition, sections were mounted with a freshly prepared STORM-specific medium containing 80 $\mu$l of 1 M DPBS (Sigma-Aldrich), 10 $\mu$l 0.5 M mercaptoethylamine, pH 8.5, 1 $\mu$l of an antibleaching oxygen scavenger that consists of 10 mg glucose oxidase, 32 $\mu$l catalase, and 93 $\mu$l DPBS, and finally 20 $\mu$l of 30% glucose in distilled water. For STORM image acquisition, a similar protocol was used as described previously (Dani et al., 2010) with a 100× objective (CFI Apo 100× oil NA 1.49 TIRF WD 0.12) and imaging cycles containing one frame of activation laser illumination (405 or 561 nm) followed by three frames of imaging laser illumination (647 nm) at 30 frames/s. To ensure the *z*-axis stability of data acquisition, Nikon Perfect Focus System was used. Image acquisition was controlled via a STORM Andor camera (iXon 897 back-illuminated EMCCD). The STORM images comprised of 1000–3000 cycles were taken using Nikon-STORM-C2 system using Nikon NIS-Elements 4.01 STORM 2.0 software. An automated algorithm was used to subtract channel crosstalk and nonspecific activation of the A647 reporter in multicolor images.

In vitro *electrophysiology.* For whole-cell patch-clamp recordings, mice (P26-P41) were killed after 1–3 weeks of viral injection. Animals were unilaterally injected with AAV-Cre/AAV-GFP or AAV-GFP (as controls) for all experiments as described above. The brains were quickly removed after brief isoflurane anesthesia and horizontal slices (300 $\mu$m) containing the ventrobasal complex (VB) and nRT were cut on a vibratome and transferred to a holding chamber containing oxygenated aCSF solution with 2 mM of divalent cations ($CaCl_2$, $MgCl_2$), myo-inositol (3 mM), and

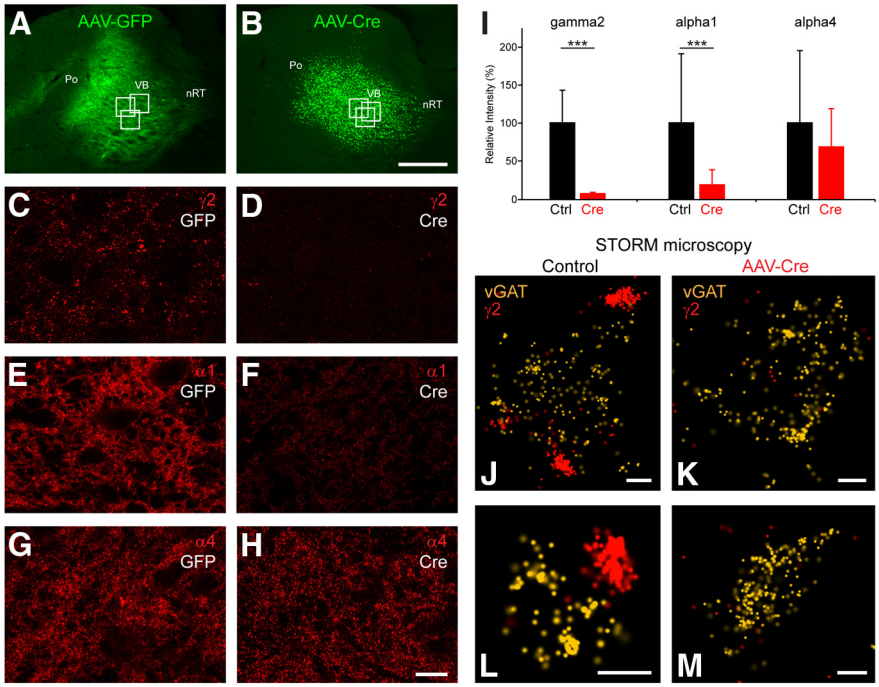


**Figure 1.** Selective removal of synaptic GABA-AR γ2 subunits in the thalamus. ***A***, ***B***, Low-power confocal images showing the injection sites of the AAV-GFP (as control) and AAV-Cre viruses in mice somatosensory thalami. White framed areas represent the position of images shown in ***C–H***, which depicts immunostaining for GABA-AR subunits in this and neighboring sections. ***C***, ***D***, High-power confocal images of γ2 subunit immunostaining in the thalamus. The punctate receptor staining present in the AAV-GFP-infected thalamus (***C***) is not detectable in the AAV-Cre-infected thalamus (***D***) 3 weeks after the viral injections. ***E***, ***F***, Large decrease in the density of α1 immunostaining can be observed in the AAV-Cre-infected thalamus (***F***) compared with control (***E***). ***G***, ***H***, No visible difference can be seen after α4 subunit immunostaining in the same animal. Quantitative analysis for the density of γ2, α1, and α4 subunits after viral interventions. Bars represent the relative intensity of each subunit in the AAV-Cre-injected thalami compared with the controls (see Materials and Methods). ***$p < 0.001$ (Student's *t* test). ***J–M***, Localization of γ2 subunit clusters (red) in the close vicinity of individual GABAergic terminals (labeled by vGAT immunostaining, yellow) by super-resolution STORM microscopy. The images represent single terminals and the associated receptor clusters. On the contralateral side, multiple (***J***) or single (***L***) receptor clusters flank the GABAergic terminals. Ipsilaterally, however, no receptor cluster can be found (***K***,***M***). Scale bars: ***A***, ***B***, 500 μm; ***C–H***, 10 μm; ***G–J***, 200 nm.

Na-pyruvate (2 mM). Slices were kept at 35°C for 30 min and then at room temperature for subsequent incubation. For recordings, slices were transferred to a submerged recording chamber held at room temperature, except for recording evoked IPSCs (eIPSCs), which was done at 34°C. The bathing solution contained the following (in mM): 131 NaCl, 2.5 KCl, 1.25 $NaH_2PO_4$, 25.6 $NaHCO_3$, 2 $CaCl_2$, 1.2 $MgCl_2$, 18 glucose, 1.7 L(+)-ascorbic acid, osmolarity 290–300 mOsm, continuously bubbled with 95%/5% $O_2$/$CO_2$ and supplemented with additional pharmacological compounds as indicated below.

Virally infected TC regions were visually identified using OptoLED Lite (Cairn Research) fluorescence illumination at 470 nm. Image acquisition was controlled via an Andor EM-CCD camera (Axon DU-897) and Andor Solis imaging software version 4.16. For patching, fluorescent cells were visualized using near-infrared DIC microscopy (BX50WI; Olympus) and recorded with a MultiClamp 700B amplifier driven by Clampex V.10.2 (Molecular Devices). Data were filtered at 2 kHz and acquired at 5 kHz using pClamp10 software. Patch pipettes were pulled from borosilicate glass (TW150F-4; World Precision Instruments) and fire-polished on a DMZ-Zeitz-Puller. Once whole-cell access was obtained, series resistance was monitored using a −10 mV test pulse throughout the recording period; cells were included for analysis only if the series resistance was <20 MΩ and the change of resistance was <25% over the course of the experiment.

For measuring cellular discharge properties in current-clamp conditions, the intracellular pipette solution contained the following (in mM): 140 $KMeSO_4$, 10 KCl, 10 HEPES, 0.1 EGTA, 2 $MgCl_2$, 4 Mg-ATP, 0.2 Na-GTP, and 10 phosphocreatine (306–309 mOsm, pH 7.23). Na-GTP was freshly added daily from concentrated stock solutions, and the solution was filtered and maintained on ice. A liquid junction potential of −10 mV was taken into account. Resting membrane potential was measured after gaining whole-cell access. Depolarizing and hyperpolarizing current square pulses were injected into the recorded cells held at different membrane potentials (−60 mV, −70 mV) through DC injections.

For sIPSC and eIPSC recordings in TC cells and to measure the cell's input resistance, the intracellular pipette solution contained the following (in mM): 120 CsCl, 10 HEPES, 2 EGTA, 8 NaCl, 0.2 $MgCl_2$, 5 QX-314-Cl, 0.2 Na-GTP, and 10 phosphocreatine (295 mOsm, pH 7.35). QX-314-Cl and Na-GTP were added freshly daily. To isolate inward currents evoked by GABA-AR activation, 6,7-dinitroquinoxaline-2,3-dione (DNQX; 40 μM; Tocris Bioscience) and D,L-2-amino-5-phosphonopentanoic acid (D,L-APV; 100 μM; Tocris Bioscience) were added to the bath. Spontaneous IPSCs (sIPSCs) were recorded at −50 mV for at least 5 min. A liquid junction potential < 5 mV was not taken into account.

To measure tonic GABA-ARs currents in TC cells, the GABA-AR blocker gabazine (SR 95531 hydrobromide/ 6-imino-3-(4-methoxyphenyl)-1(6H)-pyridazinebutanoic acid hydrobromide; 10 μM; Tocris Bioscience) was bath applied for at least 3 min to cells recorded with the patch pipette solutions used for sIPSCs and eIPSCs. Under these recording conditions, differences in holding currents and input resistance between AAV-GFP and AAV-Cre cells resulted entirely from altered tonic $Cl^-$ conductances. The holding current shift was measured as the difference in the holding current before and during drug application. For tonic current measurements, only male animals were used to avoid the disturbing effect of periodic changes in neurosteroid levels (Brickley and Mody, 2012).

For eIPSCs, a monopolar stimulation electrode filled with ACSF was placed in the nRT in a position radial to the recorded TC cell and the nRT-TC border, and the cells were recorded at 34°C. Monophasic IPSCs were elicited at 0.2 or 10 Hz with 250 μA stimulation intensity.

For monitoring evoked burst-induced IPSCs (burst IPSCs), patch pipettes contained the current-clamp recording solution supplemented with 2.5 mM QX 314-Cl. In contrast to monophasic IPSC recordings, the extracellular medium did not contain glutamate receptor antagonists. Outward burst IPSCs were recorded by voltage clamping VB cells at −30 mV. These recording conditions were chosen to promote bursting in nRT cells via glutamatergic synaptic input (Crandall et al., 2010). Burst IPSCs were evoked once every 30–60 s with 250 μA stimulation intensity, and the amplitude and kinetics were measured throughout the experiment. Under these recording/stimulation conditions, GABA-B receptor-mediated responses were negligible and application of CGP 55845 hydrochloride (2 μM, Ascent-Abcam) did not change the evoked currents.

For the establishment of $Cl^-$ reversal potential, the following intracellular solution was used (in mM): 120 Cs gluconate, 10 CsCl, 10 HEPES, 8 NaCl, 0.2 EGTA, 14 phosphocreatine, 2 Mg-ATP, 0.2 Na-GTP, pH 7.3. A junction potential (−10 mV) was taken into account.

For evoked thalamic rebound bursts, the current-clamp recording solution was used. The VB cells were held at −70 mV. Previously recorded scaled burst IPSC waveforms obtained from a control and an AAV-Cre-infected neuron were applied every 10 s.

For histological recovery of recorded cells *in vitro*, 0.2% biocytin (Sigma-Aldrich) was included in the recording solution, and the patch

pipette was carefully withdrawn at the end of the recordings. Slices were immediately transferred to a fixative solution (4% PFA, at 4°C), fixed for 1–2 h, and intensively washed in PB. Then, slices were embedded into agar (2%) and resectioned with Vibratome.

In vitro *analysis.* Action potential (AP) characteristics in tonic and burst firing mode were analyzed in Clampfit version 10.2. The peak amplitudes from AP threshold, the half-widths, and the AP afterhyperpolarizations were always determined for the first AP in a burst discharge or in tonic firing trains.

Analysis of sIPSCs was performed in Mini-Analysis 6.0 (Synaptosoft). Root-mean-square noise was determined in an event-free 60 ms time window. A minimal peak threshold of at least twice the determined root-mean-square noise was set as detection criterion. When the detection parameters were applied to traces recorded in gabazine, no events could be detected. To estimate the weighted decay time constant ($\tau_w$) in control cells, monophasic events with a rise time <2 ms were averaged and $\tau_w$ calculated from a weighted average of decay time constants in a biexponential fit, thereby accounting for occasional slow spontaneous events (see Results).

For tonic currents, all-point histograms of amplitude values were generated from 20 s segments before and during drug application and fitted by single Gaussian distribution.

Off-line analysis of eIPSCs and burst IPSCs was performed using Clampfit version 10.2. and IgorPro 5. Means of 4 successive responses were used for analysis and amplitudes calculated with respect to the baseline before stimulation. Instead of 10%–90% rise time constant, time to peak was determined, as the burst IPSC is a multiphasic event. For comparison of eIPSCs and burst IPSCs, two parameters were determined. Conductances were calculated through dividing peak event amplitudes by the driving force. Decay time courses were quantified using monoexponential fits for eIPSCs in IgorPro. To determine burst IPSC decay, responses were fit with biexponential or monoexponential curves in Igor Pro. Biexponential fits were used for burst IPSCs of AAV-GFP cells to account for the involvement of both synaptic and nonsynaptic current components, whereas AAV-Cre burst IPSCs were fit with a monoexponential time constant. Fits were applied only to traces showing smooth decay without contamination by additional spontaneous synaptic events.

In vivo *electrophysiology. In vivo* recordings were performed 3–8 weeks after the viral injections. For LFP recordings, we used 16-channel silicon probes lowered in the primary somatosensory cortex (S1, anteroposterior 1.2 and mediolateral 3.2 mm from bregma). Thalamic multiunit activity was monitored via 32-channel silicon probes using the same coordinate as for the viral injections. Silicon probe signals were high-passed filtered (0.3 Hz), amplified (2000×) by a 64-channel amplifier, and digitized at 20 kHz with two National Instruments PCI-6259 cards. TC single-unit activity was recorded by glass microelectrodes (*in vivo* impedance of 10–40 MΩ) filled with 0.5 M NaCl and 2% neurobiotin (Vector Laboratories). Neuronal signals were amplified by a DC amplifier (Axoclamp 2B, Molecular Devices), further amplified, and filtered between 0.16 and 5 kHz by a signal conditioner (LinearAmp, Supertech). Juxtacellular labeling of the recorded neurons was performed as previously described (Pinault, 1996).

Gabazine (selective GABA-AR blocker; 1 mM; Sigma) was iontophoretically applied using 1–30 μA current through small diameter glass capillaries (3–5 μm diameter) for ~30 min.

In vivo *analysis.* All data analysis was performed in MATLAB (MathWorks). Instead of using arbitrary intraburst and interburst parameters for burst detection, a custom-built semiautomatic burst detection method was used as described previously (Slézia et al., 2011). After the identification of bursts, the following firing parameters were determined: mean firing frequency, frequency of the first APs of the bursts (burst frequency), the firing frequency for the intraburst APs (intraburst frequency), the average number of spikes in bursts (intraburst spike number), the average duration of bursts measured in milliseconds (burst length), and the number of all APs in bursts relative to the number of all spikes fired (burstiness index).

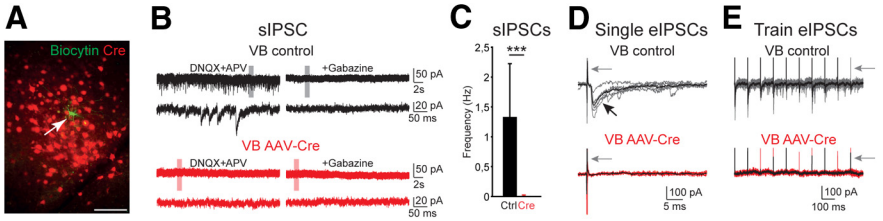


**Figure 2.** Disappearance of spontaneous and evoked, fast IPSCs in TC cells after the removal of γ2 subunits. ***A***, Low-power image of a biocytin-filled TC neuron (arrow) recorded from an acute thalamic slice in the middle of the AAV-Cre injection zone. Scale bar, 200 μm. ***B***, Recordings of spontaneous IPSCs in the VB from control (top, left, black) and AAV-Cre TC cells (bottom, left, red) in the presence of glutamatergic blockers (DNQX, D,L-APV). sIPSCs in the control cell were fully blocked by 10 μM gabazine (right). Expanded portions of the gray and red bars in the top traces are depicted in the paired lower traces. ***C***, Bar graph of average sIPSC frequencies of control ($n = 11$) and AAV-Cre cells ($n = 22$). Bars indicate mean ± SD. ***$p < 0.001$ (Student's $t$ test). ***D***, Single evoked IPSCs (black arrow) elicited by nRT stimulation in a control (top, gray) and an AAV-Cre cell (bottom, red). Averages are shown in black. No monophasic IPSC could be evoked in the AAV-Cre cell. ***E***, The 10 Hz train stimulation of the neurons shown in ***D***. Again, no eIPSCs were observed in the AAV-Cre cell. Gray arrows indicate the truncated stimulation artifacts in ***D***, ***E***.

*Polysomnographic recordings and analysis.* Surgeries for combined EEG/electromyographic (EMG) recordings and data scoring were performed on adult *GABAARγ2$^{771}$lox* mice as previously described (Franken et al., 1998). Two weeks before surgery, 4 animals were bilaterally injected with AAV-GFP (as controls) or AAV-Cre. After 10 d of recovery, the cable was plugged to the connector and mice were allowed an additional week to habituate. Undisturbed sleep–wake behavior was recorded for 48 h. The analog signals were first amplified (2000×), and the EEG and EMG signals were high-pass filtered at 0.7 Hz and 10 Hz, respectively. Signals were digitized at 2 kHz and down-sampled to 200 Hz through Somnologica 3.3.1 software (Embla System). Data were visually scored with a resolution of 4 s to determine the vigilance state (wake, NREM sleep, REM sleep). The NREM sleep power spectrum was generated from NREM sleep during both light and dark periods, but NREM sleep epochs were included only if they were both preceded and followed by other NREM sleep epochs (Wimmer et al., 2012). For analysis on spectral characteristics of the NREM-to-REM sleep transitions, only the two light phases were taken into account, as these contain the majority of transitions. Data analysis was performed as described previously (Astori et al., 2011; Wimmer et al., 2012).

*Statistics.* Statistical significance was assessed using Student's $t$ test or Mann–Whitney $U$ test based on the normality level of the dataset, and $p < 0.05$ was considered statistically significant. For quantitative receptor localization, after normalization for area of ROIs and averaging, samples from Cre- and GFP-expressing animals were compared with Student's $t$ test using Mystat (Systat Software). For analysis of EEG power spectra, univariate repeated-measures ANOVA with factor "group" and "bin" was used. In both text and figures, data are presented as mean ± SD or as whisker plots.

## Results

### Viral intervention successfully eliminates synaptic γ2 subunits

To selectively and focally delete the γ2 subunits from TC cells, we unilaterally injected Cre-recombinase-containing or, as control, GFP-containing, adeno-associated viral vectors (AAV-Cre or AAV-GFP, respectively) into the somatosensory thalamus of *GABAARγ2$^{771}$lox* mice (Fig. 1*A*,*B*). After 2–3 weeks, we com-

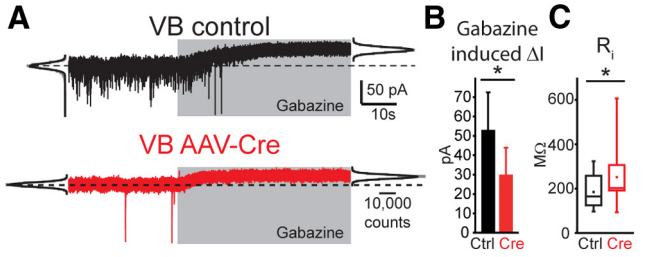


**Figure 3.** Deletion of synaptic γ2 subunits reduces tonic GABAergic inhibition. ***A***, Outward shift in the holding current of a TC cell held at −50 mV before and during gabazine (10 μM, gray shadow) application in a control (top, black) and an AAV-Cre (bottom, red) VB neuron. Gaussian curves indicate a fit to the all-points histograms of current traces before (left) and after (right) gabazine. Dotted horizontal lines indicate mean holding current level before gabazine. The large spontaneous inhibitory events recorded from the AAV-Cre VB cell are discussed in Figure 4. ***B***, Bar graph of gabazine-induced increase in the holding current (ΔI) (control, Ctrl, $n = 7$; AAV-Cre, Cre, $n = 9$). Bars indicate mean ± SD. *$p < 0.05$ (Student's $t$ test). ***C***, Box plot of cellular input resistance ($R_i$) of control ($n = 12$) and AAV-Cre VB cells ($n = 27$). The midline indicates the median. Bottom and top of the boxes represents the first and third quartiles, respectively. Whiskers represent full range. *$p < 0.05$ (Student's $t$ test).

pared ipsilateral and contralateral expression of γ2 subunits with confocal microscopy. In noninfected as well as the AAV-GFP-infected thalami, γ2 immunostaining resulted in dense punctate labeling, reflecting the predominantly synaptic localization of this subunit (Fig. 1*C*) (Nusser et al., 1998). In contrast, within the AAV-Cre-infected region, punctate γ2 immunoreactivity was not apparent (Fig. 1*D*). Next, we examined the expression of α1 subunits, which coassemble with γ2 to form functional receptors (Tretter et al., 1997) but, in addition, are also present extrasynaptically. Compared with controls, α1 labeling was reduced in the AAV-Cre-infected regions, but a weak staining, probably reflecting the extrasynaptic pool, persisted (Fig. 1*E*,*F*). Quantitative receptor localization demonstrated a nearly complete loss of γ2 immunoreactivity (relative intensity, 6.68 ± 2.11%) and a less dramatic but highly significant decrease in α1 immunostaining (relative intensity, 18.27 ± 20.18%) compared with AAV-GFP-infected regions (Fig. 1*I*). In contrast, in the case of the extrasynaptic, α4-containing GABA-ARs, which are responsible for tonic inhibition (Porcello et al., 2003; Chandra et al., 2006), no significant difference was observed between the AAV-Cre- and AAV-GFP-infected thalamic regions (relative intensity, 68.24 ± 50.82%; Fig. 1*G–I*). Based on these anatomical findings, we conclude that deletion of γ2 and the associated α1 protein was successful and selective in the infected regions.

To analyze the changes of γ2 staining at higher spatial resolution, STORM was applied (Dani et al., 2010). In these experiments, we used vesicular GABA transporter (vGAT) labeling to visualize GABAergic terminals. On the contralateral side, vGAT immunostaining labeled vesicle aggregations in the size range of nRT terminals (1–2 μm). Adjacent to these terminals, γ2 immunostaining formed dense clusters of punctae (Fig. 1*J–L*). The size of these clusters (400–500 nm) was in the range of synapses established by nRT terminals measured in serial electron microscopic images (Wanaverbecq et al., 2008). Single vGAT-positive terminals contacted one or up to four receptor clusters. In case of multiple contacts, the synapses were on different sides of the terminals, similar to earlier results (Wanaverbecq et al., 2008) (Fig. 1*J*). In contrast to the contralateral side, in the ipsilateral, AAV-Cre-infected region, γ2-labeled receptor clusters were absent around the vGAT-positive boutons (Fig. 1*K–M*). These data confirm successful viral intervention and the elimination of synaptic GABA-ARs.

### Removal of γ2 subunits eliminates fast IPSCs

To test the functional consequences of deletion of synaptic γ2-GABA-ARs, we performed whole-cell recordings from VB thalamic neurons in acute horizontal brain slices with intact nRT-TC connections forming the sole inhibitory input. When patched with pipettes containing a $K^+$-based pipette solution (Fig. 2*A*), these cells showed normal AP discharge properties both in tonic (AP amplitudes 63.1 ± 11.4 mV and 60.9 ± 6.1 mV; half-widths 1.04 ± 0.14 ms and 1.00 ± 0.18 ms; AP afterhyperpolarization −21.4 ± 5.9 mV and −21.3 ± 4.2 mV, $p > 0.05$ for all values; AAV-GFP, $n = 5$; AAV-Cre, $n = 9$) and burst mode (AP amplitudes 68.2 ± 9.8 mV and 63.8 ± 8.1 mV; half-widths 0.83 ± 0.15 ms and 0.84 ± 0.23 ms; AP afterhyperpolarization −13.4 ± 6.5 mV and −12.9 ± 3.0 mV; AP number/burst 1.7 ± 0.4 and 1.6 ± 0.4, $p > 0.05$ for all values; control, $n = 7$; AAV-Cre, $n = 8$). Moreover, cellular resting membrane potentials were unaltered (−76.6 ± 9.6 mV vs −75.0 ± 11.4 mV, $p > 0.05$; control, $n = 22$; AAV-Cre, $n = 21$ cells).

In the presence of glutamate receptor antagonists (DNQX 40 μM, D,L-APV 100 μM), all VB cells recorded in the control slices displayed fast spontaneous IPSCs (sIPSCs; rise time < 2 ms, weighted decay time constant < 11 ms) at a frequency of 1.33 ± 0.89 Hz that were blocked by the GABA-AR antagonist gabazine (Fig. 2*B*). In contrast, fast rising sIPSCs were almost completely abolished from VB cells recorded in the AAV-Cre-infected regions (0.006 ± 0.018 Hz, $p < 0.001$; Fig. 2*A–C*). In addition to fast IPSCs, slower (rise time > 30 ms) IPSCs were occasionally detected in both groups (see below).

We next examined eIPSCs elicited via activation of GABAergic inputs by extracellular stimulation in the nRT. Fast eIPSCs (rise time < 1 ms, decay time < 4 ms) were observed in 4 of 5 control cells tested with a mean amplitude of −82 ± 27 pA and 0.19 ± 0.15 pC of charge transfer. In contrast, in the AAV-Cre-infected regions, eIPSCs were absent in 5 of 6 TC cells recorded after both single and 10 Hz stimulation (Fig. 2*D*,*E*). The one AAV-Cre TC cell that responded to the stimulation showed slow kinetics (rise time 5 ms; decay time constant 28 ms) and large amplitude (~−120 pA). In summary, these data demonstrate the absence of fast synaptic inhibition mediated by γ2-GABA-ARs in AAV-Cre-infected VB cells.

To determine the effect of deleting synaptic receptors on tonic GABA-AR-mediated currents, we applied gabazine (10 μM) to cells patched with $Cl^-$-based intracellular solutions. In AAV-GFP-infected cells, gabazine induced an outward shift in the holding current (ΔI = 53 ± 19 pA), reflecting the presence of a tonic current (Fig. 3*A*). In AAV-Cre VB cells, ΔI was smaller (30 ± 14 pA, $p < 0.05$; Fig. 3*A*,*B*) and cellular input resistance was higher compared with controls (255 ± 110 MΩ vs 177 ± 84 MΩ, $p < 0.05$; Fig. 3*C*). These results suggest that either γ2-GABA-ARs account for a portion of the tonic current or existing extrasynaptic receptors have reduced functionality. More importantly, the fact that tonic currents are reduced in γ2-lacking VB cells indicates that a compensatory upregulation of nonsynaptic receptors did not occur.

### Burst-mediated IPSCs persist in the absence of synaptic GABA-ARs

Surprisingly, despite the absence of fast sIPSCs, we observed large and slow spontaneous inhibitory events in slices prepared from both control and AAV-Cre TC cells (Fig. 4*A*). These typically occurred at low frequencies (1.9 ± 3.9/min vs 1.7 ± 2.0/min, $p > 0.05$; control, $n = 16$; AAV-Cre, $n = 13$), singly or in groups of 2–4 events with interburst intervals of hundreds of milliseconds,

and are caused by spontaneous repetitive nRT burst discharge (Wimmer et al., 2012). In control cells, these events showed the typical waveform of burst IPSCs consisting of multicomponent fast events riding on a slower current envelope. In contrast, in AAV-Cre TC cells, burst IPSCs consisted of only the slow current envelope and lacked the fast phasic inhibitory currents (Fig. 4*B*), showing distinctly slower rising phases.

To quantitatively compare the burst IPSC properties in the two cell groups, we electrically stimulated the nRT to produce evoked burst IPSCs (Fig. 4*C*,*D*). Similar to spontaneous burst IPSCs, evoked burst IPSCs were abolished by gabazine (Fig. 4*C*). Compared with single AP-evoked IPSCs, the evoked burst IPSCs in control cells had a ~9.5-fold greater conductance (15.3 ± 10.0 nS for burst IPSCs, $n = 13$, vs 1.63 ± 0.60 nS for eIPSCs, $n = 4$) and slower decay kinetics (biexponential decay time constants ($\tau$1, $\tau$2) of 19 ± 10 ms and 90 ± 44 ms in $n = 8$ cells for burst IPSCs, Fig. 4*D*, third panel, vs monoexponential decay time constant ($\tau$) 3.0 ± 1.7 ms for eIPSCs, $n = 4$).

Similar to spontaneous burst IPSCs, evoked burst IPSCs were crowned by fast IPSCs in control, but not in AAV-Cre VB cells (Fig. 4*C*). Moreover, the average amplitude of the evoked burst IPSCs in AAV-Cre TC cells was diminished by ~60% compared with control (control, 425 ± 291 pA, $n = 13$; AAV-Cre, 161 ± 93 pA, $n = 20$; $p < 0.01$; Fig. 4*D*) and burst IPSCs generated in AAV-Cre cells showed decelerated time-to-peak (33.1 ± 10.0 ms in control vs 55.1 ± 25.9 ms in AAV-Cre TC cells, $p < 0.01$, Fig. 4*D*). To compare decay time courses, the slow time constant of AAV-GFP burst IPSCs was compared with a monoexponential fit of the AAV-Cre burst IPSCs, thereby taking into account the lack of a dominant fast current component resulting from the elimination of synaptic receptors. The monoexponential decay time constant of the AAV-Cre burst IPSC was comparable with the slow current component of control cells (AAV-Cre, $\tau$ = 69 ± 23 ms, $n = 15$, vs control, $\tau$2 = 90 ± 44 ms, $n = 8$; $p > 0.05$; Fig. 4*D*). The total charge transfer, calculated as the integral of the current trace, was diminished by 48% (control, 32.8 ± 26.5 pC, $n = 13$; AAV-Cre, 15.7 ± 8.3 pC, $n = 20$; $p < 0.05$; Fig. 4*D*). Moreover, burst IPSCs from both control and AAV-Cre TC cells had a reversal potential corresponding to the $Cl^-$ gradient imposed by the patch pipette. These data indicate that, in the absence of synaptic GABA-ARs, significant GABA-AR-mediated, slow, phasic events persist when the presynaptic neurons fire in burst mode. These events are independent of synaptic GABA-ARs and involve phasic recruitment of nonsynaptic GABA-ARs.

The efficiency of burst IPSCs in AAV-Cre VB cells to generate rebound low-threshold spikes could be decreased because of the missing synaptic component and the slowed-down rising phase. To test this, in current-clamped noninfected VB neurons, representative spontaneous burst IPSCs from control or AAV-Cre cells were injected as a command current (Fig. 4*E*). Injected waveforms were scaled in their amplitude (maximal peak = −420 pA) to mimic a variety of endogenous inputs of different efficacy. Cells injected with current commands obtained from control or AAV-Cre cells displayed a comparable input–output curve when considering the latency to the first AP in the rebound burst, the amplitude of the low-threshold $Ca^{2+}$-spike, or the number of elicited APs in response to a given charge injection (Fig. 4*F*–*H*). This suggests that, although rebound TC bursting may be weakened because of lower charge transfer in burst IPSCs of AAV-Cre TC cells, rebound bursting is maintained over a considerable range of burst IPSC amplitudes.

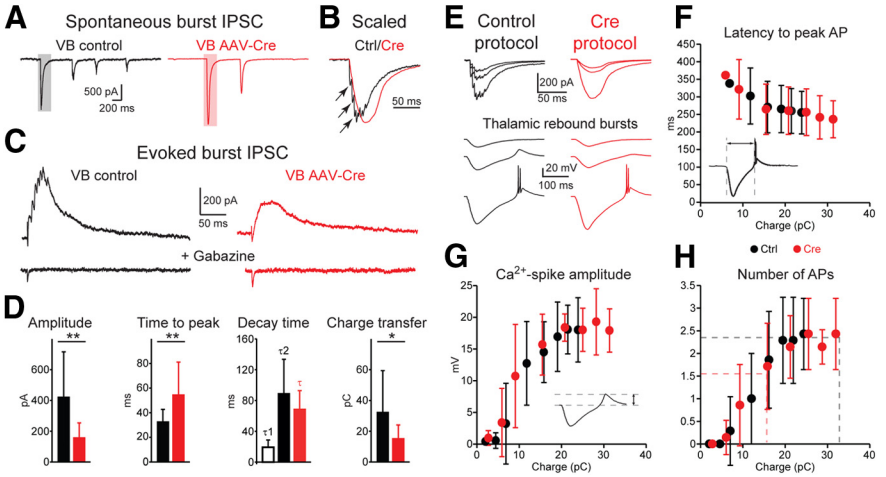


**Figure 4.** Burst IPSCs persist after the removal of $\gamma$2 subunits. ***A***, Spontaneous, repetitive burst IPSCs in a VB control and a VB AAV-Cre cell patched with high $Cl^-$ solution and held at −50 mV. There are similar interburst IPSC frequencies typical for the repetitive bursting of nRT cells and the incremental amplitude decrease of successive burst IPSCs. ***B***, Expanded traces of the first burst IPSCs for both cells shown in ***A*** (labeled with gray and red shadow). Traces are superimposed and scaled to their peak to illustrate differences in time course. Individual, fast IPSCs (arrows) crown the burst IPSCs in case of the control but not the AAV-Cre cell. ***C***, Extracellular nRT stimulation evokes gabazine-sensitive burst IPSCs in both control ($n = 13$) and AAV-Cre VB cells ($n = 20$). Cells were recorded with a $K^+$-based electrode at −30 mV in the absence of glutamatergic receptor blockers (see Materials and Methods). ***D***, Bar graphs compare evoked burst IPSC properties of control and AAV-Cre cells with respect to amplitude, kinetics, and charge transfer (control, $n = 13$; AAV-Cre, $n = 20$). Decay times were assessed in a subgroup of cells (control, $n = 8$; AAV-Cre, $n = 15$) using biexponential fits for control ($\tau$1, $\tau$2) and monoexponential fit ($\tau$) for AAV-Cre cells. ***E***, Top, Evoked burst IPSCs recorded from control (black) and AAV-Cre VB cells (red), scaled to different amplitudes and used as a current command ("Control protocol" and "Cre protocol," respectively) for control VB cells (clamped at −70 mV). Bottom, Representative voltage responses with increasing current amplitudes. ***F–H***, Quantification of rebound burst characteristics of TC cells in response to burst IPSC current commands. The Cre protocol (red) evoked APs with comparable latencies (***F***), low-threshold $Ca^{2+}$ spikes with identical amplitude (***G***), and similar numbers of APs (***H***) to control protocol (black). ***F***, ***G***, Insets, Representative response with dashed lines indicating the analyzed response property. ***H***, Red and black dashed lines indicate the number of APs corresponding to the mean charge transfer of burst IPSCs across all analyzed cells (seen in ***D***). Data are mean ± SD. *$p < 0.05$ (Student's *t* test). **$p < 0.01$ (Student's *t* test).

## Deletion of synaptic GABA-ARs does not produce aberrant oscillation

Our *in vitro* data indicate that, after the removal of $\gamma$2-GABA-ARs, a sizable portion of the slow burst IPSCs remained intact. To test the role of this slow nonsynaptic current in controlling network rhythms, we used *in vivo* assays.

We first iontophoretically injected the selective GABA-AR blocker gabazine (1 mM) into the somatosensory thalamus of control mice (Fig. 5*A*,*B*) to block both synaptic and extrasynaptic receptors. In accordance with previous data (Castro-Alamancos, 1999), gabazine application into the thalamus of mice ($n = 3$) disrupted the normal slow cortical oscillation and induced aberrant, large-amplitude regular activity in the cortex with a power spectrum peaking at 2.6 Hz (Fig. 5*A*,*B*). This indicates that, when all thalamic GABA-ARs are focally blocked, normal TC oscillations are disrupted.

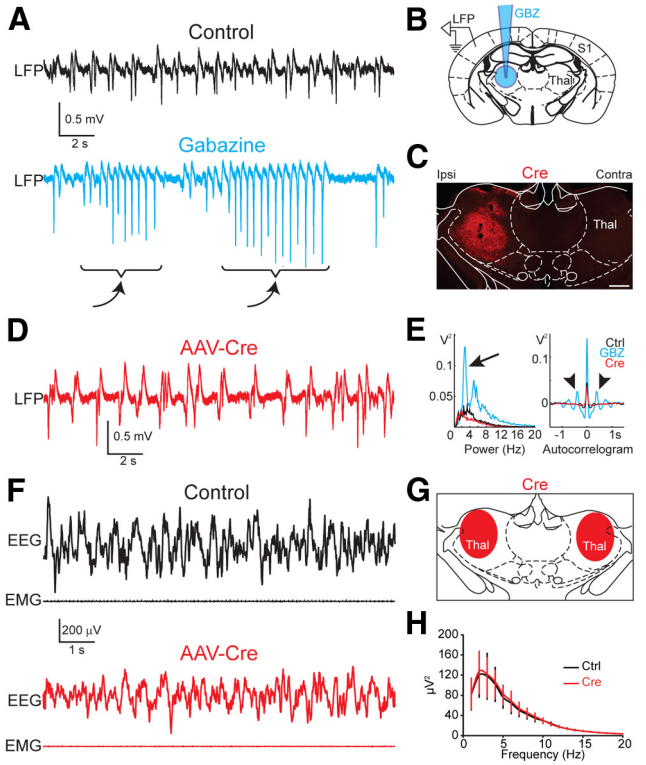


**Figure 5.** Removal of γ2-GABA-ARs in the thalamus does not cause aberrant rhythmic cortical activity. ***A***, Cortical (primary somatosensory cortex, S1) LFP recordings before (control, black) and after unilateral administration of gabazine (blue) into somatosensory thalamus under ketamine/xylazine anesthesia. There are epileptiform bouts of activity (curved arrows) in the cortical LFP recordings after gabazine. ***B***, Scheme of the unilateral, thalamic (Thal), gabazine (GBZ) injection site. ***C***, Low-power fluorescent image depicting Cre immunostaining (red) after thalamic injection of AAV-Cre. Scale bar, 500 μm. ***D***, The cortical LFP recorded from the ipsilateral S1 (red) after AAV-Cre injection to the thalamus is comparable with control (***A***). ***E***, Power spectra (left) and autocorrelograms (right) of the cortical LFPs in control condition (black), after gabazine (blue) and AAV-Cre injection (red). There is a large central peak at 2.6 Hz (marked by arrow) and the side lobes (arrowheads) in the GBZ treated animal but not in Ctrl and Cre cases. ***F***, In freely moving animals, slow oscillations are comparable in control (top black) and AAV-Cre-injected animals (top red) during NREM sleep. Bottom, Black and red traces represent the simultaneous EMG activity. ***G***, Scheme of the bilateral thalamic injection of AAV-Cre in the freely moving animals. ***H***, Power spectrum of NREM sleep over 24 h from 4 animals each of the AAV-GFP and AAV-Cre groups. Data were binned into 1 Hz bins and analyzed statistically using univariate repeated-measures ANOVA with factor "group" and "bin," yielding $p > 0.05$ for the group × bin interaction.

Next, we performed similar experiments using focal delivery of AAV-Cre (Fig. 5*C*) vectors instead of gabazine injection to examine whether deletion of synaptic receptors alone results in disturbed cortical activity. However, 3–8 weeks after viral delivery, selective deletion of only the synaptic GABA-ARs did not result in aberrant oscillations (Fig. 5*D*; $n = 9$). As a consequence, none of the cortical LFP autocorrelograms recorded from AAV-Cre-treated animals displayed the large central peaks, flanked by side lobes, which characterize the large amplitude, regular, rhythmic activity we observed after the injection of gabazine (Fig. 5*E*).

We also investigated the consequence of γ2-GABA-AR deletion on oscillatory activity during natural sleep. After bilateral thalamic injection of AAV-Cre ($n = 4$) or AAV-GFP (as control, $n = 4$), polysomnographic recordings yielded no sign of overt large-amplitude, aberrant activity during NREM sleep (Fig. 5*F*,*G*) after 3 weeks of recovery in freely moving mice. Mean power spectra across 24 h of NREM sleep were indistinguishable for AAV-GFP and AAV-Cre animals (repeated-measures ANOVA, $p > 0.05$, Fig. 5*H*). Thus, in contrast to the pharmacological blockade of all GABA-ARs, the TC system produces normal oscillatory activity even when largely devoid of thalamic γ2-GABA-ARs.

### Altered firing properties of TC cells in the absence of synaptic GABA-ARs

Complementing the EEG and LFP recordings, we also examined the firing pattern of individual TC cells in ketamine/xylazine-anesthetized mice through juxtacellular recordings (20–30 min) in two somatosensory thalamic nuclei known to have different inhibitory inputs (Pinault, 2004), the VB and the posterior nucleus (Po) (Barthó et al., 2002; Bokor et al., 2005; Wanaverbecq et al., 2008) (Fig. 6). Nuclear localizations of the juxtacellularly neurobiotin-labeled cells were *post hoc* identified using immunostaining against vGluT2 (Fig. 6*D*,*I*), whereas their phenotype was determined with Cre immunostaining (Fig. 6*E*,*J*).

The firing patterns of control, AAV-Cre-negative VB ($n = 11$) and Po ($n = 7$) cells in mice were similar to those of rats under the same recording conditions (Slézia et al., 2011). More than 90% of spikes occurred in bursts. In accordance with our previous rat data, the average intraburst frequency of spikes in VB cells was significantly faster than in Po cells (264.6 ± 47.2 Hz vs 204.3 ± 29.4 Hz, $p < 0.05$; Fig. 6 *A*,*F*).

Similar to controls, all AAV-Cre VB ($n = 9$) and Po ($n = 8$) cells were able to fire bursts of APs coupled to the rhythmic LFP activity (Fig. 6*B*,*G*). However, the properties of bursts were significantly altered in AAV-Cre cells and the alterations displayed nucleus-specific patterns (Fig. 6*C*,*H*).

In the absence of synaptic inhibition, the mean firing rate significantly decreased in case of AAV-Cre VB cells (control, 3 ± 1.3 Hz; AAV-Cre, 1.6 ± 1.1 Hz, $p < 0.05$; Fig. 6*C*). This was largely because of the reduced number of burst events (burst incidence, 0.96 ± 0.4 Hz in control vs 0.52 ± 0.36 burst/s in AAV-Cre, $p < 0.05$). In addition, the intraburst frequencies of spikes in AAV-Cre VB cells were lowered by 42 Hz (16%) (control, 264.6 ± 47.2; AAV-Cre, 222.5 ± 20.5 Hz, $p < 0.05$); however, the intraburst spike number did not change. As a consequence, the length of the AAV-Cre VB bursts increased significantly (burst length; 7.2 ± 1 ms in control vs 8.7 ± 1.7 ms, in AAV-Cre, $p < 0.05$; Fig. 6*C*).

In contrast to AAV-Cre VB cells, the mean firing rate of AAV-Cre Po cells was not altered (Fig. 6*H*). In these cells, the intraburst spike number displayed a slight decrease (3.1 ± 0.4 spike/burst in control vs 2.7 ± 0.5 spike/burst in AAV-Cre Po cells, $p < 0.05$; Fig. 6*H*). Because the intraburst frequency did not change, this resulted in a decrease of the overall burst length (control, 10.7 ± 1.6 ms; AAV-Cre, 9.0 ± 1.9 ms, $p < 0.05$; Fig. 6*H*).

These data show that TC cells retain low threshold bursts of APs in the absence of synaptic GABA-ARs, although the lack of synaptic inhibition slowed down the affected neurons, especially in VB.

### Spindle oscillations persist in the absence of synaptic GABA-ARs

Next, we examined the effect of synaptic GABA-AR removal on spindle oscillations in the thalamus of urethane-anesthetized mice through multichannel silicone probes. The probes were labeled with DiI, and their depths were registered to determine the exact position of the electrode shanks relative to the infected regions (Fig. 7*A*,*D*). For these experiments, we chose urethane anesthesia because it provides a network activity generating spindles similar to natural sleep (Steriade et al., 1993) unlike ket-

amine/xylazine anesthesia, during which short spindles are more prevalent (Slézia et al., 2011).

Spindles were detected in VB as transient rhythmic elevations of thalamic MUA, in the 7–15 Hz range, and could be quantitatively characterized (frequency, length, number of cycles, and occurrence; Fig. 7). We analyzed spindles in four experimental groups: noninjected wild-type, noninjected *GABAAR*$\gamma 2^{771}$*lox* mice; AAV-Cre injected, contralateral to the thalamus injection (AAV-Cre, contralateral, Cre; Fig. 7*A–C*) and AAV-Cre injected, ispilateral, within the injected zone (AAV-Cre, ipsilateral, Ctrl; Fig. 7*D,E*). The two noninjected groups did not differ in their quantitative measures and thus were grouped together (NonI, $n = 7$). The occurrence of spindles was variable during the recordings because of the spontaneous fluctuation in the depth of anesthesia. To overcome this variability, we performed long recordings (129 ± 60 min/animal), during which we detected together 109,762 spindles (on average 5777 ± 5509 spindle/animal, 294 ± 191 spindle/channel).

Spindles in the noninjected groups occurred at 3.36 ± 2.16 event/min (Fig. 7*F*). On average, the spindles consisted of 6.84 ± 0.78 cycles. The spindles lasted for 654 ± 74 ms and the average intraspindle frequency was 10.46 ± 0.35 Hz, which is consistent with earlier data (Steriade et al., 1993).

In all experiments of the Cre group (8 penetrations in 6 animals), normal spindle activity was detected (Fig. 7*D,E*) in the AAV-Cre-infected zone. The quantitative analysis demonstrated that the spindles had similar rates of occurrence (3.02 ± 2.05 event/min), similar numbers of spindle cycles (6.30 ± 0.39 ms), and lengths (659 ± 52 ms) to control. The only consistent change due to the deletion of synaptic inhibition was a slight decrease (10.5 ± 0.5 Hz in Ctrl vs 9.6 ± 0.4 Hz in Cre, $p < 0.01$) in intraspindle frequency (Fig. 7*F*).

We also followed on naturally occurring spindle activity through EEG recordings of NREM sleep in drug-free freely moving animals that previously received bilateral injections of either AAV-Cre or AAV-GFP (as control) vectors. NREM sleep states were analyzed with respect to the time course of power spectral densities at transitions to REM sleep. At these transitions, the power of frequencies between 5 and 25 Hz increases rapidly, notably at spindle-related EEG frequencies (Astori et al., 2011) (Fig. 8*A*). No change in the time course and power of this surge, averaged here for frequencies between 7 and 15 Hz, was found in the AAV-Cre animals (Fig. 8*B*). These data demonstrate that oscillations in the spindle frequency range are preserved after the removal of synaptic inhibition from the thalamus.

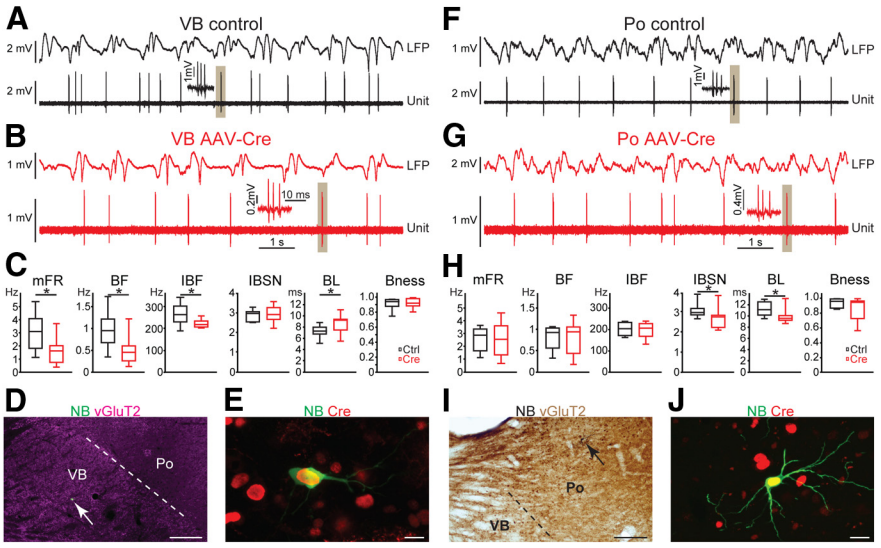


**Figure 6.** Nucleus-specific alterations in the firing properties of TC cells *in vivo* in the absence of synaptic GABA-ARs. ***A***, ***B***, Juxtacellular recordings of control (black, bottom) and AAV-Cre VB cells (red, bottom) together with cortical S1 LFP recordings (top in both cases) show typical burst firing. Shaded periods indicate selected bursts in expanded time scale. ***C***, Analysis of the properties of bursts in control (black; $n = 11$) and AAV-Cre VB cells (red; $n = 9$). There is decreased firing activity of the AAV-Cre TC cells. mFR, Mean firing rate; BF, burst frequency; IBF, intraburst frequency. The midline indicates the median. Bottom and the top of the boxes represent the first and third quartiles. Whiskers span full range. IBSN, Intraburst spike number; BL, burst length; Bness, burstiness index. *$p < 0.05$ (Mann–Whitney *U* test). ***D***, Localization of the control cell (shown in ***A***) filled with neurobiotin (NB, green) in VB. Po-VB border is identified by vGluT2 immunostaining (purple). ***E***, Confocal fluorescent image of the Cre-immunopositive (red) VB cell (green) shown in ***B***. Cre is localized to the nucleus. ***F***, ***G***, Juxtacellular recording of control and AAV-Cre Po cells together with cortical S1LFP recordings. Both control and AAV-Cre cells displayed normal burst firing. ***H***, Analysis of the burst properties in case of control ($n = 7$) and AAV-Cre Po cells ($n = 8$). Only IBSN and BL display significant changes. *$p < 0.05$ (Mann–Whitney *U* test). ***I***, Localization of the control Po cell shown in ***F***. Boundary is identified by vGluT2 immunostaining (brown). ***J***, Confocal fluorescent image of the Cre-immunopositive Po cell shown in ***G***. Scale bars: ***D***, ***I***, 200 $\mu$m; ***E***, ***J***, 10 $\mu$m.

## Discussion

We show here that oscillatory activity in thalamic circuits is under the control of inhibition that involves $\gamma 2$ subunit-independent GABA-ARs. These receptors are activated as nRT cells switch from tonic to burst discharge and suggest a "firing pattern-specific" form of inhibitory communication. Contrary to long-standing, previous views, conventional synaptic GABA-ARs are not absolutely required for TC rhythms. Phasic, nonsynaptic inhibition can efficiently drive TC cell rebound discharge and entrain slow oscillations and spindle waves during both sleep and anesthesia.

Our data demonstrate that, during burst firing of nRT cells, IPSCs in TC cells have both synaptic and nonsynaptic components in approximately equal proportions because 50% of the charge transfer remained intact after complete removal of the synaptic receptor pool in case of burst IPSCs. The remaining current had slow rise times and lacked fast-rising individual IPSCs, suggesting the contribution of extrasynaptic receptors. Most recently, an involvement of $\alpha 4$-containing GABA-ARs has been recognized during burst discharge at nRT-TC synapses in a manner that required GABA spillover, confirming our conclusions (Herd et al., 2013).

In the case of burst IPSCs, extrasynaptic receptors were recruited in a phasic, not in a tonic, manner. AP-mediated activation of extrasynaptic receptors, termed "GABA-A-slow" events, has already been demonstrated in several brain regions (Rossi and Hamann, 1998; Szabadics et al., 2007; Mańko et al., 2012). However, studying the extrasynaptic component of GABA-A-slow in isolation has not been possible with conventional pharmacological or genetic knock-out methods. Using virus-mediated gene knock-out of synaptic receptors, here we could quantitatively characterize the extrasynaptic component of GABA-AR responses and demonstrate that phasic extrasynaptic inhibition is mediated by burst discharge and powerful enough to drive global brain rhythms.

Our data disclosed a striking difference between eIPSCs when the presynaptic neuron fired in tonic as opposed to the burst

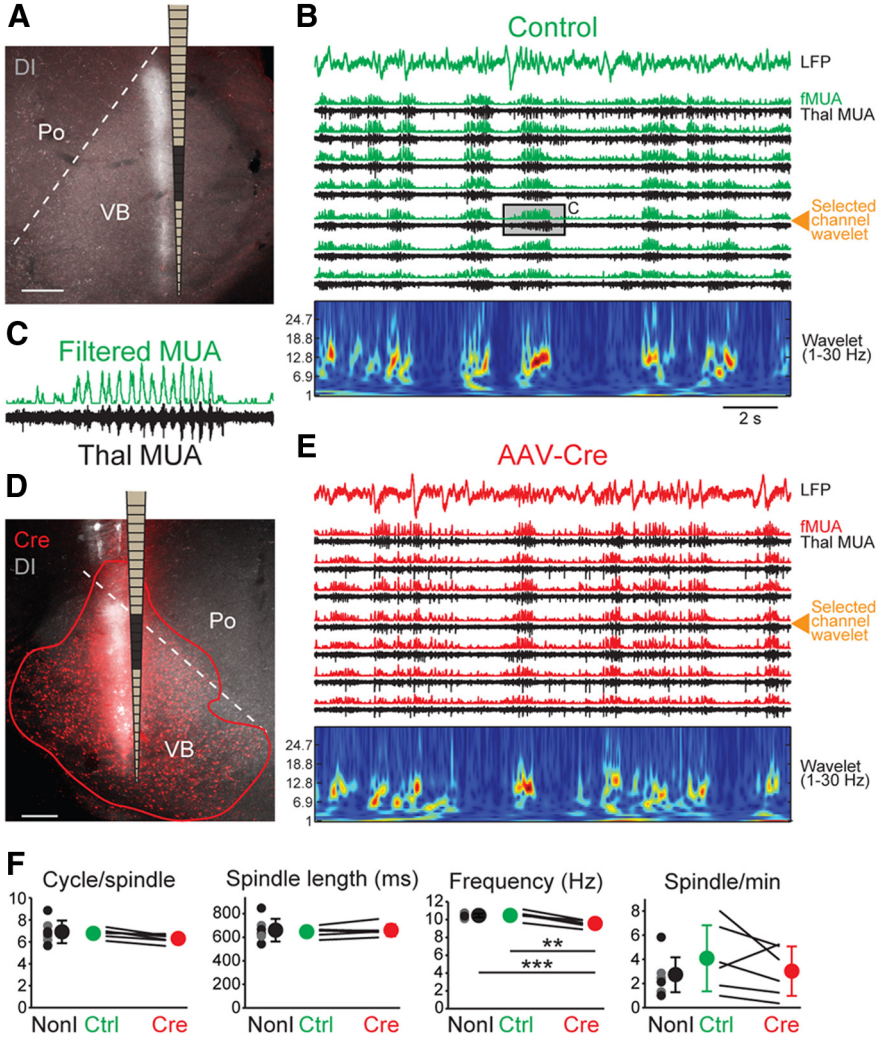


**Figure 7.** Thalamic spindle oscillations generated in the absence of synaptic GABA-ARs. ***A***, DiI-labeled track of a linear 32-channel silicon probe in the contralateral, noninfected VB. Dark gray in the schematic drawing of the silicon probe represents the position of the 7 channels shown in ***B***. ***B***, Cortical LFP recording (top) and thalamic multiunit activity in 7 adjacent channels (middle) under urethane anesthesia. Black represents raw traces; green represents filtered MUA (fMUA; 7–15 Hz). At the bottom the wavelet analysis of the raw multiunit, activity is shown in the selected channel (orange arrowhead). Wavelets represent the color-coded power of the selected MUA between 1 and 30 Hz. Warm colors represent high values. There is predominant activity in the spindle frequency range (7–15 Hz). ***C***, Two-seconds-long trace of a thalamic multiunit spindle (marked by black framed area in the channel selected for wavelet in ***B***) before (black) and after filtering (green). ***D***, ***E***, Same arrangement as in ***A***, ***B***, respectively, for a recording in the ipsilateral, AAV-Cre-infected side of the same animal. The electrode track penetrates the AAV-Cre-infected region in ***D***. Spindles are abundant in the AAV-Cre-infected region as well. Scale bars: ***A***, ***D***, 200 $\mu$m. ***F***, Quantitative analysis of spindles in noninjected (NonI; $n = 7$), AAV-Cre contralateral (Cre-C; $n = 6$) and ipsilateral (Cre-I; $n = 6$) recordings. Only the frequency of spindles shows a slight decrease (1 Hz), which reaches statistical significance. All other spindle parameters were statistically not significant. Gray dots indicate recordings from noninjected wild-type ($n = 3$); black dots indicate recordings from noninjected *GABAAR*$\gamma 2^{77I}$*lox* mice ($n = 4$). Error bars indicate $\pm$ SD. $^{**}p < 0.01$ (Student's *t* test). $^{***}p < 0.001$ (Student's *t* test).

mode. The complete disappearance of sIPSCs and eIPSCs after the removal of synaptic receptors in TC cells indicates that inhibition caused by single or tonic APs was mediated entirely by synaptic receptors. In particular, up to 10 Hz, tonic discharge did not recruit slow persistent currents (Wanaverbecq et al., 2008, Herd et al., 2013). In sharp contrast, during burst firing mode, a significant extrasynaptic receptor pool was additionally recruited that resulted in a strong increase of peak $Cl^-$ conductance (up to ~10-fold). According to Herd et al. (2013), extrasynaptic receptors contribute not only to burst IPSCs, but also prolong the decay time course of IPSCs after single APs. Small differences in the actual role of $\alpha$4-GABA-ARs could vary according to the preparation used. Herd et al. (2013) studied a complete $\alpha$4 KO, whereas in this study virally mediated gene knock-out was used in adult animals. Full KO techniques are more prone to induce compensatory changes, such as alterations in properties and exact location of remaining receptors. Intriguingly, however, this study mirrors our finding by showing that reduction of only extrasynaptic, but not synaptic GABA-ARs, also produces a 50% reduction in charge transfer.

Phasic, extrasynaptic inhibition was sufficient to promote rebound burst firing in TC cells, as demonstrated through command waveforms derived from burst IPSCs. This conclusion was also supported by the *in vivo* data showing burst firing in all TC neurons lacking synaptic GABA-ARs and preserved TC oscillations.

The burst IPSCs did not result from a temporal summation of phasic, conventional GABA-AR-mediated fast IPSCs. Instead, burst IPSCs reflect a rapid accumulation of GABA release that evokes phasic, nonsynaptic receptor activation in a manner not reached via repetitive tonic discharge up to tens of Hz (Wanaverbecq et al., 2008). As nRT-TC synapses are depressing, specific presynaptic release mechanisms activated during high-frequency discharge could contribute to the rapid increases in synaptic GABA levels, which remain the subject of further molecular characterization of nRT-TC synapses.

An unexpected change in our studies was a pronounced decrease in tonic inhibition and the associated increase in membrane resistance, without an apparent change in the expression of $\alpha$4-subunits. One explanation for the decreased tonic conductance is the disappearance of phasic inhibition in the distal dendritic region of TC cells, which is indistinguishable from the tonic conductance at the somatic level (Farrant and Nusser, 2005). Other possibilities, such as homeostatic downregulation of ambient GABA levels or involvement of nonconventional GABA-AR pools, remain to be determined. Based on our data, we currently cannot exclude the contribution of synaptic receptors to tonic inhibition.

Our experimental approach provided a unique opportunity to study the firing pattern of individual neurons lacking synaptic receptors embedded into a neuronal network oscillating normally. We performed the experiments in two thalamic nuclei, VB and Po, known to have distinct excitatory and inhibitory connectivity (Barthó et al., 2002; Bokor et al., 2005; Wanaverbecq et al., 2008; Groh et al., 2013). We found significant internuclear differences in response to the removal of synaptic GABAergic inhibition. Major changes were found in the VB, including a

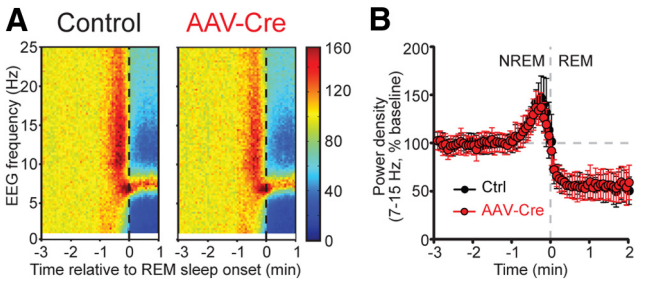


**Figure 8.** Normal spindle power density without thalamic γ2-GABA-ARs during natural sleep. ***A***, Color-coded heat maps of normalized EEG power between 0.75 and 25 Hz in 0.25 Hz bins during the NREM-to-REM sleep transitions in control ($n = 4$) and in AAV-Cre-infected mice ($n = 4$). Black dashed lines at time 0 indicate REM sleep onset. ***B***, Average mean EEG power time course between 7 and 15 Hz for all NREM-to-REM sleep transitions in the light phase. Data are normalized to the mean power in the time interval from −3 to −1 minute before the transition. Each data point corresponds to a 4 s epoch and is presented as mean ± SD.

significant drop in firing frequency, whereas changes in the Po were less prevalent. We attribute these differences to the distinct connectivity and activity pattern of the two nuclei (Hoogland et al., 1991; Groh et al., 2013). In case of VB cells, during the Up states of ketamine/xylazine induced slow oscillation, the intracellular activity is dominated by nRT-mediated rhythmic inhibition, whereas in case of Po cells fast rising EPSPs arising from layer 5 pyramidal cells determine Po activity under similar conditions (Groh et al., 2013). In agreement with these data, removal of synaptic inhibition affected VB cells to a much greater extent than Po cells. Thus, we conclude that the exact role of synaptic inhibition in controlling firing activity depends on the neuronal network the cell is embedded.

Thalamic application of GABA-AR antagonists, which block both synaptic and extrasynaptic receptors, disrupts the major TC oscillation and evokes aberrant, large-amplitude activity in ferrets and rats (Bal et al., 1995a; Castro-Alamancos, 1999), an observation that we replicated now in mice. These studies demonstrate that GABA-ARs in the thalamus have a critical role in supporting TC oscillations and GABA-B receptors alone cannot maintain normal rhythmic activity. In this study, we compared the consequences of full pharmacological blockade of GABA-ARs with those induced by virally mediated knock-out of synaptic GABA-ARs. Whereas total pharmacological blockade of thalamic GABA-ARs disrupts the major TC oscillations (Kim et al., 1995; Castro-Alamancos, 1999), the selective virus-mediated deletion of γ2-GABA-ARs did not affect the normal brain rhythms, and removal of only the synaptic GABA-ARs did not produce aberrant cortical activity. These experiments were performed under two different kinds of anesthesia (ketamine/xylazine and urethane) and in drug-free conditions as well, with identical outcomes, indicating that particular experimental conditions did not affect the results. Our data thus show that activation of extrasynaptic receptors by GABA spillover during nRT bursts alone generates sufficient amount of inhibition to maintain normal slow cortical oscillations and prevent the development of aberrant rhythmic activity.

A surprising outcome of our experiments was that spindle activity and EEG hallmarks of sleep spindles were also preserved in the brain of AAV-Cre-infected mice, indicating that relatively fast oscillations (7–15 Hz) can persist in the absence of synaptic receptors. The data demonstrate that slow GABA-A currents alone are able to maintain normal spindles with statistically similar occurrence and duration as in the intact brain. Despite the reduced charge transfer of burst IPSCs, after the removal of synaptic receptors, the phasic, extrasynaptic component of the burst IPSCs provided enough hyperpolarization to allow rebound burst discharges in TC cells. Indeed, in TC cells, a relatively small proportion of T-type $Ca^{2+}$ channels' deinactivation is sufficient for rebound burst generation (Dreyfus et al., 2010). As the frequency of rebound burst depends on the integrated membrane hyperpolarization imposed by nRT-IPSPs (Bal et al., 1995b), we found a slightly but significantly slower mean spindle frequency (~1 Hz decrease). In our experiments, the time course of thalamic GABA-A slow/burst IPSCs was 100–120 ms, which is well suited to pace a rhythm in the spindle frequency range (7–15 Hz) via the rebound mechanism. Thus, we propose here that this peculiar form of inhibition displaying dual synaptic and extrasynaptic nature was evolved to entrain a stable oscillation in the 7–15 Hz frequency range.

In conclusion, in the present study, we identified a discharge mode-specific mechanism of inhibition at a long-studied synapse implicated in a classical pacemaker activity. The synapse's main function is to synchronize TC cells to recruit them into oscillatory activity. Our data imply a complex organization of the synapse and a fine-tuned cooperation between different GABA-ARs according to the discharge mode. The molecular constitution of thalamic GABA-ARs is central to our understanding of TC synchronization during sleep, as synaptic GABA-ARs are the targets of many hypnotic and sedative drugs (Winsky-Sommerer, 2009). Here we propose that a nonsynaptic receptor entrains major sleep-associated TC oscillations in a phasic manner. Our findings provide a compelling explanation for the specific roles of different GABA-ARs in distinct behavioral states and thus open novel avenues to the development of drugs that act specifically on receptor subtypes contributing to burst IPSCs. These would have the unique potential to boost sleep yet protect phasic inhibition mediated by tonic discharge and associated wake-related functions.

## References

Astori S, Wimmer RD, Prosser HM, Corti C, Corsi M, Liaudet N, Volterra A, Franken P, Adelman JP, Lüthi A (2011) The CaV3.3 calcium channel is the major sleep spindle pacemaker in thalamus. Proc Natl Acad Sci U S A 108:13823–13828. CrossRef Medline

Bal T, von Krosigk M, McCormick DA (1995a) Role of the ferret perigeniculate nucleus in the generation of synchronized oscillations in vitro. J Physiol 483:665–685. Medline

Bal T, von Krosigk M, McCormick DA (1995b) Synaptic and membrane mechanisms underlying synchronized oscillations in the ferret lateral geniculate nucleus in vitro. J Physiol 483:641–663. Medline

Barthó P, Freund TF, Acsády L (2002) Selective GABAergic innervation of thalamic nuclei from zona incerta. Eur J Neurosci 16:999–1014. CrossRef Medline

Belelli D, Harrison NL, Maguire J, Macdonald RL, Walker MC, Cope DW (2009) Extrasynaptic GABAA receptors: form, pharmacology, and function. J Neurosci 29:12757–12763. CrossRef Medline

Blatow M, Rozov A, Katona I, Hormuzdi SG, Meyer AH, Whittington MA, Caputi A, Monyer H (2003) A novel network of multipolar bursting interneurons generates theta frequency oscillations in neocortex. Neuron 38:805–817. CrossRef Medline

Bokor H, Frère SG, Eyre MD, Slézia A, Ulbert I, Lüthi A, Acsády L (2005) Selective GABAergic control of higher-order thalamic relays. Neuron 45:929–940. CrossRef Medline

Brickley SG, Mody I (2012) Extrasynaptic GABA(A) receptors: their function in the CNS and implications for disease. Neuron 73:23–34. CrossRef Medline

Brickley SG, Cull-Candy SG, Farrant M (1999) Single-channel properties of synaptic and extrasynaptic GABAA receptors suggest differential targeting of receptor subtypes. J Neurosci 19:2960–2973. Medline

Bright DP, Aller MI, Brickley SG (2007) Synaptic release generates a tonic GABA(A) receptor-mediated conductance that modulates burst preci-

sion in thalamic relay neurons. J Neurosci 27:2560–2569. CrossRef Medline

Bright DP, Renzi M, Bartram J, McGee TP, MacKenzie G, Hosie AM, Farrant M, Brickley SG (2011) Profound desensitization by ambient GABA limits activation of δ-containing GABAA receptors during spillover. J Neurosci 31:753–763. CrossRef Medline

Capogna M, Pearce RA (2011) GABA A slow: causes and consequences. Trends Neurosci 34:101–112. CrossRef Medline

Castro-Alamancos MA (1999) Neocortical synchronized oscillations induced by thalamic disinhibition in vivo. J Neurosci 19:RC27. Medline

Chandra D, Jia F, Liang J, Peng Z, Suryanarayanan A, Werner DF, Spigelman I, Houser CR, Olsen RW, Harrison NL, Homanics GE (2006) GABAA receptor alpha 4 subunits mediate extrasynaptic inhibition in thalamus and dentate gyrus and the action of gaboxadol. Proc Natl Acad Sci U S A 103:15230–15235. CrossRef Medline

Cobb SR, Buhl EH, Halasy K, Paulsen O, Somogyi P (1995) Synchronization of neuronal activity in hippocampus by individual GABAergic interneurons. Nature 378:75–78. CrossRef Medline

Cope DW, Hughes SW, Crunelli V (2005) GABAA receptor-mediated tonic inhibition in thalamic neurons. J Neurosci 25:11553–11563. CrossRef Medline

Crandall SR, Govindaiah G, Cox CL (2010) Low-threshold $Ca^{2+}$ current amplifies distal dendritic signaling in thalamic reticular neurons. J Neurosci 30:15419–15429. CrossRef Medline

Dani A, Huang B, Bergan J, Dulac C, Zhuang X (2010) Neurotechnique superresolution imaging of chemical synapses in the brain. Neuron 68: 843–856. CrossRef Medline

Dreyfus FM, Tscherter A, Errington AC, Renger JJ, Shin HS, Uebele VN, Crunelli V, Lambert RC, Leresche N (2010) Selective T-type calcium channel block in thalamic neurons reveals channel redundancy and physiological impact of I(T) window. J Neurosci 30:99–109. CrossRef Medline

Essrich C, Lorez M, Benson JA, Fritschy JM, Lüscher B (1998) Postsynaptic clustering of major GABAA receptor subtypes requires the gamma 2 subunit and gephyrin. Nat Neurosci 1:563–571. CrossRef Medline

Farrant M, Nusser Z (2005) Variations on an inhibitory theme: phasic and tonic activation of GABA(A) receptors. Nat Rev Neurosci 6:215–229. CrossRef Medline

Franken P, Malafosse A, Tafti M (1998) Genetic variation in EEG activity during sleep in inbred mice. Am J Physiol 275:R1127–R1137. Medline

Groh A, Bokor H, Mease RA, Plattner VM, Hangya B, Stroh A, Deschenes M, Acsády L (2013) Convergence of cortical and sensory driver inputs on single thalamocortical cells. Cereb Cortex. Advance online publication. Retrieved July 3, 2013. doi: 10.1093/cercor/bht173. CrossRef Medline

Hamann M, Rossi DJ, Attwell D (2002) Tonic and spillover inhibition of granule cells control information flow through cerebellar cortex. Neuron 33:625–633. CrossRef Medline

Herd MB, Brown AR, Lambert JJ, Belelli D (2013) Extrasynaptic GABA(A) receptors couple presynaptic activity to postsynaptic inhibition in the somatosensory thalamus. J Neurosci 33:14850–14868. CrossRef Medline

Hoogland PV, Wouterlood FG, Welker E, Van der Loos H (1991) Ultrastructure of giant and small thalamic terminals of cortical origin: a study of the projections from the barrel cortex in mice using Phaseolus vulgaris leuco-agglutinin (PHA-L). Exp Brain Res 87:159–172. Medline

Kim U, Bal T, McCormick DA (1995) Spindle waves are propagating synchronized oscillations in the ferret LGNd in vitro. J Neurophysiol 74: 1301–1323. Medline

Mańko M, Bienvenu TC, Dalezios Y, Capogna M (2012) Neurogliaform cells of amygdala: a source of slow phasic inhibition in the basolateral complex. J Physiol 590:5611–5627. CrossRef Medline

Nusser Z, Sieghart W, Somogyi P (1998) Segregation of different GABAA receptors to synaptic and extrasynaptic membranes of cerebellar granule cells. J Neurosci 18:1693–1703. Medline

Pinault D (1996) A novel single-cell staining procedure performed in vivo under electrophysiological control: morpho-functional features of juxtacellularly labeled thalamic cells and other central neurons with biocytin or Neurobiotin. J Neurosci Methods 65:113–136. CrossRef Medline

Pinault D (2004) The thalamic reticular nucleus: structure, function and concept. Brain Res Brain Res Rev 46:1–31. CrossRef Medline

Pirker S, Schwarzer C, Wieselthaler A, Sieghart W, Sperk G (2000) GABA(A) receptors: immunocytochemical distribution of 13 subunits in the adult rat brain. Neuroscience 101:815–850. CrossRef Medline

Porcello DM, Huntsman MM, Mihalek RM, Homanics GE, Huguenard JR (2003) Intact synaptic GABAergic inhibition and altered neurosteroid modulation of thalamic relay neurons in mice lacking δ subunit. J Neurophysiol 89:1378–1386. Medline

Rossi DJ, Hamann M (1998) Spillover-mediated transmission at inhibitory synapses promoted by high affinity alpha6 subunit GABA(A) receptors and glomerular geometry. Neuron 20:783–795. CrossRef Medline

Sanchez-Vives MV, McCormick DA (2000) Cellular and network mechanisms of rhythmic recurrent activity in neocortex. Nat Neurosci 3:1027–1034. CrossRef Medline

Schindelin J, Arganda-Carreras I, Frise E, Kaynig V, Longair M, Pietzsch T, Preibisch S, Rueden C, Saalfeld S, Schmid B, Tinevez JY, White DJ, Hartenstein V, Eliceiri K, Tomancak P, Cardona A (2012) Fiji: an open-source platform for biological-image analysis. Nat Methods 9:676–682. CrossRef Medline

Slézia A, Hangya B, Ulbert I, Acsády L (2011) Phase advancement and nucleus-specific timing of thalamocortical activity during slow cortical oscillation. J Neurosci 31:607–617. CrossRef Medline

Steriade M, Nuñez A, Amzica F (1993) Intracellular analysis of relations between the slow (<1 Hz) neocortical oscillation and other sleep rhythms of the electroencephalogram. J Neurosci 13:3266–3283. Medline

Szabadics J, Tamás G, Soltesz I (2007) Different transmitter transients underlie presynaptic cell type specificity of GABA A, slow and GABA A, fast. Proc Natl Acad Sci U S A 104:14831–14836. CrossRef Medline

Tretter V, Ehya N, Fuchs K, Sieghart W (1997) Stoichiometry and assembly of a recombinant GABAA receptor subtype. J Neurosci 17:2728–2737. Medline

von Krosigk M, Bal T, McCormick DA (1993) Cellular mechanisms of a synchronized oscillation in the thalamus. Science 261:361–364. CrossRef Medline

Wanaverbecq N, Bodor AL, Bokor H, Slézia A, Lüthi A, Acsády L (2008) Contrasting the functional properties of GABAergic axon terminals with single and multiple synapses in the thalamus. J Neurosci 28:11848–11861. CrossRef Medline

Wei W, Zhang N, Peng Z, Houser CR, Mody I (2003) Perisynaptic localization of δ subunit-containing GABA(A) receptors and their activation by GABA spillover in the mouse dentate gyrus. J Neurosci 23:10650–10661. Medline

Wimmer RD, Astori S, Bond CT, Rovó Z, Chatton JY, Adelman JP, Franken P, Lüthi A (2012) Sustaining sleep spindles through enhanced SK2-channel activity consolidates sleep and elevates arousal threshold. J Neurosci 32:13917–13928. CrossRef Medline

Winsky-Sommerer R (2009) Role of GABAA receptors in the physiology and pharmacology of sleep. Eur J Neurosci 29:1779–1794. CrossRef Medline

Wulff P, Ponomarenko AA, Bartos M, Korotkova TM, Fuchs EC, Bähner F, Both M, Tort AB, Kopell NJ, Wisden W, Monyer H (2009) Hippocampal theta rhythm and its coupling with gamma oscillations require fast inhibition onto parvalbumin-positive interneurons. Proc Natl Acad Sci U S A 106:3561–3566. CrossRef Medline